CONTENTS

Transactions C: Aspects

International Journal of Engineering

A Hybrid Model for Supply Chain Risk Management Based on Five-dimensional Sustainability Approach in Telecommunication Industry

F. Valinejad, N. Safaie, D. Rahmani, M. R. Saadatmand*

Department of Industrial Engineering, K. N. Toosi University of Technology, Tehran, Iran

A B S T R A C T

Sustainability of supply chain risk management is one of the main competitive advantages of every organization for long-standing. There are several models in the research literature to manage sustainability risks of the supply chain. Considering that critical risks have the highest impact and have the largest share of risk management resources, they need to be identified using special techniques to make risk management more accurate and more reliable. In this paper, a new three-phase model is presented to supply chain sustainability risks management. This model includes the failure mode and effects analysis phase for identifying and assessing all risks and classification them, fuzzy VIKOR phase for ranking critical risks, and management phase to deal with critical risks. The categorization of risks was conducted according to a new five-dimensional approach to sustainable progress, including environmental, economic, social, technical, and organizational aspects on various sectors of the supply chain. The telecommunication industry of Iran is considered to show the model performance. The results indicated that consideration of the fuzzy VIKOR phase is necessary in order to accurately assess critical risks because of the priority of critical risks is not correctly identified through Failure mode and effects analysis due to the shortcomings of this method and cause errors. It was also found that the technical risks initiated by the organization are the most dangerous risk that threatens the sustainability of the supply chain.

doi: 10.5829/ije.2022.35.06c.01

1. INTRODUCTION

Development of sustainability, risk management and supply chain management are among the most important management concepts that guarantee the competitive advantage of organizations in the long run, in which risk analysis is one of the most important tools to maintain and improve the level of safety in the society and especially in industry [1]. The interconnected scope of these three scopes is "Supply chain sustainability risk management (SCSRM)", which means the management of risks that threaten the sustainability of the supply chain as illustrated in Figure 1. In comparison with traditional supply chain management, which emphasizes on logistical and economic performance [2-6], Supply Chain Sustainability Management (SCSM) is defined by integrating environmental and social ob-jectives

alongside the expansion of economic dimensions [7]. Today, Sustainable Supply Chain is a crucial head of cost reduction, increased profitability and resource allocation across the supply chain in the long term [8-12]. While one of the most key research titles is supply chain risk management, recently and it is still under development [13,14], but Supply Chain Sustainability Risk Management (SCSRM) is relatively rare in academic literature [9].

Apart from the typical supply chain risks, raising public awareness about sustainability of business practices has created more or different risks for organizations [15-16]. Based on the research background [10,17,18], the sustainability risks of the supply chain include environmental, economic and social risks [19] such as environmental impacts on natural ecosystem, pollution of environmental resources, shortage of natural

Corresponding Author Email: saadatmand.mci@gmail.com (M. R. Saadatmand)

Figure 1. Supply Chain Sustainability Risk Management (SCSRM)

resources, drought, corporate reputation, social responsibility, social inequalities, child labor, financial statements, compliance with rules, tax evasion, sanctions, bribes, fluctuations in energy prices, financial crises, demographic challenges, and so on. The potential results of the risks can possess devastating impacts for the company that the supply chain management cannot simply cope with [20].

One of the most useful and effective methods for assessing the risk is the FMEA method [21]. Failure mode and effects analysis (FMEA) was first designed in the 1960s by the NASA program as an official method for evaluating reliability risks and safety requirements. This approach provides a framework for decision-making in risk management by identifying potential risks at a single level and examining their effects on higher levels of the system [22]. Today, FMEA has been widely used as a powerful tool for analyzing the safety and reliability of systems, products, and processes in a wide range of industries such as aerospace, nuclear, automotive, electronics and medical industries [23,24].

Recently, multi-criteria decision-making methods (MCDM) have been used for risk assessment in several studies [25-30] due to their ability to consider many factors with special weight and rank risks with professional techniques. VIKOR is one of the most popular MCDM methods that has been widely used in various scientific studies [31-38] due to its ability to solve MCDM problems with conflicting and non-commensurable criteria and present a compromise ranking list.

However, the VIKOR method focuses on ranking of a set of alternatives in the presence of conflicting criteria. It determines a compromise solution that could be accepted by the decision makers. Also, FMEA is often influenced by uncertainty in real-life applications, and in such situation fuzzy set theory is an appropriate tool to

deal with this kind of problems [39]. In fact, the numerous shortcomings of FMEA published in recent studies (will be described in section 2.2), have led researchers to consider alternative approaches to risk assessment. Even scholars who referred to the limitations of FMEA method and presented several models to compensate it, have used the FMEA method in their models and then, by combining the FMEA with methods such as decision-making approaches (MCDM), have attempted to eliminate the FMEA shortcomings [25,40,41] etc. In fact, combining other methods with the FMEA method is to complement this technique and to resolve its deficiencies, and in general none of the studies conducted so far denies this method. Wang et al. [42] proposed a hybrid MCDM model in this study for improving FMEA. Liu et al. [43] propose a new model using interval 2-tuple hybrid weighted distance measure to improve the performance of the traditional FMEA. In order to assess the risk of delays of metro stations in Tehran based on the FMEA criteria, Hajiagha et al. [41] have used the VIKOR method in fuzzy environment. Safari et al. [44] evaluated enterprise architecture risks for managing all components of an enterprise using FMEA and fuzzy VIKOR.

The review of the research literature revealed some important points. First, there are some important shortcomings of FMEA and MCDM addresses to risk management when used alone. Aiming to take advantage of both methods and to cover their weaknesses, we have proposed a hierarchical approach by a combination of FMEA and fuzzy VIKOR for risk management to cover their limitations. It should be mentioned that, the approach is proposed in this paper has some differences between the works in the literature. First, the studies that have been conducted yet based on the combination of Fuzzy VIKOR and FMEA techniques, have been more focused on developing and improving the risk ranking. As a result, there is no functional and comprehensive framework for decision makers and industry experts to use FMEA's developed techniques in risk management. But in this research, by considering the managerial phase (the last phase of the three-phase model), the root causes and potential implications of each of the risks are identified and strategies to counter with them will be presented. Therefore, this study will be an operational framework for decision makers and the supply chain managers to properly manage their industry's sustainability risks based on the developed rating techniques. Second, most studies conducted on the basis of the combination of fuzzy VIKOR technique and the FMEA, have only considered the three criteria in calculating RPN (S, O & D) (section 2.1). Meanwhile, one of the limitations of the FMEA method is the lack of effective metrics. Also, according to the industry experts, more criteria should be considered to cover all aspects of risk. As a result, in this study, according to the industry

experts, more criteria are considered in addition to the three criteria (S, O & D) (section 5.2). Third, the studies that have been performed so far based on the combination of the fuzzy VIKOR and FMEA technique, have implemented the calculations of the fuzzy VIKOR method by using the three criteria proposed in calculating RPN (S, O & D). In fact, these models do not categorize any critical, semicritical, and normal risks, and only rank the identified risks. While the industry decision makers are often interested in separating critical risks from other risks and managing them in a particular way. On the other hand, these models will be operational and usable if the number of risks is low, because complex and time-consuming calculations of fuzzy VIKOR for a large number of risks, many of which are not very important, is not operational and cost effective. Regarding these points, in this study, by using the simple and fast FMEA technique, critical risks were identified and then, for accurate rating of them, the fuzzy VIKOR technique would be implemented only on the critical risks.

On the other hand, based on the literature, few studies have been managed on the supply chain sustainability risks and sustainability risk management [10]. To the best of our knowledge, no comprehensive study has analyzed the all aspects of the supply chains in view of the different dimensions of sustainability. This research gap encouraged us to develop a comprehensive model for managing the supply chain sustainability, critical risks in different echelons, which is a completely new approach and there is not any similar case in the research literature especially in telecommunication companies. The main contributions and innovations of this paper are:

- A new three-phase model for supply chain sustainability risk management is proposed
- The risks were classified based on a five-dimensional approach to sustainability
- The risks were classified based on the four parts of the supply chain
- The FMEA method is used for identifying and assessing all risks and filter critical risks
- An extended fuzzy VIKOR method with more criteria than RPN criteria is used for ranking critical risks
- The proposed model is applied to the telecommunication industry of Iran

The risk of supply chain sustainability in service organizations is far more complex than that of manufacturing organizations. Supply of telecommunication companies for which little research has been done as well as their management strategy, which is one of the main objectives of the present research.

The rest of this paper is organized as follows. In sections 2 and 3, we describe the literature review and the model development. Then, in section 4 we introduce the result presentation of the research, and find the steps of the three-phase model with respect to the studied companies. In section 5, the discussion and managerial insights are presented. Finally, the conclusion is reported in section 6.

2. LITERATURE REVIEW

2. 1. Failure Modes and Effects Analysis (FMEA)
2. 1. 1. Implementation of FMEA   To implement this method, a team of experts is formed to examine the relationship between error states, effects, causes, current controls and necessary corrective actions [45]. In order to allocate limited resources to address the most dangerous risks, each of the identified risks should be evaluated and prioritized. Typically, Risk Priority Number (RPN) is used to prioritize risks, which is the product of three risk factors (1);

$$RPN = S \times O \times P \tag{1}$$

where O is the probability of occurrence of the risk, S is the severity of the risk, and D is the probability of not detecting the risk.

According to research literature [46-48], the three risk factors are evaluated by experts using the 10-point scale de-scribed in Table 1. The risk with a higher RPN is more important and requires a higher priority to take corrective action.

2. 1. 2. Limitations of FMEA   As mentioned, FMEA is one of the most important and strong preventive measures in risk management; however, according to the

TABLE 1. Traditional FMEA scale for S, O and D

Occurrence	Rank	Severity	Rank	Detection	Rank
Very high (>1 in 2)	10	Hazardous without warning	10	Absolute uncertainty	10
Very high (1 in 3)	9	Hazardous with warning	9	Very Remote	9
High (1 in 8)	8	Very high	8	Remote	8
High (1 in 20)	7	High	7	Very Low	7
Moderate (1in 80)	6	Moderate	6	Low	6
Moderate (1in 400)	5	Low	5	Moderate	5
Moderate (1in 2000)	4	Very Low	4	Moderate high	4
Low (1 in 15,000)	3	Minor	3	High	3
Low (1 in 150,000)	2	Very Minor	2	Very high	2
Remote (<1 in 1,500,500)	1	None	1	Almost certain	1

research literature [23,24,39,40,43,45,49], this method has been severely criticized for several reasons:

1. In calculating the RPN, the relative importance of all three factors is considered to be the same, but in real applications, it is possible that each factor affects the risk ranking with a different weight.

2. Different sets of O, S, and D ranking can create similar values of RPN, but the hidden implications of these risks may be completely different, causing resource and time losses in the risk management process or in some cases lead to ignoring some risks. Small changes in the rank of each of the three parameters may lead to very different effects on the RPN.

4. The data used in risk assessment are often unclear or ambiguous, and can be expressed using descriptions such as likely, important or very high and so on. The ranking of risk factors with crisp numbers (absolute numbers 1 to 10) is often difficult and error-prone.

5. The three O, S, and D parameters are evaluated based on discrete scales, where numerical operations on a discrete scale, especially multiplication, are meaningless. Therefore, the RPN results are not only meaningless, but actually misleading.

6. RPN considers only three factors O, S and D for risk assessment and ignores other effective factors such as economic aspects, which will result in the loss of a significant amount of information and reduce the accuracy of risk assessment results.

7. The 10-point scale using to evaluate each of the O, S, and D factors is questionable; For example, a linear transformation is used to evaluate D, while a non-linear transformation is used to evaluate O.

Due to the above shortcomings of FMEA for risk assessment, a multi-criteria decision making (MCDM) methods in fuzzy environment can be used as more systematic methods to cover FMEA weakness [43]. These methods can consider many factors with special weight and rank risks with professional techniques. Also, fuzzy environment can overcome the limitations caused by crisp values in proses of RPN calculation.

2. 2. Fuzzy VIKOR   One of the MCDM methods is VIKOR technique that used to handle multi-criteria problems with conflicting and non-commensurable criteria. In the VIKOR method, a compromise solution is the closest solution to the ideal one, and the purpose of compromising is obtaining a response based on the mutual agreement between the criteria.

To implement the VIKOR method in fuzzy environment and with the presence of a group of decision makers, the following steps have been proposed in the literature of the study [30,31].

Step 1: First, a linguistic diagram is defined in accordance with the problem and decision makers weighted each criterion and evaluated each alternative using proposed description (VL, L, ML, M, MH, H and V). Then, qualitative points considered by decision makers will be converted into fuzzy numbers using these charts (see Figure 2).
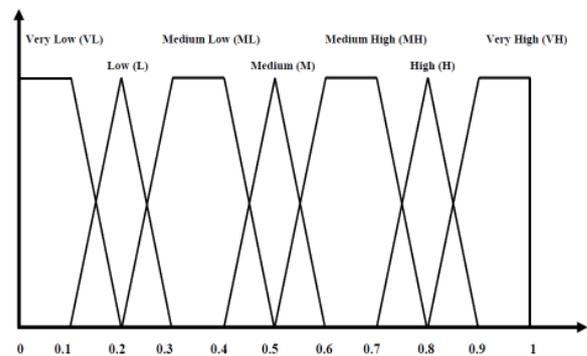
Figure 2. Linguistic variables for rankings (Sanayei et al. [31])

Step 2: Suppose that a group multi-criteria decision making (GMCDM) problem has K decision makers DM_k (k = 1, 2, ..., K), m alternatives A_i (i = 1, 2, ..., m), and n decision criteria C_j (j = 1, 2, ..., n); then the aggregated fuzzy weights ($\tilde{w}_j$) of each criterion can be calculated as follows [31]:

$$\tilde{w}_j = (w_{j1}, w_{j2}, w_{j3}, w_{j4}) \tag{2}$$

where

$$w_{j1} = \min\{w_{jk1}\}, w_{j2} = \frac{1}{k}\sum_{k=1}^{K} w_{jk2},$$
$$w_{j3} = \frac{1}{k}\sum_{k=1}^{K} w_{jk3}, w_{j4} = \max\{w_{jk4}\} \tag{3}$$

Also, the aggregated fuzzy ratings ($\tilde{x}_{ij}$) of alternatives with respect to each criterion can be calculated as follows:

$$\tilde{x}_{ij} = (x_{ij1}, x_{ij2}, x_{ij3}, x_{ij4}) \tag{4}$$

where

$$x_{ij1} = \min\{x_{ijk1}\}, x_{ij2} = \frac{1}{k}\sum_{k=1}^{K} w_{ijk2}$$
$$, w_{ij3} = \frac{1}{k}\sum_{k=1}^{K} w_{ijk3}, w_{ij4} = \max\{w_{ijk4}\} \tag{5}$$

Step 3: Then, using the COA defuzzification method to convert the fuzzy values ($\tilde{w}_j$ and $\tilde{x}_{ij}$) to crisp values (w_j and x_{ij}) [36].

Step 4: Based on the defuzzied matrix in the previous step, the VIKOR method is implemented as follows [31]:
-    Determine the best f_i^* and the worst f_i^-

$$f_i^* = max\ x_{ij}, f_i^- = min\ x_{ij} \tag{6}$$

-    Compute values S_i, R_i and Q_i

$$S_i = \sum_j W_i\left(\frac{f_j^* - f_{ij}}{f_j^* - f_j^-}\right), \tag{7}$$
$$R_i = \max\left\{\left(\frac{f_j^* - f_{ij}}{f_j^* - f_j^-}\right)\right\}W_i$$

$$Q_i = \left(\frac{S_i - S^*}{S^- - S^*}\right)v + \left(\frac{R_i - R^*}{R^- - R^*}\right)(1 - v) \tag{8}$$

where

$$S_i^* = min\ S_i,\ S_i^- = max\ S_i\ ,\ R_i^* = min\ R_i,\ R_i^- = max\ R_i \tag{9}$$

And v is introduced as a weight for the strategy of maximizing group utility, whereas $1 - v$ is the weight of the individual regret. The value of v is set to 0.5 in this study.

- The result of ranking: Based on the VIKOR method, the ranking of alternatives is arranged according to the ascending Q trend, and alternatives with lower Q will be given a higher priority.

3. THE MODEL DEVELOPMENT

According to the literature of the study, risk management generally includes five stages of identification, assessment, analysis, treatment and monitoring [10]. In this section, a three-phase model is presented for supply chain sustainability risk management based on the FMEA and fuzzy VIKOR techniques shown in Figure 3.

The reason for combining the FMEA and VIKOR techniques in this model is to use the benefits of each of the two methods and to avoid the limitations of each of them. The FMEA technique is a recognized and well-known methodology among industry experts, which is very useful for early screening of the risks due to the comprehensi-bility of the criteria and the simplicity of the calculations. From the expert's point of view, all the identified risks are not important and it is necessary to identify high and more dangerous risks, by using a simple and fast filter, so that the risk management resources are properly allocated and waste of time and money should be prevented. Therefore, by using the FMEA technique, all the identified risks are ranked to separate critical risks.

But, as discussed in section 2.2, the FMEA technique has some limitations that somewhat makes doubt about the accuracy of the results. Although the FMEA technique is valid enough to be used in the initial filtering of the risk and identifying high risk, but due to the existing deficiencies, this technique does not have the necessary accuracy to rank critical risks. Because critical risks are in fact the strategic bottlenecks for the risk management, and any errors in their identification and rating, encounters the risk management with a failure. In addition to the deficiencies, according to our industry experts, the criteria considered in the FMEA technique are not sufficient and do not cover all of the important dimensions of the industry risks. As a result, the model should include more criteria in order to achieve to the desired results. Therefore, it is proposed in this model in the continue, taking into account further criteria, by using a MCDM (fuzzy VIKOR method) approach, which is a complex and accurate ranking technique, in which the critical risks are carefully included. On the other hand,

although the fuzzy VIKOR method has a high-ranking accuracy, but due to the complexity and time-consuming of the calculations, it is not possible to use it from the beginning to rank all the identified risks. Because the identified risks are too much and the use of a complex and long-lasting fuzzy method to rank all risks, practically makes the model unusable for the industrial users. In this way, by combining the FMEA and fuzzy VIKOR techniques, we take advantage of each of the two methods, and avoid any constraints, so that risk management can be implemented quickly and accurately.

The first phase is related to FMEA technique, which includes research configuration, risk identification and risk assessment using the RPN formula. Our purpose of implementing the FMEA phase is to identify all risks and seg-regate critical risks. Given the RPN shortcomings in prioritizing risks, the critical risks that have the most impact and the largest share of risk management resources, should be prioritized using a special ranking technique [40]. So, the second phase is a fuzzy VIKOR phase that ranks the critical risks in order to risk management will be conducted more accurately. The third phase is the managerial phase that defines strategies to deal with critical risks.

3. 1. FMEA Phase   FMEA phase, including five steps that named from F1 to F5;

Step F1 - Research configuration: Each risk management project has dimensions and objectives that the project framework needs to be defined at the beginning of the FMEA phase. In other words, it should be determined that the identification of risks should take place in what field and with what goals.

Step F2 - Industry identification and selection a sample: After designing the project framework, by holding interviews with experts, the industry is carefully identified and the appropriate sample is selected.

Step F3 - Risk identification: To identify the risks, brainstorming sessions and interviews with the presence of various levels of industry experts (managers, experts, technicians, etc.) are held to provide the list of all potential risks.

Step F4 - RPN calculation: After the risk list is prepared, the risk priority number (RPN) is computed.

Step F5 - Segregation of critical risks: Generally, in the FMEA method, there is no basis for RPN to determine critical risks. For this reason, in order to determine the critical level of risks, statistical methods have been used. For this purpose, a risk index is defined and then the critical level of risks is determined based on it. So, first, the average RPN will be calculated from the relation (10) and then their standard deviation will be calculated from the relation (11).

$$\bar{X} = \frac{1}{N}\sum_{k=1}^{n} X_i \tag{10}$$

$$\sigma = \sqrt{\frac{1}{N}\sum_{k=1}^{n}(X_i - \bar{X})^2} \qquad (11)$$

Based on the results obtained from the above relations, the classification of critical levels of risk based on RPN values are defined as Table 2.

3. 2. Fuzzy VIKOR Phase VIKOR phase, including five steps that named from V1 to V5;

Step V1 - Determining the ranking criteria: Due to the configuration of the project, the criteria affecting the ranking will be determined by the experts. One of the shortcomings of the FMEA methodology is to consider only three factors (S, O, and D), therefore, in this step, the criteria proportionate to the purpose of risk ranking should be set.

Step V2 - Forming the fuzzy group decision making matrix: At this stage, decision makers determine the weight of each criterion and complete decision-making matrix, based on the linguistic chart. Then,

TABLE 2. The critical levels of the identified risks

Level	Normal	Semi critical	Critical
Risk index	$RPN < \bar{X} - \sigma$	$\bar{X} - \sigma \le RPN \le \bar{X} + \sigma$	$\bar{X} + \sigma < RPN$
Control action	Neglected	Preventive measure	Urgent preventive measure
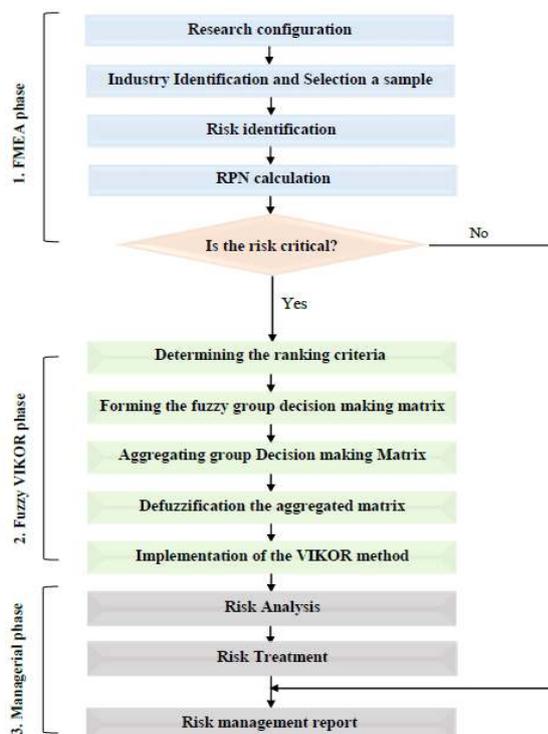
Figure 3. The flow chart of proposed model

these qualitative points are converted to fuzzy values using the graph.

Step V3 - Aggregating group decision making matrix: Group decision making matrix is aggregated based on relations (2) to (5).

Step V4 - Defuzzification the aggregated matrix: Using the COA defuzzification method, aggregated fuzzy matrix convert to crisp matrix [32].

Step V5 - Implementation of the VIKOR method: Based on the crisp matrix in the previous step, the VIKOR method is implemented as follows:

- Determine the best f_i^* and the worst f_i^-
- Compute values S_i, R_i and Q_i
- Ranking alternatives, according to the ascending Q trend

3. 3. Managerial Phase Managerial phase, including three steps that named from M1 to M3;

Step M1 - Risk Analysis: The root causes and potential consequences of each of the risks are identified by holding interviews with industry experts. Risk analysis is an important step in the process of risk management. An or-ganization can take the most appropriate strategy to deal with those risks only if they understand the root causes and correctly predict the potential consequences of the risks.

Step M2 - Risk treatment: Four major responses or strategies have been proposed in the research literature for risk treatment which includes avoiding or eliminating root causes, controlling or reducing the impact of the risk and the probability of risk occurrence, transferring or sharing the impact of the risk and the acceptance of the po-tential damages. In this step, depending on the root causes or the possible results of each risk, the appropriate strategy is selected and the Control action will be defined in accordance with this strategy.

Step M3 - Risk Management Report: Finally, the critical risks list, along with the results of the ranking, root causes and potential consequences, as well as the strategy for coping with each risk, will be presented in the risk man-agement report. Risk Management Report in this step is the introduction of two stages of implementation and monitoring of risk management strategies.

4. CASE STUDY

The companies that work in Iranian telecom industry have engaged with many challenges and unpredictability such as a complicated sustainability risk management of the supply chain in comparison with those in rest of the world. Therefore, in this research the case study described by Valinejad and Rahmani [50] in the Iranian telecommunication industry is considered. They

investigated 14 public and private sector companies operating internet service providing and bandwidth areas.

4. 1. FMEA Phase   Valinejad and Rahmani [50] used the FMEA approach to identify the mentioned supply chain sustainability risks of Iranian telecommunication companies. They designed a matrix based on the five dimensions of sustainable development and supply chain segments in Table 3 and named each cell of the table based on the first letters of the supply chain sectors and the dimensions of sustainable development.

The dimensions of the sustainable development include five dimensions of environmental, social, economic, technical and institutional that are more relevant to the business environment. Here is a brief overview of each of these five sustainability dimensions according to the literature studies [10,17]:

- Environmental dimension: Conservation of natural resources, the prohibition of waste production and environmental pollution, the proper use of non-renewable resources, etc.
- Social dimension: Reducing poverty, improving the quality of living conditions, observing ethical principles and human rights, etc.
- Economic dimension: Profitability and sustainable economic growth, avoidance of financial corruption, strict monitoring of financial statements, etc.
- Technical dimension: Technical abilities, equipment capabilities, quality of infrastructure and specialized industry issues, etc.
- Institutional dimension: Adherence to legal issues, lasting relationship with governments and partners, political stability, etc.

We have utilized the data reported by Valinejad and Rahmani [50]. They identified 15 critical risks based on the FMEA approach.

4. 2. Fuzzy VIKOR Phase

Step V1 - Determining the ranking criteria: Considering sustainable development concept, 6 criteria were introduced in order to ranking supply chain sustainability critical risks. The criteria which determined by holding interviews with experts, include two criteria used in the RPN calculation and four other criteria that were chosen with a view to sustainable development, triggered covering more dimensions of the issue of sustainability in the ranking in Table 4.

- Severity: Strength of risk in making the supply chain unsustainable
- Occurrence: The sequence of risk occurrence within a specified time period
- Uncontrollability of risk occurrence: The lack ability to prevent the risk occurrence
- The complexity of risk treatment: The difficulty in identifying, controlling and managing risk
- Comprehensiveness of risk impact: The ability of risking in making the greater parts of the supply chain un-sustainable
- Durability of risk impact: Risk capability in long-term impact on supply chain sustainability

Step V2 - Forming the fuzzy group decision making matrix: At this stage, four industry experts, as four decision makers, determined the weight of each criterion and score for each of the alternatives using qualitative terms. Table A1 (In Appendix) indicates the qualitative decision-making matrix and the weight of the criteria. In the results tables, critical risks are shown by HRi (High Risk).

Step V3 - Aggregating Group Decision making Matrix: The qualitative matrix in the previous step is converted to fuzzy matrix using the linguistic diagram as Figure 2. Then the fuzzy matrix aggregated based on relations (2) to (5). Table A2 (In Appendix) indicated the aggregated fuzzy matrix.

TABLE 3. The critical levels of the identified risks

Risks categories		The causes of sustainability risks in the supply chain			
		Suppliers (S)	Organization (O)	Consumers (C)	Environment (E)
The affected sustainability dimensions	Environmental (En)	S.En	O.En	C.En	E.En
	Economic (Ec)	S.Ec	O.Ec	C.Ec	E.Ec
	Social (S)	S.S	O.S	C.S	E.S
	Technical (T)	S.T	O.T	C.T	E.T
	Institutional (I)	S. I	O. I	C. I	E. I

TABLE 4. Research configuration

C_j	C_1	C_2	C_3	C_4	C_5	C_6
	Severity	Occurrence	Uncontrollability of risk occurrence	The complexity of risk treatment	Comprehensiveness of risk impact	Durability of risk impact

Step V4 -Defuzzification the aggregated matrix: Using the COA defuzzification method, aggregated fuzzy matrix convert to crisp matrix in Table A3 (Appendix).

Step V5 - Implementation of the VIKOR method: Based on the crisp matrix in the previous step, the VIKOR method is implemented as follows:

- Determine the best f_i^* and the worst f_i^- in Table 5.
- Compute values S_i, R_i and Q_i in Table 6.

Ranking alternatives, according to the ascending Q trend in Table 7.

4. 3. Managerial Phase   Step M1 - Risk Analysis: Root causes and potential result of each risk are presented in the risk management report in Table A4 (In Appendix).

Step M2 - Risk treatment: Strategies and control actions for each risk are presented in the risk management report in Table A4 (In Appendix).

Step M3 - Risk Management Report: The description of each risk and its position in the configuration (based on Table 3), along with the results of the ranking of VIKOR technique, root causes and potential consequences, as well as the strategy for coping with each risk, will be presented in the risk management report in Table A4 (In Appendix).

TABLE 5. The best and the worst values

Values	C_1	C_2	C_3	C_4	C_5	C_6
f_j^*	0.8625	0.84375	0.84375	0.84375	0.88125	0.73125
f_j^-	0.48125	0.35	0.5	0.43125	0.35	0.3125

TABLE 6. The values S_i, R_i and Q_i

HR	Q	R	S
HR1	0.173296	0.217647	0.980107
HR2	0.583692	0.567273	3.02006
HR3	0.416223	0.583428	1.11458
HR4	0.54001	0.63125	2.11927
HR5	0.604823	0.63125	2.81448
HR6	0.447854	0.482276	2.13726
HR7	0.647904	0.721107	2.6695
HR8	0.274703	0.304114	1.48365
HR9	0.389357	0.461076	1.65302
HR10	0.263481	0.240369	1.79395
HR11	0	0.068671	0.127762
HR12	0.660735	0.664549	3.18924
HR13	1	0.8625	5.49095
HR14	0.646066	0.565574	3.70058
HR15	0.29263	0.296926	1.72451

TABLE 7. The ranking of the critical risks by S, R and Q in ascending order

HR	by Q	by R	by S
HR1	2	2	2
HR2	10	9	12
HR3	7	10	3
HR4	9	11	8
HR5	11	12	11
HR6	8	7	9
HR7	13	14	10
HR8	4	5	4
HR9	6	6	5
HR10	3	3	7
HR11	1	1	1
HR12	14	13	13
HR13	15	15	15
HR14	12	8	14
HR15	5	4	6

5. DISSCUSION AND MANAGERIAL INSIGHTS

According to the risk management results the critical risks ranking based on fuzzy VIKOR is not consistent with prioritization of risks in terms of RPN (based on comparing "Ranking by fuzzy VIKOR" column with "RPN" column in Table 12). In other word, ranking critical risks based on the fuzzy VIKOR, does not approve the primary priority of critical risks based on the RPN. Due to the shortcomings of FMEA in calculating RPN in risk assessment on the one hand and strength of the fuzzy VIKOR to cover these limitations on the other hand, this inconsistency was predictable and validated the results of the ranking based on the fuzzy VIKOR. Furthermore, the results of the critical risk ranking by FMEA and Fuzzy VIKOR, were provided by experts. From the viewpoint of the industry experts and decision makers, rating of the critical risks based on the Fuzzy VIKOR technique was much more logical than the results of the FMEA approach.

Therefore, the need to use special ranking techniques for risk assessment, especially critical ones, is proven. However, in this study, it was attempted to use the both FMEA and Fuzzy VIKOR techniques to provide industry managers with a comprehensive and applicable framework to quickly, accurately and easily manage the sustainability risks of the supply chain. In the model presented in this paper, using the simplicity and speed of the FMEA method in risk assessment, it was attempted to identify critical risks, and then, by using the accuracy and power of Fuzzy VIKOR Method in ranking, critical risks are carefully ranked. Using this model, time and cost and risk management resources are focused on the critical

risk and the strategic risks of the supply chain are properly managed.

Also, according to the results of the ranking, mismanagement and lack of strategic management system (the technical risk generated by the organization or O.T risk) is the most dangerous risk that threatens the supply chain sustainability. This necessitates the necessity of efficient and effective implementation of the strategic management system in the supply chain.

It should be noted that the model presented in this study will be generally applicable to managers and suppliers of the supply chain experts in other industries.

According to macro policies and the 20-year vision document of Iran's development, the issue of sustainable development has become one of the most important principles of micro and macro planning. Common supply chain risks are more aimed at increasing profits and reducing costs from an economic perspective, but supply chain sustainability risks are also emphasized in addition to the social and environmental dimensions. For the sustainability of the two social dimensions, attention is paid to improving the quality of social conditions of all stakeholders. In the economic dimension, the trend of profitability is considered. For environmental sustainability, the consumption of non-renewable resources and the production of waste to protect the environment must be minimized. One of the important points for telecom managers is to discover the root causes and determine the potential consequences of each of the risks in the four areas of suppliers, organizations, consumers, and the environment and to adopt an appropriate strategy to deal with the risks and their effects.

The types of supply chain sustainability risks of telecommunication companies under three headings of critical, semi-critical and normal risks form a normal curve, so that 70% of them are semi-critical risks that require preventive action, some of which are addressed. as follow: In semi-critical risks, the power of all components of the supply chain should be focused on increasing interaction and compliance with global and national laws, as well as improving the quality and quantity of technical equipment and specialized human resource capabilities. In order to maintain the stability of the supply chain in telecommunication companies, the organization should focus on increasing the specialized capabilities of human resources, improving the quality and quantity of technical equipment and increasing the capacity of its infrastructure, invested employee motivation, creativity and participation. Emphasizes the importance of increasing the organization's interaction with suppliers, consumers and the environment as a key factor in reducing supply chain risk.

From a managerial point of view, in relation to suppliers as the largest producer of critical risks, there should be more focus and cost for the organization to interact with suppliers. Emphasis should be placed on improving the social status within the organization in order to reduce supply chain risk. Government suppliers such as the Telecommunication Company and the Telecommunications Infrastructure Company and the Radio Regulatory Company should invest in improving telecommunication infrastructure and services and products such as the quality of bandwidth, insufficient capacity of telecommunication platforms and centers. Governance risks such as sanctions, political instability, multiple and unsustainable policies are aspects of sustainable development that are most threatened.

6. CONCLUSION

Summary: In this study, it was tried to combine the advantages of each of them with the combination of fuzzy VIKOR and FMEA Technique, by avoiding the limitations of each of the two methods. After identifying all risks in the FMEA phase, the critical risks were separated and entered the fuzzy VIKOR phase for more accurate ranking. In the fuzzy VIKOR phase, critical risks were ranked and the importance and priority of dealing with each of the critical risks was precisely determined.

Then, in the management phase (last phase), the root causes and potential outcomes of each of the risks were identified and, by using the opinion of the decision makers and industry experts, an appropriate strategy for managing each of the risks was determined.

Application of the paper: Regarding to the expansion of the subjects related to the sustainable development, risk management, supply chain management and the combination of FMEA and fuzzy VIKOR, the outcome of this study are reflective for researchers who are seeking study in these areas. Also, these results help people involved in the supply chain management in the supply chain of telecommunication companies, particularly.

Limitations and future researches: Furthermore, suggestions for future research will be proposed:
1. Due to the time limitation, the sustainability risk management strategy was not deployed completely and its results were not analyzed. The future research will focus on deploy it and assess its outcomes and measure success rate.
2. Many studies have been done to combine MCDM approaches with the FMEA technique, and to overcome FMEA constraints, various techniques have been used, such as VIKOR, TOPSIS, ELECTERE, AHP, and so on. In this study, the combination of the VIKOR method with the FMEA technique was used because of the attractive features of the VIKOR method (ranking and selection from a set of alternatives in the presence of conflicting criteria and determining a compromise solution that could be accepted by decision makers). But it will be very attractive and suitable for future studies about this case, used to combine other MCDM approaches with the FMEA technique, and the results of each model are compared in terms of industry experts to the validity of each technique in this case to be determined.

7. REFERENCES

1. Esfandian. H., Goodarzian Urimi. M., Shokoohi Rad. A., "Risk Assessment of Gasoline Storage Unit of National Iranian Oil Product Distribution Company using PHAST Software", *International Journal of Engineering*, *Transactions A: Basics* Vol. 34, No. 04, (2021), 763-768, doi: 10.5829/IJE.2021.34.04A.02.

2. Goodarzian. F., Hosseini-Nasab. H., Fakhrzad. M. B., "A Multi-objective Sustainable Medicine Supply Chain Network Design using a Novel Hybrid Multi-Objective Metaheuristic Algorithm", *International Journal of Engineering, Transactions A: Basics* Vol. 33, No. 10, (2020) 1986-1995, doi: 10.5829/IJE.2020.33.10A.17.

3. Ebinger. F. Omondi. B., "Leveraging Digital Approaches for Transparency in Sustainable Supply Chains: A Conceptual Paper", *Sustainability,* Vol. 12, No. 12, (2020) 6129, doi: 10.3390/su12156129.

4. Mangla. S. K., Kumar. P., Barua. M. K., "Prioritizing the responses to manage risks in green supply chain: An Indian plastic manufacturer perspective" *Sustainable Production and Consumption*, Vol. 01, No, 03, (2015) 67-86, doi: 10.1016/j.spc.2015.05.002.

5. Stock. J. R., Boyer. S. L., "Developing a consensus definition of supply chain management: a qualitative study", *International Journal of Physical Distribution and Logistics Management*, Vol. 39, No. 8, (2009) 690-711, doi: 10.1108/09600030910996323.

6. Kaur. A., Sharma. P. C., "Social sustainability in supply chain decisions: Indian manufacturers. Environment", *development and Sustainability,* Vol. 20, No. 4, (2018) 1707-1721, doi: 10.1007/s10668-017-9961-5.

7. Nimsai. S., Yoopetch. C., Lai, P., "Mapping the Knowledge Base of Sustainable Supply Chain Management: A Bibliometric Literature Review", *Sustainability*, Vol. 12, No. 18, (2020) 7348, doi: 10.3390/su12187348.

8. Akbari-Kasgari. M., Khademi-Zare. H., Fakhrzad. M.B., M. Hajiaghaei-Keshteli. M., Honarvar. M., "A Closed-loop Supply Chain Network Design Problem in Copper Industry", *International Journal of Engineering, Transactions A: Basics* Vol. 33, No. 10, (2020) 2008-2015, doi: 10.5829/IJE.2020.33.10A.19.

9. Seuring. S. A., "Assessing the rigor of case study research in supply chain management", *Supply Chain Management: An International Journal*, Vol. 13, No. 2, (2008) 128-137, doi: 10.1108/13598540810860967.

10. Giannakis. M., Papadopoulos. T., "Supply chain sustainability: A risk management approach", *International Journal of Production Economics*, Vol. 171, No. 4, (2016) 455-470, doi: 10.1016/j.ijpe.2015.06.032.

11. Wang. Z., Sarkis. J., "Investigating the relationship of sustainable supply chain management with corporate financial performance", *International Journal of Productivity and Performance Management*, Vol. 62, No. 8, (2013) 871-888, doi: 10.1108/IJPPM-03-2013-0033.

12. Rezaei. S., Maihami. R, "Optimizing the sustainable decisions in a multi-echelon closed-loop supply chain of the manufacturing/remanufacturing products with a competitive environment. Environment", *Development and Sustainability*, Vol. 22, No 1, (2019) 1-27, doi: 10.1007/s10668-019-00491-5.

13. Gurnani. H., Ray. S., Wang. Y.," Special Issue of Production and Operations Management: Global Supply Chain Risk Management", *Production and Operations Management*, Vol. 20, No. 3, (2011) 489-489, doi: 10.1111/j.1937-5956.2011.01242.x.

14. Tang. O., Matsukawa. H., Nakashima. K., "Supply chain risk management", *International Journal of Production Economics*, Vol. 139, No.1, (2012) 1-2, doi: 10.1016/j.ijpe.2012.06.015.

15. Kakha. G., Tabasi. S., Jami. M., Danesh Narooei. D., "Evaluation of the impacting factors on sustainable mining development, using the Grey-DEMATEL approach", l*nternational Journal of Engineering*, *Transactions A: Basics* Vol. 32, No. 10, (2019) 1497-1505, doi: 10.5829/IJE.2019.32.10A.20.

16. Blackburn. W. R., "The sustainability handbook: The complete management guide to achieving social, economic, and environment", Routledge, London, (2008).

17. Anderson. D. R., "Corporate survival: The critical importance of sustainability risk management", Iuniverse Inc, (2005).

18. Business for social responsibility (BSR), "Perspectives on information management in sustainable supply chains", Available at http://www.bsr.org/reports/BSR_Info-Management-Supply-Chains1.pdf, (2007).

19. Chen. W. K., Nalluri. V., Ma. S., Lin. M., Lin. C. T., "An Exploration of the Critical Risk Factors in Sustainable Telecom Services: An Analysis of Indian Telecom Industries", *Sustainability*, Vol. 13, No. 2, (2021) 445, doi: 10.3390/su13020445.

20. MacMinn. R. D., "Value and risk", *Journal of Banking and Finance*, Vol. 26, No. 2, (2002) 297-301, doi: 10.1016/S0378-4266(01)00223-0.

21. Ravi Sankar. N., Prabhu. B.S., "Modified approach for prioritization of failures in a system failure mode and effects analysis", *International Journal of Quality & Reliability Management*, Vol. 18, No. 3, (2001) 324-336, doi: 10.1108/02656710110383737.

22. Sharma. R. K., Kumar. D., Kumar. P., "Systematic failure mode effect analysis (FMEA) using fuzzy linguistic modelling", *International Journal of Quality and Reliability Management*, Vol. 22, No. 9, (2005) 986-1004, doi: 10.1108/02656710510625248.

23. Chang. K. H., Cheng. C. H., "A risk assessment methodology using intuitionistic fuzzy set in FMEA", *International Journal of Systems Science*, Vol. 41, No. 12, (2010) 1457-1471, doi: 10.1080/00207720903353633.

24. Chin. K. S., Wang. Y. M., Poon. G. K. K., Yang. J. B., "Failure mode and effects analysis by data envelopment analysis", *Decision Support Systems*, Vol. 48, No. 1, (2009) 246-256, doi: 10.1016/j.dss.2009.08.005.

25. Hadi-Vencheh. A., Aghajan. M., "Failure mode and effects analysis: A fuzzy group MCDM approach", *Journal of Soft Computing and Applications*, Vol. 1, No. 14, (2013), doi: 10.5899/2013/jsca-00016.

26. Liu. H. C., You. J. X., You. X. Y., Shan. M. M., "A novel approach for failure mode and effects analysis using combination weighting and fuzzy VIKOR method", *Applied Soft Computing*, Vol. 28, No. C, (2015) 579-588, doi: 10.1016/j.asoc.2014.11.036.

27. Lolli. F., Ishizaka. A., Gamberini. R., Rimini. B., Messori. M., "FlowSort-GDSS–A novel group multi-criteria decision support system for sorting problems with application to FMEA", *Expert Systems with Applications*, Vol. 42, No. 17, (2015) 6342-6349, doi: 10.1016/j.eswa.2015.04.028.

28. Song. W., Ming. X., Wu. Z., Zhu. B., "A rough TOPSIS approach for failure mode and effects analysis in uncertain environments", *Quality and Reliability Engineering International*, Vol. 30, No. 4, (2014) 473-486, doi: doi.org/10.1002/qre.1500.

29. Arabzad. S. M., Razmi. J., Ghorbani. M., "Classify purchasing items based on risk and profitability attributes; using MCDM and FMEA techniques", *Research Journal of International Studies*, Vol. 1, No. 21, (2011) 80-85, doi: 10.13140/2.1.3457.0882.

30. Vahdani. B., Salimi. M., Charkhchian. M.," A new FMEA method by integrating fuzzy belief structure and TOPSIS to improve risk evaluation process", *The International Journal of Advanced Manufacturing Technology*, Vol. 77, No. 1, (2015) 357-368, doi: 10.1007/s00170-014-6466-3.

31. Sanayei. A., Mousavi. S. F., Yazdankhah. A., "Group decision making process for supplier selection with VIKOR under fuzzy

environment", **Expert Systems with Applications**, Vol. 37, No. 1, (2010) 24-30, doi: 10.1016/j.eswa.2009.04.063.

32. Yücenur. G. N., Demirel. N. Ç., "Group decision making process for insurance company selection problem with extended VIKOR method under fuzzy environment", **Expert Systems with Applications**, Vol. 39, No. 3, (2012) 3702-3707, doi: 10.1016/j.eswa.2011.09.065.

33. Girubha. R. J., Vinodh. S., "Application of fuzzy VIKOR and environmental impact analysis for material selection of an automotive component", **Materials and Design**, Vol.37, (2012) 478-486, doi: 10.1016/j.matdes.2012.01.022.

34. Hsu. C. H., Wang. F. K., Tzeng. G. H., "The best vendor selection for conducting the recycled material based on a hybrid MCDM model combining DANP with VIKOR", **Resources conservation and recycling**, Vol. 66, (2012) 95-111, doi: 10.1016/j.resconrec.2012.02.009.

35. Wu. H. Y., Chen. J. K., Chen. I. S., Zhuo. H. H., "Ranking universities based on performance evaluation by a hybrid MCDM model", **Measurement**, Vol. 45, No. 5, 856-880, doi: 10.1016/j.measurement.2012.02.009.

36. You. X. Y., You. J. X., Liu. H. C., Zhen. L., "Group multi-criteria supplier selection using an extended VIKOR method with interval 2-tuple linguistic information", **Expert Systems with Applications**, Vol. 42, No. 4, (2015) 1906-1916, doi: 10.1016/j.eswa.2014.10.004.

37. Tavana. M., Mavi, R. K., Santos-Arteaga. F. J., Doust. E. R., "An extended VIKOR method using stochastic data and subjective judgments", **Computers & Industrial Engineering**, Vol. 97, (2016) 240-247, doi: 10.1016/j.cie.2016.05.013.

38. Dong. J. Y., Yuan, F. F., Wan. S. P.,"Extended VIKOR method for multiple criteria decision-making with linguistic hesitant fuzzy information", **Computers & Industrial Engineering**, Vol. 112, (2017) 305-319, doi: 10.1016/j.cie.2017.07.025.

39. Liu. H. C., Liu. L., Lin. Q. L., "Fuzzy failure mode and effects analysis using fuzzy evidential reasoning and belief rule-based methodology", **IEEE Transactions on Reliability**, Vol. 62, No. 1, (2013) 23-36, doi: 10.1109/TR.2013.2241251.

40. Liu. H. C., You. J. X., Ding. X. F., Su. Q., "Improving risk evaluation in FMEA with a hybrid multiple criteria decision-making method", **International Journal of Quality and Reliability Management**, Vol. 32, No. 7, (2015) 763-782, doi: 10.1108/IJQRM-10-2013-0169.

41. Hajiagha. S. H. R., Hashemi. S. S., Mohammadi. Y., Zavadskas. E. K., "Fuzzy belief structure based VIKOR method: an application for ranking delay causes of Tehran metro system by FMEA criteria", **Transport**, Vol. 31, No. 1, (2016) 108-118, doi: 10.3846/16484142.2016.1133454.

42. Wang. L. E., Liu. H. C., Quan. M. Y., "Evaluating the risk of failure modes with a hybrid MCDM model under interval-valued intuitionistic fuzzy environments", **Computers & Industrial Engineering**, Vol. 102, (2016) 175-185, doi: 10.1016/j.cie.2016.11.003.

43. Liu. H. C., You. J. X., You. X. Y., "Evaluating the risk of healthcare failure modes using interval 2-tuple hybrid weighted distance measure", **Computers & Industrial Engineering**, Vol. 78, (2014) 249-258, doi: 10.1016/j.cie.2014.07.018.

44. Safari H., Faraji, Z., Majidian. S., "Identifying and evaluating enterprise architecture risks using FMEA and fuzzy VIKOR", **Journal of Intelligent Manufacturing**, Vol. 27, No. 2, (2016) 475-486, doi: 10.1007/s10845-014-0880-0.

45. Chin. K. S., Chan. A., Yang, J. B., "Development of a fuzzy FMEA based product design system", **The International Journal of Advanced Manufacturing Technology**, Vol. 36, No. 7, (2008) 633-649, 10.1007/s00170-006-0898-3.

46. Rezaee. M. J., Salimi. A., Yousefi. S., "Identifying and managing failures in stone processing industry using cost-based FMEA", **The International Journal of Advanced Manufacturing Technology**, Vol. 88, No. 9, (2017) 3329-3342, doi: 10.1007/s00170-016-9019-0.

47. Chin. K. S., Wang. Y. M., Poon. G. K. K., Yang. J. B., "Failure mode and effects analysis using a group-based evidential reasoning approach", **Computers and Operations Research**, Vol. 36, No. 6, (2009) 1768-1779, doi: 10.1016/j.cor.2008.05.002.

48. Lillie. E., Sandborn. P., Humphrey. D., "Assessing the value of a lead-free solder control plan using cost-based FMEA", **Microelectronics Reliability**, Vol. 55, No. 6, (2015) 969-979, doi: 10.1016/j.microrel.2015.02.022.

49. Ekmekçioğlu. M., Can Kutlu. A., "A fuzzy hybrid approach for fuzzy process FMEA: An application to a spindle manufacturing process", **International Journal of Computational Intelligence Systems**, Vol. 5, No. 4, (2012) 611-626, doi: 10.1080/18756891.2012.718104.

50. Valinejad. F., Rahmani. D., "Sustainability risk management in the supply chain of telecommunication companies: A case study", **Journal of Cleaner Production**, (2018), 203, 53-67, doi: 10.1016/j.jclepro.2018.08.174.

Appendix:

TABLE A1. Qualitative rating of fifteen critical risks and qualitative weight of six risk factors.

DM1	C_j	C_1	C_2	C_3	C_4	C_5	C_6	DM2	C_j	C_1	C_2	C_3	C_4	C_5	C_6
	Wj	**H**	**H**	**MH**	**M**	**M**	**ML**		**Wj**	**VH**	**H**	**MH**	**MH**	**M**	**M**
	HR1	H	H	H	VH	MH	VH		HR1	H	MH	H	H	MH	MH
	HR2	M	M	M	L	ML	L		HR2	M	ML	M	ML	L	L
	HR3	H	H	H	M	M	H		HR3	MH	H	H	H	M	H
	HR4	MH	H	H	M	ML	M		HR4	H	H	MH	M	H	M
	HR5	M	M	MH	M	L	L		HR5	MH	M	MH	M	ML	L
	HR6	H	H	M	M	M	L		HR6	H	H	H	M	M	M
	HR7	M	M	H	M	ML	L		HR7	ML	M	MH	ML	ML	L
	HR8	H	MH	H	H	H	M		HR8	H	M	H	MH	MH	ML
	HR9	M	M	VH	H	H	MH		HR9	H	M	VH	H	H	H

	HR10	H	H	VH	H	MH	M		HR10	MH	H	MH	MH	H	M
	HR11	H	H	H	H	VH	H		HR11	VH	H	H	H	VH	H
	HR12	M	H	VH	H	H	M		HR12	M	MH	H	MH	H	M
	HR13	ML	M	M	M	L	ML		HR13	M	L	M	M	L	M
	HR14	M	M	H	M	M	ML		HR14	M	ML	M	M	ML	M
	HR15	H	H	MH	H	M	ML		HR15	M	H	MH	H	M	M

DM3	C_j	C_1	C_2	C_3	C_4	C_5	C_6	DM4	C_j	C_1	C_2	C_3	C_4	C_5	C_6
	W_j	VH	MH	H	H	MH	MH		W_j	H	MH	M	M	ML	L
	HR1	VH	H	H	VH	H	H		HR1	H	MH	MH	M	M	ML
	HR2	MH	ML	ML	ML	L	L		HR2	H	VH	H	H	MH	MH
	HR3	H	H	MH	MH	H	MH		HR3	H	VH	H	H	MH	M
	HR4	MH	MH	MH	ML	H	H		HR4	M	M	MH	M	M	M
	HR5	MH	MH	MH	ML	ML	L		HR5	VH	VH	M	M	M	M
	HR6	H	H	M	MH	M	M		HR6	MH	MH	MH	M	M	M
	HR7	M	M	MH	M	M	M		HR7	H	VH	MH	H	MH	M
	HR8	MH	MH	H	H	MH	H		HR8	H	H	VH	H	VH	H
	HR9	H	MH	MH	MH	H	H		HR9	VH	MH	VH	MH	MH	MH
	HR10	MH	MH	MH	MH	MH	MH		HR10	VH	MH	MH	VH	VH	MH
	HR11	VH	H	H	VH	VH	H		HR11	H	H	VH	H	H	MH
	HR12	MH	MH	MH	MH	MH	M		HR12	M	M	ML	M	ML	ML
	HR13	ML	L	ML	ML	M	ML		HR13	MH	M	MH	M	M	M
	HR14	M	MH	M	M	MH	M		HR14	H	H	MH	MH	MH	M
	HR15	H	H	MH	H	MH	M		HR15	VH	VH	VH	VH	H	VH

TABLE A2. Aggregated fuzzy rating of fifteen critical risks and aggregated fuzzy weight of six risk factors

C_j	C_1	C_2	C_3	C_4	C_5	C_6
W_j	(0.7,0.4,0.45,0.8)	(0.7,0.4,0.45,0.8)	(0.7,0.4,0.45,0.8)	(0.7,0.4,0.45,0.8)	(0.7,0.4,0.45,0.8)	(0.7,0.4,0.45,0.8)
HR1	(.7, .825, .85, 1)	(.5, .7, .75, .9)	(.5, .75, .775, .9)	(.4, .775, .825, 1)	(.4, .625, .675, .9)	(.2, .65, .725, .9)
HR2	(.4, .6, .625, .9)	(.2, .575, .575, 1)	(.2, .525, .55, .9)	(.1, .4, .45, .9)	(.1, .325, .375, .8)	(.1, .03, .325, .8)
HR3	(.5, .75, .75, .9)	(.7, .825, .85, 1)	(.5, .75, .775, .9)	(.4, .675, .7, .9)	(.4, .6, .625, .9)	(.4, .675, .7, .9)
HR4	(.4, .625, .675, .9)	(.4, .675, .7, .9)	(.5, .65, .725, .9)	(.2, .45, .475, .6)	(.2, .6, .625, .9)	(.4, .575, .575, .9)
HR5	(.4, .65, .725, 1)	(.4, .625, .675, 1)	(.4, .575, .65, .8)	(.2, .45, .475, .6)	(.1, .325, .375, .6)	(.1, .275, .275, .6)
HR6	(.5, .75, .775,.9)	(.5, .75, .775, .9)	(.4, .6, .625, .9)	(.4, .525, .55, .8)	(.4, .5, .5, .6)	(.1, .425, .425, .6)
HR7	(.2, .525, .55, .9)	(.4, .6, .625, 1)	(.5, .65, .725, .9)	(.2, .525, .55, .9)	(.2, .425, .5, .8)	(.1, .35, .35, .6)
HR8	(.5, .75, .775, .9)	(.4, .625, .675, .9)	(.7, .825, .85, .1)	(.5, .75, .775, .9)	(.5, .725, .8, 1)	(.2, .6, .625, .9)
HR9	(.4, .75, .775, 1)	(.4, .4, .6, .8)	(.5, .825, .925, 1)	(.5, .7, .75, .9)	(.5, .75, .775, .9)	(.5, .7, .725, .9)
HR10	(.5, .725, .8, 1)	(.5, .7, .75, .9)	(.5, .675, .775, 1)	(.5, .5, .8, 1)	(.5, .5, .8, 1)	(.4, .55, .6, .8)
HR11	(.7, .85, .9, 1)	(.7, .8, .8, .9)	(.7, .7, .85, 1)	(.7, .825, .85, .1)	(.7, .875, .95, 1)	(.5, .75, .775, .9)
HR12	(.4, .525, .55, .8)	(.4, .625, .675, .9)	(.2, .65, .725, 1)	(.4, .625, .675, .9)	(.2, .625, .675, .9)	(.2, .45, .475, .6)
HR13	(.2, .425, .5, .8)	(.1, .35, .35, .6)	(.2, .475, .525, .8)	(.2, .45, .475, .6)	(.1, .35, .35, .6)	(.2, .4, .45, .6)
HR14	(.4, .575, .575, .09)	(.2, .55, .6, .9)	(.4, .6, .625,0 .9)	(.4, .525, .55, .8)	(.2, .5, .0575, .08)	(.2, .45, .475, .6)
HR15	(.4, .75, .775, 1)	(.7, .825, .85, 1)	(.5, .675, .775, 1)	(.7, .825, .85, .1)	(.4, .6, .6, .9)	(.2, .55, .6, 1)

TABLE A3. Crisp rating of fifteen critical risks and Crisp weight of six risk factors.

C_j	C_1	C_2	C_3	C_4	C_5	C_6
Wj	0.8625	0.775	0.65	0.63125	0.5	0.5875
HR1	0.84375	0.7125	0.73125	0.75	0.65	0.61875
HR2	0.63125	0.5875	0.54375	0.4625	0.4	0.38125
HR3	0.725	0.84375	0.73125	0.66875	0.63125	0.66875
HR4	0.65	0.66875	0.69375	0.43125	0.58125	0.6125
HR5	0.69375	0.675	0.60625	0.43125	0.35	0.3125
HR6	0.73125	0.73125	0.63125	0.56875	0.5	0.3875
HR7	0.54375	0.65625	0.69375	0.54375	0.48125	0.35
HR8	0.73125	0.65	0.84375	0.73125	0.75625	0.58125
HR9	0.73125	0.55	0.8125	0.7125	0.73125	0.70625
HR10	0.75625	0.7125	0.7375	0.7	0.7	0.5875
HR11	0.8625	0.8	0.8125	0.84375	0.88125	0.73125
HR12	0.56875	0.65	0.64375	0.65	0.6	0.43125
HR13	0.48125	0.35	0.5	0.43125	0.35	0.4125
HR14	0.6125	0.5625	0.63125	0.56875	0.51875	0.43125
HR15	0.73125	0.84375	0.7375	0.84375	0.625	0.5875

TABLE A4. The result of propose method

Group	Rank	Description of the risk	Root factors	Potential consequences	Strategy	Performance
O.T	1	Inefficient management and lack of strategic management system	The lack of a strategic management system	Lack of successful provision and implementation of strategic and tactical plans	Avoid	Design and implement effective strategic management
E.I	2	Problems against the privatization of the industry	Anti-privatization approach and regulations	Inability of the organizations to use all of the internal and external capacities	Reduce	Interaction and conversation with the lawmakers The creation of mechanisms to make the supply chain flexible with regulations
E.Ec	3	The impact of currency fluctuations on contracts and projects	Domestic and foreign economic and political changes	Impose additional costs on contracts and irregularities in paying and receiving the receivables	Reduce	Long-term planning in network development, which leads to time estimation and the currency of buying facilities. Providing facilities through trading card
S.T	4	Deviation from the provision time of goods and services (customs problems, lack of transfer of equipment and services on due time, lack of on time delivery of outsourcing software by the contractors, etc.)	Restrictions caused by the sanctions, custom rules and lack of proper interaction with the contractors	Loss of proper opportunity to provide services to subscribers	Reduce	A true estimation and long-term planning to relatively control and overcome predicted problems Conversation and interaction with domestic and foreign suppliers
C.Ec	5	The high sensitivity of consumers to the price of products according to the competitiveness of industry and disloyalty	Competitiveness of industry and disloyalty of customers	High probability of declining market share	Reduce	Increasing customer loyalty and belonging of the subscribers to an organization's brand by creating key competitive benefits and mechanisms such as the formation of customers' club

E.I	6	Political changes and instability in macro decisions	Political changes	Irregularities in the rules imposed on the organization and supply chain	Accept	Interaction and conversation with the lawmakers - The creation of mechanisms to make the supply chain flexible with regulations
S.T	7	Inadequacy of existing infrastructures to provide services (failing to provide the required bandwidth)	Low quality of infrastructures	Inability to provide high quality service and desired quantity to subscribers	Accept	Planning to invest in higher-quality infrastructure
S.I	8	Products and exclusive services of suppliers and the higher bargaining ability of the origin company due to the provision of exclusive services	Providing exclusive services due to the integration of broadband	Reducing the ability to bargain and increasing vulnerability of the organization	Reduce	Interaction with the origin company with the accompaniment of all companies present in the industry
S.T	9	Low capacity for the development in telecommunication centers	Exclusiveness of the available capacity by the origin company	Reducing market share	Accept	Planning to invest in centers with greater capacity
S.Ec	10	The costs of licensing and inappropriate tariffs and multiple penalties	Rules and numerous restrictions of the origin company to provide exclusive services	Imposing heavy costs to the organization	Reduce	Strict compliance of requirements and legislation Interacting with origin to meet the needs of the organizations
S.Ec	11	Higher cost of providing the exclusive bandwidth of the origin company	Exclusiveness of bandwidth by the origin company	Imposing heavy costs to the organization	Reduce	Interaction with origin company with the accompaniment of all companies present in the industry to reduce the cost of broadband
O.S	12	Problems in capabilities of human resources (Lack of motivation, lack of job satisfaction, lack of creativity and accountability, problems in work ethics and competition culture)	Problems of individuals and organizations and society	Reducing the efficiency of human force and increased absenteeism and leave of the organization	Avoid	Efforts in providing facilities and creating motivating incentives to increase creativity and involvement of employees
S.I	13	Disapproval or delay in approving the requested licenses by the origin company (intensive bureaucracy)	Intensive bureaucracy	Loss of opportunity to provide services to subscribers	Reduce	Interaction with the origin company with the accompaniment of all companies present in the industry
E.I	14	Continuation and intensification of sanctions	Problems in international relations and foreign policies	Increased economic and technological vulnerability of the organization and supply chain	Reduce	-Relying on domestic capabilities and capacities -Providing through foreign trade intermediaries -Making contracts with new supply sources of original equipment
S.T	15	Scientific dependence of the company due to problems for production, transfer and knowledge registration for the company	The lack of contractor's tendency to produce, transfer and knowledge registration for the company	Increasing technological vulnerability of the organization	Avoid	Including the act of registering and transferring knowledge in the contracts

---

Persian Abstract

چکیده

پایداری مدیریت ریسک زنجیره تامین، یکی از اصلی ترین مزیت های رقابتی برای هر سازمان بصورت پایدار است. چندین مدل در ادبیات تحقیق برای مدیریت ریسک های پایداری زنجیره تامین وجود دارد. با توجه به اینکه ریسک های بحرانی بیشترین تأثیر و سهم را از منابع مدیریت ریسک دارند، باید با استفاده از تکنیک های خاص شناسایی گردند تا مدیریت ریسک دقیق تر و قابل اطمینان تر شود. در این مقاله، یک مدل سه فازی جدید برای مدیریت ریسک های پایداری زنجیره تامین ارائه شده است. این مدل شامل فاز تحلیل حالت شکست و اثرات برای شناسایی و ارزیابی تمامی ریسک‌ها و طبقه‌بندی آنها، مرحله VIKOR فازی برای رتبه‌بندی ریسک‌های بحرانی و فاز مدیریت برای مقابله با ریسک‌های بحرانی است. طبقه‌بندی ریسک‌ها بر اساس یک رویکرد پنج بعدی جدید برای پیشرفت پایدار، شامل جنبه‌های زیست‌محیطی، اقتصادی، اجتماعی، فنی و سازمانی در بخش‌های مختلف زنجیره تامین انجام شد. صنعت مخابرات ایران برای نشان دادن عملکرد مدل در نظر گرفته شده است. نتایج نشان داد که در نظر گرفتن مرحله VIKOR فازی برای ارزیابی دقیق ریسک‌های بحرانی ضروری است، زیرا اولویت ریسک‌های بحرانی به‌دلیل کاستی‌های این روش و ایجاد خطا از طریق تحلیل حالت شکست و اثرات به درستی شناسایی نمی‌شود. همچنین مشخص شد که ریسک های فنی آغاز شده توسط سازمان خطرناک ترین خطری است که پایداری زنجیره تامین را تهدید می کند.

International Journal of Engineering

A Study of Load Demand Forecasting Models in Electricity using Artificial Neural Networks and Fuzzy Logic Model

B. R. K. Al-ani*[a], E. T. Erkan[b]

[a] Graduate School of Natural and Applied Sciences, Atilim University, Ankara, Turkey
[b] Department of Industrial Engineering, Atilim University, Turkey

A B S T R A C T

Since load time series are very changeable, demand forecasting of the short-term load is challenging based on hourly, daily, weekly, and monthly load forecast demand. As a result, the Turkish Electricity Transmission Company (TEA) load forecasting is proposed in this paper using artificial neural networks (ANN) and fuzzy logic (FL). Load forecasting enables utilities to purchase and generate electricity, load shift, and build infrastructure. A load forecast was classified into three sorts (hourly, weekly and monthly). Over time, forecasting power loads with artificial neural networks and fuzzy logic reveals a massive decrease in ANN and a progressive increase in FL from 24 to 168 hours. As illustrated, fuzzy logic and artificial neural networks outperform regression algorithms. This study has the highest growth and means absolute percentage error (MAPE) rates compared to FL and ANN. Although regression has the highest prediction growth rate, it is less precise than FL and ANN due to their lower MAPE percentage. Artificial Neural Networks and Fuzzy Logic are emerging technologies capable of forecasting and mitigating demand volatility. Future research can forecast various Turkish states using the same approach.

doi: 10.5829/ije.2022.35.06c.02

1. INTRODUCTION

Turkish Electricity Transmission Company (TEİAŞ) is responsible for power production, transmission and distribution to its users throughout Turkish. TEİAŞ provide electricity load for all residents in Turkey with constant, consistent and cost-effective electricity transport while keeping environmentally sensitive and supporting efficient resource use proudly and effectively [1]. The main objective of the demand support model forecasting is to decide whether a demanding series requires applying a classification model, a statistical or judgmental approach for forecasting demand [2]. The products are first classified according to their product life cycle status.

The classifications in the stage of the launch increase [3]; these grades have no representative historical demand data that is required for statistical estimates [4].

To create a classification model for forecasting mature goods, we use the findings of the first question of the study. The main benefit of the forecast is that it offers valuable knowledge to different stakeholders used to make future decisions—the art of estimating in a far future while anticipating/projecting for short periods [5]. The end cannot be forecast correctly. Mistakes marginalize the future forecast. Particularly when forecasting, there is a marginal error; which is widened.

Senthil Kumar et al. [6] developed net energy using Artificial neural networks (ANN) equations to calculate potential energy consumption levels in Turkey using an artificial nerve network technique. Hasheminia and Niaki [7] defined and implemented a new artificial wave forecasting network, a recurrent network with an updated algorithm. Yama and Lineberry [8] have presented an intelligent hybrid system that combines autoregressive built-in average moving models and ANN for demand

Corresponding Author's Email: barqalani@hotmail.com (B. R. K. Al-ani)

forecasting. Scholars examined the application of advanced machinery training techniques, including neural networks, new neuro networks and super-port vector machines, to forecast distorted demand at the end of the supply chain. Sharma [9] used fuzzy neural networks (FNN) with initial weights created by a genetic algorithm to learn fuzzy rules for promotion obtained by marketing experts. Mounce et al. [10] updated the changing FNN and took a weighted factor in determining the value of each element between these various rules. Also, Pezeshki and Mazinani [11] had an intelligent Fuzzy neural forecasting decision support system available.

Demand forecasting of electric loads is essential to assist power companies to plan and managing efficiently. The precise short-term load forecast is challenging since the load time series has high uncertainty levels [12]. Depending on the horizon to be considered, electricity load forecasts are classed into long-term and short-term [13]. Forecasts for short-term load cover hourly, every day, weekly and monthly forecasts; they are thoroughly covered in literature and covered in many publications. Several research papers have been produced to apply Artificial Neural Networks (ANN). Yao et al. [14] utilized a heterogeneous ANN for load prediction in the short-term forecast challenge. They also discussed the uses of minimum historical evidence to determine neural weights. Aksoy et al. [15] employed the ANN to anticipate the hourly temperatures for electricity utilities. The ANN for forecasting has also been described in the Greek power system.

Due to the complexity of the market, load forecasting in the electrical market is difficult. The instant nature of power, the complicated design of the market and frequent regulatory interventions make this complex. Artificial intelligence is a relatively recent research topic that grows in quality [16]. Computer intelligence is commonly used to refer to fuzzy parts of the system, swarm intelligence, progressive computer systems and artificial neural networks [12]. One of the area's most often employed in electricity prediction is ANNs. Artificial neural networks have gained greater attention because of their evident design, straightforward execution, and good performance [17].

Following the research in demand forecasting, several contributions address the impact of ANN and FL on short-term load forecasting, which aid the impact, benefits, and prospects (see Table 1). As a result, this study substantially contributes by anticipating demand using artificial neural networks and fuzzy logic approaches and comparing them to conventional methods. In addition, the study is made by the valuable techniques of Artificial Neural Network algorithms for forecasting demand. Since they can handle non-linear data and capture subtle functional correlations between empirical data, even when the underlying relationships are unknown or difficult to express, applying fuzzy logic

TABLE 1. Comparison of Contribution

Previous studies	Present study
Previous studies addressed the impact, challenges, and importance of ANN and FL on short-term forecasting [18-23].	This study substantially contributes by anticipating demand using artificial neural networks and fuzzy logic approaches and comparing them to conventional methods. In addition, the study is made by the valuable techniques of Artificial Neural Network algorithms for forecasting demand. Also, the MAPE indicated that ANN and FL are accurate and consistent compared to the regression method. This study showed that ANN and FL have a minimal error percentage compared to the regression analysis.

and artificial neural networks in demand forecasting will overcome many constraints encountered in the workplace. Also, the MAPE indicated that ANN and FL are accurate and consistent compared to the regression method. This study showed that ANN and FL have a minimal error percentage compared to the regression analysis. Therefore, demand forecasting of load using artificial neural network (ANN) and fuzzy logic (FL) from the Turkish Electricity load is proposed in this study.

In general, both methods and procedures are critical for accurate estimation; yet, there is a dearth of research on load forecasting methodologies. The study is classified into five broad categories based on requirements from the journal. The paper is structured as follows. Section 1, the background of the study. Section 2, the methodology of the research paper. Section 3 presented the data analysis, while section 4 presented the interpretation of the data and general discussion. The final section presented the conclusion and recommendation of the research paper.

2. METHODOLOGY

2. 1. Data Collection and Pre-processing Collecting data is the first step in creating a forecast. The amount of data necessary varies depending on the complexity of the underlying function that we are trying to approximate. The number of neurons in the neural network directly impacts the choice of the data set. A neural network is trained using pre-processed data to make forecasting easier. It is possible to perform data pre-processing, such as normalization, non-linear transformations and feature extraction.

Normalization is the first and most crucial stage in pre-processing of data. As a result, the neural network will be better able to retrieve meaningful information during training. For the most part, there are two ways to normalize data. Standardize the data to fall into a standard range - usually harmful to positive.

2. 2. Simulation of Real-Time Forecasts
Although in actuality, these variables might be dependent on forecasts, actual weather data collected at the Fort Collins Weather Station [24] for the test day is utilized to model weather-related variables in the network. Regarding weather-predicting accuracy, [24] suggests that further research in this area may be warranted.

2. 3. Artificial Neural Network   Artificial neural network undertakes calculations to replicate the learning processes of the human brain, which consists of a parallel-distributed structure of neurons that uses the gained knowledge to match inputs to outputs and make the "map" of the inputs to outputs available for usage. They are modelled after their namesakes in the brain and built to allow them to be adaptable [24]. An incomplete understanding of the brain's mechanism of neural information processing led to a variety of ANN models. An overview of ANN models for time-series forecasting is provided in the next section.

As one of the most often used ANN architectures for prediction algorithms, the multilayer perceptron (MLP) is renowned for its ability to adapt to complicated patterns [24]. Layers in MLPs comprise three layers: an input or input-output-output layer.

2. 4. The Fuzzy Logic Systems   Weekday and weekend parameters of both fuzzy logic systems were intended to be identical [25]. The fuzzy logic system's input and output sets used symmetrical Gaussian distributed membership functions, with variables and parameterized throughout the evolutionary algorithm parameterization loop [26]. There are no discontinuous spots in the Gaussian distribution where the optimization may fail [24].

2. 5. Mean Absolute Percentage Error (MAPE)
Error metrics explain that the gap between actual and expected values is successful if the model's performance is measured in terms of the difference between the actual and anticipated values. Due to the magnitude of this quantity's impact on model performance and dependability, forecasting's primary objective is to minimize it. Some error measures can be used to evaluate the model's performance. The MAPE error is the most frequently encountered among neural network researchers [12]. There are 24 forecast points in this example, and n is the number of forecast points. Calculating the most significant error across 24 hours also allows it to determine the amount of energy consumed during that period as represented by the area spanned by the load profile curve and the forecasting accuracy, referred to as the "magnitude of peak hour [24].

2. 6. Forecasting Load   In order to calculate the projected load profile, the ANN calculates the average of three load profiles. When the weights are initialized, this is done to reduce the random effects of the initialization. They are 24-hour periods with no precedent in the network, meaning that the network has never been exposed to a day like a forecast. The training and validation data sets are based on the data before the forecasting date [24].

3. SIMULATION RESULTS

The above Figure 1 shows the prediction of electricity loads using artificial neural networks and fuzzy logic at various hours, and we can see a sharp decline for ANN and an abrupt decline for FL from the 24 hours to 168 hours' horizon. The above analysis compares artificial neural networks (ANN) and fuzzy logic (FL) at various week hours. We can see that both ANN and FL show a better forecast.

The above Figure 2 reveals that regression shows a higher growth in electricity load prediction than FL and ANN from the first week of the Year, Sunday to Saturday. The electricity load consumption in Figure 2 was based daily for domestic, commercial, or industrial.
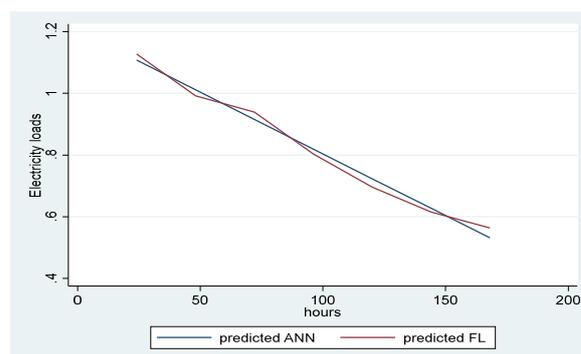

**Figure 1.** Load forecast demand using artificial neural network (ANN), fuzzy logic (FL)
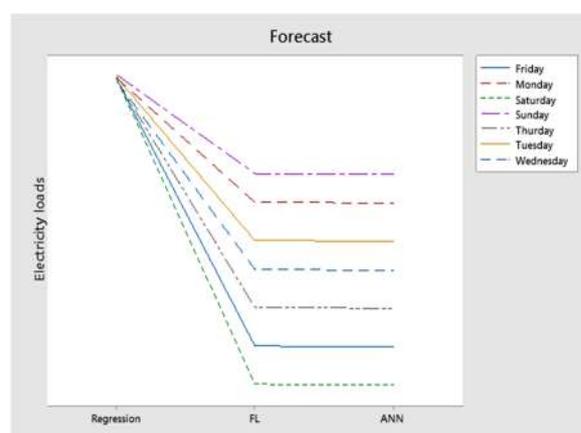
Figure 2. Comparison of Load forecast demand for the first week of the Year using artificial neural network (ANN), fuzzy logic (FL) and Multiple Linear Regression

The domestic is a people dwelling place. Commercial consumers are businesses and industries that require a more considerable volume of supplies than residential clients do. The load, however, are predicted by residential vs commercial, with the latter being the more prevalent.

Figure 3 illustrate significant discrepancies between the three models. As shown from Figure 3, fuzzy logic and ANN approaches are more accurate and dependable than regression methods. According to statistical, qualitative characteristics such as MAPE, Figure 3 indicated that ANN and FL model were more potent than the regression model in predicting load. Compared to the MLR model, the selected ANN and FL model could predict load for training, validation, and testing stages with a per cent gain in R^2. Additionally, the ANN and FL model is clearly defined compared to the MLR model by considering the relatively similar values of statistical parameters such as the median or similar distribution for the actual values (Figure 3). Additionally, a graphical representation of the actual values by the ANN, FL and MLR models shown on a graph (Figure 3) can aid in predicting load.

A short-term load forecasting model for consumption was built using ANN and FL and then compared with regression (Figure 4). The study forecasted Turkey's electricity consumption using ANN and FL techniques; regression has the highest growth (Figure 4). This figure illustrates how an ANN and FL model improved short-term electrical load predictions. The suggested ensemble technique has lower variance and bias than regression. According to the findings, the regression shows the highest growth compared to FL and ANN in Figure 4.

The above, Figure 5 shows the forecast with FL and ANN with Regression as a standard method, and this indicates that regression has the highest growth and highest mean absolute percentage error (MAPE) compared to FL and ANN. Although we can see that regression has the highest forecast growth but has lower precision
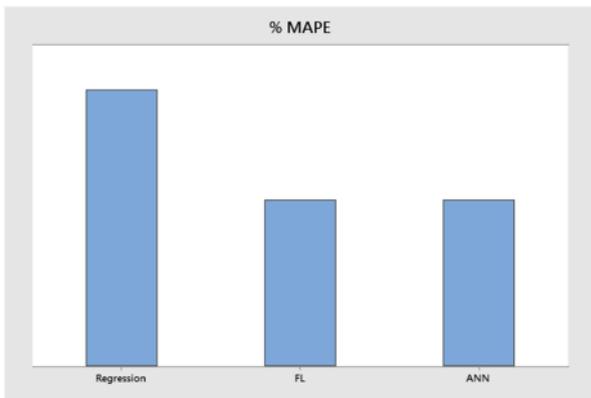
Figure 3. Comparison of MAPE (%) Load forecast demand using artificial neural network (ANN), Fuzzy Logic (FL) and Multiple Linear Regression
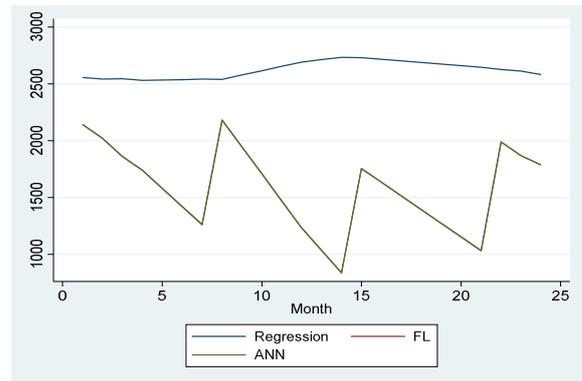
Figure 4. Comparison of Load forecast demand for months using artificial neural network (ANN), Fuzzy Logic (FL) and Multiple Linear Regression
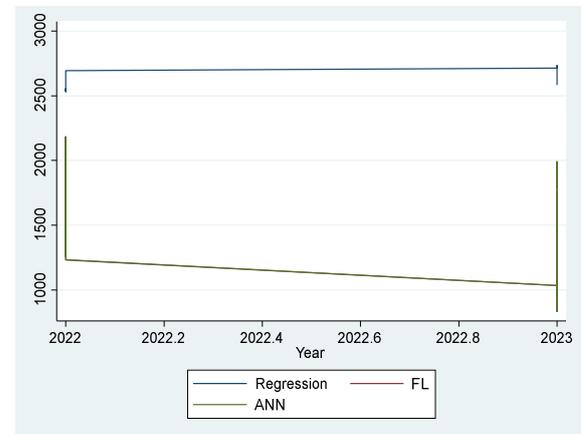
Figure 5. Comparison of Load forecast demand for months using artificial neural network (ANN), Fuzzy Logic (FL) and Multiple Linear Regression

compared to FL and ANN, both FL and ANN models keep lower MAPE per cent.

Recent years have seen a surge in interest in short-term power load forecasting, and the literature has numerous intriguing examples. Accurate load forecasting is critical for both power plants and manufacturing operations. Exogenous variables like weather, consumption time, day type, seasonal effects, and economic or political changes substantially affect the load consumption pattern. These methods have been modified to provide more precise approximations, necessitating the employment of a variety of methodologies.

The figures illustrate that non-linear linkages between input variables and load may impair ANN, FL, and MLR models. A comparison of ANN, FL, and MLR models demonstrated the critical importance of selecting the appropriate model to forecast load. ANN-based load forecasting can be enhanced on the Turkish market by using a more extensive training dataset and more detailed feature sets. The most critical aspect of developing an

effective system for anticipating electric load is selecting the appropriate input parameters. We studied the effect of these variables on the test subjects' performance. We studied the effects of these factors on the performance of load forecasting using ANN and FL then compared the results to those obtained using Regression analysis. The Turkish market's hourly load data are derived from EPIAS. We computed hourly lagged load statistics using this data, including the previous hour's load, the load at the same hour the previous day, the same hour the previous week, and the average load for the last 24 hours. As the air temperature rises, the load increases to levels more significant than those experienced during the coldest temperatures. We evaluated the accuracy of our power load forecasting models using data from the deregulated Turkish market [27].

Fuzzy logic and artificial intelligence optimization techniques and approaches are extensively applied [18, 20, 21, 28, 29]. These fuzzy models have been enhanced and adjusted here with the assistance of specialists. The specialists directly impacted the system's ability to succeed due to their skill and breadth of knowledge. The knowledge base, ruleset, and rule count all develop in lockstep with the size of the input variable and membership function. As a result, the fuzzy model must be modified regardless of whether classical or artificial intelligence approaches are utilized [26].

This paper constructs a short ANN, FL, and Regression load predictors model. The first two forecasts and ANN and FL were done, while the second part compared ANN and FL with Regression. The performance may be improved by more intricate structures, such as the combination structure presented by Emeç and Akkaya [30].

In Turkey, electricity is generated by fossil fuel-fired power stations that rely heavily on natural gas. Turkey is forced to import petroleum and natural gas due to domestic resources. This reliance on imported energy directly affects power generation. Forecasting future electricity use is a significant issue in Turkey regarding planning electricity generation. Incorrect prediction of electricity usage will result in either a power shortfall or an oversupply of electricity. A power deficit will result in unhappiness and disharmony in the household and industrial sectors. The economy will suffer adversely due to the industrial sector's disarray. Excess electricity output will also cost the country money because it would produce more than is required [18].

Model for Analysis of Energy Demand (MAED) anticipates energy consumption based on various criteria about the country's economic, technological, social, and demographic characteristics. The MAED approach is not considered reliable for forecasting Turkey's electricity consumption. Because the assumptions utilized in MAED forecasts mirror the MENR's aims, anticipated figures are typically greater than actual energy consumption. As a result, providing updated electricity

consumption predictions for Turkey has remained a priority over the years. MLR is used to decide which independent factors will anticipate future electricity usage using artificial neural networks. MLR is applied after the independent and dependent variables have been transformed logarithmically. Incorporating logarithmic transformation into the MLR allows the connection between the independent and dependent variables to remain non-linear while preserving the linear model [22,31,32].

Artificial neural networks (ANNs) have been used to forecast short-term demand. ANNs are mathematical or computational representations of biological neural networks that take structure and function into account. It comprises a network of artificial neurons that utilizes a connectionist algorithm to process information. Each artificial neural network is built on a single artificial neuron [6]; the neuron must adhere to only three rules: multiplication, addition, and activation. As a result, all input values are multiplied by a unique weight at the artificial neuron's entry site. The sum function is essential to the artificial neuron. Calculate the sum of all weighted inputs and biases. A transfer function, or activation function, is the sum of previously weighted inputs and biases that have passed through the exit of the artificial neuron [32].

From Monday to Sunday, the days of the week were allocated number values ranging from 1 to 7. The 'weekdays' are denoted by the number 1 and the 'weekends' by the number 0. Additionally, the hours of the day were allocated numbers ranging from 1 to 24, indicating 1 am to 12midnight. Adjustments to the network were now made till the optimal performance was obtained. The number of epochs, hidden layers, activation functions, and network design, among other parameters, can be modified to obtain the optimal network. Training is essentially a matter of trial and error. The activation function was the sigmoid transfer function [33-35].

Fuzzy set theory is a generalization of classical set theory. In classical set theory, an element is either a member of or not a member of a given set. As a result, the degree of membership in that set is its crisp value [26]. However, in fuzzy set theory, an element's degree of membership can be modified continually from the realm of discourse, a fuzzy set maps to the near interval 0, 1. In fuzzy sets, a membership function can represent the continuous character of data. Fuzzy set theory is a critical component of artificial intelligence (AI) and has many applications in load forecasting. For instance, it can model standard linguistic variables imprecise or ambiguous on a cognitive level. Load forecasting is fraught with uncertainty due to variations in parameters such as temperature, humidity, rainfall, wind speed, air pressure, and solar radiation about the load, and its value cannot be predicted mathematically. As a result, a fuzzy logic approach will be the most appropriate way to apply

in these circumstances [20]. Therefore, fuzzy logic is utilized to map the highly non-linear relationship between meteorological characteristics and their impact on peak demand each month of the year (membership functions). The two parameters, temperature, and humidity are employed as inputs to the fuzzy logic model in this paper, whereas load is used as an output [36].
MLR is more trustworthy than FNN, fuzzy logic, and ANN approaches. This article suggests three distinct STLF approaches: ANN, Fuzzy Logic, and Fuzzy Neural Network. The load data for the ISO New England power utility are compared to those using the multiple linear regression approach. The figures demonstrate that the more recent fuzzy logic, ANN, and FNN algorithms surpass the previous MLR strategy. We have rephrased this for clarity, but the relationship between preceding one-week and two-day time-lag loading is likely more substantial [21,29,31,33,37-39].

The electrical load is affected by the calendar effect, consumption, electricity pricing, weather, and currency. These factors have the following effects: Demand is influenced by the calendar, which includes working hours, holidays, and national or religious festivals. Consumption is directly related to demand in both the industrial and household sectors. Electricity prices are affected by both production and trade. The current weather conditions may affect electricity usage. These four weather measures are sometimes regarded as the most affectionate because they need the usage of air conditioners or electric heaters. Currency changes also affect cross-border electricity trade agreements and industrial costs [38,40].

From a utilitarian viewpoint, ANN, as a black-box technique, can lower the entrance barrier for engineers interested in load forecasting, as it does not require advanced statistical knowledge or an understanding of systems. On the other hand, an ANN-based method does not provide a systematic means for engineers to improve their understanding of the system or their knowledge of its load consumption [41]. From this advantage point, the MLR methodology offers an advantage over the ANN approach: the many impacts, such as holiday and weekend effects, can be detected and modelled transparently and methodically. They analyzed using multiple linear regression (MLR) and artificial neural networks (ANN). They employed seven independent variables to forecast energy use over time; multiple linear regression was used to analyze the proposed models. By analyzing all possible combinations of the seven independent and dependent variables, 27 equations were constructed. Three models were chosen as the best for predicting future energy use, and these three models were combined in an ANN to do so. They created the ANN using back-propagation training with a feed-forward multilayer perceptron neural network [27,32,35,42].
An error-based comparison was performed between the proposed model and the classical back propagation-

trained ANN model [43]. The suggested technique outperforms standard neural networks in terms of energy demand prediction. MENR (Ministry of Energy and Natural Resources) estimates were lower in both instances [36,44]. The word "primary energy" refers to an unaltered type of energy. Two examples are coal and natural gas. Logarithmic regression was used to generate the model, and t- and F-tests were used to validate it [24]. Additionally, he forecasted Turkey's PEC from 2010 to 2025 using three different growth rates for the CP and GDP.

Over two-thirds of the energy consumed in the United States is generated by electricity. Additionally, there are additional articles devoted to Turkey's electricity consumption predictions. There is a correlation between meteorological conditions and electrical consumption in short-term projections. The long-term electricity consumption of Turkey is calculated by Senthil Kumar et al. [6] using a recurrent neural network (RNN) and a three-layered feed-forward back-propagation network (FFBPN). Finally, the RNN is the most effective structure. The authors have forecasted Turkey's electricity demand for 2008-2014.

3. CONCLUSION

Load forecasting aids an electric utility in purchasing and generating power, load shifting, and infrastructure development. Demand forecasting is critical in a deregulated energy industry. Load forecasting has three categories—load projection for one hour to one week. Short term load forecasting can help predict load flows and minimize overloading. The daily load peak forecast is fundamental in dispatching tasks. ANN and FL short-term load forecasting models usually rely on endogenous information, generally in the active power. The proposed techniques in this study were used to forecast the load for Turkey electricity. These two methods yield a minimal MAPE value compared to regression. Artificial Neural Networks and Fuzzy logic are recent technologies that predict and reduce actual and forecasted demand. There was no historical data for the load forecast for the selected years. As a result, the data was forecasted for these two years. Therefore, future studies should investigate the other new technologies to forecast; future studies can also forecast for different states in Turkey using the same techniques.

4. REFERENCES

1.   Hausmann, P. Demand Forecast. (2020), 39-49.

2.   Ivanov, D., Tsipoulanidis, A., and Schönberger, J. Demand Forecasting. (2017), 301-315.

3.   Bhattacharyya, S. Energy Demand Forecasting. (2019), 121-145.

4.   Karaçor, A. G., and Erkan, T. E. "Exploiting Visual Features in Financial Time Series Prediction." *International Journal of Cognitive Informatics and Natural Intelligence*, Vol. 14, No. 2, (2020), 61-76.

5.   Islam, M., Che, H., Hasanuzzaman, M., and Rahim, N. A. Energy Demand Forecasting. (2020), 105-123.

6.   Senthil Kumar, A., Goyal, M., Ojha, C., Singh, R., and Swamee, P. "Application of Artificial Neural Network, Fuzzy Logic and Decision Tree Algorithms for Modelling of Streamflow at Kasol in India." *Water Science and Technology: a Journal of the International Association on Water Pollution Research*, Vol. 68, (2013), 2521-6. https://doi.org/10.2166/wst.2013.491.

7.   Hasheminia, H., and Niaki, S. "A Hybrid Method of Econometrics and Artificial Neural Networks for Forecasting Economic Phenomena." *Sharif Journal of Science and Technology*, Vol. 24, (2008), 39-45.

8.   Yama, B. R., and Lineberry, G. T. "Artificial Neural Network Application for a Predictive Task in Mining." *Mining Engineering (Littleton, Colorado)*, Vol. 51, (1999), 59-64.

9.   Sharma, M. "Artificial Neural Network Fuzzy Inference System (ANFIS) For Brain Tumor Detection." (2012).

10. Mounce, S., Boxall, J., and Machell, J. An Artificial Neural Network/Fuzzy Logic System for DMA Flow Meter Data Analysis Providing Burst Identification and Size Estimation. (2007).

11. Pezeshki, Z., and Mazinani, S. M. "Comparison of Artificial Neural Networks, Fuzzy Logic and Neuro Fuzzy for Predicting Optimization of Building Thermal Consumption: A Survey." *Artificial Intelligence Review*, Vol. 52, (2019), 495-525. https://doi.org/10.1007/s10462-018-9630-6.

12. Lin, M., Huang, C., Chen, R., Fujita, H., and Wang, X. "Directional Correlation Coefficient Measures for Pythagorean Fuzzy Sets: Their Applications to Medical Diagnosis and Cluster Analysis." *Complex & Intelligent Systems*, Vol. 7, No. 2, (2021), 1025-1043. https://doi.org/10.1007/s40747-020-00261-1.

13. Sekerci, H. Load Demand Forecast of Organized Industrial Zone and Imbalance Cost Analysis. (2019).

14. Yao, A. W. L., Liao, H., and Liu, C. "A Taguchi and Neural Network Based Electric Load Demand Forecaster." *The Open Automation and Control Systems Journal*, Vol. 1, (2008), 7-13. https://doi.org/10.2174/1874444300801010007.

15. Aksoy, A., Öztürk, N., and Sucky, E. "Demand Forecasting for Apparel Manufacturers by Using Neuro-Fuzzy Techniques." *Journal of Modelling in Management*, Vol. 9, No. 1, (2014), 18-35. https://doi.org/10.1108/JM2-10-2011-0045.

16. Rama, K., and Gooda Sahib-Kaudeer, N. A Predictive Analysis of Residential Electrical Load Demand in Mauritius. (2020).

17. Sikora, R., Baniukiewicz, P., Chady, T., Lopato, P., Psuj, G., Grzywacz, B., and Misztal, L. Artificial Neural Networks and Fuzzy Logic in Nondestructive Evaluation. In *Studies in Applied Electromagnetics and Mechanics*, (2014), 137-151.

18. Mamun, A. A., Sohel, Md., Mohammad, N., Haque Sunny, Md. S., Dipta, D. R., and Hossain, E. "A Comprehensive Review of the Load Forecasting Techniques Using Single and Hybrid Predictive Models." *IEEE Access*, Vol. 8, (2020), 134911-134939. https://doi.org/10.1109/ACCESS.2020.3010702.

19. Chen, K.-L., Yeh, C.-C., and Lu, T.-L. "A Hybrid Demand Forecasting Model Based on Empirical Mode Decomposition and Neural Network in Tft-Lcd Industry." *Cybernetics and Systems*, Vol. 43, No. 5, (2012), 426-441. https://doi.org/10.1080/01969722.2012.688691.

20. Sina, A., and Kaur, D. "An Accurate Hybrid Approach for Electric Short-Term Load Forecasting." *IETE Journal of Research*, (2021), 1-16. https://doi.org/10.1080/03772063.2021.1905085.

21. Azadeh, A., Neshat, N., Rafiee, K., and Zohrevand, A. M. "An Adaptive Neural Network-Fuzzy Linear Regression Approach for Improved Car Ownership Estimation and Forecasting in Complex and Uncertain Environments: The Case of Iran." *Transportation Planning and Technology*, Vol. 35, No. 2, (2012), 221-240. https://doi.org/10.1080/03081060.2011.651887.

22. Srisaeng, P., Baxter, G. S., and Wild, G. "An Adaptive Neuro-Fuzzy Inference System for Forecasting Australia's Domestic Low Cost Carrier Passenger Demand." *Aviation*, Vol. 19, No. 3, (2015), 150-163. https://doi.org/10.3846/16487788.2015.1104806.

23. Gordini, N., and Veglio, V. "Customers Churn Prediction and Marketing Retention Strategies. An Application of Support Vector Machines Based on the AUC Parameter-Selection Technique in B2B e-Commerce Industry." *Industrial Marketing Management*, Vol. 62, (2017), 100-107. https://doi.org/10.1016/j.indmarman.2016.08.003.

24. Tapoglou, E., Karatzas, G., Trichakis, I., and Varouchakis, E. Uncertainty Analysis of a Combined Artificial Neural Network - Fuzzy Logic - Kriging System for Spatial and Temporal Simulation of Hydraulic Head. (2015).

25. Moosavi, S. M. S., and Seifbarghy, M. "A Robust Multi-Objective Fuzzy Model for a Green Closed-Loop Supply Chain Network under Uncertain Demand and Reliability (A Case Study in Engine Oil Industry)." *International Journal of Engineering*, Vol. 34, No. 12, (2021), 2585-2603. https://doi.org/10.5829/ije.2021.34.12c.03.

26. Lin, M., Li, X., Chen, R., Fujita, H., and Lin, J. "Picture Fuzzy Interactional Partitioned Heronian Mean Aggregation Operators: An Application to MADM Process." *Artificial Intelligence Review*, (2021). https://doi.org/10.1007/s10462-021-09953-7.

27. Bozkurt, Ö. Ö., Biricik, G., and Tayşi, Z. C. "Artificial Neural Network and SARIMA Based Models for Power Load Forecasting in Turkish Electricity Market." *PLOS ONE*, Vol. 12, No. 4, (2017), e0175915. https://doi.org/10.1371/journal.pone.0175915.

28. Farahbakhsh, H., Pourfar, I., and Lashkar Ara, A. "A Modified Artificial Bee Colony Algorithm Using Accept–Reject Method: Theory and Application in Virtual Power Plant Planning." *IETE Journal of Research*, (2021), 1-16. https://doi.org/10.1080/03772063.2021.1973597.

29. Verma, D., Dong, Y., Sharma, M., and Chaudhary, A. K. "Advanced Processing of 3D Printed Biocomposite Materials Using Artificial Intelligence." *Materials and Manufacturing Processes*, (2021), 1-21. https://doi.org/10.1080/10426914.2021.1945090.

30. Emeç, Ş., and Akkaya, G. *TURKEY'S ELECTRICITY CONSUMPTION FORECASTING with ARTIFICIAL NEURAL NETWORKS*. (2019).

31. Chen, K.-L., Yeh, C.-C., and Lu, T.-L. "A Hybrid Demand Forecasting Model Based on Empirical Mode Decomposition and Neural Network in Tft-Lcd Industry." *Cybernetics and Systems*, Vol. 43, No. 5, (2012), 426-441. https://doi.org/10.1080/01969722.2012.688691.

32. Almasri, R. A., and Narayan, S. "A Recent Review of Energy Efficiency and Renewable Energy in the Gulf Cooperation Council (GCC) Region." *International Journal of Green Energy*, Vol. 18, No. 14, (2021), 1441-1468. https://doi.org/10.1080/15435075.2021.1904941.

33. Fahad, M., and Arbab, N. "Factor Affecting Short Term Load Forecasting." (2014). https://doi.org/10.7763/JOCET.2014.V2.145.

34. Kumaran, J., and Ravi, G. "Long-Term Sector-Wise Electrical Energy Forecasting Using Artificial Neural Network and Biogeography-Based Optimization." *Electric Power Components and Systems*, Vol. 43, No. 11, (2015), 1225-1235. https://doi.org/10.1080/15325008.2015.1028115.

35. Çunkaş, M., and Altun, A. A. "Long Term Electricity Demand Forecasting in Turkey Using Artificial Neural Networks." *Energy Sources, Part B: Economics, Planning, and Policy*, Vol. 5, No. 3, (2010), 279-289. https://doi.org/10.1080/15567240802533542.

36. Blancas, J., and Noel, J. Short-Term Load Forecasting Using Fuzzy Logic. Presented at the 2018 IEEE PES Transmission Distribution Conference and Exhibition - Latin America (T D-LA), (2018).

37. Gonzalez-Fernandez, I., Iglesias-Otero, M. A., Esteki, M., Moldes, O. A., Mejuto, J. C., and Simal-Gandara, J. "A Critical Review on the Use of Artificial Neural Networks in Olive Oil Production, Characterization and Authentication." *Critical Reviews in Food Science and Nutrition*, Vol. 59, No. 12, (2019), 1913-1926. https://doi.org/10.1080/10408398.2018.1433628.

38. Wang, R., Chen, S., and Lu, J. "Electric Short-Term Load Forecast Integrated Method Based on Time-Segment and Improved MDSC-BP." *Systems Science & Control Engineering*, Vol. 9, (2021), 80-86. https://doi.org/10.1080/21642583.2020.1843088.

39. Oğcu, G., Demirel, O. F., and Zaim, S. "Forecasting Electricity Consumption with Neural Networks and Support Vector Regression." *Procedia - Social and Behavioral Sciences*, Vol. 58, (2012), 1576-1585. https://doi.org/10.1016/j.sbspro.2012.09.1144.

40. Fatema, I., Kong, X., and Fang, G. "Electricity Demand and Price Forecasting Model for Sustainable Smart Grid Using Comprehensive Long Short-Term Memory." *International Journal of Sustainable Engineering*, Vol. 0, No. 0, (2021), 1-19. https://doi.org/10.1080/19397038.2021.1951882.

41. Siddharth, D., Saini, D. K. J., and Singh, P. "An Efficient Approach for Edge Detection Technique Using Kalman Filter with Artificial Neural Network." *International Journal of Engineering*, Vol. 34, No. 12, (2021), 2604-2610. https://doi.org/10.5829/ije.2021.34.12c.04.

42. Borade, A. B., and Bansod, S. V. "Comparison of Neural Network-Based Forecasting Methods Using Multi-Criteria Decision-Making Tools." *Supply Chain Forum: An International Journal*, Vol. 12, No. 4, (2011), 4-14. https://doi.org/10.1080/16258312.2011.11517276.

43. Antonopoulos, V. Z., Gianniou, S. K., and Antonopoulos, A. V. "Artificial Neural Networks and Empirical Equations to Estimate Daily Evaporation: Application to Lake Vegoritis, Greece." *Hydrological Sciences Journal*, Vol. 61, No. 14, (2016), 2590-2599. https://doi.org/10.1080/02626667.2016.1142667.

44. Demiroren, A., and Ceylan, G. "Middle Anatolian Region Short-Term Load Forecasting Using Artificial Neural Networks." *Electric Power Components and Systems*, Vol. 34, No. 6, (2006), 707-724. https://doi.org/10.1080/15325000500419284.

Persian Abstract

چکیده

از آنجایی که سری های زمانی بار بسیار متغیر هستند، پیش بینی تقاضای بار کوتاه مدت بر اساس تقاضای پیش بینی بار ساعتی، روزانه، هفتگی و ماهانه چالش برانگیز است. در نتیجه، پیش‌بینی بار شرکت انتقال برق ترکیه (TEA) در این مقاله با استفاده از شبکه‌های عصبی مصنوعی (ANN) و منطق فازی (FL) پیشنهاد شده است. پیش‌بینی بار، شرکت‌های برق را قادر می‌سازد تا برق بخرند و تولید کنند، تغییر بار و زیرساخت بسازند. پیش‌بینی بار به سه دسته (ساعتی، هفتگی و ماهانه) طبقه‌بندی شد. با گذشت زمان، پیش‌بینی بارهای توان با شبکه‌های عصبی مصنوعی و منطق فازی، کاهش شدید ANN و افزایش تدریجی FL را از ۲٤ ساعت به ۱٦۸ ساعت نشان می‌دهد. همانطور که نشان داده شد، منطق فازی و شبکه های عصبی مصنوعی از الگوریتم های رگرسیون بهتر عمل می کنند. این مطالعه بالاترین نرخ رشد و میانگین درصد خطای مطلق (MAPE) را در مقایسه با FL و ANN دارد. اگرچه رگرسیون بالاترین نرخ رشد پیش‌بینی را دارد، اما به دلیل درصد MAPE پایین‌تر از FL و ANN دقیق‌تر است. شبکه های عصبی مصنوعی و منطق فازی فناوری های نوظهوری هستند که قادر به پیش بینی و کاهش نوسانات تقاضا هستند. تحقیقات آتی می تواند کشورهای مختلف ترکیه را با استفاده از همین رویکرد پیش بینی کند.

International Journal of Engineering

Performance Evaluation of Hollow Concrete Blocks Made with Sawdust Replacement of Sand: Case Study of Adama, Ethiopia

K. Shantveerayya[a], M. Kumar C. L.*[b], K. G. Shwetha[b], F. Jima[a], K. Fufa[a]

[a] Department of Civil Engineering, Adama Science & Technology University, Ethiopia
[b] Department of Civil Engineering, Nitte Meenakshi Institute of Technology, Yelahanka, Bengaluru, Karnataka, India

P A P E R I N F O	*A B S T R A C T*
	Hollow concrete blocks (HCBs) are substitutes for conventional bricks and stones in building construction. Experimental testing has been performed on the feasibility of producing HCBs from sawdust (SD). Sawdust is substituted with fine aggregate (pumice) by weight proportions 3, 6, and 9%. Sawdust is treated with tap water to remove foreign materials. Different tests were performed on blocks in order to find the effect of sawdust and to confirm whether blocks produced will satisfy the minimum acceptable standards. Different tests were conducted on the samples for 21 days as in Ethiopia to reflect the pratical application. Compressive strength of sawdust with additions of 3, 6, and 9% was 1.17, 0.99, and 0.51 N/mm², respectively. Replacement with 9% resulted in a higher rate of water absorption. The density of HCBs was found to be between 633.06 and 638.21 kg/m³. In light of the results, it is concluded that 3% of sawdust can be optimized for the production of blocks.

1. INTRODUCTION AND BACKGROUND STUDY

Wood is exploited in the construction industry for residential and public buildings in all parts of the world. Woodworking is done by cutting, drilling, and sanding, which generates waste in powder and coarser form. Wood powder is also generated by wood-dwelling insects such as woodpeckers and carpenter ants. The residue in the form of powder is called sawdust. An increase in unmanaged waste, particularly in developing countries, has heightened environmental concerns. In addition to tackling the pollution problem, recycling waste as a building material can also contribute to a more cost-effective structure. Sawdust has various practical uses. It can be used as a building material in concrete, solid and hollow concrete blocks, ceiling tiles, furniture, plywood etc. [1].

In rural Ethiopia, sawdust is used as fuel and reformed into charcoal briquettes. The construction industry in Ethiopia has skyrocketed over the past two decades, and many middle-class. Ethiopians have typically reached for building blocks due to high prices. Many small carpentry and sawmills have started operations in Ethiopia over the past few decades and are facing challenges when it comes to disposing of this waste. It was observed that sawdust was being deposited in landfills or in uncontrolled outdoor rubbish pits outdoors. This suggests that sawdust is relatively abundant and could increase in the future. There is no clear statistical data on the availability of sawdust in Ethiopia. However, the export volume of sawdust is estimated at 184.93 tons, which was exported in 2018 [2].

The study will aid in reducing the amount of construction material (Pumice) utilized in the production of HCBs. Thus, promoting the optimum utilization of lumber received from nature and facilitating in the campaign for environmental consideration. Additionally, lumber companies will be able to dispose of their waste materials at the same time as generating additional revenue. In the present study, fine powder sawdust is utilized to produce HCBs.

Corresponding Author Institutional Email: maheshkumar.cl@nmit.ac.in (M. Kumar C. L.)

Several studies have been carried out with rice husk ash, concrete waste, fly ash, blast furnace slag, rubber waste, glass powder and paper waste for manufacture of concrete and hollow concrete blocks [3]. In order to produce concrete with different mixed fractions for the first time [1]; the volume of cement was substituted with sawdust, and noticed a sustainable enhancement in strength properties of concrete. Compressive strength and density properties of sawdust ash and slaked lime mixture with cement substitute were investigated by [4]. A combination of cement/SDA-lime proportions of 90:10 (cement: SDA-lime) was perceived to have the highest strength and the density reduced with an incremental in SDA-lime.

Limestone dust and sawdust have been used in various combinations to prevent brittle failure of bricks [5]. Compressive strength and weight of HCBs were compared for different mixed proportions [6] of sawdust with sand by volume replacement. Accordingly, the addition of 10% sawdust did not meet the minimum strength requirements. This is because sawdust contains a large amount of tannin, which inhibits the internal hydration process and reduces the strength. Blocks were lighter when 10 percent sawdust is added. [7] also investigated the compressive strength, water absorption and thermal properties of sawdust treated with engine oil. The thermal conductivity of the blocks decreased with increasing sawdust content, and the strength decreased with the addition of 10% sawdust. Boob [8] investigated how curing type affects the compressive strength and density of HCBs when replacing sand with sawdust. With 15 % and substituted sawdust, a cement/sand mix of 1:6 demonstrated effective strength properties compared to sprinkling, the gunny bag method is found to be more efficient. For the production of HCBs, Albera [9] used a different volume ratio to replace sawdust with sand. According to his results, an optimal replacement rate of 15% can be used for strength, but an increase in water absorption was also observed. Recent studies has been done on Fly ash-based GPC which has exceptional compressive strength, making it ideal for structured applications [10]. A Study on roof tiles using metakolin with different percentages of EPS, sodium silicate and flexi cool coating paint was studied by Raheem and Sulaiman [11] .The researcher suggested 20% metakolin has higher strength compared to ordinary tile, which is 9.1% and 39.6% in terms of compressive strength and transverse breaking strength.

Furthermore, several studies were performed using sawdust ash as a substitute for cement and sand to determine density, compressive strength, and water absorption rate of HCBs for 28 and 56 days. According to Raheem and Sulaiman [11], based on their observations, the 28-day strength did not meet the national building code (NBC) standards, but the 56-day strength increased by 20%. For the production of concrete, different proportions of sawdust ash were used as supplementary of cement by weight in order to produce concrete [12]. An amount of 5% has been used as an optimal ratio for achieving optimum compressive strength. Additionally, the addition of sawdust ash to concrete at an early age has a lower strength, but improves significantly up to 90 days, adding sawdust ash to concrete will lead to a reduction in workability of concrete. Concrete blocks with coconut shells (CS) was studied [13] and stated that addition of CS has improved the strength property by 32%. Stabilized blocks made up of rice husk with different percentage is studied by Mousavi [14] and suggested optimum percentage of rice husk was 12% with 1.6 % increment in strength.

Several researchers studied the behavior of concrete, concrete blocks, and bricks mixed with different mix proportions by volume and weight of sawdust, sawdust ash with the combination's other mineral admixtures. The use of sawdust in HCBs is usually limited to 10% due to its organic nature and higher affinity towards the water absorption. It has also been observed that there is an increase in strength for lower percentage up to 10% replacement but not the same for higher replacements. However, it is also observed that addition of sawdust has low strength property at early age but enhances the strength at later stage up to 90 days. In addition, it has good thermal conductivity and decrease in weight of the blocks with increase in percentage of sawdust. To date, there is a dearth of information in Ethiopia, on the application of sawdust on HCBs. Hence, this study aims to works on locally available sawdust from Adama science and technology university (ASTU), Ethiopia production unit to investigate the effect of sawdust in HCBs. This research presents some physical and mechanical properties of HCBs of different mix proportion of 3, 6 and 9% by volume. This percentage is selected to determine the optimization from the previous study and utilize the large quantity of sawdust and reduce the usage of natural resource fine aggregate. Due to limited laboratory resources, chemical composition of materials and microscopic studies could not be conducted. It is observed that the usage of sawdust by volume replacement will have impact of the quantity of usage in sawdust compared to weight replacement. In this research, in order to reduce the weight of HCBs and increase the quantity of sawdust and reduce the environmental dumping problem, we have used sawdust by weight replacement and overcome the workability problem with an increase in the quantity sawdust. Sawdust was pre-soaked for 30 minutes before in use.

2. MATERIALS AND METHODOLOGY

To investigate the effect of sawdust on Hollow concrete blocks, 63 samples were casted with 3, 6, and 9% of

sawdust, replacing sand with mixing ratio of 1:8 (cement: sand). The samples were tested to study the mechanical and durability properties of HCBs for 21 days. It is observed the sawdust has a high-water absorption capacity when soaked for 30 minutes. The water absorbed by the sawdust during mixing and curing time will releases its moisture content to the surrounding medium and act as an internal curing during the hydration process once curing of the blocks is stopped through external. This keeps the blocks to satisfy the both industrial and codal requirement indirectly by curing the samples for 21 days. 21 samples were taken from the local factory for comprative studies. Initially the material properties of cement, aggregate and sawdust are examined according to Ethiopia Standard Agency [15]. Table 1 summarizes the quantity of materials required to produce HCBs. SD indicates sawdust and 0 indicates percentage of sawdust.

2. 1. Properties of Materials   32.5 grade Portland Pozzolana cement brand produced by Ethio cement is used as binding materials for the production of blocks. Pumice and scoria are commonly used for the production of HCBs in Adama city, Ethiopia. This research only uses pumice as an aggregate, available from Mikiyas Concrete Block Factory at Kebele 14, Adama City to produce HCBs. To compare the results directly, all blocks were made with the same sawdust and pumice stone (see Figure 1). The properties of sawdust and pumice are summarized in Table 2.

From Figure 2, it is observed that the crushed pumice size is not within the limits of upper and lower limits of ASTM D6913 [16] for coarser grain size. The crushing percentage is high and within the limits which indicates that the most of the aggregate size are smaller than the

TABLE 1. Mix Design of HCBs

Notation	Cement (kg)	Sand (kg)	Sawdust (kg)
SD 0	32.13	226.5	-
SD 3	32.13	219.71	6.79
SD 6	32.13	212.91	13.58
SD 9	32.13	206.11	20.39

TABLE 2. Characteristic properties of pumice and sawdustused in the production of reference and sawdust blocks

Properties	Pumice	Sawdust
Specific gravity (g/cm^3)	1.34	1.34
Density (kg/m^3)	850	365
Water absorption (%)	52	98.87
Cc	10	7.5
Cu	1.225	1.225
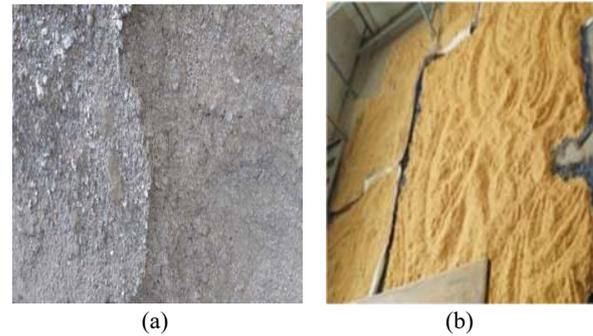
(a)   (b)
Figure 1. (a) Crushed pumice and (b) Cleaned sawdust
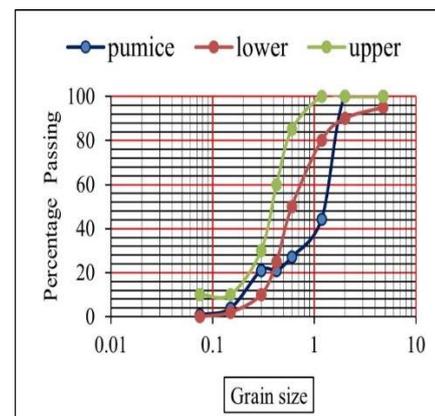
Figure 2. Grain distribution of pumice

requirement needed for the production of blocks. This is due to the random crushing of the coarser aggregates at the production site. Due to the smaller particle size, high-water absorption and an increase in weight of the blocks are to be expected. It is observed that the curve for pumice shows a gradation gap between the particle size, which influences the strength of HCBs [17]. It is also observed the particles size between 0.6 and 0.3. Figure 2 shows flattened horizontal, which indicates that there is absence of grain size. These uneven variations of aggregate size can impact on the strength and density of the block. The grain distribution of sawdust is shown in Figure 3.

2. 2. Mixing, Casting, Curing and Drying Sawdust HCBs   Concrete blocks with dimensions of 400 x 150 x 200 mm (L x W x H), were cast in the Mikiyas Block Factory in Adama Kebele 14, Ethiopia using different sawdust ratios. The pumice is initially crushed to produce fine aggregate without particular attention. Sawdust is washed with water and dried before it used for mixing. Later it is again soaked in water for 30 minutes to absorb maximum water before it is in used for mixing process. According to Portland cement association, it has substantial improvement in properties of concrete through the addition of washed sawdust. The required
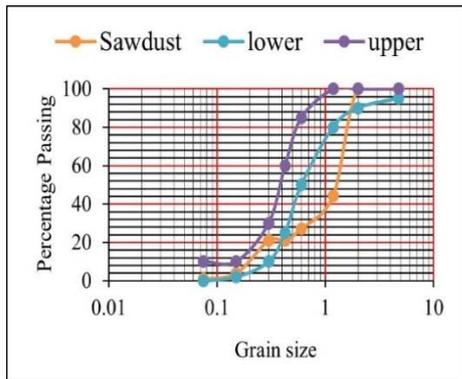
Figure 3. Grain distribution of Sawdust

quantities of materials are subsequently dry mixed until homogeneity is achieved. Depending on the workability of each mix design, a certain amount of water is added until consistency is achieved without special care being required to promote homogeneity. The mixing of the materials took longer with a comparative sample with an increased proportion of sawdust. Similar observation was made by Paramasivam and Loke [1]. The forms were made of wood that was neither damp nor strewn with sand (to ensure easy removal) and were filled with a shovel and compacted in the vibrating device as shown in Figure 4. To reduce evaporation of water and increase the strength of blocks, casting and curing samples were done in the evening. For the initial 12 hours, samples were dried on wooden planks and then placed on a non-absorbent surface and cured by spraying three times a day for 21 days. Once the external curing process is stopped at 21 days, the water absorbed from the sawdust will start releasing to the surrounding medium through channels at microlevel and act as on internal curing. Which indirectly satisfies the standard curing period of 28 days.

2. 3. Methodology   The experimental procedures are followed for mechanical and durability properties. All

Figure 4. Methodology for casting of samples

samples are examined for compressive strength, water absorption, density, fire resistance, dimension measurement and tolerance and weight. The samples are tested for various parameters and are done in accordance to ASTM standards [15]. The casting method for preparation of samples is shown in Figure 4.

2. 3. 1. Compressive Strength   To determine the compressive strength, randomly six samples from each mix ratio are tested by applying uniaxial compressive load. Steel sheets of 10 mm are attached to the top and bottom to ensure even loading. The specimens are tested under controlled loading at a constant rate of 2.5 mm/min. The crushing strength of the specimens are calculated using according to Equation (1).

$$f_c = \frac{P}{A} \tag{1}$$

where, fc= compressive strength, P = load at which the specimen sustained maximum load and A = net area on which the load was applied.

2. 3. 2. Water Absorption   Three samples are taken from each mixture ratio. All samples are oven dried for 24 hours at 115 °C, and their weights are recorded. These samples are then soaked in water for 24 hours while their weight was recorded every two hours for the first six hours and final weight at 24 hours. Equation (2) is used to calculate the percentage of water absorption.

$$\% \text{ of water absorption} = \frac{\text{Weight of wet sample} - \text{weight of dry sample}}{\text{weight of dry sample}} \times 100 \tag{2}$$

2. 3. 3. Density   Three samples of each blend portion was oven-dried at 100°C for 24 hours to examine the density propertiesThe samples were gradually brought to room temperature and their weights were recorded. The Density of blocks is calculated using Equation (3).

$$\text{Density of blocks} = \frac{\text{Weight of dried blocks}}{\text{Volume of spciemen}} \tag{3}$$

2. 3. 4. Fire Resistance   Three samples of each mixed proportions are open fired for one hour in an uncontrolled temperature by keeping in a practical condition. After firing process, the samples are set to cool and it was observed whether the material bond was lost. The fire resistnce test is depicted in Figure 5.

2. 3. 5. Dimension and Tolerance Measurement Six samples are selected to conduct the test. The measurements of each sample are recorded in all three dimensions and compared to the mold size as filled with wet mix.

2. 3. 6. Weight Measurement   Three samples were randomly selected from each and the accuracy

Figure 5. Fire resistance test

weighted to 0.1 g. An average of three sample weights were taken. All blocks with a mixed design are compared to the reference to control weights, the blocks are light/ heavy. The reference HCBs and sadust HCBs are shown in Figure 6.

3. ANALYSIS RESULTS AND DISCUSSION

3. 1. Effect of Compressive Strength on HCBs using Sawdust   From the test results, it is observed that 3% sawdust substitute is more effective than the reference sample. Replacement of 3 and 6% of fine aggregate with sawdust, the strength of sawdust blocks is increased by 81 and 52.3 %, respectively. Adding a higher percentage of sawdust decreases the compressive strength. Similar trends were observed in literature [16-20] for a replacement of 2% and higher with sawdust.
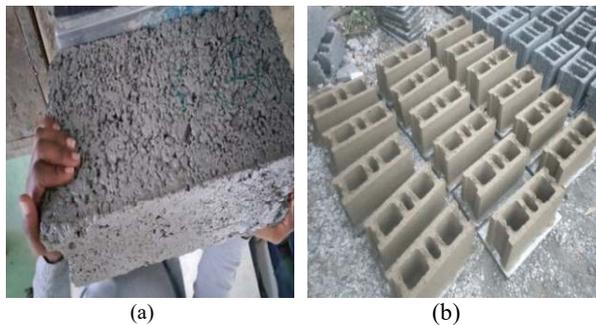

(a)   (b)
Figure 6. (a) Reference HCBs and (b) Sawdust HCBs

Since saw dust is finer than the pumice and fills the gap between the particles and increases bonding strength at the microscopic level. The strength attained for 3% replacement is below the minimum requirement of 1.8 N/mm^2 according to ASTM standards [15] for class D classification of non-load bearing walls. The sawdust contains bark, which prevents from hydration at initial stage. Hence, there is a reduction in strength at early ages. If curing process is carried out for 28 days as per codal requirement, the strength of blocks is expected to increase, as its observed in several studies [8, 21-23]. In Figure 7, the strength of blocks are reduced at 6% and 9%. From the physical observation of the blocks it is observed, with the addition of higher percentage of sawdust, cement mortar is coated with the ample amount of sawdust (organic material) instead of fine aggregate which impacts in the reduction of the bond between at micro level which makes the reduction in strength of the blocks.

3. 2. Effect of Compressive Strength on Water Absorption Property using Sawdust   The average percentage of water absorption of three samples were 17.94, 20.86, 22.12 and 26.60%, for 0, 3, 6 and 9%, respectively and test results are presented in Table 3. These results are consistent with the results reported in
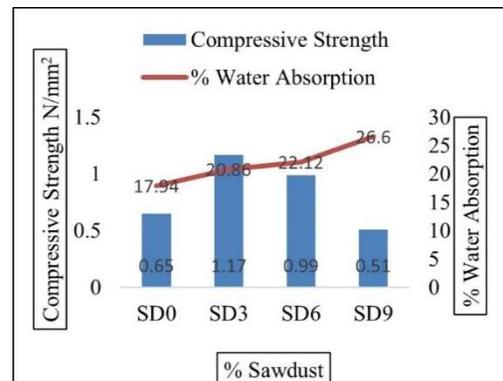
Figure 7. Effect of Compressive strength, Water Absorption Vs Sawdust

TABLE 3. Summary of the experiments

Notation	HCBs	Compressive strength (N/mm²)	Water absorption (%)	Density (kg/m³)	Dimension (cm)			Weight (kg)
					L	W	H	
Reference	SD0	0.65	17.94	638.21	39.7	14.8	20.05	7.47
	SD3	1.17	20.86	689.45	40	15.1	20.15	8.068
Sawdust	SD6	0.99	22.12	683.47	39.9	14.9	20	8.002
	SD9	0.51	26.6	633.06	40	15.15	20.25	7.401

literature [19, 21] a significant increase in water absorption was observed. with an increase in sawdust percentages up to 6%. This is due to the high absorption capacity of sawdust at an early stage. The percentage of water absorption decreases with an increased percentage for above 6%, which indicates that the optimum moisture capacity is reached at 6%. It is also obsrved that the compressive strength is maximum at 3 % replacement and gradually decreases thereafter, which is observed in Figure 7. At 3% replacement of sawdust, the water absorption rate is slightly higher than the specified [15]. The effect of reduction in water absorption can ve achieved coating the sawdust with kerosene as its an non-absorbent proerty.

3. 3. Effect of Compressive Strength Versus Density on HCBs using Sawdust

From results, for 0, 3, 6 and, 9% the density of blocks are 638.21, 689.45, 683.47 and 633.06 kg/m^3, respectively. [18,19,24] observed a similar effect in blocks as well as in the concrete. Figure 8 shows that the density of HCBs for 3% is higher than that of other percentage replacement. This increase in density of blocks is due to the finer grain size of the sawdust, which is finer than fine aggregate [25], which is similar and is observed in Figure 3. This finer sawdust fills the voids between the aggregates and increases the density of blocks. In contrast, the density of the blocks for reference and other mixed proportions is decreased. The oversaturation of water absorption in the sawdust at the initial stage and the subsequent evaporation during the oven drying of the samples will form the air pockets at the micro level, which lead to the reduction in the density of the blocks. These blocks meets the class D classification according to ASTM standards [15].

From Figure 8, it is observed that the compressive strength decreases with decrease in density of the blocks. With the increased density of blocks, the compressive strength of the blocks for 3% replacement is found to be
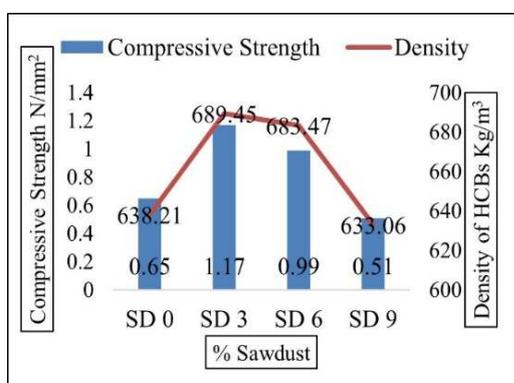
Figure 8. Effect of Compressive Strength Vs Density of HCBs

increased. From this it is concluded that density of blocks has significant effect in compressive strength. Similar results were reported by Omar et al. [24].

3. 4. Effect of Fire Resistance on HCBs with Sawdust

This test is done for hollow concrete blocks to ensure that they are non-flammable and is their any reduction in cross sectional dimensions as well to now the effect of bond strength in the matrix if the blocks are burnt for one hour as per the Indian Standard (IS: 1077-1992) [25]. Random tests were performed on three samples from each mixture. Physical observations was done on all the blocks, and it is observed smouldered like charcoal but didn't burn the blocks and slight reduction in size was observed. The edges of the blocks were damaged for the small application of force for all the mix proportions except 3% replacement of sawdust. The damage at the edges was found due to its brittle nature and due to the reduction in bond strength between the sawdust and cement matrix and fine aggregate. Similar observations were reported by Popoola et al. [18] for the blocks made with waste material of papercrete.

3. 5. Effect of Weight on HCBs with Addition of Sawdust

In comparision to the reference blocks, the blocks with addition of sawdust are found to be 8% higher. The reference blocks are lighter because combined use of scoria and pumice and their density ranges 500 -1000 kg [26]. The results showed a slight increase in the weight of 0.5 kg for 3 and 6% of sawdust blocks compared to the reference blocks and the same observation was reported by Sunagar and his coworkers [27]. It was expected the weight of blocks would be reduced to its low density when compared to pumice. However, it was found to be higher than the expected, this is due to the finer particles filling the voids leading to the addition of weight to the blocks, as well as the high-water absorption of sawdust. In the presence of 9% sawdust, the weight of the blocks decreased. This is the result of over-saturation of water absorption and the formation of air pockets after curing and creating micro voids in the matrix. The additional weight of blocks can be compansiated with the strength, drop fall and fire resistance properties of the blocks.

4. CONCLUSIONS

The feasibility of HCBs using sawdust, with different percentage replacements of 3%, 6% and 9% by sand has been investigated for various properties.

The research showed that 3% sawdust replacement with sand is effective. The compressive strength of the blocks for 3% is 80% higher than the reference blocks. Water absorption for 3% is found to be 15% higher than

the recommended. Density and weight of blocks for reference blocks is 8% lower than sawdust blocks. A 3% replacement of fine aggregate with sawdust is found to be better at fire resistance than any other mix ratios. Dimensions tolerance along width and length are reduced, and the reduction are within the permissible limits. Hence, it is recommended that 3% of the fine aggregate can be replaced with sawdust as it meets the standard requirements. As their strengths are higher than the reference blocks. The use of sawdust with treatment could be further explored to improve water absorption property of blocks.

5. ACKNOWLEDGEMENT

6. REFERENCES

1. Paramasivam, P., and Loke, Y. O., "Study of sawdust concrete", *International Journal of Cement Composites and Lightweight Concrete*, Vol. 2, No. 1, (1980), 57-61, doi: 10.1016/0262-5075(80)90008-1.

2. Fetene, Y., Addis, T., Beyene, A., Kloos, H. "Valorisation of solid waste as key opportunity for green city development in the growing urban areas of the developing world", *Journal of Environmental Chemical Engineering*, Vol. *6*, No. 6, (2018). 7144-7151.

3. Shantveerayya, K., Murthy, H. C. A., and C. Gadafa, "Evaluation of strength and durability of hollow concrete blocks prepared by using concrete waste materials from Adama", *International Journal of Engineering Research and Applications*, Vol. 10, No. 5, (2020), 25-32, doi: 10.9790/9622-1005032532.

4. Tyagher, S., Utsev, J., and Adagba T., "Suitability of saw dust ash-lime mixture for production of sandcrete hollow blocks", *Nigerian Journal of Technology*, Vol. 30, No. 1, (2011), 79-84.

5. Turgut, P., and Murat Algin H., "Limestone dust and wood sawdust as brick material", *Building and Environment*, Vol. 42, No. 9, (2007),3399-3403, doi: 10.1016/j.buildenv.2006.08.012.

6. Adebakin and Adeyemi, A., "Uses of sawdust as admixture in production of lowcost and light-weight hollow sandcrete blocks", *American Journal of Scientific and Industrial Research*, Vol. 3, No. 6, (2012), 458-463, doi: 10.5251/ajsir.2012.3.6.458.463.

7. Al-Qysi, Y., "Effect of adding treated sawdust on the characteristics of the solid and hollow concrete block", *Journal of Environmental Studies*, Vol. 11, No. 1, (2013), 5-10, doi: 10.21608/jesj.2013.192101.

8. Boob, T. N., "Performance of saw-dust in low cost sandcrete blocks", *American Journal of Engineering Research*, Vol. 03, No. 04, (2014), 2320-847.

9. Abera, M. A., "Investigating the acceptable quantity of fine aggregate to be replaced with sawdust to obtain strong, light weight, and economical result for HCB production", *International journal of Advance Research, Ideas and Innovations in Technology*, Vol. 5, No. 5, (2019), 391-395.

10. Arunraj, E., Hemalatha, G., and Noroozinejad Farsangi, E., "A novel lightweight phase-changing cooling roof tile", *International Journal of Engineering, Transactions C: Aspects*, Vol. 34, No. 6, (2021), 1398-1406, doi: 10.5829/ije.2021.34.06c.02.

11. Raheem, A. A. and Sulaiman, O. K., "Saw dust ash as partial replacement for cement in the production of sandcrete hollow blocks", *International Journal of Engineering Research and Applications*, Vol. 3, No. 4, (2013), 713-721.

12. Raheem, A. A., Olasunkanmi, B. S., and Folorunso, C. S., "Saw dust ash as partial replacement for cement in concrete", *Organization, Technology and Management in Construction: An International Journal*, Vol. 4, No. 2, (2012), 474-480, doi: 10.5592/otmcj.2012.2.3.

13. Anu S Das, Ansu V, Megha P, Nithin M Thomas, and Sachin A K, "Assessment of Strength of Hollow Concrete Blocks with Holes Reinforced with Half Portion of Coconut Shells", *Journal on Today's Ideas - Tomorrow's Technologies*, Vol. 6, No. 2, (2018), 93-98, doi: 10.15415/jotitt.2018.62008.

14. Mousavi, S. E., "Performance of Non-fired Green Brick Containing Rice Husk as Sustainable Building Material", *International Journal of Engineering, Transactions C: Aspects*, Vol. 29, No. 3, (2016), 306-312, doi: 10.5829/idosi.ije.2016.29.03c.04.

15. E. Ethiopia Standard Agency, "Compulsory Ethiopian Standard Design of Concrete Structures-Part 1-1 : General rules and rules for buildings", *CES EN 1994-1-1*, Vol. PART 1-1, 2015.

16. ASTM D6913-04R2009, "Standard Test Methods for Particle-Size Distribution (Gradation) of Soils Using Sieve Analysis", *ASTM International, West Conshohocken, PA,* Vol. 04, No. Reapproved (2009), 1-35, doi: 10.1520/D6913-17.1.6.

17. Birhane, S., "Experimental study on some mechanical properties of papercrete concrete", *Advances in Materials,* Vol. 6, No. 1, 1, (2017). doi: 10.11648/j.am.20170601.11.

18. Popoola, O. C., Ayegbokiki, S. T., and Gambo, M. D., "Saw dust ash as partial replacement for cement in the production of sandcrete hollow blocks", *IOSR Journal of Engineering*, Vol. 05, No. 05, (2015), 30-34.

19. Ekhuemelo, D., Tembe, E. T., and Versue, A. M., "Some aspects of physical and mechanical properties of hollow blocks procuced from hot water treated sawdust", *Sustainability, Agri, Food and Environmental Research*, Vol. 5, No. 4, (2017), 82-97, doi: 10.7770/safer-v5n4-art1304.

20. Ekhuemelo, D. O., Gbaeren, E. T., and Tembe, E. T., "Evaluation of lime treated mixed sawdust as fractional replacement for sand in the production of sandcrete hollow blocks", *International Journal of Science and Engineering Investigations*, Vol. 6, No. 65, (2017), 21-27.

21. Qatta, H. I., "Improvement the mechanical and thermal properties of concrete hollow blocks by using local materials in Iraq", *The Iraqi Journal for Mechanical and Material Engineering,* Vol. 13, (2013), 410-421.

22. Kumar, D., Singh, S., Kumar, N., and Gupta, A., "Low-cost construction material for concrete as sawdust", *Global Journal of Researches in Engineering*, Vol. 14, No. 4, (2014),1-5.

23. Gambo, S., Ibrahim, K., and Daikwo, G. A., "Sawdust types effective as partial replacements of fine aggregate in concrete", *ATBU Journal of Environmental Technology*, Vol. 6, No. 65, (2017), 21-27.

24. Omar, M. F., Abdullah, M. A. H., Rashid, N. A., and Abdul Rani, A. L., "Partially replacement of cement by sawdust and fly ash in lightweight foam concrete", IOP Conference Series: Materials Science and Engineering, Vol. 743, No. 1, (2020),12-35, doi: 10.1088/1757-899X/743/1/012035.

25. IS:1077 (BIS 1992), "IS 1077, Common Burnt Clay Building

Bricks -Specification", *Bureau of Indian Standard*, 1992.

26. Gunduz, L., "Use of quartet blends containing fly ash, scoria, perlitic pumice and cement to produce cellular hollow lightweight masonry blocks for non-load bearing walls", *Construction and Building Materials*, Vol. 22, No. 5, (2008), 747-754, doi: 10.1016/j.conbuildmat.2007.01.008.

27. Sunagar, P., Kumari, T. G., Jyothilakshmi, R., Mahesh Kumar, C. L., Shwetha, K. G., Sumalatha, J., and Naveen, G. M. "Sustainable Medium Strength Geopolymer with Fly Ash and GGBS as Source Materials". *Nveo-Natural Volatiles & Essential Oils Journal NVEO*, 3114-3124.

Persian Abstract

چکیده

بلوک های بتنی توخالی (HCBs) جایگزین آجر و سنگ های معمولی در ساخت و ساز ساختمان هستند. آزمایشات تجربی بر روی امکان سنجی تولید HCB از خاک اره (SD) انجام شده است. خاک اره با نسبت های وزنی ۳، ۶ و ۹ درصد با سنگدانه های ریز (پومیس) جایگزین می شود. خاک اره برای حذف مواد خارجی با آب لوله کشی تصفیه می شود. آزمایش‌های مختلفی بر روی بلوک‌ها به منظور یافتن اثر خاک اره و تأیید اینکه آیا بلوک‌های تولید شده حداقل استانداردهای قابل قبول را برآورده می‌کنند، انجام شد. آزمایش‌های مختلف روی نمونه‌ها به مدت ۲۱ روز مانند اتیوپی انجام شد تا کاربرد عملی را منعکس کند. مقاومت فشاری خاک اره با افزودن ۳، ۶ و ۹ درصد به ترتیب ۱.۱۷، ۰.۹۹ و ۰.۵۱ نیوتن بر میلی‌متر مربع بود. جایگزینی با ۹٪ منجر به نرخ بالاتر جذب آب شد. چگالی HCBs بین ۶۳۳.۰۶ و ۶۳۸.۲۱ کیلوگرم بر متر مکعب است. با توجه به نتایج، می توان نتیجه گرفت که ۳ درصد خاک اره را می توان برای تولید بلوک بهینه کرد.

International Journal of Engineering

Finite Element Analysis on Behavior of Single Battered Pile in Sandy Soil Under Pullout Loading

M. S. Al-Tememy, M. A. Al-Neami*, M. F. Asswad

Civil Engineering Department, University of Technology, Baghdad, Iraq

A B S T R A C T

Batter piles are the piles driven in the soil at an inclination with the vertical to withstand oblique loads or large horizontal loads and have been widely used to support high buildings, offshore buildings, and bridges. These constructions are risky because of the exposure to moments and overturning resulting from winds, waves, and ship impact. A 3D FEA using PLAXIS 3D software was used to investigate the effect of several variables that affect the behavior of single batter piles under pull-out loads. The study is achieved on a steel pipe pile model embedded in a dry sandy soil with three relative densities (loose, medium, and dense) at different inclination angles and three embedment ratios, L/D of 25, 37.5, and 50, respectively. The numerical results showed that the ultimate pull-out resistance of the battered pile raise as the battered angle increases reaches a maximum value, then decreases. The ultimate pull-out load capacity of a single battered pile is directly proportional to the slenderness ratio and relative density; the ultimate pull-out load increases with the increase in the ratio of slenderness and relative density. The ultimate uplift load of the battered pile was less affected by the free-standing length. Vertical and battered piles at a battered angle of (10° and 20°) and free-standing lengths equal to zero have higher ultimate pull-out capacity; by increasing the free-standing length, the ultimate pull-out capacity decreased.

doi: 10.5829/ije.2022.35.06c.04

1. INTRODUCTION

Batter piles are used to support marine structures, towers, bridges, and tall chimneys since the type of structures are subjected to lateral load, pullout load, and/or overturning moments due to wind, waves, and ship impact. Battered piles transfer the induced overturning moment and the lateral load partially into compression or/and tension forces. A few studies have been carried out experimentally as well as numerically to evaluate the batter piles capacity under pullout loading.

Zhang et al. [1] performed an experimental investigation to study the effect of the batter pile angle in addition to sand density on the lateral load capacity of a battered pile. Results showed that the batter pile angle and soil density affect lateral pile capacity. Bose and Krishnan [2] performed experimental tests on vertical and batter model piles constructed in sandy soil and subjected to pullout loads to investigate the effect of pile

inclination and pile length. The results showed that the ultimate pullout capacity increases with an increase in a length to diameter ratio; also, the ultimate pullout capacity increases with increasing pile batter angle attain a maximum value and then decreases.

Rahimi and Bargi [3] carried out a three-dimensional finite element analysis using ABAQUS software to study the effect of pile inclination angle. The results showed that the change in the pile inclination could significantly influence the distribution of pile forces and moments; as the pile inclination angle increases, the pile displacement decreases.

Nazir and Nasr [4] conducted tests on the steel pipe pile model in loose, medium, and dense sand with different embedded lengths and with various batter angles to study the effect of different parameters on the ultimate pullout load capacity of battered pile. The results indicated that when the batter angle increases, the ultimate pullout capacity of a battered pile constructed in

*Corresponding Author Institutional Email:
40008@uotechnology.edu.iq (M. A. Al-Neami)*

dense and medium sand increases, while in loose sand, the ultimate pullout capacity decreases with an increase in the pile batter angle. The ultimate pullout capacity increases with an increase in the embedment ratio and relative density of sand.

Gaaver [5] conducted experimental model tests on single piles and pile in groups embedded in the sand and subjected to uplift loading to investigate the effect of pile embedment depth, relative density of soil, and piles arrangement in a group on the uplift capacity. The results concluded that the pile capacity increased with an increase in the relative density of the soil and the pile embedment ratio.

Al-Neami et al. [6] studied the ultimate capacity of a single pile model subjected to a compression load. The results indicate that an increase in battered angle would increase the pile capacity until it reached the peak value at 20°; then, the capacity decreased. Also, they studied the effect of relative density and slenderness ratio on pile load capacity. Increasing the relative density of the sand by 1.5 times will increase the pile load capacity twice, and the load capacity of the battered pile is less affected by an embedded ratio (L/D). Gebrselassie [7] presented FEA to investigate the response of a battered pile under horizontal, vertical, and oblique loads. It was noted that when the batter angle increases, a pile load-carrying lateral capacity increases until the angle reaches -20°; then, the resistance decrease and as the load inclination angle increased, the total and lateral deformation increases. Vali [8] studied the effects of the water table changes on the behavior of a geogrid reinforced soil-footing system on marine soft soil layers in Qeshm Island, Iran. The impacts of the water table and the geogrid layer specifications were evaluated by the finite element analysis to investigate the system's behaviors. The results indicate that water tables played a substantial role in the behaviors of the soil-footing systems. By decreasing the water table, the settlement decreased while the safety factor of the soil-footing system increased. Increasing the tensile strength of the geogrid layer resulted in decreasing the soil-footing system settlement and improving the safety factor of the system. Russo et al. [9] investigated the mechanical behavior of three hybrid piles equipped with strain gauges along the shaft via three loading tests. A new installation procedure for a foundation pile of a new Mall under design in a disused factory area and numerical simulations of the energy hybrid pile behavior was presented. The FEM package PLAXIS 2D was demonstrated to be capable of modeling the most important features of the complex behavior of a heat exchanger pile even with simple constitutive models for soil. The FE package PLAXIS 2D was used to simulate the behavior of an isolated hybrid energy pile installed in pyroclastic sandy soils and subjected to both thermal and mechanical loadings. In the technical literature, many studies were limited to permanent situations where only the maximum temperature variations were considered.

Many factors influence batter piles under pullout loads. Thus, it becomes necessary in geotechnical engineering to understand how they behave and know the variables that affect the design of the pullout capacity of batter piles. Therefore, further investigation is required to provide insight into the influence of different parameters on the batter pile response. In this study, the behavior of the batter pile under a pullout load embedded in the sand is evaluated under different parameters (relative densities, embedment ratio, battered angles, and free-standing length). The recent paper will focus on the behavior of batter piles subjected to pullout loading driven in dry sandy soil by conducting three-dimensional numerical model tests using PLAXIS software on a full scale.

2. VALIDATION OF NUMERICAL MODEL

To check the validity of PLAXIS software, the research carried out by Al-Neami et al. [6] was used. The problem represents pile models with five different inclinations of 0, 10°, 20°, 30°, and 40° constructed in dense sand with a relative density of 80%. The model's domain used in the analysis was 100 cm in length, 75 cm in width, and 70 cm in depth. The dry unit weight of soil is 18.7 kN/m^3, and the internal friction angle equals 40°. The soil was modeled using the Mohr-Coulomb model. The pile used is circular steel solid with a cross-section of 20 mm in diameter pile and an embedment ratio equal to 15. The single vertical and batter piles were modeled as an embedded beam element which is discretized with solid elements. The interface strength reduction factor (R$_{inter}$) was taken as a manual, and it equals 0.7 as reported by Waterman [10]. A fine mesh was used to obtain accurate numerical results. Figure 1 shows the finite element mesh for soil and pile.
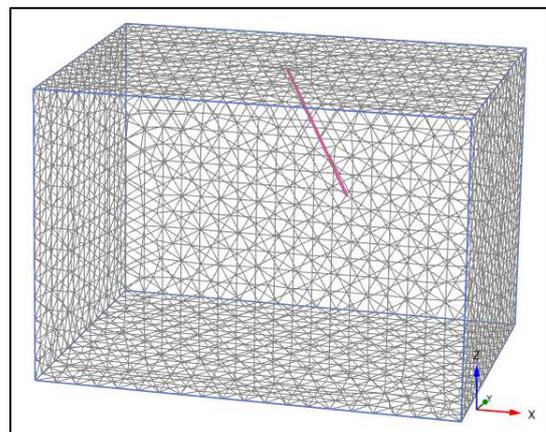

Figure 1. Problem finite element mesh

The load-settlement curves estimated from the numerical model compared with the experimental results of Al-Neami et al [6] as shown in Figure 2 . PLAXIS-3D analysis resulted in excellent agreement with the experimental results.

3. PARAMETRIC STUDY

3. 1. Method of Analysis   The pullout capacity of a battered pile is predicated by using PLAXIS 3D software that works on the finite element approach. PLAXIS 3D software is a 3D finite-element analysis program for the nonlinear properties of soil and rock and soil-structure interaction problems. In this studying, the loading is applied axially through a prescribed displacement equal to 0.1D, (where D diameter of the pile) instead of applying the axial load for a better comparison of the results.

3. 2. Soil Modeling   The properties of the sand used in this analysis are taken directly from laboratory tests carried out by Al-Neami et al. [6]. The soil is assumed to obey the advanced Mohr-Coulomb yield criterion. The soil properties used are listed in Table 1.
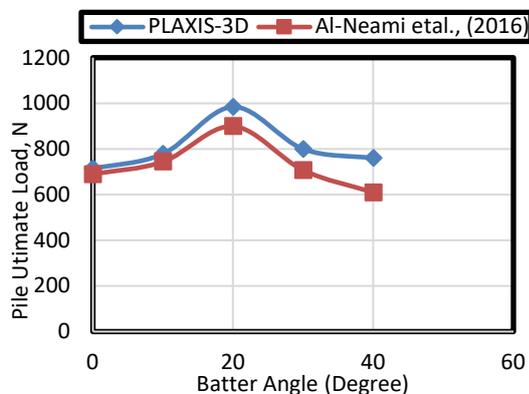
Figure 2. Validation of the result obtained from PLAXIS-3D and Al-Neami et al. [6]

TABLE 1. Properties of soil

Parameters	Unit	Loose sand	Medium sand	Dense sand
Relative density, RD	%	40	60	
Dry weight, γ_d	kN/m^3	17.3	18	18.7
Internal friction angle, φ	°	33	37	40
Dilaatancy angle, ψ	°	3	7	10
Young's modulus, E	kN/m^2	10000	20000	30000
Poisson's ratio, μ	-	0.15	0.2	0.25

*assumed values from Budhu [11].

3. 3. Pile Modeling   The pile used in this study is a circular pipe with a 0.4 m diameter, and the corresponding lengths are 10, 20, and 30 m. The pile has been modeled as elastic; where the elastic model describes the pile material. The pipe pile is modeled as closed-ended from top and bottom. The strength reduction factor R_{inter} is assumed to be 0.7 based on the interaction between steel and sand, which ranges from (0.6 - 0.7) depending on the surface roughness of the pile Waterman [10]. The input parameters of the pile in PLAXIS 3D analysis are listed in Table 2.

3. 4. Geometry and Boundary Conditions   The testing box geometry was constructed by dimensions of 60 m x 60 m in the x-axis and y-axis. The soil layer's top boundary is at a depth of z equals zero, while the soil layer's bottom boundary is at a depth of z = 40 m, then the soil characteristics were identified as the soil block. The simulation is performed under drained conditions where the phreatic level is kept at the bottom of the soil.

4. MESH GENERATION

Mesh is a term used to describe a collection of finite elements. PLAXIS allows for a fully automatic generation of finite element mesh. So to acquire precise numerical results, the mesh should be fine enough. Extremely fine meshes must be avoided because they would result in excessive calculation. To perform the finite element computations in this numerical study; the geometry of the model was divided into the numbers of finite elements to be fully defined. The soil elements of the 3D-finite element mesh are the 10-node tetrahedral elements. Figure 3 shows the soil model, pile geometry, and mesh generated in PLAXIS 3D.

5. RESULT AND DISCUSSION

5. 1. Single Pile Load-Displacement Curve The ultimate axial pullout load of vertical and batter pile was obtained from load-displacement curves. The

TABLE 2. Properties of the pile

Parameters	Unit	Value
Material type	-	Steel
Diameter, D	m	0.4
Wall thickness, t	m	0.01
Unit weight,	kN/m^3	78
Young's modulus, E	kN/m^2	200x10^6
Poisson's ratio	-	0.3
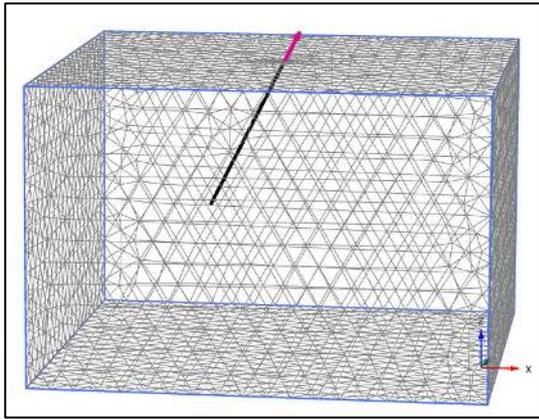
Figure 3. 3D FE mesh for soil and pile

Figure 4. Load-displacement curve for vertical and batter pile under different embedment ratio in loose sand RD = 40%

ultimate pullout capacity of the pile is obtained from the load-displacement curve as 10% D (Where D is the pile diameter). Figures 4-6 show the axial pullout load versus displacement for piles having different L/D ratios for different batter angles in soil with different relative densities.

5. 2. Effect of Pile Batter Angle   The effect of battered angle (α) on the ultimate pullout load capacity is investigated through a selection of vertical and inclined piles with angles (10°, 20°, 30°, 40°) installed in the

Figure 5. Load-displacement curve for vertical and batter pile under different embedment ratio in medium sand RD = 60%
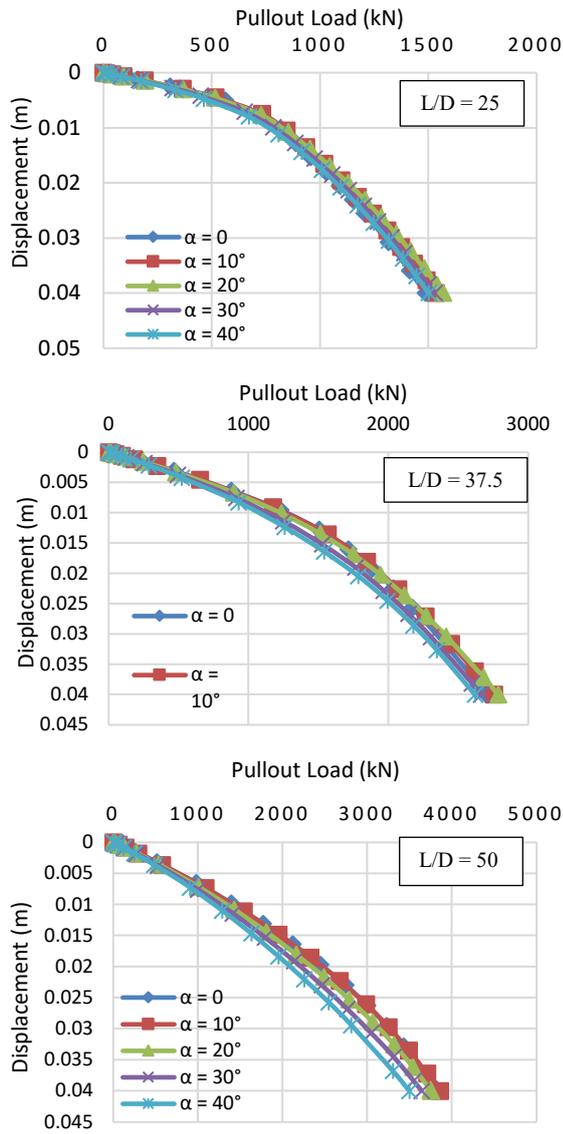
Figure 6. Load-displacement curve for vertical and batter pile under different embedment ratio in dense sand RD = 80%

loose, medium, and dense sand with different embedment ratio (L/D) equals 25, 37.5, and 50. Figure 7 shows the variation of the ultimate pullout load with batter angle. It is seen that the ultimate pullout load capacity increases with an increase in batter angle, reaches its maximum value, and then decreases. For piles constructed in loose sand, RD = 40% maximum value is attained at batter angle equal to 10° for all L/D ratios, and it is about 2.6 to 4.5 % higher than that of the vertical pile. For piles constructed in medium and dense sand, the increasing of battered angles increases the pile load capacity until the maximum value is attained at angle 20°, after which the resistance decreases for L/D ratio equal to 25 and 37.5. The increased percentage of the battered pile at 20°

ranges between (3.08-6.67) % higher than that of the vertical piles. Results obtained were close to the finding of Nazir and Nasr [4].

5. 3. Effect of Pile Embedment Ratio   Three different L/D ratios (25, 37.5, and 50) were used to study the effect of the pile embedment ratio of vertical and batter piles. Figure 8 gives the relationship between the ultimate pull out capacity and pile embedment ratios L/D with different batter angles at 40%, 60%, and 80% relative densities. The embedment ratio has a major
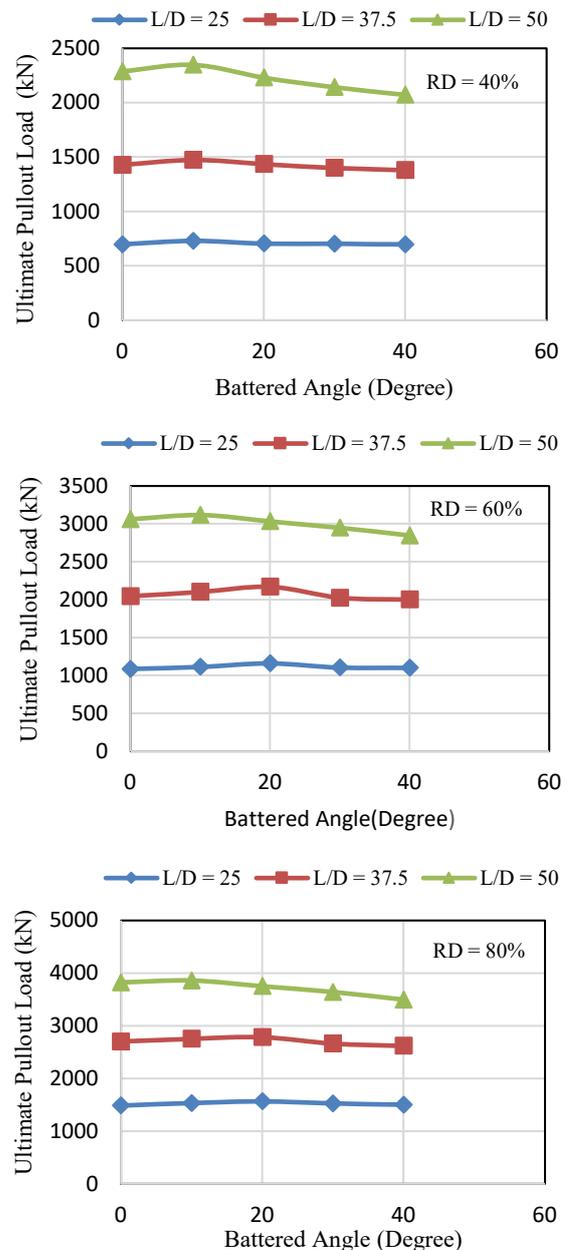
Figure 7. Ultimate pullout load capacity variation with batter angle under different embedment ratios

influence on a single pile's ultimate pull out load capacity. Results obtained were close to the finding of Gaaver's [5].

5. 4. Effect of Relative Density of Sand

Figure 9 shows the ultimate pull out load capacity variation with a batter angle for different sand densities. The figure confirmed that an increase in the relative density improves the ultimate pull out load capacity of vertical and batter piles for all L/D values.

When the relative density of sand increases from 40% to 60%, the ultimate pulls out load capacity increases by
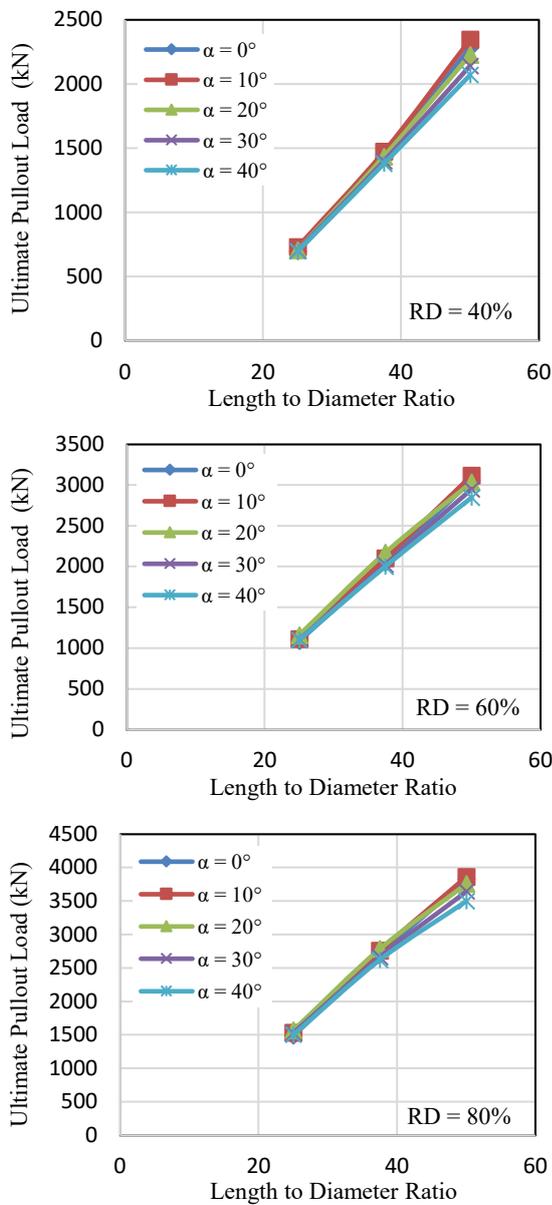
Figure 8. Ultimate pullout load capacity with length to diameter ratio under different batter angles
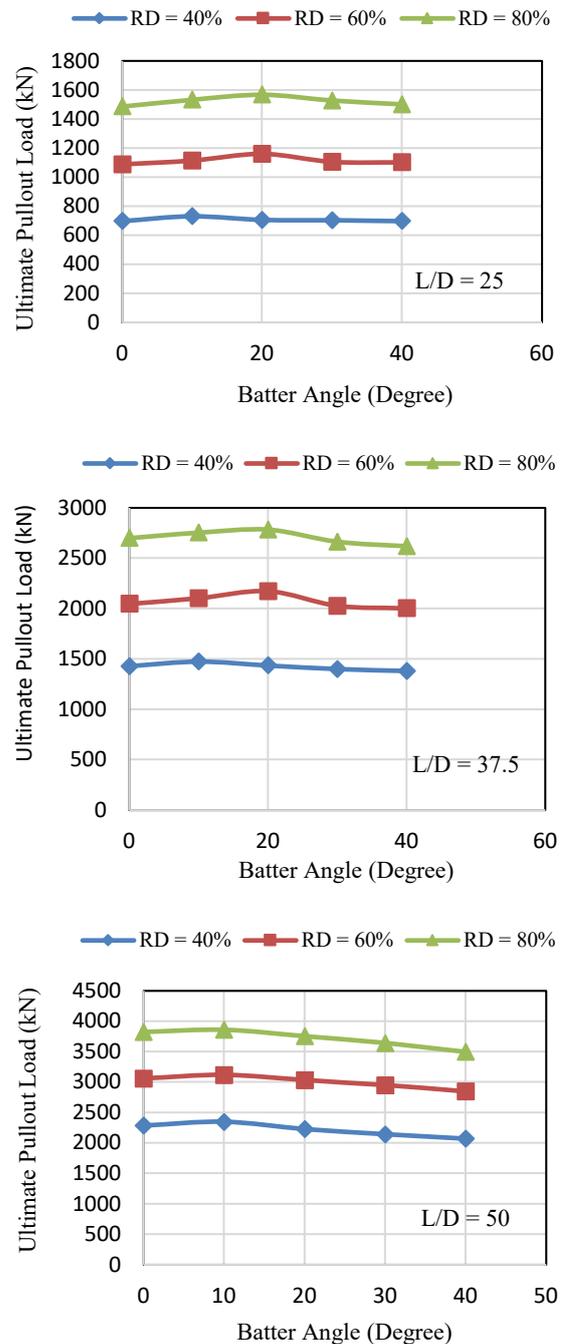
Figure 9. Ultimate pullout load capacity variation with batter angle under different relative densities

about 34-56% for vertical pile and 36-64% for battered pile at angle 20°. When the relative density of sand increases from 40% to 80%, the ultimate pulls out load capacity improves by 67-112% for vertical piles, and 68-122% for batter piles at an angle of 20°. When relative density increases, the angle of friction between the soil

and pile increases, and thus, the effective stress and skin friction also increase. These results are conjugated with Al-Neami et al. [6] results.

5. 5. Effect of Free-Standing Length   Free-standing of the pile (unsupported pile length) is the pile height above the ground level, in which the pile cap doesn't in contact with the underlying soil. The effect of free-standing length e on the ultimate pull out load capacity has been studied for single vertical and batter piles. PLAXIS 3D model has built for the sandy soil of 80% relative density; the pile length has kept a constant and equal to 15m, while the free-standing length was varied (e = 0.0, 10 cm, and 20 cm) as shown in Figure 10.

Figure 11 shows the ultimate pull out load capacity variation with the free-standing length for different batter pile angles.

It can be found that the vertical pile at zero free-standing has a higher ultimate pull out load capacity, while for batter piles, the pull out load is the highest at the batter angle of 20° and the free-standing length is zero. After which, the pull out load starts decreasing with an increase in the free-standing length. When the angle of inclination reaches more than 20° (30° or 40°), it can be noticed that the pull out load decreases at zero free-standing, and when the (e) increases to 0.1 m, the pull out load increases, then it shows a slight decrease at 10cm e.
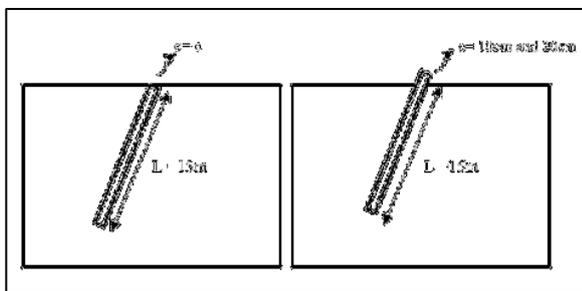

Figure 10. Free-standing length, e.
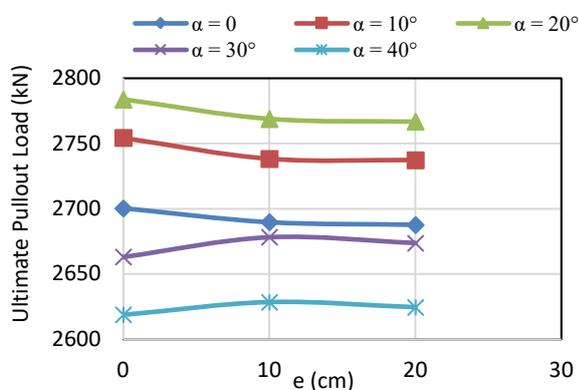
Figure 11. Variation of ultimate pull-out load capacity with free-standing length, RD = 80%

This behavior is attributed to the surrounding soil that will provide sufficient support to the embedded pile. Therefore, the free-standing slightly affects ultimate pull out load capacity due to mobilizing the skin friction.

6. CONCLUSION

This research implicated a 3D FEA to study the influence of several parameters affecting the pullout capacity of battered piles. The overall results may be ordered as follows:
1. The ultimate pullout load capacity of a single battered pile increases with an increase in batter angle α, reaches its maximum value, and then decreases. The maximum value of ultimate pullout load capacity corresponds to batter angle α, dependent on the relative density of soil and the length to diameter ratio L/D of the pile.
2. For piles constructed in loose sand, the batter angle that equal to 10° has the highest pullout load capacity for all L/D ratios, and it is about 2.6 to 4.5 % higher than that of the vertical pile
3. In medium and dense sand with a slenderness ratio equal to 25 and 37.5, the ultimate pullout load value is at a battered angle of 20°. While for batter pile with L/D equal to 50, the ultimate value is at 10°.
4. The increse in the ultimate pullout load capacity with increasing the pile inclination angle has occurred as a result of the interfacial bonding effect due to the increase of the friction angle between the pile shaft and surrounding soil.
5. The slenderness ratio influences the ultimate pullout load resistance of vertical and battered piles; the increase of ultimate uplift capacity when L/D increased from 25 to 50 was approximately doubled.
6. The ultimate pullout capacity of vertical pile bent in loose sand was increased about 227% when the L/D was increased from 25 to 50, while in dense sand, the increase in ultimate pullout capacity was 157%.
7. The increase in ultimate pullout capacity with an increased L/D ratio is due to the increase in the skin friction resistance between the soil and the pile; when the slenderness ratio increases, the shaft resistance increases. The increase in the shaft resistance is due to the increase in the overburden pressure with the slenderness ratio generates the horizontal earth pressure that acts as a normal force on the pile shaft.
8. The relative density has an impact on the ultimate resistance pullout load capacity of vertical and battered piles. When the relative density of sand increases from 40 % to 60%, the ultimate pullout capacity increases by about 34-56% for vertical pile and 36-64% for battered pile at an angle of 20°.

When the relative density of sand increases from 40% to 80%, the ultimate pullout capacity improves by 67-112% for vertical piles and 68-122% for batter piles at an angle of 20°.

9. The relative density of sand greatly affects the ultimate load pullout capacity. When relative density increases, the friction angle between the pile and soil increases, and thus, the effective stress and skin friction also increase.

10. Vertical and batter pile at a battered angle (10° and 20°) and free-standing lengths equal to zero have higher ultimate pullout capacity; by increasing the free-standing length, the ultimate pull-out capacity decreased. This behavior is attributed to the surrounding soil that will provide sufficient support to the embedded pile. Therefore, the free-standing slightly affects ultimate pullout load capacity due to mobilizing the skin friction.

11. The ultimate pullout load capacity of the battered pile was less affected by the free-standing length.

7. REFERENCES

1. Zhang, L., McVay, M., and Lai, P., "Centrifuge modelling of laterally loaded single battered piles in sands". *Canadian Geotechnical Journal*, Vol. 36, No. 6, (1999), 1074-1084. https://doi.org/10.1139/t99-072

2. Bose, K., and Krishnan, A. "Pullout capacity of model piles in sand". *Indian Geotechnical Society Chennai Chapter*, *Student Competition Paper*, (2009), 49-54.

3. Rahimi, M., and Bargi, K., "Efficient arrangement of batter piles of a pile-supported wharf in the sand", *Electronic Journal of Geotechnical Engineering*, Vol. 15 (2010), 729-738. http://dx.doi.org/10.28991/HEF-2021-02-03-010

4. Nazir, A., and Nasr, A. "Pullout capacity of batter pile in sand". *Journal of Advanced Research,* Vol. 2, (2013), 147-154. https://doi.org/10.1016/j.jare.2012.04.001

5. Gaaver, K. "Uplift capacity of single piles and pile groups embedded in cohesionless soil". *Alexandria Engineering Journal,* Vol. 52, No. 3, (2013), 365-372, https://doi.org/10.1016/j.aej.2013.01.00.

6. Al-Neami, M. Rahil, F., and Al-Bayati, K., "Bearing capacity of batter piles embedded in sandy soil". *International Journal of Geotechnical Engineering*, Vol. 10, No. 5, (2016), 529-532, https://doi.org/10.1080/19386362.2016.1203094.

7. Teklearegay, W., "Numerical Investigation of Single Batter pile Due to Inclined Loads". AAU Institutional Repository, (2020). http://etd.aau.edu.et/handle/123456789/23542

8. Vali, R. "Water Table Effects on the Behaviors of the Reinforced Maine Soil-footing Systems". *Journal of Human, Earth, and Future*, Vol. 2, No. 3, (2021), 296-305. http://dx.doi.org/10.28991/HEF-2021-02-03-09

9. Russo, G., Marone, G., and Di Girolamo, L., "Hybrid Energy Piles as a Smart and Sustainable Foundation". *Journal of Human, Earth, and Future*, Vol. 2, No. 3, (2021), 306-322. http://dx.doi.org/10.28991/HEF-2021-02-03-010

10. Waterman, D., "Structural elements and excavations". Presentation in CG1 Chile, (2006).

11. Budhu, M. "Soil mechanics and foundations" Wiley, No. 1, (2020).

Persian Abstract

چکیده

شمع های خمیر شمع هایی هستند که در خاک با شیب عمودی رانده می شوند تا بارهای مورب یا بارهای افقی بزرگ را تحمل کنند و به طور گسترده برای حمایت از ساختمان های مرتفع، ساختمان های فراساحلی و پل ها استفاده می شوند. این سازه‌ها به دلیل قرار گرفتن در معرض لحظات و واژگونی ناشی از باد، امواج و برخورد کشتی خطرناک هستند. یک FEA سه بعدی با استفاده از نرم افزار PLAXIS 3D برای بررسی اثر چندین متغیر که بر رفتار شمع های خمیر منفرد تحت بارهای کششی تأثیر می گذارد، استفاده شد. این مطالعه بر روی یک مدل شمع لوله فولادی تعبیه شده در خاک شنی خشک با سه تراکم نسبی (سست، متوسط و متراکم) در زوایای شیب مختلف و سه نسبت تعبیه، L/D به ترتیب ۲۵، ۳۷.۵ و ۵۰ به دست آمد. نتایج عددی نشان داد که مقاومت نهایی شمع ضربه‌خورده با افزایش زاویه ضربه خورده به یک مقدار حداکثر می‌رسد و سپس کاهش می‌یابد. ظرفیت بارکشی نهایی یک شمع کوبیده شده مستقیماً با نسبت باریکی و چگالی نسبی متناسب است. بار کشش نهایی با افزایش نسبت باریکی و چگالی نسبی افزایش می یابد. بار بالابر نهایی شمع ضربه خورده کمتر تحت تأثیر طول ایستاده آزاد قرار گرفت. شمع‌های عمودی و ضربه‌خورده با زاویه ضربه‌خورده (۱۰ و ۲۰ درجه) و طول‌های ایستاده برابر با صفر ظرفیت بیرون‌کشی نهایی بالاتری دارند. با افزایش طول ایستادن، ظرفیت خروجی نهایی کاهش یافت.

International Journal of Engineering

Investigation of Carbon Black/ Polyester Micro-composites: An Insight into Nano-size Interfacial Interactions

M. Karevan*

Department of Mechanical Engineering, Isfahan University of Technology, Isfahan, 84156-83111, Iran

P A P E R I N F O	*A B S T R A C T*
	In the micro/nanomaterial reinforced composites, interfacial interactions at the interface of filler/polymer lead to the formation of a third layer called interphase as the secondary reinforcing mechanism. The interphase may be formed due to local adsorption of polymer chains at the interface, mechanical interlocking, and interdiffusion of polymer chains. Since the interactions govern the load transfer at the filler/polymer interface, they play a key role in the mechanical response of reinforced composites. However, there exist only a few well-established and validated studies in the description of the interfacial interactions presented in thermosetting composites. This research aims at the understanding of correlations amongst the mechanical properties of thermosetting polyester composites reinforced with 0-15 wt. % of carbon black (CB) focusing on the nano-size cooperative rearranging region (CRR). To estimate the length of CRR, thermal analysis of the variations in the specific heat capacity or the relaxation strength within the glass transition temperature (T_g) range was measured using a thermodynamic model. A nano-size CRR of 10 nm on average was estimated and correlated to the enhanced impact and toughness behavior of the specimens. The results suggested the presence of softer interphase based on the T_g values influenced by the CBs agglomeration level and cross-linking density, which in turn governs the mechanical response of the composites. The methodology introduced in this study can be used in the explanation of changes in mechanical and physical properties of reinforced composites with a focus on the underlying role of nano-size interfacial interactions. *doi: 10.5829/ije.2022.35.06c.05*

NOMENCLATURE

ΔC_p	Calorimetric relaxation strength (J/K.g)	V_α	The volume of the CRR (nm³)
CI	Crystalline index	K_B	The Boltzman constant (1.380649×10^{-23} J/K)
CRR	The cooperative rearranging region (nm)	**Greek Symbols**	
C_v	Specific heat capacity (J/K.g)	ρ	Density (g/cm³)
P.I	Peak intensity	θ	Half of XRD characteristic peak (°)
T_g	Glass transition temperature (°C)	δ	The characteristic length of the glass transition (nm)

1. INTRODUCTION

The interfacial interactions govern the polymer properties at or near the interface between the filler and polymer resulting in the creation of an interfacial zone or "interphase" [1, 2]. The modified interfacial chains control communication between fillers and polymer chains away from the filler surface and have chemical, physical, microstructural, and mechanical properties other than those of the composite constituents [3].

Interfacial interactions may be governed by the thermodynamic compatibility and the chemical affinity of the reinforcement and polymer, the dispersion/distribution quality of fillers, crystallization characteristics of the matrix, and the processing technique used. The latter is reported to govern overall performance of thermosetting parts filled with

Corresponding Author Institutional Email: mkarevan@iut.ac.ir
(M. Karevan)

micro/nano-reinforcements [4, 5]. It has been reported that the higher the strength of the interfacial interactions, the greater the level of fillers dispersion [6]. The higher degree of dispersion means the existence of greater reinforcing sites, stronger filler/polymer adhesion and thus more enhanced mechanical properties of composites. The latter may be also resulted from hindering deformation and shearing of polymer chains around the filler.

The main challenge is that weak interfacial interaction cannot be avoided due to the tendency of fillers to agglomerate leading to a significant decrease in the mechanical and electrical properties compared to the initial expectations and predicting elastic models that fail due to wrong assumptions regarding the filler/polymer bonding [7, 8]. Although surface modifications or applying high shear force during the dispersion state in the fabrication of micro/nanocomposites have been widely used, a useful tool to better understand the formation and changes in the extent of the interfacial interactions is still needed. This is in particular of higher importance when considering effect particles agglomeration/dispersion and the need for advanced methods in the qualification or quantification of the interactions [9, 10]. For instance, characterization techniques such as the atomic force microscopy and nano-indentation not only can be considered as rather expensive and time-consuming method and high level of skills, but also these methods cannot estimate the representative thickness of interphase through the composite bulk [11].

Methods such as Raman spectroscopy, FTIR spectroscopy and X-ray photoelectron spectroscopy (XPS) have been also reported as those useful in the characterization of the interphase [12, 13]. However, such methods normally are not able to give quantitative data about the size/geometry of the interphase. Scanning electron microscopy (SEM) and transmission electron microscopy (TEM) provide qualitative information, too [14]. The presence of agglomeration has been widely reported to unfavorably influence the overall mechanical response of composites, too [15, 16]. The latter is believed to directly affect the strength of interfacial interaction due mainly to the attractive nature of particles when their hydrophobicity differs from that of the parent matrix. Although numerous studies have reported the effect of carbon-based fillers on the mechanical properties of polymeric composites [17, 18], less research has been conducted on the correlations among the mechanical behavior and the interfacial interaction at the filler/polymer and in particular in the case of thermosetting composites [19, 20].

This research emphasizes the characterization of mechanical performance including the tensile response, impact resistance and toughness and thermal behavior of polyester composites reinforced CB followed by the quantification of the interphase represented by the cooperative rearranging region (CRR). The CRR was estimated using a thermodynamic model through variations of the specific heat capacity or the calorimetric relaxation strength (ΔC_p) of the composites over the glass transition temperature (T_g) [21]. The findings were further correlated with the microstructure of the composites to better understand the role of CRR on the mechanical response of the fabricated CB reinforced composite parts. The hypothesis is that the interfacial interactions govern the degree of interfacial bonding and thus the T_g and mechanical performance of the composites [22]. The current study could open up a novel methodology more specifically in the case of thermosetting matrices to quantify the interfacial polymer chains of modified properties linked to the bulk behavior of micro/nano reinforced polymeric composites.

2. EXPERIMENTAL

2. 1. Material For fabrication of CB/Polyester composites, industrial-grade CB was used as the reinforcement purchased from Doodeh Sanati Pars Co. (Iran). The CB used is a black powder with particle size estimated from the scanning electron microscopy (SEM) method to be ~ 5 μm and a density of ~ 1.7 g/cm³. An industrial-grade polyester thermoset resin with clear appearance was provided by a local supplier and used as the base polymer matrix. The resin components of hardener and catalyst were used as described by the manufacturer. The curing time of the resin used appeared to be around 20-30 min depending on the catalyst ratio.

2. 2. Fabrication of CB/Polyester Micro-composites Composites of CB/Polyester reinforced with 0 to 10 wt. % of CB were prepared using
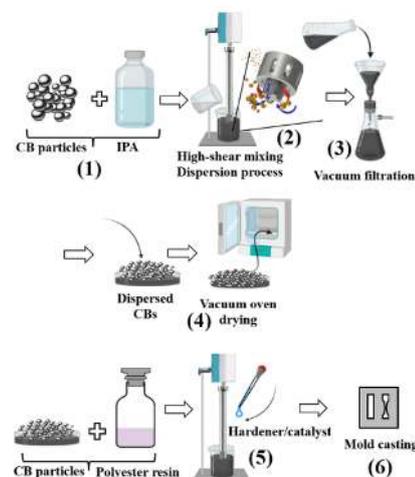
Figure 1. Schematic of CB/polyester composites fabrication route from the mixing to mold casting step

direct mixing of CB within the resin utilizing a high shear mixer at the rpm of 3000 for 15 minutes. The CB particles initially were dispersed within isopropyl alcohol and then vacuum filtered. The CB particles were collected and vacuum dried at 80 ℃ and 8h to ensure removal of the residual IPA and water. To fabricate the polyester based microcomposites, a given wt. % of CB from 0 to 15 wt. % was added into the resin part of the polyester and mixed using a high shear mixer at the rpm of 3000 for 30 minutes. Then, the two-phase compound was mixed with the catalyst and hardener phases as prescribed by the maufacturer. The mixture of resin/hardener/catalyst and CB was then cast into cavities of silicon molds using a mold release agent following the respective standards as required for mechanical behavior characterization with the curing process at the ambient condition. Figure 1 represents the fabrication route used in this study from step 1 (mixing) to 6 (mold casting) as described in details earlier. The same fabricated samples were used for the X-ray diffraction (XRD), scanning electron microscopy (SEM) and differential scanning calorimetry (DSC) analysis.

2. 3. Characterization of CB/Polyester Micro-composites

2. 3. 1. Mechanical Response of CB/Polyester composites
Tensile response of the composites including the Young' modulus, tensile strength and strain at break of composites was determined per the ASTM D638 test method using a universal tensile testing machine (Sanaf Co., Iran). The testing was run using typeV specimens with 3.2 mm thickness with a gage length of 10 mm. Three tensile test specimens were used in the case of each composite system and at least average of two specimens were reported. Measurements were conducted at the deformation rate (stroke speed) of 2.54 mm/min at room temperature. The apparatus used applies tensile loading on the specimen fixed within the grippers measuring force (Newton) versus displacement (mm) until the specimens break. The Izod impact resistance of the specimens was measured per ASTM D256 to understand the effect of the addition of CB particles on the impact performance of the specimens. A homemade loadcell was utilized to conduct testing of the energy absorption of the composites based on the elastic stored energy concerning the initial potential energy of a dropped weight.

2. 3. 2. Thermal Analysis of Micro-composites
The thermal properties of the composites including the T_g and calorimetric relaxation strength were characterized using DSC (Sanaf Co., Iran) utilizing a temperature ramp-up to 200 ℃ with the rate of 10 ℃/min to determine the effect of the addition of fillers on the thermal response and the interfacial characteristics around the reinforcement phase. To provide the DSC test conditions, small material masses, ranging between 10 and 15 mg, were cut from each composite specimen and analyzed using aluminum pans.

2. 3. 3. Microstructural and Morphological Studies
The SEM method was used to assess the morphology of the fractured surface of the fabricated composites including the dispersion quality and microstructural properties of the fracture surface of the samples. The surface of the CB reinforced composites was gold-sputtered before the SEM analysis to ensure the absence of charging effects on the non-conductive fractured surface. The XRD technique was performed to examine the structure of CB reinforced composites and the dispersion quality of the CB within the polyester composites. The XRD analysis was performed using an XRD machine with a Cu Kα radiation source (λ= 1.5406 Å) generating X-rays on the incident beam monochromator setting. The specimens were scanned in the 2θ range from 5° to 70° with a 0.05° step size. The X-ray equipment was operated at 45 KV and 40 mA.

3. RESULTS AND DISCUSSION

3. 1. Mechanical Response of CB/Polyester Micro-composites
Figure 2 depicts the changes in the tensile Young's modulus and tensile strength of the composites as a function of the filler content as previously reported in our studies elsewhere. It can be understood from the results that generally the tensile strength of the parts decreases with the addition of fillers whilst the modulus increases up to an optimized value of the filler content (Figures 2a and 1b, respectively). It is hypothesized that the decrease in the strength might be attributed to the presence of a weaker (softer) interfacial CB/polymer zone so far called interphase and agglomerated regions that will be discussed in the current study. Other factors are thought to be contributing to the decreased tensile strength such as the lower possibility of crosslinking among the polyester monomers and, thus, lowered crosslink density [23]. Moreover, it is believed that the presence of defects including the bubble formed during the processing stage might be a key factor that unfavorably influences the tensile strength of the composites. The findings are in good agreement with results reported elsewhere [24]. Further studies were performed to better support the variations in the tensile response of the composites as described in next sections. The impact resistance of the CB/polyester composites with the addition of filler content is represented in Figure 3. It is realized that with an increase in the CB content, an overall initial improvement in the impact resistance of samples is obtained. The finding could be correlated to the disrupted degree of cross-links formed at the vicinity of the CB particles leading to the presence of weak interphase compared to the stiffness of the pure matrix away from the interfacial surface [25].
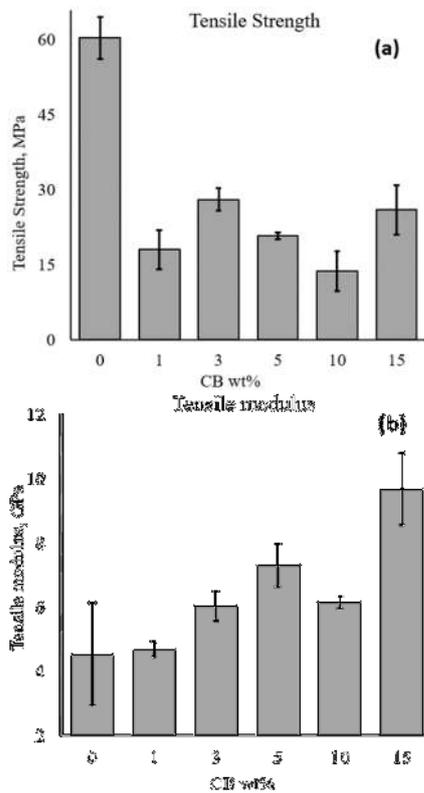
Figure 2. (a) Tensile strength and (b) modulus of the composites as a function of the CB filler content
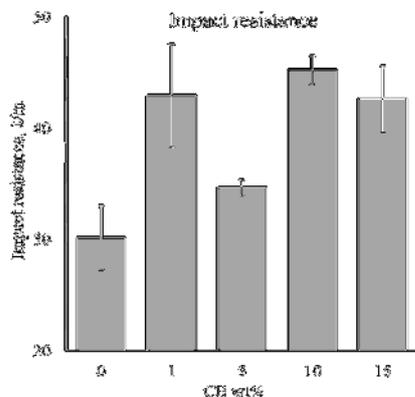
Figure 3. Izod impact resistance of the CB/polyester vs. the filler content

The observed decrease in the impact resistance followed by addition of CB content is further correlated to the formation of competing effects. The inherent stiffness of CB particles normally is believed to decrease the impact behavior of composites. However, as described in the next sections, the generation of softer interphase as a result of poor interfacial interactions and altered degree of cross-links at the vicinity of the fillers contribute to the enhanced impact behavior of the fabricated composites. The findings were further supported by the measured energy absorption of the

composites in the drop weight experiments. An overall enhancement in the absorbed energy is observed upon addition of the CB content.

The increase in toughness properties of the composites is related to the presence of softer interphase and the inherent properties of carbon-based materials in absorbing energy (Table 1) [26]. However, with further addition of the CB beyond 10 wt. % a drop in the toughness of the specimens was noticed. The observed finding could be ascribed to the extensive level of CB agglomeration as described earlier leading to the presence of stress concentration and shear slippage amongst CB fillers due to shortage of polymer chain and, thus, the decrease in wetting ability of polyester [27].

3. 2. Glass Transition Temperature and Interphase Quality   The variations in the Tg of the CB/polyester composites are shown in Table 2. It is sown that the Tg values decrease with an increase in the CB wt. % followed by an increase when the filler content exceeds 10 wt.%. The presence of the weak interphase can be supported by the Tg decrease due mainly to the weaker interfacial interactions or disrupted cross-link density around the surface of the CB [28, 29]. An increase in Tg upon the addition of the greater amount of CB concentration can be correlated to the existence of lower specific surface to volume area of fillers exposed to the polymer matrix leaving a greater amount of polymer network intact due to agglomeration of fillers. It has been shown that the changes in the Tg of polymer composites are strongly related to the extent of the interfacial zone which in turn governs the length of the CRR [30, 31]. To understand the links in the range of the interphase that in the context of polymer composites filled with rigid particles could be correlated to the CRR, the thickness of the CRR was evaluated [3, 21]. It was further released that the changes in the Tg values could be associated with the changes in the crystalline phase as described in the next parts.

3. 3. CRR Estimation as a Measure of Relaxation Strength   The changes in the calorimetric heat capacity of polymeric composites near Tg can be considered as a

TABLE 1. The absorbed energy of the CB reinforced polyester as a function of CB wt.%

Absorbed Energy (J)	Composite system CB wt.%
12.2	0
12.6	1
12.5	3
15	5
15.1	10
12.6	15

TABLE 2. T_g, C_p and calorimetric relaxation strength of the CB/polyester v.s. CB wt.%

T_g (°C)	ΔT_g (°C)	T_g (°C) Liquid	T_g (°C) Solid	ΔC_p ($\frac{J}{g \cdot °C}$)	C_p Final ($\frac{J}{g \cdot °C}$)	C_p Onset ($\frac{J}{g \cdot °C}$)	CB wt. %
65.8	26.4	74.0	47.6	0.054	0.375	0.321	**0**
62.3	17.8	70.5	52.7	0.03	0.307	0.277	**1**
61.2	13.2	70.2	57.0	0.002	0.154	0.152	**3**
61.9	23.6	71.5	47.9	0.046	0.375	0.329	**5**
65.5	16.1	70.6	54.5	0.027	0.331	0.304	**10**
65.7	14.9	72.2	57.3	0.006	0.214	0.208	**15**

key factor in understanding the presence and quantity of the interphase. This effect arises from the fact that upon heating a polymeric specimen, the extent of chains mobility increases over the T_g transition zone. This results in a transitional behavior of reinforced polymers from solid-like to liquid-like state where the C_p of the specimens increases. The immobilized chains therefore exhibit greater C_p values than those restricted at the interface. Table 2 further shows the C_p values together with the calorimetric relaxation strength ΔC_p observed with the addition of the interphase.

The opposite case is also true when the weak interfacial interactions or polymers with the lowered degree of cross-link accommodate a greater region of mobile chains that can easier slide over each other leading to a decrease in the T_g. It has been previously reported that in carbon-based reinforced thermosetting composites, the ratio of hardener/resin is adversely altered resulting in a lower cross-link density at the interface of the filler/polymer. So far, it was already shown that an addition of CB decreased the T_g values that could be correlated with the extent of the generated CRR. The CRRs have been explained as the cooperative dynamics that predict the length of the immobilized region so far called the interphase and are highly correlated to the specific heat capacity (C_p) before and after T_g as mentioned earlier. In the current study, a model first introduced by Donth [21] was used to estimate the CRRs length using the changes in the heat capacity from solid to liquid behavior of CB/polyester around the T_g of the fabricated parts on the bases of the DSC thermograms obtained over the heating scan of the specimens (Equations (1) and (2)):

$$V_\alpha = \frac{\Delta\left(\frac{1}{C_v}\right)}{\rho(\delta T)^2} K_B T^2 \tag{1}$$

$$\delta = \sqrt[3]{V_\alpha} \tag{2}$$

where V_α is the volume of the cooperative region, C_v is the specific heat capacity, ρ is the density of the specimen, K_B is the Boltzman constant, δ is temperature fluctuation, and δ is the characteristic length of the glass

transition. Table 3 displays the changes in the nano-size CRR namely the representative of the interphase thickness with the addition of the CB content. It is illustrated that the CRR length increases at 1 wt. % of CB concerning that in the case of pure polymer. Nevertheless, the length of CRR starts decreasing upon by addition of 15 wt. % of fillers. As previously shown through the changes in Tg values, when the CB loading grows, the presence of agglomeration results in suppressed filler/polymer interaction as the effective CB/polyester interface decreases. The latter is clearly confirmed by the decrease in the CRR length (Table 3). The CRR predicted in the pure matrix is related to the presence of softer interphase or/and weaker bonding around the harder region regardless of the presence of any fillers. The latter can be related the loose packing perfection of the polymer chains under the unfavourable effect of the weak interactions. Further decrease followed by the addition CB wt. % is correlated to the presence of agglomeration contributing to lower surface area of fillers. As expected, with an addition of CB wt.% beyond 3 wt.%, the increased specific surface of the fillers overcomes the adverse effect of the agglomeration phase. The observed results are in good agreement with the changes in Tg confirming weaker CB/polymer adhesion and interfacial interaction against imperfect interfacial bonding or destroyed cross links.

It is noted that the lower CRR corresponds to an overall lower effect of fillers surface interaction from the interfacial polymer to regions away from this surface [32]. The results further confirm the improvement in the tensile modulus is associated with the inherent properties of CBs, which overcomes the effect of softer interphase than polyester [33]. In opposite, the enhanced absorbed energy as well as the impact resistance of the specimens upon an increase in the CB content could be thought of the growing amount of soft interphase as expected.

It should be noted that the picture of interfacial interactions in the case of thermosetting polymers is more complicated due to the presence of a three-dimensional network of polymer chains from the high degree of cross-link. However, the changes in the density of cross-links due to the nano/microscale effect of the

TABLE 3. CRR thickness in nm vs. the CB wt.% in CB/polyester composites

| CRR (δ) (nm)	CB wt. %
9.2	**0**
11.1	**1**
8.4	**3**
9.3	**5**
10.7	**10**
8.83	**15**

interfacial interactions should be taken into account as a key factor altering the cross-links density through the polymer bulk. Another important observation is that the use of thermosetting polymers should fall within the measurement of T_g where the resolution and sensitivity of the thermal device could capture the changes in the C_p. Moreover, whilst the presence of harder interphase may result in the decrease in impact resistance and toughness, this may on the opposite side lead to an enhanced tensile response of the specimens. Therefore, when the application of multi-functional composites comes into account, the optimized values of fillers fraction need to be considered when overall improvement in mechanical properties is desired. The interrelation amongst the structure, filler/polymer adhesion and the filler wt. % with the specific emphasis on the role of interfacial interactions is thus an elemental factor governing the overall properties of reinforced micro/nanocomposites.

3. 4. XRD Microstructural Analysis   The XRD patterns of the CB reinforced composites are represented in Figure 4. The results indicate two main halos associated with the amorphous hill and the crystalline rigid phase. The first peaks appear around $\sim 20^\circ$ and the second peaks are observed $\sim 38^\circ$ to 41° as characteristic peaks of the polyester resin. The results, however, show that with the addition of CB into the polyester resin, the

second peaks disappear at the loading above 10 wt. % reflecting the decrease in the amorphas shoulder as supported with the T_g values observed at higher loadings of CB. The results further confirm there a slight change in the first characteristic angle associated with the first halo with respect that observed in the case of pure polyester [24, 34].

It is suggested that by the addition of filler into the polyester matrix, a rigid interphase forms around the fillers leading to the composites with greater solid-like behavior. The findings are in good agreement with the CRR and T_g values where at the higher CB content greater interactions are present at the interfacial surface of CB/polymer. As understood from the results reported, a little increase in 2θ values of the first halo by the addition of filler concerning that in the case of pure polyester indicates lower d-spacing between the galleries of the crystalline phase showing a more compact (denser) structure of the composites according to the Bragg's law [35]. This finding may explain an increase in the elastic modulus of the parts as an underlying synergistic effect as well as the reinforcing function of the CB particles.

Figure 4 further indicates the characteristic peak of CB occurring $\sim 29.5^\circ$ that is in good agreement with that reported elsewhere in the literature. The summary of the XRD structural analysis is reported in Table 4. It is
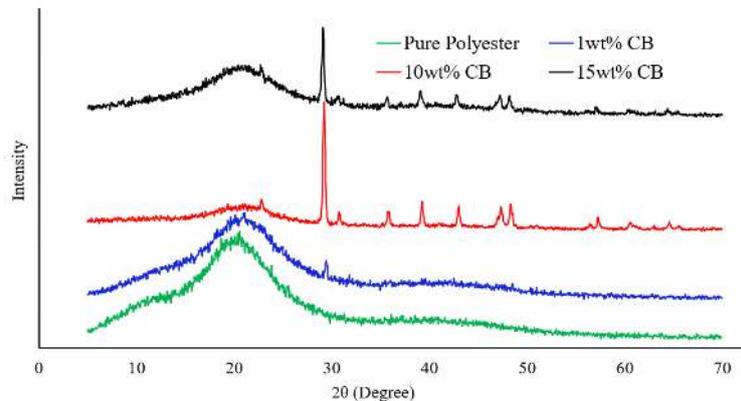
Figure 4. XRD diffraction traces of the CB/polyester composites as a function of the CB wt%

TABLE 4. XRD characteristic peaks, crystalline index and peak intensity of the CB reinforced polyester composites against

Composite system	Polyester							CB	
CB wt. %	$2\theta^{\circ a}$ First Halo	$2\theta^{\circ a}$ Second Halo	P.I^b (a.u) First peak Amorph	P.I^b (a.u) Second peak Amorph	$2\theta^{\circ a}$ Crystal peak	P.I^b (a.u) Crystal peak	CI^c (%)	$2\theta^{\circ a}$	P.I^b (a.u)
0	20.4	38.3	290	40	20.5	493	59	-	-
1	21.3	41.6	223	26	20.6	395	61	29.4	124
10	20.9	41.0	32	32	21.2	74	53	29.2	955
15	20.9	39.7	87	30	20.9	221	65	29.1	680

^{a} 2-theta (degree) ^{b} Peak intensity ^{c} Crystalline Index ^{c} Crystallite size

shown that when the CB filler is incorporated into the polyester, the peak intensity related to the first halo decreases followed by a second increase confirming the presence of the greater amount of rigid phase (so far linked to the crystalline phase). According to Table 4, it is understood that the peak intensity associated with the presence of CB fillers experience an initial increase compared with the neat polyester followed by the decrease in the peak intensity of CB reinforcement. The results are thought off a better dispersion state of the CB within the polyester matrix at the filler loading of 10 wt. %. The latter supports the increase in the CRR values when the greater surface area of the CB particles contributes to more significant immobilized polymer chains around the fillers due to stronger interfacial interactions. This further confirms the increase in Young's modulus, the absorbed energy quality and the impact resistance of the fabricated part at the filler loadings of 10 wt.%. However, the decrease in the absorbed energy of the specimens at the filler content above wt.% could be correlated with the presence of greater fractions of rigid phase resulting in a more brittle nature of the parts as expected. The crystalline index (CI%) of the composites as proposed by Segal et al. [36] as an empirical approach in the determination of the crystallinity is calculated by Equation 3 and reparented in Table 4.

$$CI\% = \frac{P.I_{crystal}}{P.I_{crystal} + P.I_{amorph}} \quad (3)$$

in which $P.I_{amorph}$ and $P.I_{crystal}$ are the peak intensities associated with the amorphous and crystalline phases, respectively. An overall increase is observed in the crystallinity of the fabricated composites with the addition of the fillers as explained earlier (Table 4). However, the decrease in the amount of the crystalline phase at the filler loading of 10 wt.% might be ascribed to the presence of the agglomeration phase or decreased degree of crosslinking density. It is noted that the level of interfacial interaction is also correlated to the number of crystalline rigid phases not the number of crystals as the latter acts mainly as the sites immobilizing the polymer chains movement [3, 37].

3. 4. SEM Microstructural Study of CB/Polyester Composites   Figure 5 represents the SEM images of the fracture surface of pure polyester and composites reinforced with 15 wt.% of CB particles. Figure 5a indicates that there exist complex and greater crack marks on the fractured surface of the 15 wt. % CB reinforced specimen compared to that observed in the case of pure polyester parts. This finding supports the extended number of parallel crack marks when the CB loading increases as previously shown by the decrease in the impact resistance and absorbed energy quality of the composites filled with higher loadings of CB.
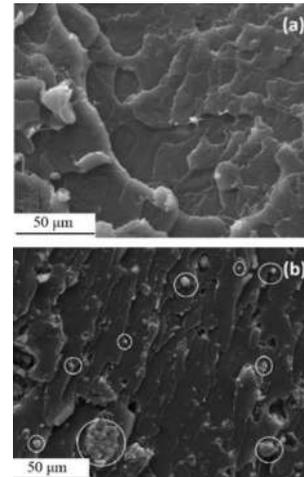
Figure 5. Representative SEM images of (a) pure polyester and (b) CB/polyester composite fracture surface filled with 15 wt.% of CB

The SEM images further indicates he presence of both the dispersed and agglomerated phase of CB particles that contributes to the observed CCR values as well as the mechanical response of the fabricated composites. However, minimal presence of agglomeration is represented confirming the extended values of the relaxation strength released by the thermal analysis. The SEM results further suggest multiple stress concentration sites leading to the observed river crack traces in the reinforced composites.

Although the fractured surface of the neat polyester exhibits a greater plastic deformation, as displayed by the roughness and undulation marks, which in turn shows the greater capability of the pure specimens in the energy absorption, the inherent properties of carbon-based materials provide the reinforced parts with improved toughness against the undesired local stress concentration zones within the composite bulk [34].

4. CONCLUSIONS

To better understand the role of filler/polymer interactions and their correlation with mechanical properties including tensile behavior, impact resistance and energy absorption, composites of thermosetting polyester reinforced with 0 to 15 wt. % of CB were fabricated using shear mixing method followed by silicon mold casting of the CB/resin/hardener composites. The results indicated that the extent of interfacial interactions estimated to be ~10 nm highly governs the thermal and mechanical properties of the composites. It was revealed that the weaker strength of interaction as a result of suppressed cross-links leads to lower Tg values and calorimetric ΔCp contributing to a smaller length of nano-size CRR. The improved mechanical properties

including the impact resistance and energy-absorbing behavior were linked to the weaker interfacial bonding and, thus, the presence of softer interphase as the damping phase. The results further suggested the adverse effect of the agglomeration phase on the decrease in the tensile strength and the lower amount of generated interphase at higher fillers ratio up to 10 wt.% of CBs as shown by the changes in the Tg values of the composites.

5.REFERENCES

1. Zare, Y. and Rhee, K.Y., "Study on the effects of the interphase region on the network properties in polymer carbon nanotube nanocomposites", *Polymers*, Vol. 12, No. 1, (2020), 182. doi: 10.3390/polym12020404.

2. Irzhak, V., "The interphase layer in polymer nanocomposites", *Polymer Science, Series C*, Vol. 62, No. 1, (2020), 51-61. doi: 10.1134/S1811238220010038.

3. Karevan, M. and Kalaitzidou, K., "Formation of a complex constrained region at the graphite nanoplatelets-polyamide 12 interface", *Polymer*, Vol. 54, No. 14, (2013), 3691-3698. doi: 10.1016/j.polymer.2013.05.019.

4. Saindane, U.V., Soni, S. and Menghani, J.V., "Friction and wear performance of brake pad and optimization of manufacturing parameters using grey relational analysis", *International Journal of Engineering, Transactions C: Aspects*, Vol. 35, No. 3, (2022), 552-559. doi: 10.5829/ije.2022.35.03C.07.

5. Tajammul, H.M., Gouda, P.S., Siddhalingeshwar, I. and Kodancha, K.G., "Effect of alcoholic treated mwcnt on tensile behavior of epoxy composite", *International Journal of Engineering, Science and Technology*, Vol. 8, No. 1, (2016), 57-63. doi: 10.4314/ijest.v8i1.5.

6. Wan, C. and Chen, B., "Reinforcement and interphase of polymer/graphene oxide nanocomposites", *Journal of Materials Chemistry*, Vol. 22, No. 8, (2012), 3637-3646. doi: 10.1039/C2JM15062J.

7. Govorov, A., Wentzel, D., Miller, S., Kanaan, A. and Sevostianov, I., "Electrical conductivity of epoxy-graphene and epoxy-carbon nanofibers composites subjected to compressive loading", *International Journal of Engineering Science*, Vol. 123, (2018), 174-180. doi: 10.1016/j.ijengsci.2017.11.014.

8. Faghidian, S.A., Żur, K.K. and Reddy, J.N., "A mixed variational framework for higher-order unified gradient elasticity", *International Journal of Engineering Science*, Vol. 170, (2022), 103603. doi: 10.1016/j.ijengsci.2021.103603.

9. Xia, X., Weng, G.J., Hou, D. and Wen, W., "Tailoring the frequency-dependent electrical conductivity and dielectric permittivity of cnt-polymer nanocomposites with nanosized particles", *International Journal of Engineering Science*, Vol. 142, (2019), 1-19. doi.

10. Pant, G., "Analysis of properties of polymer nanocomposites on the basis of nature of interphase property variation", *Materials Today: Proceedings*, Vol. 25, (2020), 893-897. doi: 10.1016/j.matpr.2019.12.207.

11. Watcharotone, S., Wood, C.D., Friedrich, R., Chen, X., Qiao, R., Putz, K. and Brinson, L.C., "Interfacial and substrate effects on local elastic properties of polymers using coupled experiments and modeling of nanoindentation", *Advanced Engineering Materials*, Vol. 13, No. 5, (2011), 400-404. doi: 10.1002/adem.201000277.

12. Gwon, J.G., Lee, S.Y., Doh, G.H. and Kim, J.H., "Characterization of chemically modified wood fibers using ftir

spectroscopy for biocomposites", *Journal of Applied Polymer Science*, Vol. 116, No. 6, (2010), 3212-3219.

13. Sun, N., Ji, R., Zhang, F., Song, X., Xie, A., Liu, J., Zhang, M., Niu, L. and Zhang, S., "Structural evolution in poly (acrylic-co-acrylamide) ph-responsive hydrogels by low-field nmr", *Materials Today Communications*, Vol. 22, (2020), 100748. doi: 10.1016/j.mtcomm.2019.100748.

14. Barber, A.H., Cohen, S.R. and Wagner, H.D., "Measurement of carbon nanotube–polymer interfacial strength", *Applied Physics Letters*, Vol. 82, No. 23, (2003), 4140-4142.

15. Sheikh, K. and Shahrajabian, H., "Experimental study on mechanical, thermal and antibacterial properties of hybrid nanocomposites of PLA/CNF/AG", *International Journal of Engineering, Transactions B: Applications*, Vol. 34, No. 2, (2021), 500-507. doi: 10.5829/ije.2021.34.02b.23.

16. Yudhanto, F., Jamasri, J., Rochardjo, H. and Kusumaatmaja, A., "Experimental study of polyvinyl alcohol nanocomposite film reinforced by cellulose nanofibers from agave cantala", *International Journal of Engineering, Transactions A: Basics*, Vol. 34, No. 4, (2021), 987-998. doi: 0.5829/ije.2021.34.04a.25.

17. Saindane, U.V., Soni, S. and Menghani, J.V., "Dry sliding behavior of carbon-based brake pad materials", *International Journal of Engineering, Transactions B: Applications*, Vol. 34, No. 11, (2021), 2517-2524. doi: 10.5829/ije.2021.34.11b.14.

18. Jesthi, D., Nayak, A., Routara, B. and Nayak, R., "Evaluation of mechanical and tribological properties of glass/carbon fiber reinforced polymer hybrid composite", *International Journal of Engineering*, Vol. 31, No. 7, (2018), 1088-1094. doi: 10.5829/ije.2018.31.07a.12.

19. Bagheri, R., Peason, R. and Marouf, B., "Modeling of stiffening and strengthening in nano-layered silicate/epoxy (research note)", *International Journal of Engineering, Transactions A: Basics*, Vol. 30, No. 1, (2017), 93-100. doi: 10.5829/idosi.ije.2017.30.01a.12

20. Saindane, U.V., Soni, S. and Menghani, J.V., "Recent research status on synthesis and characterization of natural fibers reinforced polymer composites and modern friction materials–an overview", *Materials Today: Proceedings*, Vol. 26, (2020), 1616-1620. doi: 10.1016/j.matpr.2020.02.334.

21. Donth, E., "Characteristic length of the glass transition", *Journal of Polymer Science Part B: Polymer Physics*, Vol. 34, No. 17, (1996), 2881-2892. doi: 10.1002/(SICI)1099-0488(199612)34:17<2881::AID-POLB3>3.0.CO;2-U.

22. Zhang, W., Emamy, H., Vargas-Lara, F., Betancourt, B.A.P., Meng, D., Starr, F.W. and Douglas, J.F., The interfacial layers around nanoparticle and its impact on structural relaxation and glass transition in model polymer nanocomposites, in Theory and modeling of polymer nanocomposites. 2021, Springer.101-131. doi: 10.1007/978-3-030-60443-1_5.

23. Kim, B., Choi, J., Yang, S., Yu, S. and Cho, M., "Influence of crosslink density on the interfacial characteristics of epoxy nanocomposites", *Polymer*, Vol. 60, (2015), 186-197. doi: 10.1016/j.polymer.2015.01.043.

24. Alam, M., Islam, M., Mina, M. and Gafur, M., "Structural, mechanical, thermal, and electrical properties of carbon black reinforced polyester resin composites", *Journal of Applied Polymer Science*, Vol. 131, No. 13, (2014).

25. Dong, J., Jia, C., Wang, M., Fang, X., Wei, H., Xie, H., Zhang, T., He, J., Jiang, Z. and Huang, Y., "Improved mechanical properties of carbon fiber-reinforced epoxy composites by growing carbon black on carbon fiber surface", *Composites Science and Technology*, Vol. 149, (2017), 75-80.

26. Chandrasekaran, S., Sato, N., Tölle, F., Mülhaupt, R., Fiedler, B. and Schulte, K., "Fracture toughness and failure mechanism of graphene based epoxy composites", *Composites Science and*

Technology, Vol. 97, (2014), 90-99. doi: 10.1016/j.compscitech.2014.03.014.

27. Ma, P.-C., Mo, S.-Y., Tang, B.-Z. and Kim, J.-K., "Dispersion, interfacial interaction and re-agglomeration of functionalized carbon nanotubes in epoxy composites", *Carbon*, Vol. 48, No. 6, (2010), 1824-1834. doi: 10.1016/j.carbon.2010.01.028.

28. Qiao, R., Deng, H., Putz, K.W. and Brinson, L.C., "Effect of particle agglomeration and interphase on the glass transition temperature of polymer nanocomposites", *Journal of Polymer Science Part B: Polymer Physics*, Vol. 49, No. 10, (2011), 740-748. doi: 10.1002/polb.22236.

29. Rittigstein, P. and Torkelson, J.M., "Polymer–nanoparticle interfacial interactions in polymer nanocomposites: Confinement effects on glass transition temperature and suppression of physical aging", *Journal of Polymer Science Part B: Polymer Physics*, Vol. 44, No. 20, (2006), 2935-2943. doi: 10.1002/polb.20925.

30. Kim, J.-K. and Hodzic, A., "Nanoscale characterisation of thickness and properties of interphase in polymer matrix composites", *The Journal of Adhesion*, Vol. 79, No. 4, (2003), 383-414. doi.

31. Lachman, N. and Daniel Wagner, H., "Correlation between interfacial molecular structure and mechanics in cnt/epoxy nano-composites", *Composites Part A: Applied Science and Manufacturing*, Vol. 41, No. 9, (2010), 1093-1098. doi.

32. Seiler, J. and Kindersberger, J., "Insight into the interphase in polymer nanocomposites", *IEEE Transactions on Dielectrics and Electrical Insulation*, Vol. 21, No. 2, (2014), 537-547.

33. Lu, X., Detrez, F., Yvonnet, J. and Bai, J., "Identification of elastic properties of interphase and interface in graphene-polymer nanocomposites by atomistic simulations", *Composites Science and Technology*, Vol. 213, (2021), 108943.

34. Maradini, G.d.S., Oliveira, M.P., Guanaes, G.M.d.S., Passamani, G.Z., Carreira, L.G., Boschetti, W.T.N., Monteiro, S.N., Pereira, A.C. and de Oliveira, B.F., "Characterization of polyester nanocomposites reinforced with conifer fiber cellulose nanocrystals", *Polymers*, Vol. 12, No. 12, (2020), 2838.

35. Chu, B. and Hsiao, B.S., "Small-angle x-ray scattering of polymers", *Chemical Reviews*, Vol. 101, No. 6, (2001), 1727-1762. doi: 10.1021/cr9900376.

36. Segal, L., Creely, J.J., Martin Jr, A. and Conrad, C., "An empirical method for estimating the degree of crystallinity of native cellulose using the x-ray diffractometer", *Textile Research Journal*, Vol. 29, No. 10, (1959), 786-794.

37. Kalaitzidou, K., Fukushima, H., Askeland, P. and Drzal, L., "The nucleating effect of exfoliated graphite nanoplatelets and their influence on the crystal structure and electrical conductivity of polypropylene nanocomposites", *Journal of Materials Science*, Vol. 43, No. 8, (2008), 2895-2907.

Persian Abstract

چکیده

در کامپوزیت های تقویت شده میکرو/نانومواد، برهمکنش‌های سطحی در سطح مشترک پرکننده/پلیمر منجر به تشکیل لایه سومی به نام فازمیانی به عنوان مکانیزم تقویت کننده ثانویه می شود. فاز میانی ممکن است به‌دلیل لایه نشینی سطحی موضعی زنجیره های پلیمری در سطح مشترک، و به هم پیوستگی مکانیکی و انتشار میان زنجیره های پلیمری تشکیل شود. از آنجایی که برهمکنش بر انتقال بار در رابط پرکننده/پلیمر حاکم هستند، نقش کلیدی در پاسخ مکانیکی کامپوزیت های تقویت شده دارند. با این حال، تنها چند مطالعه به خوبی پایه گذاری شده و معتبر در توصیف برهمکنش های سطحی ارائه شده در رابطه با کامپوزیت های ترموست وجود دارد. هدف این تحقیق درک ارتباط بین خواص مکانیکی کامپوزیت‌های پلی‌استر ترموست تقویت‌شده با ۰ تا ۱۵ درصد وزنی کربن سیاه با تمرکز بر منطقه بازآرایی مقید با اندازه نانو (CRR) است. برای تخمین طول CRR، آنالیز حرارتی تغییرات در ظرفیت گرمایی ویژه یا استحکام رهایش مقاومت در ظرفیت گرمایی در محدوده دمای انتقال شیشه‌ای با استفاده از یک مدل ترمودینامیکی اندازه‌گیری شد. یک CRR با اندازه ۱۰ نانومتر به طور متوسط تخمین زده شد که با تاثیر اثر افزایشی در رفتار ضربه‌پذیری و چقرمگی نمونه‌ها مرتبط بود. نتایج حاکی از وجود فازمیانی نرم‌تر بر اساس مقادیر دمای شیشه‌ای تحت تأثیر سطح تجمع ذرات کربن سیاه و چگالی اتصال متقابل است که به نوبه خود پاسخ مکانیکی کامپوزیت‌ها را کنترل می‌کند. روش معرفی شده در این مطالعه را می توان در تبیین تغییرات خواص مکانیکی و فیزیکی کامپوزیت های تقویت شده با تمرکز بر نقش اساسی برهمکنش‌ها در اندازه نانو استفاده کرد.

International Journal of Engineering

Journal Homepage: www.ije.ir

Experimental Investigation Joining Al 5083 and High-density Polyethylen by Protrusion Friction Stir Spot Welding Containing Nanoparticles using Taguchi Method

A. Rafiee*[a], S. Nickabadi[b], M. A. Nobarian[c], H. Tagimalek[d], H. Khatami[a]

[a] Mechanical Engineering Department, Faculty of Engineering, Urmia University, Urmia, Iran
[b] Mechanical Engineering Department, Faculty of Engineering, Guilan University, Guilan, Iran
[c] Mechanical Engineering Department, Tabriz University, Tabriz, Iran
[d] Faculty of Mechanical Engineering, Semnan University, Semnan, Iran

A B S T R A C T

One of the most important challenges of the Friction Stir Spot Welding (FSSW) process is the appearance of a void in the welded parts. This causes the stress to be stacked against the created void, and as a result, the mechanical properties would be reduced. To solve this problem in this research, the aluminum and polyethylene sheets are joined by means of H13 steel tools, protruding fixtures, and also three types of nanoparticles. Appending three types of Nano-particles, namely Al_2O_3, TiO_2, SiO_2, the constituent materials of Al 5083 and high-density polyethylene sheets have been prepared. To improve the mechanical properties of the welded samples, these three types of Nano-materials are integrated to the Stir Zone (SZ). In order to find the maximum strength of welded composite plates, the Design of Experiment (DOE) is performed using the Taguchi method. The Rotation Speed, Dwell Time, Tool d/ Protrusion d besides the type and percentage of Nano-material are chosen as input parameters. The maximum fracture force and the maximum strength are respectively as 2249 N and 4.13 MPa. Without using nanoparticles, a rupture is occurred in the tensile tests of polyethylene samples. Thus, the polyethylene samples capture more sediment by addition of nanoparticles, and the nanoparticles' deposition improves the mechanical properties of the Al/PE composite. Compared to the base material of pure aluminum and polyethylene, a nearly eightfold increment of the mechanical properties of the Al/PE composite sample is observed by addition of nanoparticles in the welding nugget. According to the S/N ratio analysis, the rotation speed of 2500 rpm, dwell time of 12 s, tool d/ protrusion d of 3 mm, Nano-material's type of Sio_2 and percentage of 10% are considered as the optimum states.

doi: 10.5829/ije.2022.35.03c.06

1. INTRODUCTION

Aluminum alloys and high-density polyethylene are very useful materials in various industries [1]. Al 5083 contains 4% magnesium and about 0.25% chromium [2]. The properties of aluminum include excellent corrosion resistance, good fatigue resistance, welding ability and moderate strength [3]. High-density polyethylene belongs to the family of thermoplastic polymer and is used due to its high flexibility and bending ability [4]. The composite joining of these two materials helps different industries to reduce weight and maintain performance. Weight loss is a major challenge in various

industries to maintain performance and reduce fuel consumption [5]. Composites can also be structurally better by compromising between two materials that operate independently. From polymer/metal joints, lighter, safer, less polluting and environmentally friendly products are obtained [6]. FSW welding is a solid-state welding process that was invented in 1991 [7]. In solid-state welding, FSW welding is developing rapidly. It is possible to join non-uniform materials with excellent quality in this process [8]. Protrusion friction stir spot welding (PFSSW) is one of the newest FSW welding methods for eliminating keyhole defects in a pin-less tool with a protrusion in the middle of the fixture [9].

*Corresponding author E-Mail: st_a.rafiei@urmia.ac.ir (A. Rafiei)

Zarghani et al. [10] studied the protrusion friction stir spot welding (PFSSW) on the plates of Al 2024. A pin-less tool and a specially designed fixture (protrusion) have been used with a clamp plate on the surface. The effect dwell time of 6, 12 and 18 seconds were investigated on the microstructure and mechanical properties of samples. The appearance of the welding surface showed that the keyhole would not form and the weld was relatively smooth. Microstructure and mechanical results showed that the welding zone was a uniform and refined structure since the structural regeneration gives more resistance to the base metal while it can be influenced by stress relaxation time. The penetration depth of the tool increased with increasing the dwell time, stir zone (SZ), and heat-affected zone (HAZ) of the two sheets. The maximum failure load (6000 N) was achieved in the present work compared to other methods of welding. Shahrabadi et al. [11] investigated PFSSW as a new method for producing welds without a keyhole on the specific carbon steel, which eventually introduced the technique to be a high-quality method for welding effects of the parameters such as tool rotational speed and penetration depth on mechanical and metallurgical properties. The microstructure and hardness of the welding region were affected by the dispersion and deformation of materials in the welding zone. The amount of hardness of the weld zone by this method was much lower than the weld produced by resistance welding due to the lack of martensitic in the metallic microstructure in the weld zone. Nateghi and Hosseinzadeh [12] investigated a new method of interconnected friction welding process, including cooling the weld to increase the weld strength and reduce the angular distortion of friction-welded polyethylene sheets. The taguchi experimental method and the response surface methodology were used to analyze the effects of tool rotation speed, passage speed and cooling gas inlet pressure on tensile strength and angular distortion. Also, non-destructive ultrasonic evaluation was used to measure residual stress to justify the change in angular distortion. The results showed that the use of cooling caused to a better combination of plastic materials. It also released residual stress and reduced angular distortion. Abibe et al. [13] examined two traditional techniques for joining metals and polymers, including fastening brackets and adhesive fasteners. Abibe et al. [13] argued that the use of the adhesive method creates a continuous relationship between the surface of the parts, which manifests the uniformity of the stresses and exhibits good mechanical properties while affected by stretching. They bound the polyetherimide (PEI) aluminum fusion joints (F-ICJ) of the 6080-T6 series F-ICJ method, which increased the resistance of the ultrasonic method by 18%. Moreno et al. [14] have investigated the effects of rotational speed and welding on the mechanical properties and thermal behavior of high-density polyethylene friction welded joints using non-rotating combs on their study. The results showed that tensile strength, hardness and crystallization decreased with increasing rotational speed and the effect of welding speed. Lambiase and Genna [15] studied on Laser-Welding technique (LAJ) and the welding on dissimilar AA5053 materials into PVC that had the tensile strength of 15.3 MPs, which compared to the previous ones and achieved 71% tensile strength. Geo et al. [16] investigated dissimilar lap joints of high-density polyethylene (HD-PE) and acrylonitrile butadiene styrene (ABS) sheets in the presence of multilayer carbon nanotubes (MWCNT) by immersion friction welding. Complete microstructural joints made in different process parameters were observed using field diffusion scanning electron microscopy (FESEM). Some defects such as pores and cracks were observed in improper processing parameters. Dashatan et al. [17] joined dissimilar ABS to PMMA by friction stir spot welding method. The thermal distribution and the thermal penetration of the sample indicated a suitable thermal distribution for welding. With the parametric evaluation of the dwell time of the velocity and degree of penetration, it was found that these parameters affect the strength of welding, so that in the test section, by increasing the dwell time, welding resistance increases. Gonçalves et al. [18] created a new method for joining polymer materials using the FSPW method, which resulted in maximum tensile strength of 1700 N. Haghshenas and Khodabakhshi [19] in a review paper examined solid-state technology for the dissimilar bonding of metals and non-metals such as polymers. This type of joint design was very interesting for structural applications, especially in the automotive industry. Goushegir et al. [20] used the FSPJ method to join dissimilar Al 2024 into phenyl sulfide. They studied three welding regions for spot welding and the results of their work that showed the temperature of the welding zone increases with a rotational speed of 2900 rpm to about 400 °C. Sahu et al. [21] have investigated the possibility of welding the Al6063 friction mixing spoon with polypropylene for cylindrical and threaded tool pin profiles in various tool positions such as tool compensation and slotted edge base plate as edge joining to improve weld quality. The joint behavior due to tensile load and the coupling mechanism in the weld stirrer region have been investigated using stress-strain diagrams and scanning electron micrographs, respectively. The weld joining interface was the weakest region instead of the weld stirring region due to the presence of carbon maturation steps due to micro-hardness changes through the weld midline along with energy dispersion spectroscopy analysis. The maximum join efficiency was 23.33% at tool rotation of 700 rpm and scrolling speed of 30 mm/min using a threaded pin in the slotted edge-based design. Khodabakhshi et al. [22]

were able to weld two dissimilar materials, aluminum and polyethylene by friction stir welding for the first time. In this research, the effective parameters on mechanical properties for PFSSW joining aluminum sheets to polyethylene sheets are studied. Whereas polymer and aluminum have different properties such as thermal conductivity, electrical conductivity, flexibility, tensile strength, and many other properties, they are also used in conjunction with a variety of industrial and commercial applications. Besides, the production of plates with low weight and cost and high efficiency has become a challenge for engineers to use these compounds and methods to join metals and polymers. To achieve this goal, first, the Al 5083 sheet welding High-density polyethylene with the PFSSW method was investigated.

Based on previous research, appropriate studies have been performed on the effect of different nanoparticles on two metal/polymer composites. In the present study, an approach based on optimization of a PFSSW method of Al 5083/HD-PE composite sheets using nanomaterials has been investigated. Three nanoparticles can improve the quality of welded nuggets due to their different properties. In this research, the effect of adding three nanoparticles with different weight percentages along with experimental design in PFSSW process was investigated. Figure 1 shows a schematic of the PFSSW process.

2. MATERIALS AND METHOD

In this study, the new PFSSW method was used to join Al 5083 sheet and high-density polyethylene. The dimensions of the samples used are 45×100×4 mm with a joint surface of two materials of 30 mm. In this process, the standard dimensions of AWS C1.1M/C1.1:2012 spot welding were used. Before starting the welding operation, the aluminum sheets were subjected to annealing operation. Acetone was used to clean the weld area. To investigate and optimize the effect of nanoparticles on the mechanical properties of the welded area, Al_2O_3, T_iO_2, S_iO_2 nanomaterials of Tecnan company of Spain with weight ratios of 1, 5 and 10 % were used. The mechanical properties of the samples Al 5083 and HD-PE stated in Table 1.
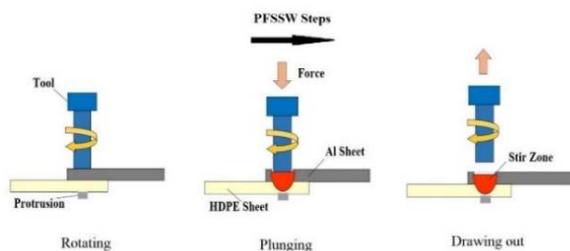
TABLE 1. Mechanical properties of Al5083 and HDPE samples

Type metal	Properties	Test results
	Tensile Strength (MPa)	225
Al 5083	Yield Strength (MPa)	318
	Elongation (%)	19
	Tensile Strength (Kg/cm²)	287.2
HD-PE	Yield Strength (Kg/cm²)	307.8
	Elongation (%)	655

In this study method, a specially designed fixture with a protrusion in the center with a diameter of 7 mm was used. This bulge and space around it improved the mechanical properties during the process. The reason for using specially designed fixtures was the forces involved in the work-piece and the slipping of the sheet due to the lack of coordination of the tools. In order to control the applied torque forces and increase the welding quality, two M12 straps and four screws were used to close the parts. The sheet and nanomaterials are shown in Figure 2. The FP4M milling machine was used for welding and the desired fixture was mounted separately on the machine. A measuring clock with an accuracy of 0.05 mm was used to center the tool with the protrusion. After placing the samples and fixing the sheets on top of each other, the welding adjustment process was applied by adjusting the considered parameters. The spot welding process in the present study was performed in three stages. Penetration of the tool to a depth of 0.6 mm, dwell time in the sample and removal of the tool from the welding site were performed. The tool used was made of H13 steel without pins with three diameters of 7, 14 and 21 mm. Figures 3 and 4 show machine tools and dimensions and geometry of the tools accessories used in the experiments, respectively.


Figure 1. Schematic of the PFSSW process
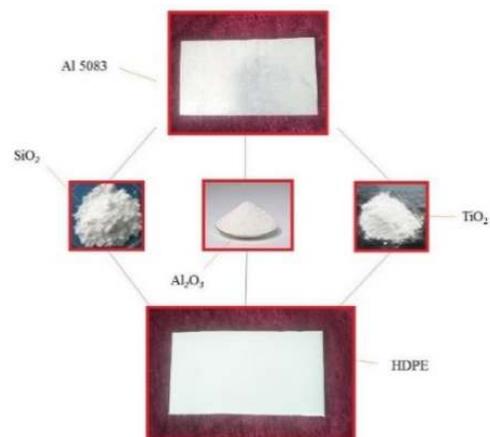
Figure 2. Nanomaterials and samples in this research
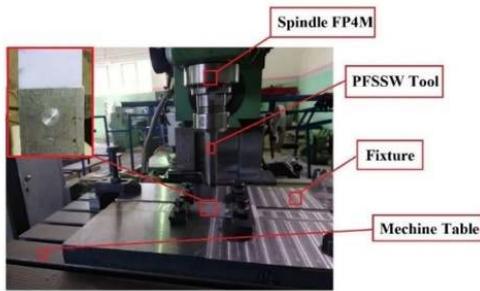
**Figure 3.** Machine tools and accessories used in empirical test
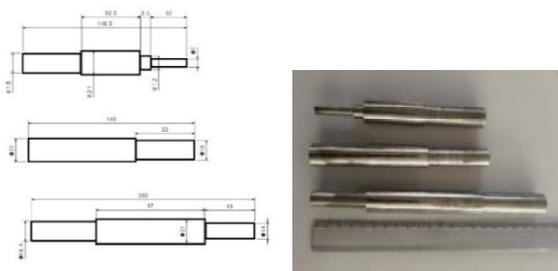
Figure 4. Dimensions and geometry of the tool

Figure 5, shows a composite Al/PE jointed sample in the PFSSW process with the presence of nanoparticles. Mini-tab software was used to design experiments with five parameters in three levels, according to the design of Taguchi experiments, L27 array was used.

3. DESIGN OF EXPERIMENTS

The purpose of designing an experiment is to make purposeful changes in the effective factors of the process

Figure 5. Composite Al/PE jointed sample in the PFSSW process with the presence of nanoparticles

and to examine the changes in the output. In designing an experiment, the first step is to determine the response variables. The experiments are performed according to the parameters and levels intended for each parameter. These effective factors are divided into two categories of response variables: the first group of material parameters including the type and percentage of base materials and nanomaterials used, the second group of process parameters including rotation speed, dwell time and tool diameter. After identifying the response variables and parameters affecting the problem, the next step is to determine the number of levels studied and the range of parameters. Table 2 shows the parameters and scope of work at three levels. According to studies, rotation speeds of 500, 1250 and 2500 rpm were selected. The purpose of selecting the minimum rotation speed of 500 rpm was not to join polyethylene and aluminum samples. The diameters of the tool were 7, 14 and 21 mm, respectively. The ratio of tool diameter to the protrusion in three ratios of 1, 2 and 3 and pause time is considered as the third parameter of 6, 12 and 18 seconds. Given the number of variable parameters and the number of levels associated with each variable in the problem, the number of tests required to analyze and evaluate the research was in the full factorial model. This means that this experiment consists of 125 tests to examine the types of possible cases for experimental research that requires a lot of time and cost. Due to available resources, it was not possible to perform all of these tests. Therefore, it is necessary to use a suitable test plan to reduce the number of tests. Test design methods such as the Taguchi method are known as a method that reduces the number of tests. According to the conditions, the orthogonal array L27 was selected by the Taguchi method. This test design is shown in Table 3.

4. RESULTS AND DISCUSSION

4. 1. Tensile Test   The mechanical properties of the joined composite samples were measured from the tensile test. The experiment was performed at ambient temperature at a rate of 10 mm/min. Tensile tests were performed on 27 design samples. The tensile test was performed by the Ryan-Joyner method with a tensile

TABLE 2. Parameters and level of research

Factor	Unit	Levels	Values
Rotational speed	rpm	3	500, 1250, 2500
Dwell Time	s	3	6, 12, 18
tool d/protrusion d	mm	3	1, 2, 3
Nano type	Type	3	Al_2O_3, TiO_2, SiO_2
Nano Material Percentage	(%)	3	1, 5, 10

TABLE 3. Designing experiments by the L27 Taguchi array

Exp. No.	Rotational Speed	Dwell Time	Tool d/ Protrusion d	Nano Material Percentage	Nano Type
1	500	6	1	1	Al_2O_3
2	500	6	1	5	Al_2O_3
3	500	6	1	10	Al_2O_3
4	500	12	2	1	T_iO_2
5	500	12	2	5	T_iO_2
6	500	12	2	10	T_iO_2
7	500	18	3	1	S_iO_2
8	500	18	3	5	S_iO_2
9	500	18	3	10	S_iO_2
10	1250	6	2	1	S_iO_2
11	1250	6	2	5	S_iO_2
12	1250	6	2	10	S_iO_2
13	1250	12	3	1	Al_2O_3
14	1250	12	3	5	Al_2O_3
15	1250	12	3	10	Al_2O_3
16	1250	18	1	1	T_iO_2
17	1250	18	1	5	T_iO_2
18	1250	18	1	10	T_iO_2
19	2500	6	3	1	T_iO_2
20	2500	6	3	5	T_iO_2
21	2500	6	3	10	T_iO_2
22	2500	12	1	1	S_iO_2
23	2500	12	1	5	S_iO_2
24	2500	12	1	10	S_iO_2
25	2500	18	2	1	Al_2O_3
26	2500	18	2	5	Al_2O_3
27	2500	18	2	10	Al_2O_3

boundary and the welding nugget. Figure 7 the sample connected in the process PFSSW was shown. Samples from the bottom and top and sides and section A-A was examined. In solid-state thermal joining, it was observed that aluminum and polyethylene are homogeneously joined at a certain boundary. Figures 8 and 9 show the macrostructure of the spot welding zone with and without the presence of nanomaterials.
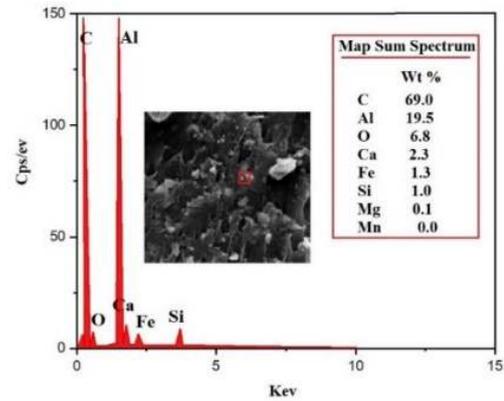
Figure 6. X-ray diffraction from Al/PE composite sample
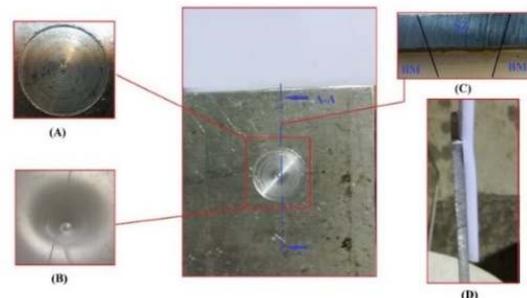
Figure 7. Sample connected in the process PFSSW: a) Top surface, b) bottom surface, c) cutting section A-A along and d) side view

testing device of Urmia University. The highest fore of failure was in 27 samples from the polyethylene sample.

4. 2. Joint Line Metallography   The analysis of Al/PE composite elements from X-ray diffraction made by the German broker company with the D8ADVANCE model and Cobalt lamp. Figure 6 shows the x-ray diffraction of an Al/PE composite sample. Complete mixing and proper joining border indicate that the resulting weld is approved. After performing the tensile test on Al/PE composite samples, light microscopy and SEM was used to observe and examine the fracture surfaces. The spot welding area with and without the presence of nanomaterials is studied for the joining
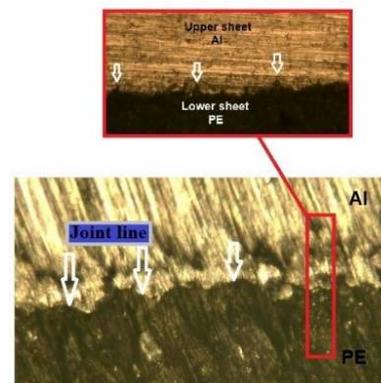
Figure 8. Boundary join of Al/ PE composite without the presence of nanoparticles with X100 magnification
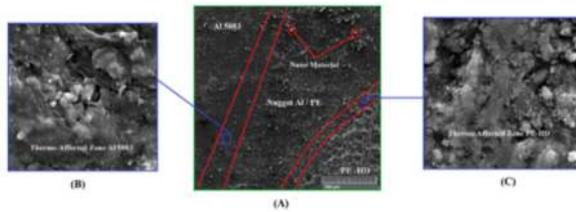
Figure 9. SEM microscope images of fracture mode after tensile test; a) Al/ PE composite, b) Thermal affected zone Al5083, c) Thermal affected zone PE-HD
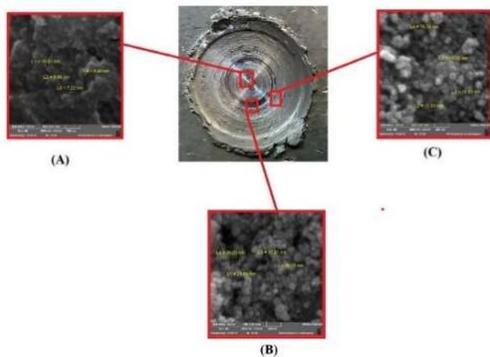
Figure 10. SEM microscope image of the composite Al /PE nugget area; a) Stir Zone, b) Thermal affected zone, c) Base metal

Figure 10 showed SEM microscope images of the fracture after a tensile test on the weld joint. In Al/PE composite, the welding microstructures vary Rotational speed, Dwell Time, on the tool d/protrusion d. Compared to welds produced by pin-less tools, Keyhole is not visible. Due to the lack of depth of tool penetration in the samples in this process, keyhole defects, hook defects and surface cracks were not seen in the microstructure. The reason for this is the thermal zone and the onion ring structures (mechanical) are not available due to the lack of tool pins. The keyhole defect was completely removed and no other defect was detected.

4. 3. Optimization

4. 3. 1. Analysis of Tensile Test Results   By analyzing the results and adding these results in Minitab software, the normal diagram of the output data obtained is presented in Figure 11. Equation (1) is the statistical modeling of the larger-better equation, which is why the choice of this equation is to find the maximum force of choice. According to the analysis of the results in Table 4, the P-value increased by 0.05, indicating that the tensile strength results of the welded samples follow the normal distribution.

$$S/N = -10 \log \log \left[\sum_{i=1}^{n} \frac{1}{y_i^2} \right] \tag{1}$$

Regression YTS = 1057.9 - 738.2 RS1 - 202.3 RS2 + 940.5 RS3 - 1.6 DT1   + 116.5 DT2   - 114.8 DT3   - 408.2 D/d1   + 91.4 D/d2

+ 316.8 D/d3   + 90.2 NT1   - 332.5 NT2   + 242.3 NT3   + 48.2 NMP1 + 8.6 NMP 2 - 56.8 NMP3

Based on the P-value of the analysis of the variance table, which shows that the rotation speed has a greater effect on the tensile strength of welded samples than other welding parameters. Besides, the R-Sq value was 89.62%, indicating that this model covers more than 90% of the data. It should be noted that for higher R-Sq values, it's more realistic and consistent with the regression model.

TABLE 4. Analysis and variance of tensile test results

Source	DF	Adj SS	Adj MS	F-Value	P-Value
Rotational speed	2	13233863	6616931	51.96	0.000
Dwell Time	2	240848	120424	0.95	0.409
tool d/protrusion d	2	2477759	1238880	9.73	0.002
Nano type	2	1596512	798256	6.27	0.010
Nano Material Percentage	2	50661	25331	0.20	0.822
Error	16	2037443	127340	-	-
Total	26	19637086	-	-	-
R-sq=89.62%		R-sq(adj)= 83.14%		R-sq(pred)= 70.45%	
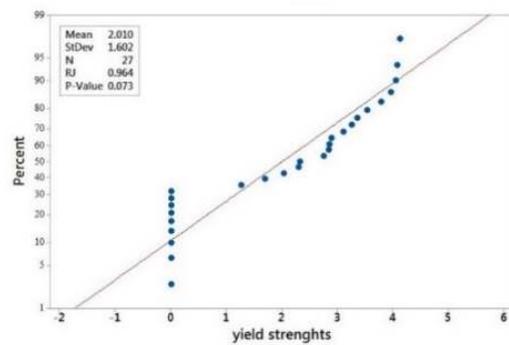
Figure 11. Normal diagram for experimental data of Al/PE composite
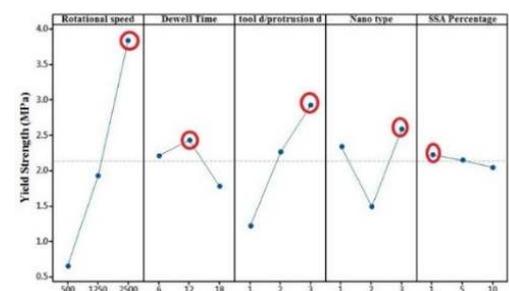
Figure 12. Effect of processing parameters on tensile strength

Since in the study of tensile strength, the aim is to maximize the amount of response, signal-to-noise (the larger is better) analysis has been used to investigate the main effects of the parameters and the order of their importance on the tensile strength of the samples. The maximum fracture force was 2249 N and the maximum tensile strength was 4.13 MPa in the tensile test (Figure 13). Due to the normal distribution of data, analysis of variance of the data obtained from the tensile test is considered. Also, Figures 14 and 15 show the diagrams of the response surface method and the contours of the tensile test. Based on the results of these graphs, the effects of variable effective factors on each other and finally on the yield strength are presented. Eq. 2 regression model is the criterion for submission to an analysis of variance.
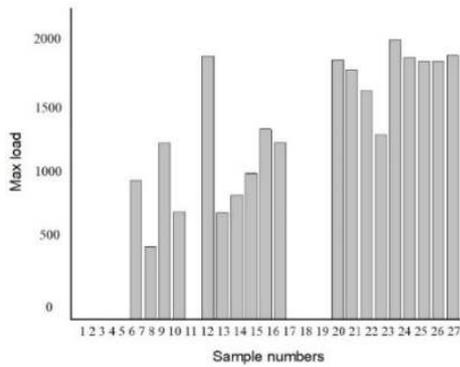
Figure 13. Tensile test results for the basis of yield strength
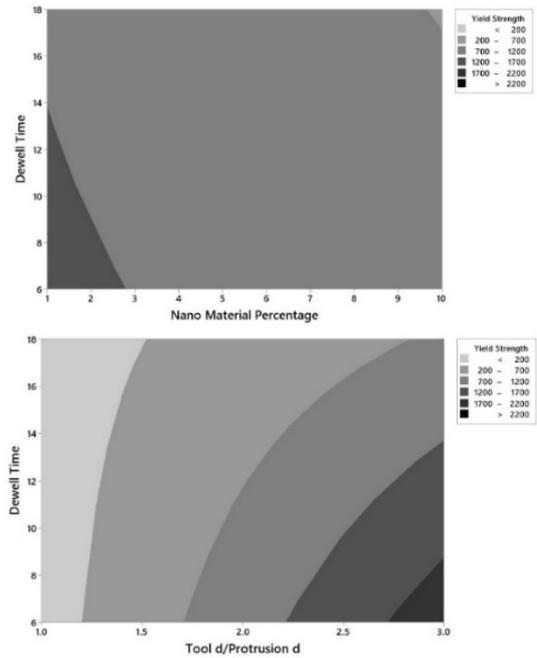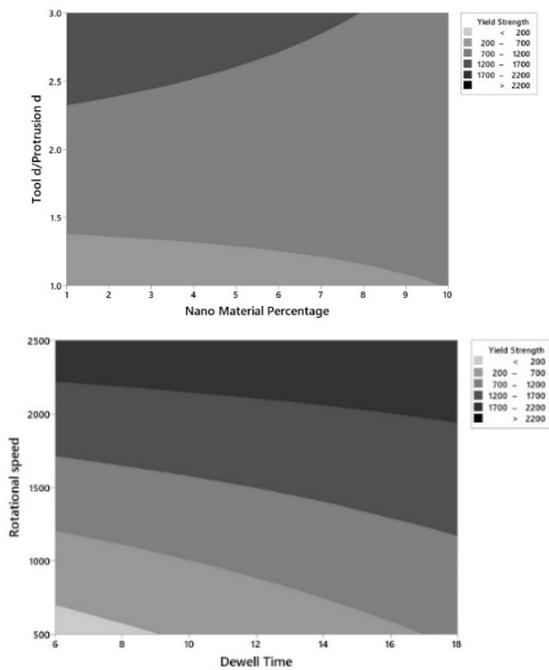
Figure 14. Contours of effective factors based on yield strength
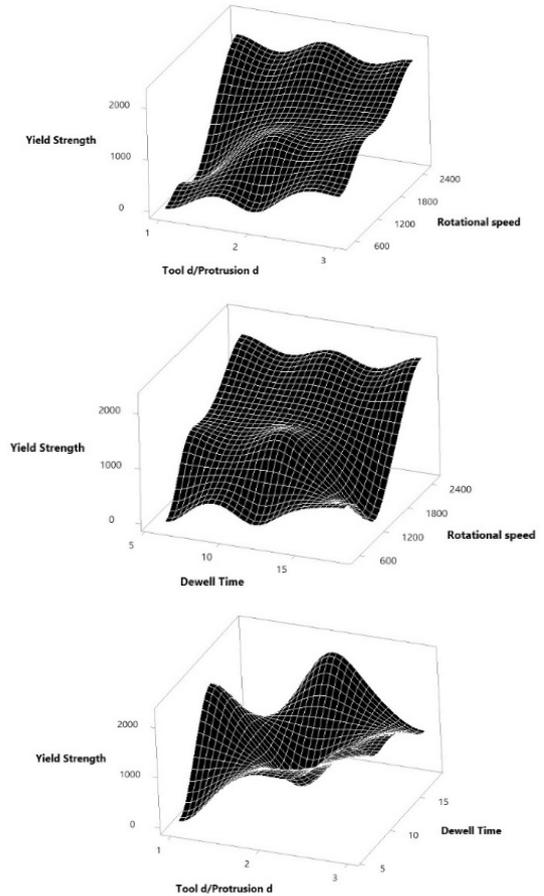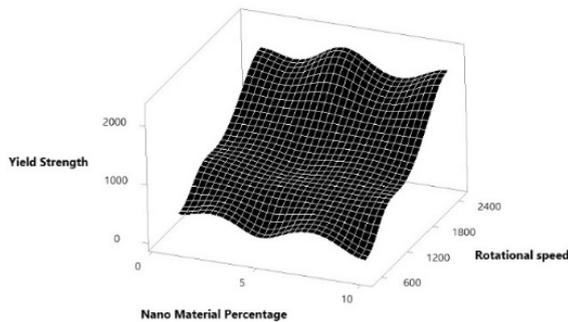
Figure 15. Effective parameter response surface method

The interaction effect of the parameters on the maximum strength is depicted in Figure 16.

4. 3. 2. Signal to Noise Tensile Test Results
According to the results of signal-to-noise analysis in Table 6, for the tensile strength of the samples, the parameters are ranked based on impact degree, tool speed, Tool d/protrusion d, nanomaterial type, dwell time and percentage of nanoparticles, respectively, with the results and percentage. The share corresponds to the analysis of the variance table. The ratings are obtained from the delta values and the delta values are obtained from the difference between the maximum and minimum column values of that factor. According to the results of signal-to-noise analysis in Table 5, for the tensile
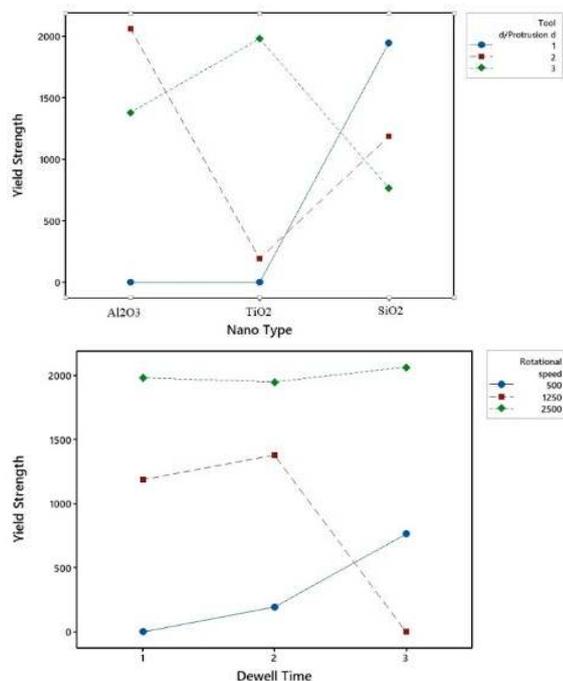
Figure 16. Interaction effect of the parameters on maximum tensile force yield strength

strength of the samples, the parameters are ranked based on impact degree, tool speed, Tool d/protrusion d, type of nanomaterial, pause time and percentage of nanoparticles, respectively with the results and also Corresponds to the percentage share of the analysis of variance table. The ranking is obtained from the delta values and the delta values are obtained from the difference between the maximum and minimum column values of that factor.

Table 5 shows the signal-to-noise results of the test design. In these results, the effect of 5 input factors with three levels has been investigated. According to the analysis of variance presented in Table 5, the percentage of participation in the parameters shows that the rotational speed had the greatest effect on tensile strength and other parameters such as Tool d/protrusion d, nanomaterial type, static time and percentage of nanoparticles had the most effect, respectively.

The optimal value of the parameter for the rotation speed of the maximum level tool with the maximum speed (2500 rpm) is considered to be the third level. Because increasing the temperature due to increasing the speed of the tool, causes more friction of the material. As the temperature increases, the strength of the melt and viscosity decrease and the materials in the weld zone integrate well and ultimately lead to an increase in tensile strength. The optimal parameter value for the dwell time in the second level was 12 seconds. The reason for this was that the low and excessive heat required (due to tool friction) reduced the mechanical properties of the welding area. The optimal value was in 12 seconds and a more uniform cross-section was achieved at the welding surface than in 6 and 18 seconds.

The optimal parameter for Tool d / Protrusion d is in the third level with a diameter of 21 mm. The reason for this was the greater contact of the work-piece and the presence of useful friction. The optimal effect of the studied parameters for the nanomaterial was the third level of the nanomaterial (S_iO_2) which had the greatest effect on the tensile strength of the welded parts. Also, the last parameter was the effect of the optimal percentage of nanoparticles. At the first level, 1% of the nanoparticles were selected. In nanoparticles about 1% to the welding area, the tensile strength of the welded

TABLE 5. Signal-to-Noise Analysis Table Tensile strength results

Level	Rotational speed	Dwell Time	Tool d/ protrusion d	Nano type	Nano Percentage
1	0.6513	2.2084	1.2213	2.3362	2.2240
2	1.9296	2.4316	2.2660	1.4911	2.1484
3	3.8344	1.7753	2.9280	2.5880	2.0429
Delta	3.1831	0.6562	1.7067	1.0969	0.1811
Rank	1	4	2	3	5

samples increases. The reason for this increase was good nanoparticle distribution, stress distribution and tensile strength.

5. CONCLUSION

In this study, a novel approach called the PFSSW process was investigated in order to join different materials, consisted of high-density polyethylene and Al5083, with different parameters at the ambient temperature and normal conditions. To discover the impact of process parameters on mechanical properties, these materials were applied using DOE analysis. The high-density polyethylene and Al5083 besides the structural and mechanical properties of flawless welds, such as debarment of void defects on the welding surface, were employed. The results of S/N Analysis and Analysis of Variance reveals that the most effective parameter on the tool's tensile strength is the rotation speed, and other parameters are respectively as the Tool d/ Protrusion d, Nano-materials' percentage, Nano-materials' type, and dwell time. At the next level, the same results of maximum tensile strength are applied. The increment in both the welding area and the joint spot is due to the heat exchange resulting from the friction between the tool and the upper sheet (Al5083).

In this research, the chosen parameters of Taguchi experiments play an important role in rising the welded areas' temperature. As the temperature increases, whether soft or hard materials' mass would be proliferated and a better balance struck. For the lack of strength, TiO_2 nanoparticles have no impact on enhancing the welding properties. In the absence of nanoparticles, a rupture was witnessed in the tensile tests of polyethylene samples. Therefore, more sediment was grabbed by the polyethylene sample through adding nanoparticles and so the mechanical properties of the Al/PE composite are improved by deposition of nanoparticles. The analysis of variance was attained at reliability of R (Sq) = 89%. Based on the S/N ratio analysis, the optimum states of input parameters are considered as the rotation speed of 2500 rpm dwell time of 12 s, Tool d/ Protrusion d of 3 mm, Nano-material's type of Sio_2 and percentage of 10%.

6. REFERENCES

1. Tagimalek, H., Maraki, M.R., Mahmoodi, M. "A new approach of the constrained groove pressing process on Al5083-O alloy using PMMA polymer, without die non-friction coefficient: nanostructure, mechanical Properties and hardness", *Journal of Engineering Research*, (2021). https://doi.org/10.36909/jer.12957

2. Maraki, M.R., Tagimalek, H., Azargoman, M., Khatami, H., & Mahmoodi, M., "Experimental Investigation and Statistical Modeling of the Effective Parameters in Charpy Impact Test on AZ31 Magnesium Alloy with V-shape Groove Using Taguchi Method", *International Journal of Engineering, Transactions C: Aspects*, Vol. 33, No. 12, (2020), 2521-2529. doi: 10.5829/ije.2020.33.12c.13

3. Pasoodeh. B., Tagimalek. H., "Analytical and Numerical Evaluation of Wire Flat Rolling Process Based on the Slab Method and DEFORM-3D", *Journal of Advanced Materials and Processing*, Vol. 8, No. 4, (2020), 3-16. DOR: 20.1001.1.2322388.2020.8. 4.1.6

4. Grujicic, M., Sellappan, V., Omar, M.A., Seyr, N., Obieglo, A., Erdmann, M., Holzleitner, J., "An overview of the polymer-to-metal direct-adhesion hybrid technologies for load-bearing automotive components" *Journal of Materials Processing Technology*, Vol. 197, No. 1-3, (2008), 363-373. https://doi.org/10.1016/j.jmatprotec. 2007.06.058

5. Tagimalek, H., Maraki, M.R., Mahmoodi, M., Mohammad Zadeh, P., "Investigation Experimental and Finite Element Method of Mechanical Properties of Hot Forging on Ti6Al4V Alloy", *Iranian (Iranica) Journal of Energy and Environment*, Vol. 12, No. 2, (2021), 149-154. Doi: 10.5829/ijee.2021.12.02.07

6. Mahmoodi, M., Tagimalek. H., Sohrabi. H., Maraki. M.R., "Using the artificial neural network to investigate the effect of parameters in square cup deep drawing of aluminum-steel laminated sheets", *International Journal of Iron & Steel Society of Iran*, Vol. 17, No. 2, (2020), 1-13. DOI: 10.22034/ijissi.2021.528568.1196.

7. Tagimalek, H., Maraki, M.R., Mahmoodi, M., Azargoman, M., "A Hybrid SVM-RVM Algorithm to Mechanical Properties in the Friction Stir Welding Process", *Journal of Applied and Computational Mechanics*, Vol. 8, No. 1, (2022), 36-47. DOI:10.22055/ JACM.2019. 31017.1811.

8. Isam Jabbar I, Guney Guven. Y., "Application of a novel friction stir spot welding process on dissimilar aluminum joints", *Journal of Manufacturing Processes*, Vol. 35, (2018), 282-288. https:// doi.org/10.1016/j.jmapro.2018.08.018.

9. Tagimalek, H., Maraki, M.R., M. Mahmoodi, kardan-Moghaddam, H., & Farzad-Rik, Salar, "Prediction of mechanical properties and hardness of friction stir welding of Al 5083/pure Cu using ANN, ICA and PSO model", *SN Applied Sciences*, (2021). DOI: 10.1007/s42452-021-04884-y

10. Zarghani, F., Mousavizade, S. M., Ezatpour, H. R., Ebrahimi, G. R. "High mechanical performance of similar Al joints produced by a novel spot friction welding technique", *Vacuum*, Vol. 147, (2018), 172-186. https://doi.org/10.1016/j.vacuum.2017.10.035.

11. Shahrabadi, A. R., Mousavizade, S. M., Ezatpour, H. R., Pouranvari, M. "Achieving high mechanical performance in protrusion friction stir spot welding (PFSSW) of DQSK steel compared to other techniques", *Materials Research Express*, Vol. 5, No. 10, (2018), 106519. https://doi.org/10.1088/2053-1591/aada37

12. Nateghi, E., Hosseinzadeh, M. "Experimental investigation into effect of cooling of traversed weld nugget on quality of high-density polyethylene joints", *The International Journal of Advanced Manufacturing Technology*, Vol. 84, (2016), 581-594. https://doi.org/10.1007/s00170-015-7663-4

13. Abibe, A. B., Sônego, M., Dos Santos, J. F., Canto, L. B., & Amancio-Filho, S. T. On the feasibility of a friction-based staking joining method for polymer–metal hybrid structures. *Materials & Design*, Vol. 92, (2016), 632-642. https://doi.org/10.1016/j.matdes.2015. 12.087.

14. Moreno, M.M., Romero, Y.M., Zambrano, H.R., Afonso, C.R.M., Silgado, J. U. "Mechanical and thermal properties of friction-stir welded joints of high density polyethylene using a non-rotational shoulder tool" *The International Journal of Advanced Manufacturing Technology*, Vol. 97, (2018), 2489-2499. https://doi.org/10.1007/s00170-018-2102-y.

15. Lambiase, F., Genna, S. "Laser assisted joining of AA5053 aluminum alloy with polyvinyl chloride (PVC)" Optics & Laser Technology", Vol. 107, (2018), 80-88. https://doi.org/10.1016/j.optlastec.2018.05.023.

16. Geo, J., Li, C., Shilpakar, U., Shen, Y. "Microstructure and tensile properties of dissimilar submerged friction stir welds between HDPE and ABS sheets" *The International Journal of Advanced Manufacturing Technology*, Vol. 87, (2016), 919-927. https://doi.org/10.1007/s00170-016-8539-y

17. Dashatan, S. H., Azdast, T., Ahmadi, S. R., Bagheri, A. "Friction stir spot welding of dissimilar polymethyl methacrylate and acrylonitrile butadiene styrene sheets" *Materials & Design*, Vol. 45,   (2013),   135-141. https://doi.org/10.1016/j.matdes.2012.08.071.

18. Gonçalves, J., Dos Santos, J. F., Canto, L. B., Amancio-Filho, S. T. "Friction spot welding of carbon fiber-reinforced polyamide 66 laminate" *Materials Letters*, Vol. 159, (2015), 506-509. https://doi.org/10.1016/j.matlet.2015.08.036.

19. Haghshenas, M., & Khodabakhshi, F. "Dissimilar friction-stir welding of aluminum and polymer: a review" *The International Journal of Advanced Manufacturing Technology*, Vol. 104, (2019), 333-358. https://doi.org/10.1007/s00170-019-03880-2.

20. Goushegir, S. M., Dos Santos, J. F., Amancio-Filho, S. T. "Friction spot joining of aluminum AA2024/carbon-fiber reinforced poly (phenylene sulfide) composite single lap joints: microstructure and mechanical performance" *Materials & Design*,   Vol.   54,   (2014),   196-206. https://doi.org/10.1016/j.matdes.2013.08.034

21. Sahu, S.K., Pal, K., Mahto, R.P., Dash, P. "Monitoring of friction stir welding for dissimilar Al 6063 alloy to polypropylene using sensor signals" *The International Journal of Advanced Manufacturing Technology,* Vol. 104, (2019), 159-177. https://doi.org/10. 1007/s00170-019-03855-3

22. Khodabakhshi, F., Haghshenas, M., Sahraeinejad, S., Chen, J., Shalchi, B., Li, J., Gerlich, A. P. "Microstructure-property characterization of a friction-stir welded joint between AA5059 aluminum alloy and high-density polyethylene" *Materials Characterization*,   Vol.   98,   (2014),   73-82. https://doi.org/10.1016/j.matchar .2014.10.013

Persian Abstract

چکیده

یکی از مهمترین چالش‌های جوشکاری اصطکاکی اغتشاشی نقطه‌ای وجود یک جای پین در قطعات جوش داده شده است. این جای پین باعث جمع شدن تنش در حفره حاصل شده و در نتیجه باعث کاهش خواص مکانیکی آن می‌شود. برای حل این مشکل در این تحقیق، ورق‌های آلومینیوم و پلی اتیلن با استفاده از ابزارهای فولادی گرم کار H13 و سه نوع نانوذرات اتصال داده شدند. آلومینیوم و پلی اتیلن با چگالی بالا با افزودنی سه نوع نانوذرات Al2O3، TiO2، SiO2 اتصال داده شد. برای بهبود خواص مکانیکی نمونه‌های جوش داده شده، سه نوع نانو مواد به ناحیه ناگت جوش اضافه شد. طراحی آزمایشی با استفاده از روش تاگوچی برای یافتن حداکثر مقاومت صفحات کامپوزیت جوش داده شده انجام شد. سرعت دورانی، مکث زمانی، نسبت قطر ابزار به قطر پین، نوع نانو و درصد مواد نانو به عنوان پارامترهای ورودی انتخاب شدند. حداکثر نیروی خرابی ۲۲۴۹ نیوتن و بیشترین مقاومت ۴.۱۳ مگاپاسگال بود. در آزمایشات کششی نمونه‌های فاقد نانوذرات، پارگی توسط نمونه پلی اتیلن انجام شد. برای این منظور، نمونه پلی اتیلن با افزودن نانوذرات رسوب بیشتری جذب کرده و رسوب نانوذرات باعث بهبود خواص مکانیکی کامپوزیت Al / PE می‌شود. علاوه بر این، در نمونه همراه با نانوذرات، خواص مکانیکی نمونه کامپوزیت Al / PE در مقایسه با ماده پایه آلومینیوم و پلی اتیلن، حدود ۸ برابر افزایش یافته است. تجزیه و تحلیل نسبت سیگنال به نویز نشان داد که سرعت چرخش ۲۵۰۰ دور در دقیقه، زمان ساکن ۱۲ ثانیه، قطر ابزار بر قطر برآمدگی ۳ میلی متر، نوع نانو SiO2 و درصد مواد نانو ۱۰٪ شرایط بهینه هستند.

International Journal of Engineering

Design of a Knowledge Flow Network for the Personnel of an Organization under Various Scenarios and its Solution using Lagrangian Relaxation

A. Makarchi, H. R. Dezfoulian*, P. Samouei

Department of Industrial Engineering, Faculty of Engineering, Bu-Ali Sina University, Hamedan, Iran

A B S T R A C T

Knowledge transfer can occur on two levels: intra-organizational and inter-organizational. Acquiring knowledge from outside an organization usually requires significant budget and considerable time. However, through awareness and reliance on knowledge already acquired by the personnel, and creating a knowledge flow network, knowledge level of the organization can be increased in the shortest possible time. The present paper addresses the design of a knowledge flow network between the personnel of an organization according to the professional and personal trust levels, teaching and learning capabilities, knowledge level of the personnel, organizational commitment level, type and importance of each knowledge, and the stochastic nature of the knowledge transfer duration. This problem was formulated as a stochastic multi-objective mixed-integer programming. The objectives of the proposed model were maximizing the knowledge level and minimizing the knowledge transfer time. The model was solved using the Lagrangian relaxation algorithm and the CPLEX solver. Results indicate the high efficiency of the Lagrangian relaxation algorithm specially in computational time of large-sized problems. Moreover, the results show that the organizational commitment parameter has more significant influence on the knowledge transfer duration, followed by teaching and learning capabilities.

doi: 10.5829/ije.2022.35.06c.07

1. INTRODUCTION

Knowledge has been overgrown in the past decades, such progress in gained knowledge for the last decade is known by many to be larger than that accumulated throughout history up to the previous decade. It has earned knowledge the status of an essential competitive advantage, and every firm bears responsibility for gaining and applying knowledge [1, 2].

Knowledge can be transferred between organizations (inter-organizational) or within an organization (intra-organizational) [3]. Clearly, effective intra-organizational knowledge transfer is critical for a sustainable competitive advantage [4, 5]. The main topic of the present research is intra-organizational knowledge transfer, because knowledge transfer between the personnel of an organization can be led to considerable time and budget saving.

This research primarily focuses on answering the question of how to use the existing knowledge in an organization to guide the knowledge flow between the personnel to maximize the knowledge level and to minimize the duration time of knowledge transfer. To realize this goal, considering budget constraints and the parameters affecting the model, one must determine the knowledge, the field, and the personnel involved in knowledge transfer so that the overall level of knowledge in the organization can be maximized in the shortest possible time.

To this end, first, the existing literature on the subject is reviewed, and the research gap is highlighted. Then, the problem is stated, and the associated mathematical model is introduced. In the subsequent section, the solution method is explained, after which the different solution methods are compared, and the sensitivity analysis is performed. Finally, the results are discussed, and suggestions are made for future research.

Corresponding Author Institutional Email: hrdezfoolian@basu.ac.ir
(H. R. Dezfoulian)

The remaining structure of the paper is as follows: the literature review of the related papers is presented in section 2. Problem description, assumptions, and mathematical model are given in section 3. Using solving methods consist of the LP-metric, and the Lagrangian relaxation methods are in section 4. Section 5 introduces examples and sensitivity analysis for the determination of important parameters. Finally, computational results and discussions for small, medium, and large-sized problems with 25 different samples and two methods are presented in the last section.

2. LITERATURE REVIEW

The literature review of this paper is organized in knowledge flow networks, factors affecting knowledge transfer, and mathematical modeling. First, research on knowledge flow networks is mentioned. Rózewski et al. [6] have stated that an open atmosphere encouraging knowledge transfer and an appropriate field of cooperation are required for successful knowledge discovery. Collaborative learning in an organizational social network is based on knowledge resource distribution via creating a knowledge flow network. In this network, the nodes represent the persons in an organization and contain information about their social and cognitive abilities. In addition, the persons are described by their skill sets, their knowledge level in these skills, and their collaborative learning behavior, which can be recognized by analyzing the knowledge flow. They assume knowledge level increasing is the result of collaborative learning. In other words, cooperative learning can be analyzed as a process involving the flow of knowledge in the network. Chandra et al. [7] aimed to understand the knowledge sharing in projects based on knowledge flow patterns. An interpretive structural model for the knowledge network in knowledge-based organizations (specifically, an automotive research and development center) was discussed by Rezaeian et al. [8]. They identified and ranked the factors affecting the formation of knowledge networks and their relationships in knowledge-based organizations. Environmental factors, knowledge content, cultural factors, IT and network systems, communication mechanisms, organizational structures, and management processes were the factors influential in knowledge network formation in their research.

The second topic investigated in the literature review is the factors affecting knowledge transfer within an organization. In another research, Lin [9] concluded that organizational commitment is directly related to implicit knowledge transfer. Duan et al. [10] explored, confirmed, and mapped the significant factors affecting transnational knowledge transfer (TKT). Ten factors had been selected by more than 50 percent of specialists as the significant

factors influencing TKT projects. These were cultural relations and awareness, language, motivation, knowledge gap, appropriate selection of teacher and learner, scope and focus, transfer channel, trust, and constraint removal. Knowledge transfer and learning capacity in multinational corporations (MNCs) addressed by Lee and Wu [11]. The knowledge absorption capacity of the learner is the most critical factor in internal knowledge transfer in MNCs. This research defines absorption capacity as the personnel's capability and motivation. The impact of trust on selecting the knowledge transfer mechanism was investigated by Sreckovic and Windsperger [12]. Alexopoulos and Buckley [13] stated that, despite the fundamental role of trust in facilitating intra-organizational knowledge flows, the existing limited empirical research shows what kind of trust is related to the adequate knowledge transfer between persons and when these types of trust gain significance. Hence, they examined the effects of personal and professional trust on knowledge transfer. They found that professional trust and personal trust are both positively and considerably related to knowledge transfer. Moreover, they demonstrated that professional trust has a remarkably more substantial positive effect than personal trust on knowledge transfer. Swart et al. [14] investigated the reasons of knowledge sharing with the colleagues. The impact of commitment, personal and professional trust on the transfer and application of knowledge was studied by Ouakouak and Ouedraogo [15]. The relationship between trust, knowledge transfer and organizational commitment in small and medium companies was investigated by Curado. and Vieira [16]. The results indicated that trust has a remarkable positive effect on knowledge transfer and organizational commitment. Knowledge transfer is somehow the intermediary between trust and organizational commitment. García-Almeida and Bolívar-Cruz [17] identified the main factors contributing to the success of knowledge transfer in service-based companies during the creation or sale of new units. Regional transfer of experience, compatibility between the cultural background of the knowledge and that of the learners, the absorption capacity of the learners, motivation of the teachers and learners, and incompatibility during the transfer process are key factors influencing several aspects of success in knowledge transfer in service-based companies. By investigating the effect of commitment on the common intentions of knowledge collaborators in virtual societies in China, Lou et al. [18] attempted to fill the research gap in this area. Their results indicated that emotional and normative commitment could considerably influence the knowledge transfer goals of users.

The third part of the literature review concerns the mathematical modeling of knowledge flow networks. A mixed-integer programming (MIP) model for the

systematic analysis and proper understanding of knowledge flow networks between the personnel in an organization was formulated by Dong et al. [19]. They demonstrated how centralized organizations could facilitate knowledge transfer using knowledge transfer networks and reduce the number of relationships required in a multi-knowledge environment for effective knowledge management. Dezfoulian et al. [2] formulated knowledge transfer between the members of an industrial cluster using a new MIP model. They maximized knowledge transfer between the companies considering the budget and time constraints. Dezfoulian and Samouei [20] formulated knowledge transfer between the members of a chain level using a novel MIP model and implemented it for the producer level of a dairy supply chain. Moreover, they identified the parameters influencing the knowledge flow network.

A comparison between the few mathematical models (of the knowledge flow network) in terms of the objective function indicates that only Dong et al. [19] presented single-objective, where Dezfoulian et al. [1] and Dezfoulian and Samouei [20] discussed multi-objective. Most papers in this area have considered increasing the level of knowledge. The second objective of Dezfoulian et al. [1] was maximizing knowledge transfer between companies in the cluster with the most substantial level of relationship. Also, the second objective of Dezfoulian and Samouei [20] has been to reduce the knowledge transfer cost. The focus of Dezfoulian et al. [1] and Dezfoulian and Samouei [20] was on inter-organizational knowledge transfer, while that by Dong et al. [19] was on intra-organizational knowledge transfer. Dong et al. [19] solved their model using a heuristic method, while the other two papers have used exact methods.

A review of previous studies showed that the maximization of the knowledge level of personnel in an organization and considering budget and time and the associated formulation in the form of a mathematical model as a powerful analysis tool has been rarely addressed. Furthermore, given the importance of knowledge as an essential resource in organizations and the scarcity of resources (especially budget and time), any action to enhance the level of knowledge is a significant step toward improving the competitive status of the organization. For this reason, the present research focuses on mathematical modeling to improve the level of organizational knowledge using intra-organizational knowledge transfer. For this purpose, professional and personal trust, organizational commitment (which has not been considered in previous research), teaching and learning capabilities, which affect the knowledge transfer process, were considered. For a more realistic model, the stochastic nature of the knowledge transfer duration has been considered. However, previous works have considered all the variables and parameters to be deterministic. The problem has been formulated as a

stochastic MIP model and solved using the CPLEX solver and the Lagrangian relaxation algorithm.

3. PROBLEM DESCRIPTION AND MODELING

Knowledge is a critical resource in every organization. It has motivated numerous advanced organizations to manage knowledge and use it to their best advantage. In general, the personnel in an organization do not share equal awareness of different types of knowledge. Each personnel member may be an expert in a particular knowledge and a beginner or an intermediate in the others. The personnel can cooperate in knowledge transfer to improve the overall knowledge level. For the best results, it is necessary to maximize the knowledge in the shortest possible time considering the budget limitation. To this end, the knowledge level of each member must be determined at the outset of the knowledge transfer plan. Beginner, intermediate, and expert levels are defined for each knowledge type. Persons with higher levels of knowledge can teach their knowledge to persons with lower levels. Knowledge transfer is affected by various factors. This model considers professional and personal trust, teaching and learning capability, and organizational commitment for knowledge sharing. The duration of knowledge transfer is impacted by the teaching and learning abilities and the organizational commitment. Therefore, to get closer to the real-world situation, the necessary time of knowledge sharing is considered stochastic. Different areas of knowledge have different levels of significance for other persons. Therefore, different knowledge must be prioritized for each person according to their needs and jobs. Hence, this paper presents a stochastic MIP model for knowledge sharing between the personnel of an organization according to professional and personal trust, teaching and learning abilities, organizational commitment, and type and significance of each knowledge. The objectives of this model are to maximize the knowledge level and minimize the duration of knowledge transfer. The proposed model is considered based on three scenarios, namely optimistic, likely, and pessimistic. Then, the problem is solved for each scenario. Finally, the average of the results is reported based on the opinion of the decision-maker and the probability of each scenario. Clearly, the knowledge transfer time in the pessimistic case is longer than the likely and the optimistic cases.

3. 1. Assumptions
The assumptions are as follows:
- The knowledge possesses beginner, intermediate, or expert levels, denominated 1, 2, and 3, respectively.
- The knowledge level of a person who teaches another person is higher than the learner knowledge level.

- The teacher cannot learn knowledge from another person during the teaching period.
- At the end of the teaching period, the learner's level is upgraded by 1.
- The significance of different knowledge types is equal for other persons during the planning horizon.
- Knowledge transfer does not occur during regular work hours.
- The knowledge transfer duration depends on the type of knowledge and the teaching capability, learning capability, and organizational commitment.
- Knowledge transfer that is impossible to complete during the planning horizon is excluded.
- The knowledge transfer cost depends on the type of knowledge and the teaching and learning persons.
- The cost of knowledge transfer between the organization's personnel must not exceed the allocated budget.
- The persons are unable to teach and learn several types of knowledge simultaneously.
- Teaching and learning happen one-on-one and not in groups.
- The pessimistic, likely, and optimistic cases (for the given knowledge transfer duration) have the same probability of occurrence.

The indexes, parameters, and decision variables and their definitions in this model are as follows:

Indexes

k	Teacher
l	Learner
s	Knowledge type
t	Periods

Parameters

K	Total number of persons
T	Planning horizon duration
S	Total number of knowledge types
γ_{ks}	Significance of knowledge type s for person k
α_{kl}	Professional level of trust between person k and person l
β_{kl}	A personal level of trust between person k and person l
$\widetilde{tt_s}$	Duration of teaching (learning) knowledge type s
θ_k	Teaching capability of person k
λ_l	Learning capability of person l
$(\pi_l)\,\pi_k$	Organizational commitment of the teacher (learner)
ζ_{kls}	Cost of transferring knowledge type s from person k to person l
M	A sufficiently large number
C	The total budget allocated to knowledge teaching in the organization
A	The threshold for professional trust
B	The threshold for personal trust

Decision variables

X_{kls}^t	1, if transferring knowledge type s from person k to person l begins in period t; 0, otherwise.
E_{ls}^t	1, if person l is learning knowledge type s during period t; 0, otherwise.

F_{ks}^t	1 if person k is teaching knowledge type s during period t; 0, otherwise.
W_{ks}^t	Level of person k in knowledge type s at the beginning of period t

3. 2. Mathematical Programming Model   The model presented in this paper is a development of the models by Dezfoulian et al. [1], Dong et al. [19], Dezfoulian and Samouei [20]. The problem is modeled as a bi-objective, linear, stochastic MIP model according to Equations (1)-(17).

$$Max \sum_{k=1}^{K} \sum_{s=1}^{S} \gamma_{ks} \times W_{ks}^T \qquad (1)$$

$$Min \sum_{k=1}^{K} \sum_{\substack{l=1 \\ k \neq l}}^{K} \sum_{s=1}^{S} \sum_{t=1}^{T} \big(\widetilde{tt_s} \times (1.5 - \theta_k \times \pi_k) \times (1.5 - \lambda_l \times \pi_l)\big) \times X_{kls}^t \qquad (2)$$

$s.t.:$

$$\sum_{s=1}^{S} E_{ls}^t \leq 1 \quad \forall l \in \{1,2,\dots,K\}, \forall t \in \{1,2,\dots,T\} \qquad (3)$$

$$\left(\frac{\sum_{\substack{k=1 \\ k \neq l}}^{K} \sum_{p=t-\widetilde{tt_s}+1}^{t} X_{kls}^p}{M}\right) \leq E_{ls}^t \quad \forall l \in \{1,2,\dots,K\}, \forall s \in \{1,2,\dots,S\}, \forall t \in \{1,2,\dots,T\} \qquad (4)$$

$$\sum_{s=1}^{S} F_{ks}^t \leq 1 \quad \forall k \in \{1,2,\dots,K\}, \forall t \in \{1,2,\dots,T\} \qquad (5)$$

$$\left(\frac{\sum_{\substack{l=1 \\ l \neq k}}^{K} \sum_{p=t-\widetilde{tt_s}+1}^{t} X_{kls}^p}{M}\right) \leq F_{ks}^t \quad \forall k \in \{1,2,\dots,K\}, \forall s \in \{1,2,\dots,S\}, \forall t \in \{1,2,\dots,T\} \qquad (6)$$

$$X_{kls}^t \leq W_{ks}^t - W_{ls}^t + M \times (1 - X_{kls}^t) \quad \forall k,l \in \{1,\dots,K\}, k \neq l, \forall s \in \{1,\dots,S\}, t < (T - \widetilde{tt_s} + 1) \qquad (7)$$

$$X_{kls}^t \leq \alpha_{kl} - A + M \times (1 - X_{kls}^t) \quad \forall k,l \in \{1,\dots,K\}, k \neq l, \forall s \in \{1,\dots,S\}, t < (T - \widetilde{tt_s} + 1) \qquad (8)$$

$$X_{kls}^t \leq \beta_{kl} - B + M \times (1 - X_{kls}^t) \quad \forall k,l \in \{1,\dots,K\}, k \neq l, \forall s \in \{1,\dots,S\}, t < (T - \widetilde{tt_s} + 1) \qquad (9)$$

$$\sum_{p=T-\widetilde{tt_s}+1}^{T} X_{kls}^p \leq 0 \quad \forall k,l \in \{1,\dots,K\}, k \neq l, \forall s \in \{1,\dots,S\} \qquad (10)$$

$$W_{ls}^{t+1} = W_{ls}^t \quad l \in \{1,2,\dots,K\}, s \in \{1,2,\dots,S\}, t < \widetilde{tt_s} \qquad (11)$$

$$W_{ls}^t = W_{ls}^{t-1} + \sum_{\substack{k=1 \\ k \neq l}}^{K} X_{kls}^{t-\widetilde{tt_s}} \quad l \in \{1,2,\dots,K\}, s \in \{1,2,\dots,S\}, t > \widetilde{tt_s} \qquad (12)$$

$$\sum_{k=1}^{K} \sum_{\substack{l=1 \\ k \neq l}}^{K} \sum_{s=1}^{S} \sum_{t=1}^{T} \zeta_{kls} \times X_{kls}^t \leq C \qquad (13)$$

$$W_{ks}^t \leq 3 \quad \forall k \in \{1,2,\dots,K\}, s \in \{1,2,\dots,S\}, \forall t \in \{1,2,\dots,T\} \qquad (14)$$

$$\sum_{\substack{k=1 \\ k \neq l}}^{K} \sum_{p=t+1}^{t+\widetilde{tt_s}-1} X_{kls}^{p} \leq \left(1 - \sum_{\substack{k=1 \\ k \neq l}}^{K} X_{kls}^{t}\right) \; \cdot \forall l \in \tag{15}$$
$$\{1 \cdot 2 \cdot \ldots \cdot K\} \cdot s \in \{1 \cdot 2 \cdot \ldots \cdot S\} \cdot t \leq (T - \widetilde{tt_s} + 1)$$

$$\sum_{\substack{k=1 \\ k \neq l}}^{K} \sum_{p=t}^{t+\widetilde{tt_s}} X_{kls}^{p} \leq 1 \quad \cdot \forall l \in \{1 \cdot 2 \cdot \ldots \cdot K\} \cdot \forall s \in \tag{16}$$
$$\{1 \cdot 2 \cdot \ldots \cdot S\} \cdot \forall t \in \{1 \cdot 2 \cdot \ldots \cdot T\}$$

$$\sum_{\substack{l=1 \\ k \neq l}}^{K} \sum_{p=t}^{t+\widetilde{tt_s}} X_{kls}^{p} \leq 1 \quad \cdot \forall k \in \{1 \cdot 2 \cdot \ldots \cdot K\} \cdot \forall s \in \tag{17}$$
$$\{1 \cdot 2 \cdot \ldots \cdot S\} \cdot \forall t \in \{1 \cdot 2 \cdot \ldots \cdot T\}$$

The model consists of two objective functions. The first objective, shown in Equation (1), is maximizing the knowledge level of the organization's personnel in the last period of the planning horizon, and the second objective, shown in Equation (2), is minimizing the duration of knowledge transfer between the organization's personnel. Equations (3) and (4) indicate that person l can learn knowledge from at most one person during period t. Equations (5) and (6) indicate that person k can teach at most one person during period t. Equations (7), (8), and (9) show that person k transfers knowledge type s to person l during period t if the knowledge of person k is at least one level higher than person l and if the professional trust level (α_{kl}) and personal trust level (β_{kl}) are higher than A and B, respectively. Constraint (10) indicates that the last period of teaching knowledge type s in the planning horizon cannot begin in $\widetilde{tt_s} - 1$, since there is insufficient time to learn that knowledge type. Equation (11) shows that the level of knowledge type s in person l is the same as the initial level during the $\widetilde{tt_s}$ initial periods of the planning horizon. Equation (12) indicates that the knowledge type s in person l increases by 1 level after training (period tt_s). Constraint (13) shows that the total cost of transferring knowledge from the teachers k to the learners l during the planning horizon cannot exceed the allocated budget C. Constraint (14) shows that the knowledge level of all persons in all the knowledge types must not exceed the highest level defined for expertise during the planning horizon. Equation (15) indicates that if X_{kls}^{t} equals one at the beginning of period t, person l cannot learn from another person during the subsequent $\widetilde{tt_s} - 1$ periods. Equation (16) indicates that while person l is learning knowledge type s from person k, learning a higher level of this knowledge from other persons is impossible. Constraint (17) shows that no more than one person can simultaneously learn knowledge s from person k during period t.

4. SOLUTION METHOD

The Lagrangian relaxation method is used to solve the model of the knowledge flow network between an organization's personnel. Hence, first, the algorithm is introduced and, then, the results obtained from solving the model in small, medium, and large scales are presented.

4. 1. LP-Metric Method   A multi-objective decision-making model consists of a vector of decision variables, objective functions, and constraints to maximize or minimize the objective functions. Since such problems rarely have a unique solution, the decision-maker selects a solution from among a set of efficient solutions.

The LP-Metric method is a multi-criteria decision-making method (MCDM) that can solve multi-objective decision-making models (MODMs). This method minimizes the sum of the powers of the relative deviations of the objectives from their optimal values and combines several objective functions into a single objective. The LP-Metric method drew interest for two reasons:

- It requires less information from the decision-maker.
- It is practically simple to use.

The point x* is called an ideal point if it simultaneously optimizes all the objectives in a problem. However, such a solution does not usually exist due to the conflicts between different objectives. Another definition for the ideal point is when the optimal value of each objective function is determined separately. Then, the metric distance in the LP methods is used to measure the proximity of a solution to the ideal solution.

The parameter $1 \leq P \leq \infty$ determines the LP family. The value of P determines the degree of priority on the present deviations, such that the higher this value is, the higher the emphasis will be on the most considerable variations. Moreover, $P = \infty$ means that the most significant variations will be considered from among the existing variations for the optimization. The values P=1, P=2, and $P = \infty$ are usually used in the calculations and it depends on the decision-maker in any case.

Since the value of LP-Metric can be affected by the measurement scale of the objectives (in case these scales are different), the following formula can be used to resolve this issue:

$$LP = \left\{ \sum_{i=1}^{k} w_i \left[\frac{f_i(x^{*i}) - f_i(x)}{f_i(x^{*i}) - f_i(\tilde{x}^i)} \right]^{p} \right\}^{\frac{1}{p}} \tag{18}$$

The metric distance obtained from Equation (18) varies between zero and one. The maximum values of the objectives are desired. x^{*i} denotes the ideal solution in optimizing the ith objective, $\tilde{x}^i$ is a solution that minimizes f_i, x represents a given solution, and w_i indicates the significance (weight) of the ith objective. The LP-Metric function must be minimized to minimize deviations from the ideal value. If the objectives are minimization, the LP formula is obtained as Equation (19):

$$LP = \left\{ \sum_{i=1}^{k} w_i \left[\frac{f_i(x) - f_i(\tilde{x}^i)}{f_i(x^{*i}) - f_i(\tilde{x}^i)} \right]^p \right\}^{\frac{1}{p}} \tag{19}$$

All the objective functions (minimization and maximization) are added via the LP-Metric method, and the minimum value of the overall function is calculated. In the LP-Metric technique, the preferences of the decision-maker to various objectives are represented by their related weights.

For this purpose, we used lower bound, and upper bound for each objective function, and calculated Z3 according to the following equation:

$$Z3 = w1\left(\frac{UB1 - z1}{UB1 - LB1}\right) + w2\left(\frac{z2 - LB2}{UB2 - LB2}\right) \tag{20}$$

UB1 (upper bound 1), LB1 (lower bound 1), UB2 (upper bound 2), and LB2 (lower bound 2) are the bounds of Z1, and Z2, respectively. For UB1, LB1, UB2, and LB2 calculation, we used the following relations:

$$UB1 = \sum_s \sum_k 3\gamma_{ks} \tag{21}$$

The first objective function is maximizing the knowledge level of the organization's personnel in the last period of the planning horizon. Clearly, according to situations, knowledge is transferred from the first to the last period. Since the maximum level of each knowledge (for the experts) is three, we used this value for UB1. Because this objective function value cannot exceed this value.

$$LB1 = \sum_s \sum_k w_{ks}^1 \gamma_{ks} \tag{22}$$

In lower bound 1 we used the knowledge level of each person at the first period. Clearly, after knowledge sharing, the level of the organization's personnel in the last period of the planning horizon cannot be less than their initial levels.

$$LB2 = 0 \tag{23}$$

The second objective function is minimizing the duration of knowledge transfer between the organization's personnel. We choose LB2=0. If we don't have any knowledge sharing, we will not consume any time for teaching or learning. Therefore, this value can be 0.

$$UB2 = \sum_{\substack{l=1 \\ k \neq l}}^{K} \sum_{s=1}^{S} \sum_{k=1}^{K} \left(\widetilde{tt}_s \times (1.5 - min1(\theta_k \times \pi_k)) \times (1.5 - min2(\lambda_l \times \pi_l)) \right)(3 - w_{ks}^1) \tag{24}$$

For upper bound 2 calculation, we considered to maximum necessary time for all persons to become experts or have level 3 in all the fields. In the worst case, we assume two persons with the first and the second-lowest organizational commitment to be teacher and learner. Clearly, for these persons minimum teaching and learning capabilities are considered. Therefore, in UB2 we used $min1(\theta_k \times \pi_k)$ and $min2(\lambda_l \times \pi_l)$.

4. 2. Lagrangian Relaxation Method

The Lagrangian relaxation method is a common technique for solving some optimization problems. This method was first introduced by Held and Krap to solve the Traveling Salesman Problem (TSP) and is a technique that solves a constrained and hard optimization problem via a more straightforward problem. The main idea behind Lagrangian relaxation is relaxing the complicated constraints, multiplying them by coefficients called Lagrangian multipliers, and adding them to the objective function of the problem. The relaxed problem is expected to be easier to solve than the original problem due to eliminating some of the constraints and the enlargement of the feasible region.

The relaxation of the Lagrangian multipliers as a method to obtain the upper (lower) bounds of the objective functions of mathematical problems attracted interest after the successful solution of the TSP, the scale of which was considerably large compared to the computational power of the time, in 1970. Given the computational burden in large-sized problems, determining the upper and lower bounds is of utmost significance in increasing the method's efficiency.

The Lagrangian relaxation algorithm begins by considering a λ for each constraint. The λ's, called Lagrangian multipliers, act as shadow prices in linear programming (λ represents the variation of the objective function for a unit change in the number to the right of the corresponding constraint). Then, the Lagrangian function, which is a combination of the constraints and the objective function, is formulated as Equation (25):

$$\theta(x \cdot \lambda) = f(x) + \sum_{i=1}^{m} \lambda_i [b_i - g_i(x)] \tag{25}$$

In this equation, $\theta(x, \lambda)$ denotes the objective function of the relaxed problem, $f(x)$ represents the objective function of the original problem. b_i is the right side of the relaxed constraint, and $g_i(x)$ denotes the left side of the relaxed constraint. Finally, the derivatives of the Lagrangian function are calculated for each of the variables separately [21].

In this research, Lagrangian relaxation is used to solve the presented model. It is done by adding each relaxed constraint to the objective function of the problem with a Lagrangian multiplier. To find appropriate Lagrangian multipliers a loop is formed, and the problem is solved with different values. The solution obtained from the Lagrangian relaxation algorithm may violate the relaxed constraints. The steps of the Lagrangian relaxation algorithm are presented as follows:

1. Calculate an initial upper bound (UB) and LB*= -∞ and the vector of the initial Lagrangian coefficient (λ).
2. Solve the released problem (D) and compute x* and LB.
3. If LB>LB*, then LB*=LB.

4. $\lambda^{(t)} = \lambda^{(t-1)} + k(b-Ax)$ while $k = \theta \frac{UB-LB^*}{\sum_{i=1}^{n}(b_i - a_i x^*)^2}$

5. If after m consecutive repetitions there is no improvement in the amount of the best limit then $\theta = \theta/2$.

6. Refer to the second step and continue until the algorithm stops.

5. Sensitivity analysis

In this section, Table 1 introduces several small, medium, and large-sized problems. Then, various sensitivity analysis results are presented. After ensuring the model's validity, the sample problem is solved using the Lagrangian relaxation method at the mentioned scales in pessimistic, likely, and optimistic cases.

Sample problem 1 consists of 5 persons, three types of knowledge, and a 4-period planning horizon. The sensitivity of this problem was analyzed using the LP-Metric objective function, with the result shown in Figures3-9. Figures 1 and 2 show the Pareto layer of the

TABLE 1. Sample problem size

| Sample Problems	Size	Number of Persons	Number of Knowledge	Planning Horizon
1		5	3	4
2		10	3	4
3	Small	15	4	5
4		20	4	5
5		25	5	6
6		50	5	6
7		55	6	7
8	Medium	60	6	7
9		65	6	8
10		70	7	8
11		100	7	8
12		105	8	8
13		110	8	9
14		120	7	9
15		130	8	10
16		130	11	12
17		130	12	12
18	Large	135	13	12
19		135	14	12
20		140	15	12
21		140	16	12
22		145	17	12
23		145	18	12
24		150	19	12
25		150	20	12

objective functions and the Pareto layer of the probability of the pessimistic, likely, and optimistic cases.

Figure 1 displays all eleven cases of the Pareto layer for the average objective functions in pessimistic, likely, and optimistic conditions. In the first case, the weight of the first objective function is considered 1, and that of the second objective function is regarded zero. Then, 0.1 is deducted from the weight of the first objective function and added to that of the second objective function case by case until all the eleven cases are formed.

As shown in Figure 1, up to the 5th case, the weight of the first objective function is reduced and the weight of the second objective function is increased. In these conditions, the LP-Metric objective function varies from zero in the first case to 0.275 in the 5th case. From the 5th case up to the 11th case, the weight of the first objective function is reduced and the weight of the second objective function is increased. The LP-Metric objective function varies from 0.275 to zero.

Figure 2 shows the results of the objective function for the optimistic (1), likely (2), pessimistic (3) and average (4) situations for a problem. Average situation is calculated as follows:

$$\frac{\text{pessimistic situation} + 4 * \text{likely situation} + \text{optimistic situation}}{6} \quad (26)$$
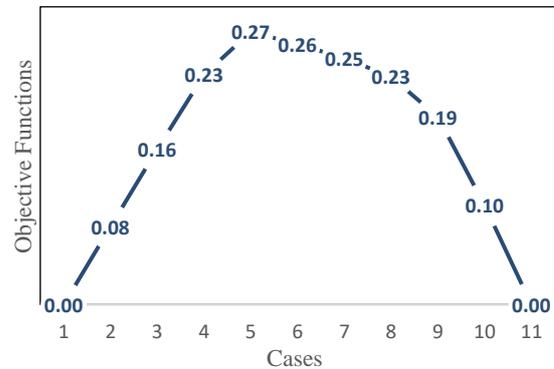
**Figure 1.** Pareto layer of the LP-Metric objective function
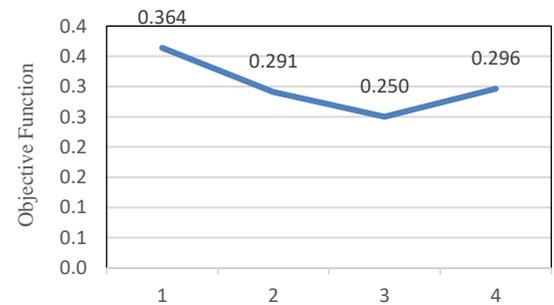
Figure 2. Pareto layer of the probability of occurrence of random cases

It must be noted that the sensitivity analysis in this section, performed in sample problem 1 for likely situation.

Figure 3 shows that an increase in the planning horizon increases the time available for knowledge transfer, leading to a rise in the knowledge level and an increase in the duration of knowledge transfer in the organization.

Figures 4-9 display sensitivity analysis of the teaching and learning capabilities, the organizational commitment, and the professional and personal trust in a range of -100 to 100%.

Figures 4 and 5 show that an increase in the teaching capability and learning capability merely reduces the second objective function, i.e., duration of knowledge transfer, and does not affect the first objective function, i.e., knowledge level of the organization. Also, the teaching capability has more significant effect on the second objective function than does the learning capability, such that a 100% increase in the teaching capability leads to a 12% decrease in the second objective function. In comparison, a 100% increase in the learning capability results in only a 5% decrease in this function. Furthermore, a 100% reduction in the teaching capability


Figure 5. Effect of a change in the learning capability on the objective functions

increases the second objective function by about 107%, while a reduction in the learning capability increases it by only about 41%.

The impact of changes in the organizational commitment on the objective function is shown in Figure 6. Similar to the last two parameters, organizational commitment only reduces the duration of knowledge transfer (second objective function) and does not affect on the knowledge level in the organization. A 100% increase in this parameter reduces the knowledge transfer duration by 35%, and a 100% decrease in it increases the knowledge transfer duration by 194%. These values indicate that the influence of organizational commitment on knowledge transfer duration is greater than those of teaching and learning capabilities.

Regarding Figures 6, 7, and 8, it must be mentioned that the model constraints associated with professional and personal trust indicate that these parameters are inter-dependent, and knowledge transfer occurs only when they exceed the specified thresholds.

Figure 7 indicates the sensitivity analysis of professional trust. As can be seen, the knowledge transfer and its duration increase by 4 and 103%, with a 100%

Figure 3. Effect of a change in the planning horizon on the objective functions
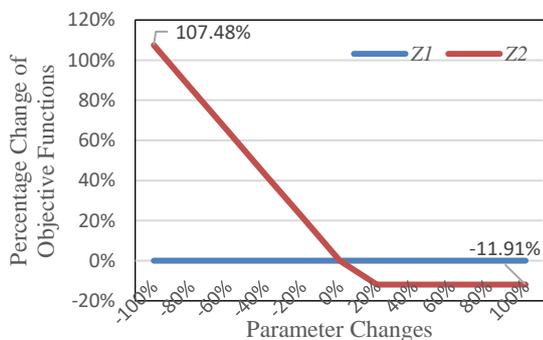
Figure 4. Effect of a change in the teaching capability on the objective functions
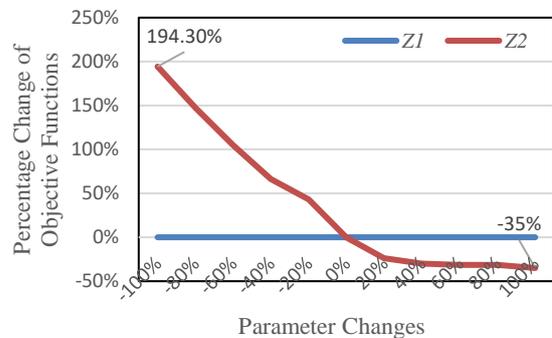

Figure 6. Effect of a change in organizational commitment on the objective functions
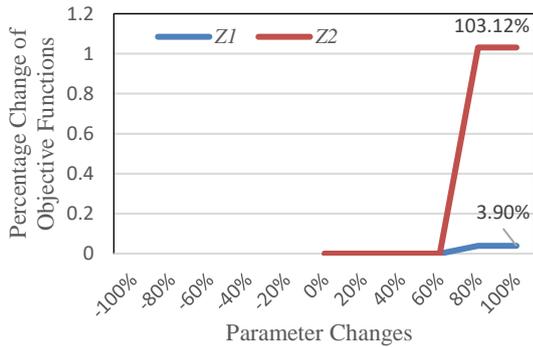
Figure 7. Effect of a change in professional trust on the objective functions

increase in professional trust. In addition, a reduction in this parameter does not change the objective function since it violates the threshold and Constraint 8.

As observed in Figure 8, in this particular problem, a 100% increase in personal trust has no impact on the two objective functions due to the dependence of this parameter on professional trust. This is evident in Figure 9, which displays the simultaneous change of professional and personal trust.
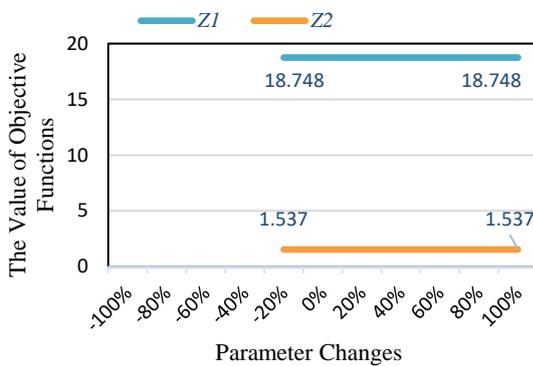
Figure 8. Effect of a change in personal trust on the objective functions
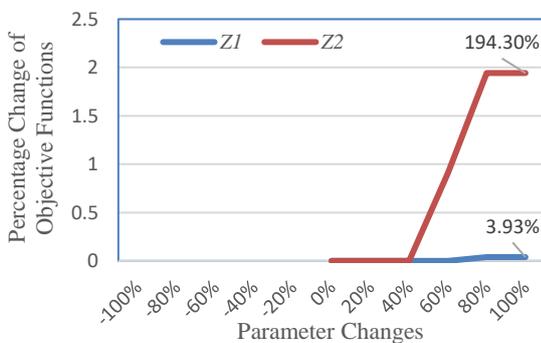
Figure 9. Effect of simultaneous changes in professional and personal trust on the objective functions

Simultaneous changes in personal trust and professional trust these parameters are analyzed in Figure 9. It shows a 100% increase in professional and personal trust increases the first and second objective functions by 4 and 194%, respectively.

6. COMPUTATIONAL RESULTS AND DISCUSSION

In this section, the problems are solved at small, medium, and large scales using the CPLEX solver and Lagrangian relaxation and compared. It is worth mentioning that knowledge transfer occurs between persons if the professional and personal trust values are higher than the specified thresholds. The thresholds considered for the professional and personal trust values in all the problems studied in this paper were selected based on the quantitative research presented by Ouakouak and Ouedraogo [16], conducted among 307 employees in Canadian organizations. All the structures in their study have been measured according to the 5-point Likert scale. The following questions were asked of the employees for professional and personal trust. The resulting average professional trust and personal trust threshold values obtained for knowledge transfer were 0.822 and 0.653, respectively (see Table 2).

6. 1. Solution of Small-scale Problems   In this section, 5 sample problems are evaluated. The pessimistic, likely, and optimistic cases were generated for each sample problem and solved using the LP-metric method in GAMS software and the Lagrangian relaxation algorithm. The objective function values and computation time for each sample are shown in Tables 3 and 4.

Figures 10-13 are for a better comparison of the solution methods using the values in Tables 3 and 4. These figures show the Lagrangian relaxation method usually produces better results than the CPLEX solver for the first objective function.

TABLE 2. Factors affecting the determination of professional and personal trust [16]

Parameter	Question
Professional Trust	I believe my colleagues trust me to perform my tasks correctly.
	I trust my colleagues in their ability to perform their tasks correctly.
	I believe that my colleagues perform tasks assigned to them professionally and committedly.
Personal Trust	My colleagues are honest.
	I believe that the intentions and motivations of my colleagues are sincere.
	I believe that my colleagues look after my interests.

**TABLE 3.** Solution of the small-scale problems using GAMS software

Problem	Indicator	GAMS Software		
		Pessimistic	Likely	Optimistic
1	Z1	18.748	18.748	19.082
	Z2	1.537	1.537	2.149
	Solve Time	0.311	0.335	0.344
2	Z1	34.657	35.002	35.002
	Z2	8.119	6.368	6.368
	Solve Time	0.639	0.558	0.697
3	Z1	52.654	53.019	55.598
	Z2	9.948	9.948	17.568
	Solve Time	1.213	1.236	1.342
4	Z1	87.510	87.510	88.418
	Z2	8.978	8.978	12.086
	Solve Time	1.798	1.909	1.900
5	Z1	142.234	143.123	143.123
	Z2	36.046	41.339	40.016
	Solve Time	3.365	3.714	3.892

TABLE 4. Solution of the small-scale problems using the Lagrangian relaxation method

Problem	Indicator	Lagrangian Relaxation Method		
		Pessimistic	Likely	Optimistic
1	Z1	21.101	21.553	23.570
	Z2	5.618	7.132	9.857
	Solve Time	3.096	3.223	3.387
2	Z1	38.779	40.012	40.843
	Z2	14.933	14.367	17.567
	Solve Time	4.864	4.459	4.850
3	Z1	58.305	63.115	67.844
	Z2	21.595	36.120	33.315
	Solve Time	5.786	7.910	7.922
4	Z1	97.333	101.076	103.308
	Z2	22.278	33.476	32.650
	Solve Time	9.120	10.561	11.233
5	Z1	147.855	154.252	156.588
	Z2	47.983	79.270	81.115
	Solve Time	15.066	17.088	17.076

6. 2. Solution Of Medium-Scale Problems

In this section, Sample Problems 6-10 are evaluated. The pessimistic, likely, and optimistic cases were generated
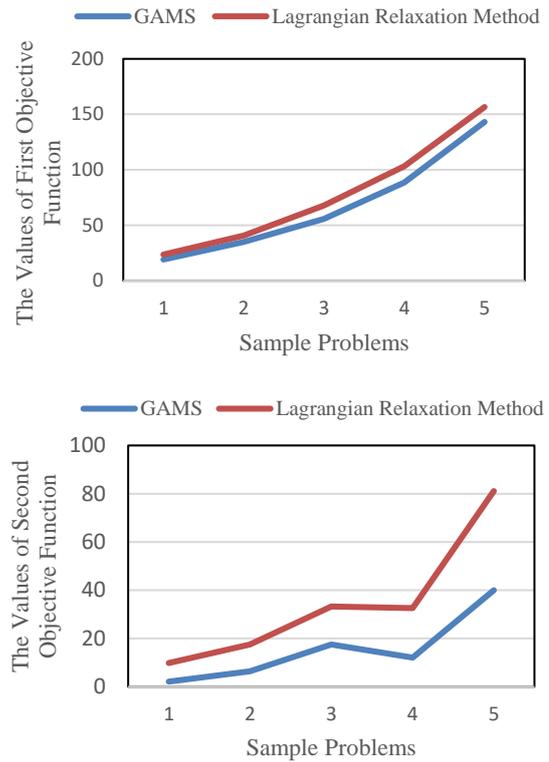
Figure 10. Average graph of the objective functions of the small-scale sample problems in the optimistic case
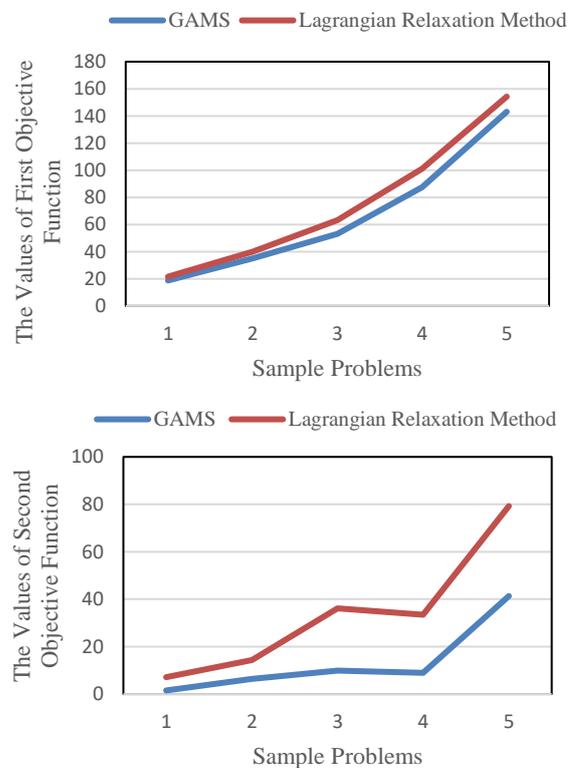
Figure 11. Average graph of the objective functions of the small-scale sample problems in the likely case
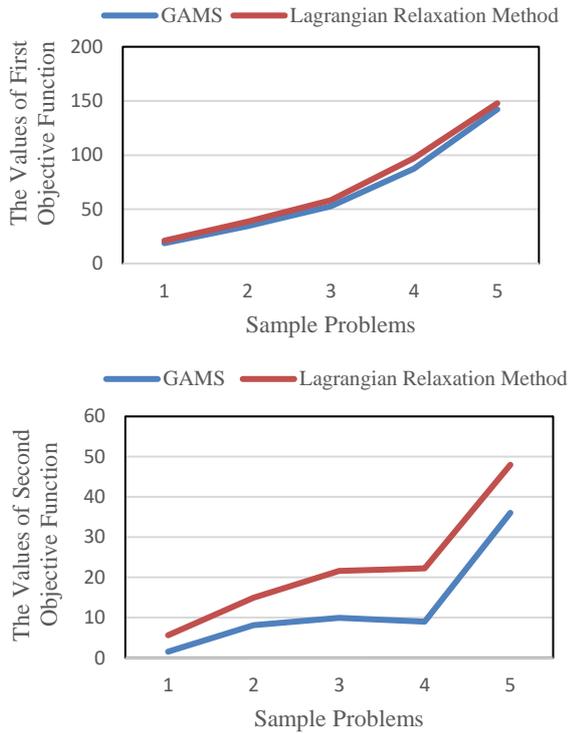
Figure 12. Average graph of the objective functions of the small-scale sample problems in the pessimistic case
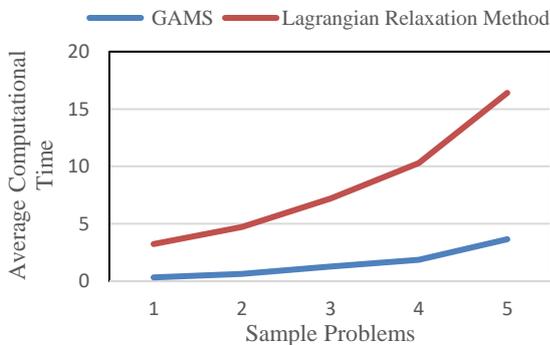
Figure 13. Average graph of the objective functions of the small-scale sample problems

for each sample problem and solved using the CPLEX solver in the GAMS software and the Lagrangian relaxation algorithm. The objective function values and computation time for each sample are shown in Tables 5 and 6.

Figures 14-17 are for a better comparison of the solution methods using the values in Tables 5 and 6. As can be seen in these figures, more knowledge transfer occurs in the Lagrangian relaxation method than in the solution using the CPLEX solver. For the larger problems the Lagrangian relaxation method reaches the solution faster than the CPLEX solver.

TABLE 5. Solution of the medium-scale problems using GAMS software

| Problem	Indicator	GAMS Software		
		Pessimistic	Likely	Optimistic
6	Z1	275.881	282.607	291.186
	Z2	98.708	114.969	107.113
	Solve Time	8.448	9.969	14.502
7	Z1	364.446	382.337	401.684
	Z2	134.560	142.362	166.802
	Solve Time	16.821	82.720	41.422
8	Z1	433.738	449.019	475.594
	Z2	157.475	184.731	194.095
	Solve Time	17.951	43.481	1018.640
9	Z1	424.076	435.798	451.921
	Z2	219.634	240.629	232.977
	Solve Time	40.534	68.920	1022.911
10	Z1	550.981	569.321	592.896
	Z2	280.773	259.136	305.025
	Solve Time	48.365	1028.467	1032.434

TABLE 6. Solution of the medium-scale problems using the Lagrangian relaxation method

Problem	Indicator	Lagrangian Relaxation Method		
		Pessimistic	Likely	Optimistic
6	Z1	287.648	302.342	308.466
	Z2	136.683	165.540	136.014
	Solve Time	39.641	42.345	43.945
7	Z1	381.857	400.260	420.441
	Z2	161.919	166.660	163.821
	Solve Time	75.320	84.547	98.482
8	Z1	452.527	472.922	498.502
	Z2	177.705	171.519	161.457
	Solve Time	88.704	110.981	110.111
9	Z1	438.723	449.753	474.080
	Z2	233.201	240.780	248.319
	Solve Time	148.017	139.822	164.320
10	Z1	551.391	595.708	615.980
	Z2	229.225	311.712	310.039
	Solve Time	170.700	175.286	190.954

6. 3. Solution of Large-scale Problems   In this section, five large-scale sample problems are evaluated. The pessimistic, likely, and optimistic cases were

generated for each sample problem and solved using the CPLEX solver and the Lagrangian relaxation algorithm. The objective function values and computation time for each sample are shown in Tables 7 and 8.
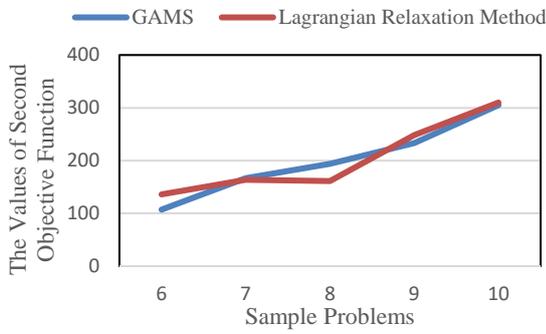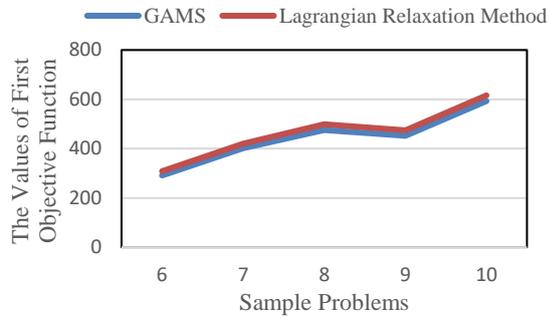
Figure 14. Average graph of the objective functions of the medium-scale sample problems in the optimistic case
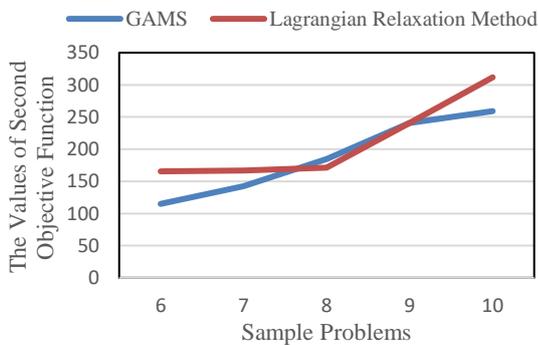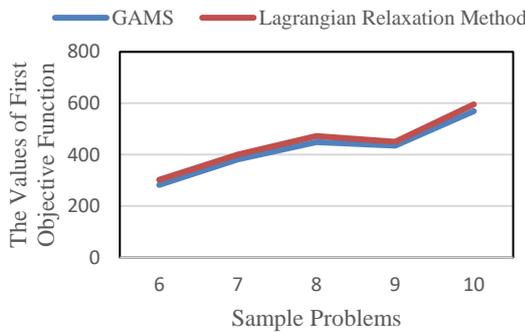
Figure 15. Average graph of the objective functions of the medium-scale sample problems in the likely case
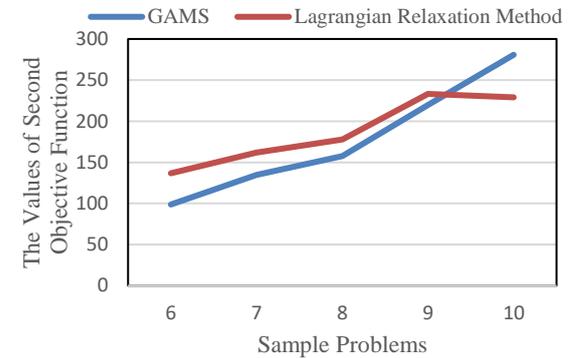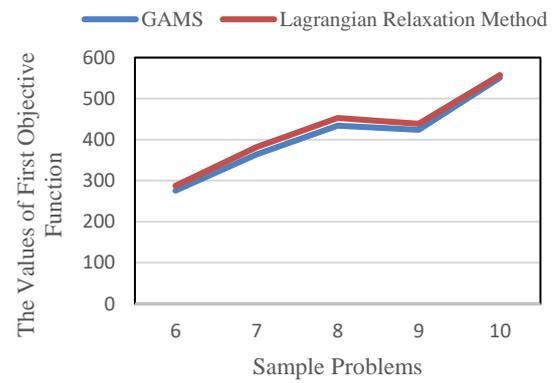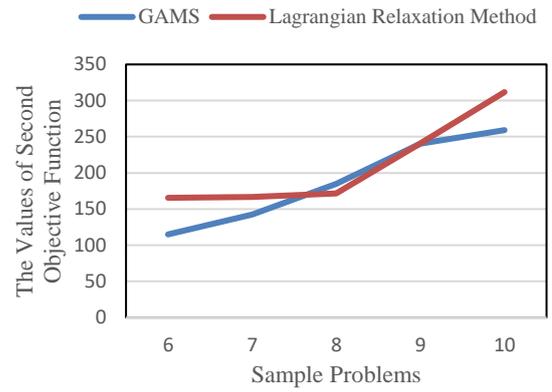
Figure 16. Average graph of the objective functions of the medium-scale sample problems in the pessimistic case
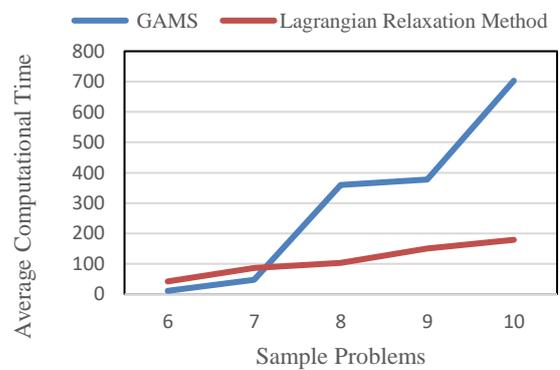
Figure 17. Average graph of the objective functions of the medium-scale sample problems

TABLE 7. Solution of the large-scale problems using GAMS software

| Problem	Indicator	GAMS Software		
		Pessimistic	**Likely**	**Optimistic**
11	Z1	825.429	867.715	901.553
	Z2	342.826	394.597	371.124
	Solve Time	1060.848	1068.224	1067.315
12	Z1	986.869	1006.240	1030.502
	Z2	312.949	332.498	403.207
	Solve Time	1083.767	1092.608	1095.609
13	Z1	987.680	1033.086	1067.017
	Z2	453.209	551.923	563.889
	Solve Time	1109.767	1116.027	1122.732
14	Z1	963.671	983.462	1008.336
	Z2	446.644	438.087	429.772
	Solve Time	1114.210	1123.539	1122.166
15	Z1	1207.750	1227.054	1233.216
	Z2	382.905	416.643	425.026
	Solve Time	1161.307	1167.212	1174.656
16	Z1	1168.396	1283.952	1475.807
	Z2	416.603	457.806	526.214
	Solve Time	1493.652	1573.324	1634.021
17	Z1	1412.303	1569.225	1705.679
	Z2	452.956	503.284	547.048
	Solve Time	1721.320	1764.378	1813.225
18	Z1	1631.315	1773.169	2086.081
	Z2	390.268	424.204	499.063
	Solve Time	1853.326	1893.601	1961.254
19	Z1	1952.676	2194.018	2411.009
	Z2	486.913	547.093	601.201
	Solve Time	2002.336	2010.325	2029.321
20	Z1	2414.407	2624.355	2948.714
	Z2	474.915	516.212	580.014
	Solve Time	2098.356	2180.957	2259.325
21	Z1	2686.056	2951.710	3354.216
	Z2	509.380	559.758	636.089
	Solve Time	2323.255	2490.521	2501.378
22	Z1	2756.253	3178.452	3695.874
	Z2	486.981	559.748	650.870
	Solve Time	2651.355	2730.301	2681.021
23	Z1	2750.099	3197.790	3997.238
	Z2	445.547	518.078	647.598
	Solve Time	2932.631	3110.665	3054.221
24	Z1	3527.419	3876.285	4259.654
	Z2	497.898	547.141	601.254
	Solve Time	3742.332	3893.602	3721.225
25	Z1	3645.842	4050.936	4501.040
	Z2	569.065	632.294	702.549
	Solve Time	4398.021	4553.221	4630.232

**TABLE 8.** Solution of the large-scale problems using the Lagrangian relaxation method

Sample Problems	Indicator	Lagrangian Relaxation Method		
		Pessimistic	**Likely**	**Optimistic**
11	Z1	980.408	1009.717	1005.554
	Z2	1013.379	917.578	635.009
	Solve Time	409.579	448.384	441.293
12	Z1	1123.060	1179.430	1208.948
	Z2	948.131	1067.769	913.085
	Solve Time	618.205	655.781	696.747
13	Z1	1184.371	1214.392	1215.821
	Z2	1102.582	1341.834	1035.959
	Solve Time	843.691	903.050	956.417
14	Z1	1086.948	1128.485	1167.396
	Z2	1027.694	1200.839	1037.956
	Solve Time	886.937	967.430	1005.905
15	Z1	1291.978	1465.508	1492.896
	Z2	989.330	1166.494	1006.252
	Solve Time	892.354	973.231	1016.325
16	Z1	1193.562	1311.607	1507.594
	Z2	671.088	737.459	847.654
	Solve Time	1034.393	1136.696	1306.547
17	Z1	1552.706	1725.229	1875.249
	Z2	793.620	881.800	958.478
	Solve Time	1088.844	1209.827	1315.029
18	Z1	1681.032	1827.209	2149.658
	Z2	781.732	849.709	999.658
	Solve Time	1099.247	1194.834	1405.687
19	Z1	2106.723	2367.104	2601.213
	Z2	686.515	771.365	847.654
	Solve Time	1299.314	1459.903	1604.289
20	Z1	2558.147	2780.595	3124.264
	Z2	797.641	867.001	974.158
	Solve Time	1366.588	1485.422	1669.014
21	Z1	2840.915	3121.885	3547.597

|				
	Z2	764.431	840.034	954.584
	Solve Time	1433.109	1574.845	1789.597
	Z1	2843.906	3268.857	3800.997
22	Z2	633.885	728.604	847.214
	Solve Time	1413.265	1624.443	1888.887
	Z1	2806.825	3263.750	4079.687
23	Z2	515.002	598.838	748.547
	Solve Time	1385.652	1611.223	2014.029
	Z1	3760.662	4132.596	4541.314
24	Z2	784.338	861.910	947.154
	Solve Time	1861.567	2045.678	2247.998
	Z1	3889.328	4321.475	4801.639
25	Z2	847.191	941.323	1045.914
	Solve Time	1993.308	2214.787	2460.874

Figures 18-21 were plotted for a better comparison of the solution methods using the values in Tables 7 and 8. They showed that the Lagrangian relaxation method can transfers more knowledge than GAMS. Furthermore, the Lagrangian relaxation method is usually faster than the GAMS computational time.


Figure 19. Average graph of the objective functions of the large-scale sample problems in the likely case

Figure 18. Average graph of the objective functions of the large-scale sample problems in the optimistic case
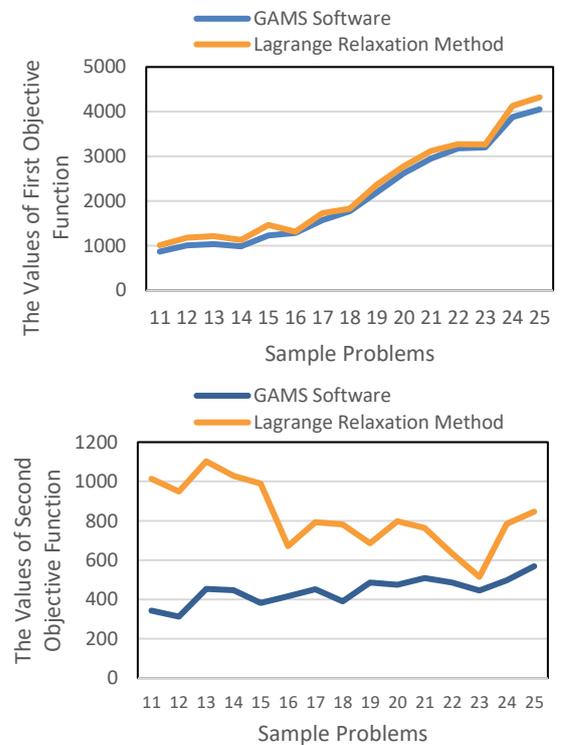
Figure 20. Average graph of the objective functions of the large-scale sample problems in the pessimistic case
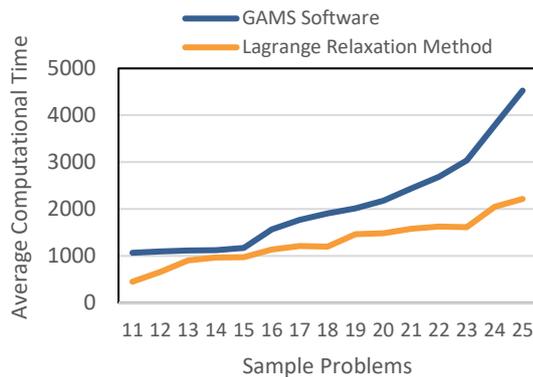
Figure 21. Average graph of the objective functions of the large-scale sample problems

The Lagrangian relaxation method transfers more knowledge than CPLEX solver in all the optimistic, likely, and pessimistic situations. Consequently, the knowledge transfer duration is longer in the Lagrangian relaxation method. Concerning computation time, the larger the sample problems become, the shorter the solution time using Lagrangian relaxation becomes compared to the CPLEX solver.

In addition, Montazer [22] developed a new approach for knowledge based systems reduction using rough sets theory

7. CONCLUSION AND SUGGESTIONS

In the present knowledge-based era, knowledge as the most valuable capital in organizations, requires a novel management approach toward issues concerning the organization and the personnel. A change in the nature of activities performed in organizations toward knowledge-based ones has increased the essential of knowledge management. One of the most important knowledge management processes is knowledge transfer, which it can be done by internal or external resources of an organization. Clearly, knowledge upgrade in an organization using external resources requires more time and budget. For this reason, reliance on internal resources is preferred in organizations. Factors such as professional and personal trust and organizational commitment play a key role in such knowledge transfer.

This paper designs a knowledge flow network between the personnel of an organization using stochastic MIP for maximizing the knowledge level and minimizing the knowledge transfer duration time. To solve the knowledge flow network model, several sample problems were designed; then, sensitivity analyses were performed on one of the sample problems. After model's validity several small, medium, and large-sized problems in pessimistic, likely, and optimistic cases were solved

using the CPLEX solver and the Lagrangian relaxation method. Finally, a comparison was drawn between the methods. The results indicate that organizational commitment has the most considerable effect on the knowledge transfer duration, followed by teaching and learning capabilities. Moreover, the effect of an increase in professional trust is considerably more significant on the reduction in the knowledge transfer duration than on the increase in the knowledge level. It indirectly contributes to a decrease in the costs of knowledge transfer. Comparing the two solution methods indicates that the Lagrangian relaxation algorithm produces better results than the CPLEX solver in all cases and reaches the solution faster in larger problems.

Given the increasing importance of knowledge management and knowledge transfer in organizations and the lack of quantitative research on this topic, various approaches can be taken to develop the work in this paper. Examples include using multiple teaching methods in the knowledge transfer process, considering the possibility of group teaching, and assuming stochastic learning. Furthermore, using rough set theory in the field of knowledge management is another direction of developing our future investigans.

8. REFERENCES

1. Dezfoulian, H.R., Afrazeh, A. and Karimi, B., "A new model to optimize the knowledge exchange in industrial cluster: A case study of semnan plaster production industrial cluster", *Scientia Iranica*, Vol. 24, No. 2, (2017), 834-846, https://dx.doi.org/10.24200/sci.2017.4065

2. Leyer, M., Schneider, C. and Claus, N., "Would you like to know who knows? Connecting employees based on process-oriented knowledge mapping", *Decision Support Systems*, Vol. 87, (2016), 94-104, https://doi.org/10.1016/j.dss.2016.05.003

3. Van Wijk, R., Jansen, J.J. and Lyles, M.A., "Inter-and intra-organizational knowledge transfer: A meta-analytic review and assessment of its antecedents and consequences", *Journal of Management Studies*, Vol. 45, No. 4, (2008), 830-853, https://doi.org/10.1111/j.1467-6486.2008.00771.x

4. Li, H., Li, C. and Wang, Z., "An agent-based model for exploring the impacts of reciprocal trust on knowledge transfer within an organization", *Journal of Business & Industrial Marketing*, (2021), https://doi.org/10.1108/JBIM-12-2019-0528

5. Liu, D.-R., Lin, C.-W. and Chen, H.-F., "Discovering role-based virtual knowledge flows for organizational knowledge support", *Decision Support Systems*, Vol. 55, No. 1, (2013), 12-30, http://dx.doi.org/10.1016/j.dss.2012.11.018

6. Różewski, P., Jankowski, J., Brodka, P. and Michalski, R., "Knowledge workers' collaborative learning behavior modeling in an organizational social network", *Computers in Human Behavior*, Vol. 51, (2015), 1248-1260, https://doi.org/10.1016/j.chb.2014.12.014

7. Chandra, R., Iyer, R.S. and Raman, R., "Enabling organizations to implement smarter, customized social computing platforms by leveraging knowledge flow patterns", *Journal of Knowledge Management*, (2015), https://doi.org/10.1108/JKM-11-2014-0455

8.   Rezaeian, A., Bagheri, R. and Fartoukzadeh, H., "Identifying, prioritizing and modeling factors of knowledge networks formation in knowledge-based organizations", ***Journal of Management Improvement***,   Vol. 11, No. 31-24, http://www.behboodmodiriat.ir/article_57684.html?lang=en

9.   Lin, C.-P., "To share or not to share: Modeling tacit knowledge sharing, its mediators and antecedents", ***Journal of business ethics***,   Vol. 70, No. 4, (2007), 411-428, https://doi.org/10.1007/s10551-006-9119-0

10.   Duan, Y., Nie, W. and Coakes, E., "Identifying key factors affecting transnational knowledge transfer", ***Information & Management***,   Vol. 47, No. 7-8, (2010), 356-363, https://doi.org/10.1016/j.im.2010.08.003

11.   Choong, Y.L. and Fang, C.W., "Factors affecting knowledge transfer and absorptive capacity in multinational corporations", (2006),   https://www.semanticscholar.org/paper/Factors-affecting-knowledge-transfer-and-absorptive-Choong-Fang/39a2cece2098f2a10b09c4c8eef1d1aa3a62a1de

12.   Srećković, M. and Windsperger, J., The impact of trust on the choice of knowledge transfer mechanisms in clusters, in Network governance. 2013, Springer.73-85.

13.   Alexopoulos, A.N. and Buckley, F., "What trust matters when: The temporal value of professional and personal trust for effective knowledge transfer", ***Group & Organization Management***, Vol. 38,   No.   3,   (2013),   361-391, http://dx.doi.org/10.1177/1059601113488939

14.   Swart, J., Kinnie, N., Van Rossenberg, Y. and Yalabik, Z.Y., "Why should i share my knowledge? A multiple foci of commitment perspective", ***Human Resource Management Journal***,   Vol. 24, No. 3, (2014), 269-289, http://dx.doi.org/10.1111/1748-8583.12037

15.   Ouakouak, M.L. and Ouedraogo, N., "Fostering knowledge sharing and knowledge utilization: The impact of organizational commitment and trust", ***Business Process Management Journal***, (2019), https://doi.org/10.1108/BPMJ-05-2017-0107

16.   Curado, C. and Vieira, S., "Trust, knowledge sharing and organizational commitment in smes", ***Personnel Review***, (2019), https://doi.org/10.1108/PR-03-2018-0094

17.   García-Almeida, D.J. and Bolívar-Cruz, A., "Successful replication of knowledge in the growth of service organizations: Evidence from spanish hotel chains", ***Journal of Knowledge Management***,   (2020), https://doi.org/10.1108/JKM-12-2019-0700

18.   Luo, C., Lan, Y., Luo, X.R. and Li, H., "The effect of commitment on knowledge sharing: An empirical study of virtual communities", ***Technological Forecasting and Social Change***, Vol.   163,   (2021),   120438, https://doi.org/10.1016/j.techfore.2020.120438

19.   Dong, S., Johar, M. and Kumar, R., "Understanding key issues in designing and using knowledge flow networks: An optimization-based managerial benchmarking approach", ***Decision Support Systems***,   Vol. 53, No. 3, (2012),   646-659, http://dx.doi.org/10.1016/j.dss.2012.04.007

20.   Dezfoulian, H. and Samouei, P., "The optimal network design for knowledge sharing in a supply chain for horizontal integration", ***Journal of Business Administration Researches***,   Vol. 11, No. 22, (2020), 101-128, doi. 20.1001.1.2645386.1398.11.22.5.7

21.   Wolsey, L.A., "Mixed integer programming", Wiley Encyclopedia of Computer Science and Engineering, (2007), 1-10.

22.   Montazer, G.A., "A new approach for knowledge based systems reduction using rough sets theory (research note)", ***International Journal of Engineering***, ***Transactions A: Basics,*** Vol. 16, No. 2, (2003), 157-162, https://www.ije.ir/article_71439.html

Persian Abstract

چکیده

انتقال دانش در دو سطح درون سازمانی و بین سازمانی می‌تواند انجام شود. یادگیری دانش از خارج از سازمان نیاز به بودجه و زمان قابل توجهی دارد، در حالی که با اشراف و اتکاء به دانش موجود در سازمان که نزد کارکنان است می‌توان با ایجاد یک شبکه جریان دانش بین کارکنان اقدام به ارتقاء سطح دانش آن‌ها با صرف کم‌ترین زمان نمود. طراحی یک مدل شبکه جریان دانش بین کارکنان سازمان با توجه به سطح اعتماد حرفه‌ای و شخصی، توان آموزش و یادگیری، سطح دانش کارکنان، میزان تعهد سازمانی، نوع و اهمیت هر دانش و همچنین غیرقطعی بودن مدت انتقال دانش مسأله‌ای است که در این مقاله به آن پرداخته می‌شود. این مسأله در قالب یک مدل ریاضی برنامه‌ریزی عدد صحیح مختلط غیرقطعی با توابع هدف حداکثر کردن سطح دانش و حداقل کردن مدت انتقال دانش موزون فرموله شد. مدل به کمک حل‌کننده CPLEX و الگوریتم آزادسازی لاگرانژ حل گردید. نتایج بدست آمده از حل مدل در همه اندازه‌های مورد نظر، نشان از کارایی بالای الگوریتم آزادسازی لاگرانژ در یافتن کران بالا برای مسأله اصلی در هر سه اندازه کوچک، متوسط و بزرگ دارد. همچنین نتایج نشان می‌دهد که پارامتر تعهد سازمانی تأثیر بیشتری نسبت به توان آموزش و یادگیری در مدت زمان انتقال دانش دارد.

International Journal of Engineering

Optimal Selection of Cutting Parameters for Surface Roughness in Milling Machining of AA6061-T6

K. Danesh Narooei*[a], R. Ramli[b]

[a] Department of Industrial Engineering, Faculty of Industry and Mine Khash, University of Sistan and Baluchestan, Zahedan, Iran
[b] Department of Mechanical and Manufacturing Engineering, Faculty of Engineering and Built Environment, Universiti Kebangsaan Malaysia, Malaysia

A B S T R A C T

Due to its ability to remove material quickly while maintaining optimum surface quality, end milling is considered one of the most frequent metal cutting procedures in industry. The present study aimed to investigate the impacts of cutting parameters and tool geometry on milling of Aluminum Alloy 6061-T6 to examine the impact surface roughness by utilizing response surface methodology (RSM). RSM was used to create a second-order mathematical model of surface roughness for this purpose. A multiple regression analysis used the analysis of variance to demonstrate the effect of machining settings on surface roughness and determine experiment performance. The trials for optimizing surface roughness were set up utilizing the central composite design (CCD) method and various cutting parameters such as spindle speed, feed rate and depth of cut. Also the parameters used in tool geometry are the radial rake angle (10, 13, 16, 19 and 22 degrees), and nose radius (0, 0.2, 0.4, 0.6 and 0.8 mm). The result shows that the nose radius has more significant effect on the surface roughness followed by the radial rake angle. Moreover, the effect of the depth of cut on surface roughness is more dominant than cutting speed. The optimum combinations of cutting and tool geometry parameters were cutting speed (60.53 m/min), feed rate (0.025 mm/tooth), depth of cut (0.84 mm), radial rake angle (12.72 degree) and nose radius (0.34 mm).

1. INTRODUCTION

The oldest process to shape components is metal cutting or machining in the manufacturing industry [1]. It is evaluated that 15% of the all-mechanical part produced worldwide is derived from machining operation. Metal cutting is a general term applied to a group of processes that includes material removal and shaping process to generate parts with various methods [2]. Material removal is desirable necessary in manufacturing operation for multiple reasons such as dimensional accuracy, high surface finish, and sharp corners and flatness [3]. The machining process can produce a variety of shapes and parts. The machining operation can be defined as a system including workpiece, cutting tool and the machine. The interactions among these elements are necessary to determine an efficient and economical machining process [4,5]. The general machining process are turning, milling, boring, drilling, planning, shaping, broaching, and sawing [6]. One of the common machining processes is milling to produce complicated parts in the various industries [7,8].

In the last decade, the metal cutting process continued to grow significantly with time to obtain optimum machining process efficiency. The offering optimum machining parameters is often the primary factor in attaining this specific purpose to develop along with implement a high effective procedure control intended for machining operations through parameter optimization [9]. The cutting process is affected by several factors such as tool geometry, cutting parameters, temperature and tool wear. The tool geometry parameters have high influence when compared by other factors on the quality of surface product [10,11].

Corresponding Author: kh_dnarooei@eng.usb.ac.ir (K. Danesh Narooei)

The milling process is capable of producing a variety of configuration with the utilized different milling cutter. The basic types of milling cutters with common milling operation are slab milling, face milling and end milling [10]. In milling process the main goal is to produce the parts with high quality in minimum machining time. In minimizing the machining time, the researcher utilized various optimization methods to determine the optimum airtime motion. The optimization method employed to determine the minimum distance between each node. The quality and machining time in milling process may be affected by various cutting conditions and tool geometry. The cutting conditions are feed rate, cutting speed, axial depth of cut and radial depth of cut. The main tools of geometry are radial rake angle, nose radius, helix angle, radial relief angle and axial relief angle [12] as shown in Figure 1. These parameters play a significant role in success of aforementioned matters in machining.

The qualities of machining, production rate and operational cost are the main three objectives in machining application. These three objectives are conflicting objectives for the machining process. Setting up effective machining parameters and appropriate airtime motion has been an issue for industrial companies for approximately a century and is still the focus of several studies. Obtaining optimal cutting conditions is a major challenge in the manufacturing industry, where the economy of machining operations is critical in a competitive market. In terms of improving machining quality, dimensional accuracy and surface roughness are mentioned [13, 14]. The effectiveness of the machining process and the optimal surface roughness are always dependent on selecting the proper cutting conditions [15, 16]. This cutting condition is divided into two parts: cutting parameters and tool geometry. Cutting parameters are cutting speed, feed rate and cutting depth of cut [17, 18]. Nose radius, helix angle and radial rake angle are considered the three most important tool geometries parameters.

Given the importance of the milling operation in contemporary manufacturing industries, it is required to improve machining quality and minimize machining time
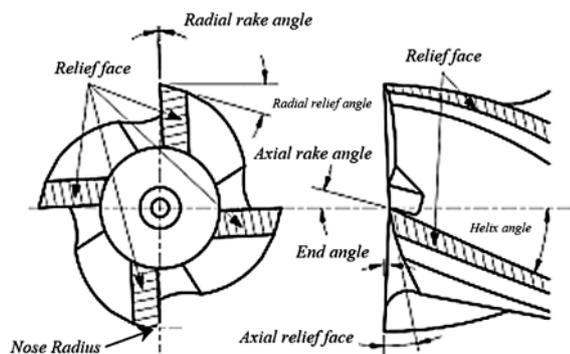
for such an operation. However, an attempt has been made in this work to investigate the effect of tool geometry (nose radius and radial rake angle) and cutting parameters (feed rate, cutting speed, and depth of cut) on the surface quality achieved during the end milling process.

A functional series of advantageous statistical and mathematical methods that are successfully employed to model and optimize the issues and problem related to the engineering field is called RSM. RSM is a technique whose major aim is to enhance and optimize the obtained responses which were affected by different factors related to the input process [19]. Besides, the connections between received responses and the factors related to manageable input are quantified by RSM. RSM has some significant practical functions. Among the applications assigned to the RSM, the ones in new products designing, improving and organizing as well as in the existing product designing and improving can be mentioned [20]. Independent variables work in isolation or in combination. These variables cause some influences that affect the processes. Here, RSM clarifies these effects on the processes created by the independent variables. When manufacturing processes need to be modelled and optimized by RSM technique, enough data and information is gathered using planned experimentation.

2. MATERIALS AND METHODS

2. 1. Materials　　　　Aluminium is the third most abundant element in the earth's crust, as well as the second most consumed metal by weight, trailing only iron and its alloys [21]. Modern aluminum alloys are useful for structural applications and as steel replacements to their low density and attractive features such as high ductility and corrosion resistance. Table 1 shows the commercial designations of many aluminum alloys, together with their principal alloying elements and applications in industry.

T temper is further classified into ten conditions. T6, which has been solution treated and artificially aged, is one of the most frequent tempers [22]. Magnesium and silicon are components of the aluminum alloy-T6. Aluminium alloy-T6 has medium strength, good machinability, formability, and weldability, as well as high corrosion resistance. The chemical properties of AA 6061-T6 are summarized in Tables 1.

2. 2. Preparation　　　　The experiment were designed based on five factors feed rate, cutting speed, depth of cut, noise radius and radial rake angle in five factor levels as listed in Table 2. These five levels for each cutting condition selected from literature review determined by previous researcher as mentioned as optimum range of cutting conditions. These five factors in five levels


Figure 1. Tool geometry definition

TABLE 1. Chemical composition of AA 6061-T6

Component	Weight, %
Silicon	0.8
Iron	0.7
Copper	0.4
Manganese	0.15
Magnesium	1.2
Chromium	0.35
Zinc	0.25
Titanium	0.15
Other elements	0.15
Remainder Aluminium	95.85

selected to design experiment for surface roughness test by central composite design method (CCD). The experiments were performed on AA 6061-T6 using high speed steel end mill cutter based on central composite design containing of 32 coded value as summarized in Table 3. The Minitab 19.1.1 software version 2019 was utilized to arrange the experimental design and analyses the results obtained.

2. 3. Characterization After the finished milling machining process according to the experimental design, the R_a arithmetic surface roughness was adopted and measured on the machined surface roughness. The measurements were taken after finished all the 32 experiments with surface roughness tester Mitutoyo SV-C3100W4 as shown on Figure 2. Averaging surface

TABLE 2. Process parameters and their levels

Parameters	Symbol	Unit	Factor levels				
			-2	-1	0	1	2
Cutting speed	N	m/min	31.4	39.25	47.1	54.95	62.8
Feed rate	F	mm/tooth	0.025	0.03	0.035	0.04	0.045
Depth of cut	D	mm	0.4	0.6	0.8	1	1.2
Radial rake angle	α	degree	10	13	16	19	22
Nose radius	r	mm	0	0.2	0.4	0.6	0.8

TABLE 3. Experimental design for central composite design in coded value

Run	Coded value				
	N	F	D	α	r
1	-1	-1	-1	-1	1
2	1	-1	-1	-1	-1
3	-1	1	-1	-1	-1
4	1	1	-1	-1	1
5	-1	-1	1	-1	-1
6	1	-1	1	-1	1
7	-1	1	1	-1	1
8	1	1	1	-1	-1
9	-1	-1	-1	1	-1
10	1	-1	-1	1	1
11	-1	1	-1	1	1
12	1	1	-1	1	-1
13	-1	-1	1	1	1
14	1	-1	1	1	-1
15	-1	1	1	1	-1
16	1	1	1	1	1
17	-2	0	0	0	0
18	2	0	0	0	0
19	0	-2	0	0	0
20	0	2	0	0	0
21	0	0	-2	0	0
22	0	0	2	0	0
23	0	0	0	-2	0
24	0	0	0	2	0
25	0	0	0	0	-2
26	0	0	0	0	2
27	0	0	0	0	0
28	0	0	0	0	0
29	0	0	0	0	0
30	0	0	0	0	0
31	0	0	0	0	0
32	0	0	0	0	0

roughness values at sites located (D1, D2, and D3) on the cutting path of the workpiece generated the R_a values of the machined surface roughness. Figure 3 illustrated the

surface roughness experiment and measured region for surface roughness test. The failure criterion for the surface roughness experiment was kept at 6 µm.

For the prediction of R_a, a second-order polynomial response is designed. Finally, ANOVA is used to assess the model's appropriateness. The optimization methods' objective function results in the lowest value of R_a.

3. RESULTS

R_a was evaluated in the dry milling process of AA 6061-T6 using HSS tool under various cutting parameters. The surface roughness predicted model developed based on five response cutting parameters, which are N, F, D, α and r. The milling process in the dry machining process utilized for this experiment. All constant parameters selected from the data handbook. The parametric study and design optimization were performed utilized RSM in the design of the experiment statistical methods. This method is simple to use and provides a thorough review of the factors that influence a specific response.

The experiment is carried out to collect the required data, and regression analysis is utilized to generate a realistic surface roughness prediction model. Table 4 shows the design matrix with the results of completed

**Figure 2.** Surface roughness tester Mitutoyo SV-C3100W4
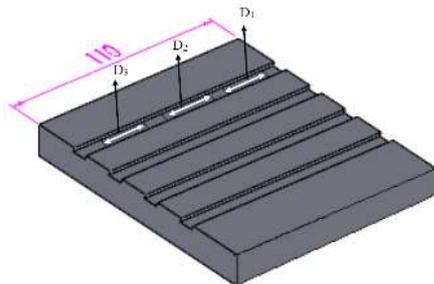
Figure 3. The surface roughness experiment in milling process

TABLE 4. Design matrix and results for surface roughness

Run	Coded value					Response Surface roughness
	N	F	D	α	r	R_a
1	-1	-1	-1	-1	1	1.66
2	1	-1	-1	-1	-1	1.74
3	-1	1	-1	-1	-1	2.69
4	1	1	-1	-1	1	1.95
5	-1	-1	1	-1	-1	2.92
6	1	-1	1	-1	1	2.50
7	-1	1	1	-1	1	2.20
8	1	1	1	-1	-1	3.13
9	-1	-1	-1	1	-1	3.01
10	1	-1	-1	1	1	2.44
11	-1	1	-1	1	1	2.36
12	1	1	-1	1	-1	3.30
13	-1	-1	1	1	1	2.27
14	1	-1	1	1	-1	3.28
15	-1	1	1	1	-1	3.33
16	1	1	1	1	1	2.06
17	-2	0	0	0	0	2.79
18	2	0	0	0	0	2.83
19	0	-2	0	0	0	3.31
20	0	2	0	0	0	3.58
21	0	0	-2	0	0	3.46
22	0	0	2	0	0	4.07
23	0	0	0	-2	0	1.16
24	0	0	0	2	0	2.04
25	0	0	0	0	-2	2.75
26	0	0	0	0	2	1.34
27	0	0	0	0	0	3.11
28	0	0	0	0	0	3.07
29	0	0	0	0	0	3.03
30	0	0	0	0	0	2.88
31	0	0	0	0	0	3.27
32	0	0	0	0	0	3.25

surface roughness. The minimum and maximum surface roughness were 1.16 m and 3.58 m for runs 23 and 20, respectively. The minimum surface roughness determined by combination of cutting conditions N (47.1 m/min), F (0.025 mm/tooth), D (0.8 mm), and tool geometry r (0.4 mm) and α (10 degree).

In this research, the MINITAB software is employed to analyze and generate a prediction mathematical model. The analysis of variance (ANOVA) of statistical analysis results of R_a is shown in Table 5. In Table 5, the F and P values from the model are 52.42 and <0.0001, respectively; indicates that the selected model is significant. The other p-values higher than 0.05 implies the model terms are insignificant. In this case, N, the interaction of the cutting condition and tool geometry, NF, ND, Nα and interaction of the Nr are insignificant. These five effects have p-values of higher than 0.05, which means that they are insignificant for a confidence level of 95%. The ANOVA table shows the linear, square and interaction components. The linear, square and interaction components are significant with small p-values. Also, the R^2 with 98.96% and Adj R^2 with 97.07% are shown the other adequacy of the experiment.

The large p-value 0.9021 compared to the pure error indicates that the model does not effectively fit the response surface. In addition, Table 5 demonstrates that the α and r have the greatest influence on surface roughness, with F-values of 77.08 and 235.96, respectively. Furthermore, with a P-value of 0.9444 and greater than 0.05, N is negligible.

R^2 statistic indicates that the fitted second-order model accounts for 98.96 percent of variability in surface roughness by the independent variables. For model adequacy; they were checking utilized normal. They used normal probability and residual versus predicted graphs to test model adequacy.

Figure 4, the normal probability plot of the standardized residuals demonstrates that the errors from the R_a model are normally distributed, since the points on the plot are pretty close to the straight line. It can be used to ensure that the basic assumptions underlying the analysis are met. Figure 5 demonstrates that the residuals for a specific location in standardized residuals vs.

TABLE 5. ANOVA table for surface roughness test

Source	Sum-of-Square	DF	Mean-square	F-Ratio	P-value
Model	14.29	20	0.71	52.42	< 0.0001
N	6.943E-005	1	6.943E-005	5.093E-003	0.9444
F	0.13	1	0.13	9.41	0.0107
D	0.59	1	0.59	43.32	< 0.0001
α	1.05	1	1.05	77.08	< 0.0001
r	3.22	1	3.22	235.96	< 0.0001
N*N	3.595E-003	1	3.595E-003	0.26	0.6177
F*F	0.019	1	0.019	1.40	0.2620
D*D	4.076E-003	1	4.076E-003	0.30	0.5954
α*α	0.059	1	0.059	4.33	0.0615
r*r	0.18	1	0.18	13.05	0.0041
N*F	0.074	1	0.074	5.46	0.0394
N*D	0.20	1	0.20	15.01	0.0026
N*α	0.52	1	0.52	37.83	< 0.0001
N*r	0.11	1	0.11	7.84	0.0173
F*D	0.16	1	0.16	11.78	0.0056
F*α	0.24	1	0.24	17.34	0.0016
F*r	0.14	1	0.14	10.26	0.0084
D*α	0.66	1	0.66	48.32	< 0.0001
D*r	4.52	1	4.52	331.31	< 0.0001
α*r	2.31	1	2.31	169.11	< 0.0001
Residual	0.15	11	0.014		
Lack of Fit	0.041	6	6.907E-003	0.32	0.9021
Pure Error	0.11	5	0.022		
Cor Total	14.44	31			< 0.0001
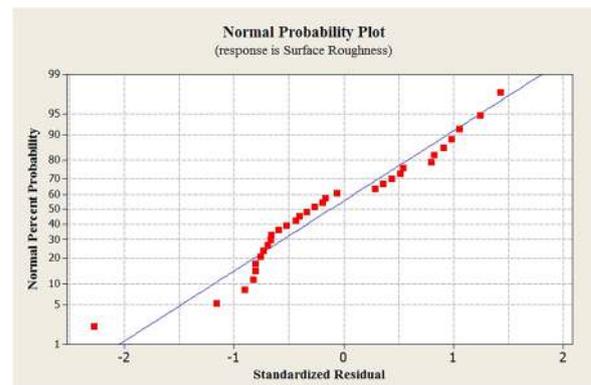
Figure 4. Normal probabilities of residuals for surface roughness
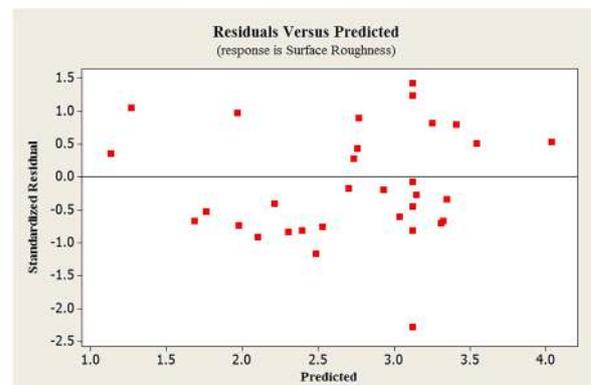

Figure 5. The plot of residuals versus predicted response for surface roughness

expected values of R_a are fairly distributed, and the plot revealed no obvious patterns or distinctive structures. As a result, it is possible to conclude that the suggested model is adequate.

Therefore, according to the previous definition, can confidently generate the predicted mathematical model. It can be utilized to perform the parametric study from the model and response optimization. The predicted mathematical model of the surface roughness generated by RSM as shown by Equation (1).

$$R_a = -19.0651 + 0.00164844 \ N + 0.00692201 \ F + 2.4234 \ D$$
$$+ 1.87551 \ \alpha + 9.65229 \ r - 0.000000359095 \ N^2$$
$$+ 0.000027617 \ F^2 + 3.74607 \ D^2 - 0.043598 \ \alpha^2$$
$$- 7.00831 \ r^2 - 0.00000059955 \ NF + 0.000345113 \ ND \quad (1)$$
$$+ 0.0000106408 \ N\alpha + 0.000607637 \ Nr - 0.0105439 \ FD$$
$$- 0.000454575 \ F\alpha - 0.0113086 \ Fr - 0.299227 \ D\alpha$$
$$- 2.04341 \ Dr - 0.166981 \ \alpha r$$

where R_a indicates the surface roughness in μm, N represents the cutting speed (m/min), F shows the feed rate (mm/tooth), D is the depth of cut (mm), α shows the radial rake angel (degree), and r is the nose radius (mm). Equation 1 can be used to estimate the influence of the chosen cutting parameters on surface roughness and to determine the best range of values.

The three-dimensional surface plots were used to determine the effect of the cutting parameter on R_a. Based on a model equation, these charts explain how a response variable interacts with the two components. Additionally, these graphs can be used to determine ideal response values and design circumstances. Figure 6 depicts the surface plot's interaction effect on N and D on R_a. This graph indicates that the faster the N, the lower the R_a. The cure has a steeper upward slope in the side to the D, according to this plot. However, the D has a wide range of effects on R_a. To establish the minimal R_a, it is important to keep the D at a lower value and the N at a greater value. These trends are similar to the finding of Reddy and Rao [23] and Kumar et al. [24]. The surface plot of the effect of α and N on R_a as shown in Figure 7. As shown in this figure, the curve has a greater upward slope on the α side and a slight curvature on the N side. The quadratic terms in the N and α directions cause the curvatures in the N and α directions, respectively. This appears to determine the minimal R_a; the α must be maintained at lower levels. These trends are similar to the finding of Maheshesh et al. [15].

The interaction effects on the r and N on the R_a are depicted on a surface plot as shown in Figure 8. In the side of the r appeared convex curve from lower for higher values. According to surface plot, the N increases from 31.4 to 62.8 m/min has an insignificant effect of the R_a. As shown, the minimum R_a was produced at lower and higher values of r of the higher value of N. These trends are similar to the finding of Reddy and Rao [23].
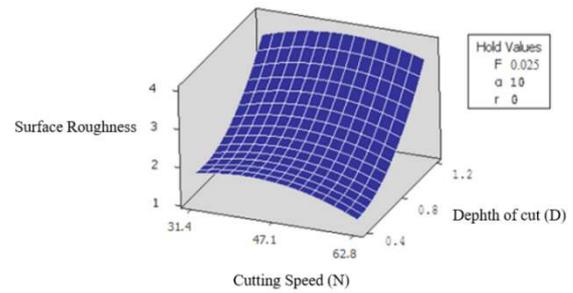
**Figure 6.** The three-dimensional surface of the surface roughness against N and D
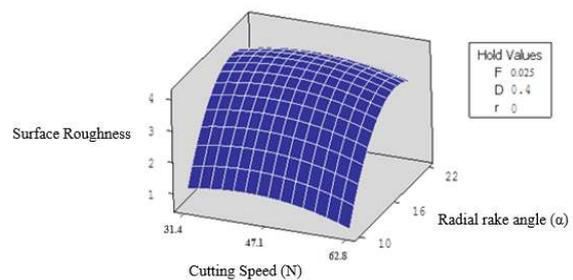
**Figure 7.** The three-dimensional surface of the surface roughness against N and α
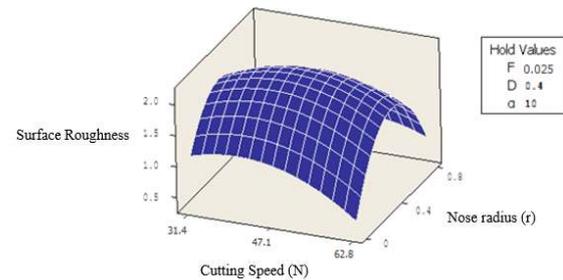
Figure 8. The three-dimensional surface of the surface roughness against N and r

The interaction impact of α and D on R_a is depicted in Figure 9. The minimal R_a calculated for lower α and D values. As shown, the variation in α has considerable different effects on R_a at lower values at the D. The curvature on the α side demonstrates that a change in this value reduces the R_a quality. In addition, increasing the D value decreases the R_a quality on the side to the D values. These trends are similar to the finding of Raja and Baskar [25].

The interaction effect of D and r on R_a is shown on Figure 10. The curve shows the curvature from the r side view while it shows the steeper upward curve from the D side view. Considering the D effects, as can be seen, the R_a quality decreases as the D increase. This trend is similar to the finding of Li et al. [26]. The three-dimensional surface of the R_a in a micrometer against to the two cutting parameter's α and r are shown in Figures 11. The curve is shows the convex curvature from the r
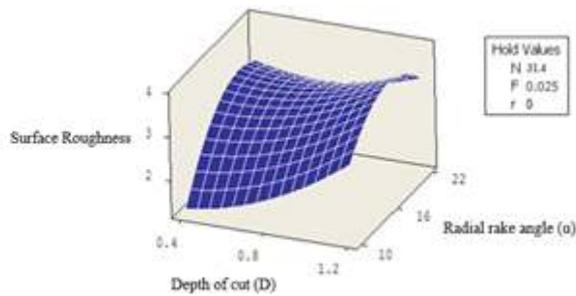
Figure 9. The three-dimensional surface of the surface roughness against D and α
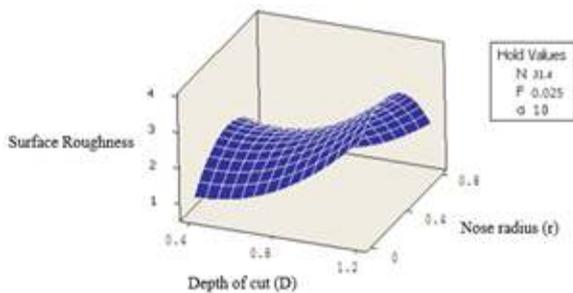
Figure 10. The three-dimensional surface of the surface roughness against D and r
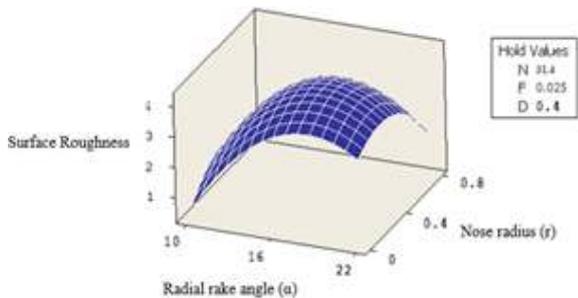
Figure 11. The three dimensional surface of the surface roughness against α and r

side view while it shows the steeper upward curve from the D. As shown, increasing the α has a significant diverse effect of the R_a with a peak at about 16 degrees. Then the R_a quality starts to increase in 3 μm on the r of 22 mm. In the side of r, the convex curvature shows the optimum R_a determined as lower and higher r values. These trends are similar to the finding of Maheshesh et al. [15] and Zain et al. [27].

4. CONCLUSION

In this research, the optimization of R_a under the various cutting parameters in the dry milling process on AA 6061-T6 has been investigated. An investigation of the cutting parameters which are N, D, F, r and α, it is found

that the r has a more significant effect on the R_a followed by α. R_a is least affected by N. It was observed that the R_a increased at the F, α and D increased. Moreover, the R_a was decreased as the N increased. In the r parameters, the R_a has minimum values on lower and higher values of the r factors. The minimum R_a determined by combination of cutting condition N (47.1 m/min), F (0.025 mm/tooth), D (0.8 mm) and in tool geometry, r (0.4 mm) and α (10 degree).

5. REFERENCES

1. Zhuang, K., Fu, C., Weng, J., Hu, C. "Cutting edge microgeometries in metal cutting: a review. " *The International Journal of Advanced Manufacturing Technology*, Vol. 116, No. 7, (2021), 2045-2092. https://doi.org/10.1007/s00170-021-07558-6

2. Li, S., Sui, J., Ding, F., Wu, S., Chen, W., Wang, C. "Optimization of Milling Aluminum Alloy 6061-T6 using Modified Johnson-Cook Model" *Simulation Modelling Practice and Theory*, Vol. 111, (2021), 102330. https://doi.org/10.1016/j.simpat.2021.102330

3. Jawahir, I., Brinksmeier, E., M'saoubi, R., Aspinwall, D., Outeiro, J., Meyer, D., Umbrello, D., Jayal, A. "Surface integrity in material removal processes: Recent advances" *CIRP Annals-Manufacturing Technology,* Vol. 60, No. 2, (2011), 603-626. https://doi.org/10.1016/j.cirp.2011.05.002

4. Kim, Y. M., Shin, S. J., Cho, H. W. "Predictive modeling for machining power based on multi-source transfer learning in metal cutting" *International Journal of Precision Engineering and Manufacturing-Green Technology*, Vol. 9, No. 1, (2022), 107-125. https://doi.org/10.1007/s40684-021-00327-6

5. Saligheh, A., Hajialimohammadi, A., Abedini, V. "Cutting Forces and Tool Wear Investigation for Face Milling of Bimetallic Composite Parts Made of Aluminum and Cast Iron Alloys" *International Journal of Engineering, Transactions C: Aspects,* Vol. 33, No. 6, (2020), 1142-1148. DOI: 10.5829/ije.2020.33.06c.12

6. Zhu, K. "Modeling of the Machining Process", In Smart Machining Systems Springer, Cham., (2022), 19-70, DOI: 10.1007/978-3-030-87878-8_2

7. Kant, T., Pare, V. "Study of optimum process selection parameter in high speed cnc end milling of composite materials using meta heuristic optimization" *International Journal of Science & Technology,* Vol. 1, No. 2, (2022), 9-18.

8. Prasanth, I. S. N. V. R., Ravishankar, D. V., Manzoor Hussain M., "Analysis of Milling Process Parameters and their Influence on Glass Fiber Reinforced Polymer Composites (RESEARCH NOTE)" *International Journal of Engineering, Transactions A: Basics,* Vol. 30, No. 7, (2017), 1074-1080 DOI: 10.5829/ije.2017.30.07a.17

9. Zailani, Z. A., Rusli, N. S. N., Shuaib, N. A., "Effect of Cutting Environment and Swept Angle Selection in Milling Operation" *International Journal of Engineering, Transactions C: Aspects*, Vol. 34, No. 11, (2021), 2578-2584 DOI: 10.5829/ije.2021.34.11bc.02

10. Gao, X., Cheng, X., Ling, S., Zheng, G., Li, Y., Liu, H. "Research on optimization of micro-milling process for curved thin wall structure" *Precision Engineering*, Vol. 73, (2022), 296-312. https://doi.org/10.1016/j.precisioneng.2021.09.015

11. Venkata Vishnu, A., Sudhakar Babu, S., "Mathematical Modeling and Multi Response Optimization for Improving Machinability of

Alloy Steel using RSM, Grey Relational Analysis and Jaya Algorithm" *International Journal of Engineering, Transactions C: Aspects,* Vol. 34, No. 09, (2021), 2157-2166. DOI: 10.5829/IJE.2021.34.09C.13

12. Reddy, N. S. K., Rao, P. V. "Selection of optimum tool geometry and cutting conditions using a surface roughness prediction model for end milling", *The International Journal of Advanced Manufacturing Technology,* Vol. 26, No. (11-12), (2005), 1202-1210. https://doi.org/10.1007/s00170-004-2110-y

13. Esfandiari, A. "Cuckoo Optimization Algorithm in Cutting Conditions During Machining" *Journal of Advances in Computer Research* Vol. 5, No. 2, (2014), 45-57.

14. Hassan, A., El-Hamid, A., Wagih, A., Fathy, A. "Effect of mechanical milling on the morphologyand structural evaluation of Al-Al$_2$O$_3$ nanocomposite powders" *International Journal of Engineering, Transactions A: Basics,* Vol. 27, No. 4, (2014), 625-632. DOI: 10.5829/idosi.ije.2014.27.04a.14

15. Mahesh, G., Muthu, S., Devadasan, S. "Prediction of surface roughness of end milling operation using genetic algorithm" *The International Journal of Advanced Manufacturing Technology* Vol. 77, No. (1-4), (2015), 369-381. https://doi.org/10.1007/s00170-014-6425-z

16. Nakhaei, M. R., Naderi, G. "Modeling and Optimization of Mechanical Properties of PA6/NBR/Graphene Nanocomposite Using Central Composite Design" *International Journal of Engineering, Transactions C: Aspects,* Vol.33, No. 9, (2020), 1803-1810. DOI: 10.5829/ije.2020.33.09c.15

17. Lauro, C. H., Pereira, R. B., Brandão, L. C., Davim, J. P. "Design of Experiments—Statistical and artificial intelligence analysis for the improvement of machining processes: A review" *Design of Experiments in Production Engineerin,* (2016), 89-107. DOI: 10.1007/978-3-319-23838-8_3

18. Edem, I. F., Balogun, V. A. "Energy efficiency analyses of toolpaths in a pocket milling process" *International Journal of Engineering, Transactions B: Application,* Vol. 31, No. 5, (2018), 847-855. DOI: 10.5829/ije.2018.31.05b.22

19. Sahith Reddy, S., Achyutha Kumar Reddy, M. "Optimization of Calcined Bentonite Clay Utilization in Cement Mortar using Response Surface Methodology" *International Journal of Engineering, Transactions A: Basics* Vol. 34, No. 7, (2021), 1623-1631. DOI: 10.5829/ije.2021.34.07a.07

20. Vahdani, M., Ghazavi, M., Roustaei, M. "Prediction of Mechanical Properties of Frozen Soils Using Response Surface Method: An Optimization Approach" *International Journal of Engineering, Transactions A: Basics* Vol. 33, No. 10, (2020), 1826-1841. DOI: 10.5829/ije.2020.33.10a.02

21. Ozdemir, F., Witharamage, C. S., Darwish, A. A., Okuyucu, H., Gupta, R. K. "Corrosion behavior of age hardening aluminum alloys produced by high-energy ball milling" *Journal of Alloys and Compounds,* Vol. 900, (2022), 163488. https://doi.org/10.1016/j.jallcom.2021.163488

22. Kadirgama, K., Noor, M. M., Rahman, M. M., Rejab, M. R. M., Haron, C. H. C., Abou-El-Hossein, K. A. "Surface roughness prediction model of 6061-T6 aluminium alloy machining using statistical method" *European Journal of Scientific Research,* Vol. 25, No. 2, (2009): 250-256.

23. Reddy, N. S. K., Rao, P. V. "Selection of an optimal parametric combination for achieving a better surface finish in dry milling using genetic algorithms." *The International Journal of Advanced Manufacturing Technology,* Vol. 28, No. (5-6), (2006): 463-473. https://doi.org/10.1007/s00170-004-2381-3

24. Kumar, M. S., Prasad, J., Krishna, D. A., Narayana, M. V., Anusha, M., Saravanakumar, A. "Parametric optimization of aluminium alloy milling using Taguchi method for surface roughness" *International Journal of Scientific Research and Review,* Vol. 7, No. 3, (2018), 516-522.

25. Raja, S. B., Baskar, N. "Application of particle swarm optimization technique for achieving desired milled surface roughness in minimum machining time" *Expert Systems with Applications* Vol. 39, No. 5, (2012), 5982-5989. https://doi.org/10.1016/j.eswa.2011.11.110

26. Li, B., Tian, X., Zhang, M. "Modeling and multi-objective optimization of cutting parameters in the high-speed milling using RSM and improved TLBO algorithm" *The International Journal of Advanced Manufacturing Technology,* Vol. 111, No. 7, (2020), 2323-2335. https://doi.org/10.1007/s00170-020-06284-9

27. Zain, A. M., Haron, H. Sharif, S. "Simulated annealing to estimate the optimal cutting conditions for minimizing surface roughness in end milling Ti-6Al-4V" *Machining Science and Technology,* Vol. 14, No. 1, (2010), 43-62. https://doi.org/10.1080/10910340903586558

Persian Abstract

چکیده

فرآیند فرزکاری یکی از متداول ترین مراحل برش فلزات در صنعت است زیرا توانایی آن در حذف سریع مواد با کیفیت سطح مطلوب ثابت شده است. در این مقاله بر اساس روش سطح پاسخ (RSM) اثرات پارامترهای مختلف برشکاری و هندسه ابزار در فرزکاری بر زبری سطح مورد بررسی قرار گرفته است. در همین راستا یک مدل ریاضی مرتبه دوم از زبری سطح با استفاده از RSM توسعه داده شده است. همچنین تجزیه و تحلیل رگرسیون چندگانه با استفاده از تجزیه واریانس برای نشان دادن اثر پارامترهای ماشینکاری بر زبری سطح و تعیین عملکرد آزمایش انجام شده است. در بهینه سازی زبری سطح، آزمایش ها با استفاده از روش طراحی مرکب مرکزی (CCD) با استفاده از پارامترهای مختلف سرعت برش، نرخ پیشروی، عمق براده برداری انجام شده است. همچنین پارامترهای زاویه آزاد ابزار (۱۰، ۱۳، ۱۶، ۱۹ و ۲۲ درجه) و زاویه نوک ابزار (۰، ۰.۲، ۰.٤ ، ۰.٦ و ۰.۸ میلی متر) در هندسه ابزار مورد بررسی قرار گرفته است. نتیجه نشان می دهد که زاویه نوک ابزار و به دنبال آن زاویه آزاد ابزار تأثیر چشمگیری در زبری سطح دارد. علاوه بر این، تأثیر عمق براده برداری بر زبری سطح بیشتر از سرعت برش است. در نهایت ترکیب بهینه پارامترهای برش و هندسه ابزار، سرعت برش (۶۰.۵۳ متر در دقیقه)، نرخ پیشروی (۰.۰۲۵ میلی متر بر دندانه) ، عمق براده برداری (۰.۸٤ میلی متر) ، زاویه آزاد ابزار (۱۲.۷۲ درجه) و زاویه نوک ابزار (۰.۳٤ میلی متر) بدست آمده است.

International Journal of Engineering

Journal Homepage: www.ije.ir

RESEARCH NOTE

Development of a Method for Estimating Thermal Conductivity of Organic Deposits on the Wax Flow Loop Laboratory Installation

P. Y. Ilyushin[a,b], K. A. Vyatkin*[a,b], A. V. Kozlov[a]

[a] *Perm National Research Polytechnic University, Mining and Oil Faculty, Perm, Russian Federation*
[b] *Scientific and educational center of geology and development of oil and gas deposits, Perm 614013, Russian Federation*

P A P E R   I N F O

A B S T R A C T

During the oil production, the occurrence of such a complication as the formation of wax deposits is not uncommon. The fight against these deposits, as well as the development of modern methods of dealing with them, is one of the most important tasks of the subsoil user. Many modern methods of modeling deposits require the exact determination of such a quantity as the thermal conductivity of organic deposits. Based on the analysis of scientific literature, it can be concluded that there is no method developed for estimating this value under conditions of wax formation without affecting their pore structure. The paper describes a method for determining this value based on the results of a study of the process of formation of organic deposits on the laboratory installation "Wax Flow Loop" based on the laws of heat and mass transfer. Based on the results of applying this technique, it becomes possible to determine the thermal conductivity of organic deposits, the value of which correlates with the values given in the reference and scientific literature. In addition, the presence of a correlation between the value of the thermal conductivity of deposits and the component composition of the studied fluid was determined. The application of the described technique will make it possible to most accurately simulate the processes of oil production and determine the technological effectiveness of the use of modern methods of combating organic deposits.

doi: 10.5829/ije.2022.35.06c.09

NOMENCLATURE

C_T	heat capacity of oil (J/(kg· °K))	υ	flow rate (m/s)
d_1	inner diameter of the test section before wax deposition (m)	**Greek Symbols**	
d_2	outer diameter of the test section (m)	α	coefficient of heat transfer from the fluid to the wall (W/($m^2 \cdot °K$))
d_3	inner diameter of the test section after the formation of organic deposits (m)	β	temperature coefficient of volumetric expansion (deg^{-1})
Gr	Grashof number	ΔP	pressure drop in the test section (MPa)
g	acceleration due to gravity (m/s^2)	ΔT	difference between the cooling temperature of the test section and the temperature at the outlet of the test section (℃)
l	pipe length (m)	η	viscosity of the oil (m^2/s)
Nu	Nusselt number	λ_T	thermal conductivity of oil (W/(m· °K))
Pr	Prandtl number	λ_{steel}	coefficient of thermal conductivity of the test section material (W/(m· °K))
Pr_s	Prandtl number at wall temperature	λ_{wax}	coefficient of thermal conductivity of wax deposits (W/(m· °K))
Pr_{oil}	Prandtl number at the temperature of oil at the outlet of the test section	μ	kinematic viscosity of the liquid at average temperature, mPa·s;
Q	volumetric flow rate of the oil (m^3/s)	ν	kinematic viscosity of the liquid (m^2/s)

*Corresponding Author Institutional Email: kirill.vyatkin@girngm.ru (K. A. Vyatkin)

q_l	value of the linear heat flux density (W/m)	$\sum(C_{17} - C_{60})$	total content of high weight components in oil (%)
Re	Reynolds number	$\sum(C_5 - C_{16})$	total content of low molecular weight components in oil(%)
R_l	thermal resistance of test section befor formation of wax deposition ((m· °K) / W)	π	number Pi
R_l^*	thermal resistance of test section after formation of wax deposition ((m· °K) / W)	ρ_{15}^{15}	relative density of oil at a temperature 15℃ (kg/m³)
T	temperature at the entrance to the test section (°К)	ρ	density of the fluid (kg/m³)

1. INTRODUCTION

Most of the oil fields in the Russian Federation and, in particular, the Perm Krai are entering the final stages of development [1]. In addition to a decrease in oil production rates and an increase in the water cut of the produced liquid, intensification of the processes of formation of asphalt-resin-paraffin deposits (ARPD) is observed in these fields [2]. The formation of these deposits causes a decrease in the hydraulic radius of the production string, an increase in pressure in the oil gathering system and a decrease in the service life of oilfield equipment [3].

At the present time, there are many methods of dealing with these deposits, but all these methods can be divided into two groups: prevention of the formation of deposits and their removal [4,5]. There is also a classification based on the active physical field: chemical, mechanical, physical and thermal [6]. The most widespread, at the moment, among the technologies for removing organic deposits are various scrapers, treatment of a well or an oil pipeline with hydrocarbon solvents, hot oil or water [7,8]. Among the methods for preventing the formation of deposits are the dosage of wax deposits inhibitors, the use of smooth coatings on the inner surface of the tubing and heating cables [9,10]. Also, many modern methods of dealing with deposits find their place in oil production, among which we can identify the technology of the "controlled layer", oil treatment with ultrasound, selection of the speed mode of the well, etc. [11-13]. As part of the review of the scientific literature, it was noted that for the application of these methods, the required value is the thermal conductivity of organic deposits.

An important note is the need to assess the thermal conductivity of organic deposits without physical impact on their pore structure. The volume of these deposits is heterogeneous in its properties, deposits can have different porosity values, and the pore space is filled with various fluids [14].

At the same time, in many scientific publications, including literature [15,16], this value was taken equal to a constant, the justification for which was not given.

In the modern oil industry, there is a strong trend towards the digitalization of production, including the development and implementation of "digital twins" of fields and computer modeling of oil production and transportation processes. For the successful implementation of these technologies, it is necessary to have a large amount of data on the properties of fluids, the laws of their flow and heat and mass transfer. So, for example, in the well-known methods for determining the temperature of the inner surface of the tubing string, the processes of paraffin formation and related changes in the heat and mass transfer regime are not taken into account [17,18]. To take into account these changes, it is required to use not only more modern methods for determining the temperature of the production wellbore but also a number of studies to determine the actual thermal conductivity of organic deposits. This fact confirms the importance of this parameter for the process of modeling the fluid flow along the production wellbore.

Another important trend in modern oil production is the environmental friendliness of the field. In this regard, new methods are being developed for using oilfield waste, including paraffin deposits. Their use is possible as thermal insulation, as part of the road surfaces and for petrochemical purposes [19,20]. All these areas require a deep study of the properties and composition of the formed deposits, including their thermal conductivity.

Modeling of wax formation processes is also of fundamental importance in the design of production and transportation of formation fluids. The assessment of the probability of formation of these deposits and the nature of their distribution along the length of the production tubing or linear oil pipeline makes it possible to assess the need to apply methods to combat wax deposits for the trouble-free operation of oilfield equipment.

Modeling of the processes of formation of organic deposits occurs in various software systems using a variety of models for the formation of these deposits. Most of the models described in the scientific literature take into account the composition of the fluid, the thermobaric and velocity conditions of its flow [21]. A common parameter taken into account in all considered models is the presence of a temperature gradient between the fluid flow and the cold surface. However, when modeling the processes of formation of organic deposits, the thermal conductivity of these deposits, which can have a significant impact on the kinetics of this process, is not taken into account. Veiga et al. [22], Sousa et al. [23], they have demonstrated that the thermal resistance of organic deposits is the dominant resistance when the thickness of organic deposits reaches 5% of the pipe diameter. As a result of modeling the thickness of organic deposits in the annular geometry of the laminar flow, it

was found that a change in the thermal conductivity of organic deposits from 0.1 to 0.4 W/(m· °K) leads to a change in the thickness of wax deposits by 50%, which confirms the importance of this parameter in modeling paraffin formation.

Based on the foregoing, it becomes obvious that for the most detailed modeling of the processes of oil production and transportation, as well as the introduction and assessment of the technological efficiency of the modern methods of combating organic deposits, it is necessary to develop a method for determining the thermal conductivity of organic deposits. This work presents a method that allows estimating this value with sufficient accuracy in the study of the process of organic deposits formation on the laboratory installation "WaxFlowLoop".

2. MATERIALS AND METHODS

The "WaxFlowLoop" laboratory installation is a closed hydraulic circuit for studying the process of paraffin formation. This unit as an experimental setup is shown in Figure 1. The principle of operation of the installation is to constantly maintain the temperature of the test fluid circulating through the system and to cool the test section to create a temperature gradient between the flow and the wall. The pressure in the system is set due to the injection of nitrogen into the feed tank through a special channel (not shown in the figure).

Conducting research on this installation involves simulating the movement of fluid in a real oil pipeline. The achievement of this goal is provided by kinematic, thermal and technological similarities. The kinematic is provided by controlling the mass flow rate of the oil in the test section by means of frequency control of the motor. Thermal similarity is provided by setting the required oil and test section temperatures. Technological similarity means the study of the real fluid, as well as the

execution of the test section of their stainless steel. Providing these similarities allows us to speak about the similarity of the modes of formation of organic deposits in the test section and in a real oil pipeline.

During the operation of this laboratory installation, in order to simulate the process of fluid transportation in a real pipeline, the mass flow rate of the pump is selected based on the requirements for observing kinematic similarity. Compliance with this requirement, as well as the execution of the test section from stainless steel and correct sampling, allows us to speak about the similarity of the conditions for the formation of organic deposits in the considered laboratory stand and the real pipeline. As part of this work, studies were carried out under the laminar regime of fluid flow in the test section.

During the study, many different parameters are recorded, among them: pressure drop between the inlet and outlet of the test section, temperature at the inlet and outlet of the test section, oil mass flow rate, oil density, temperature in the installation and thermostats, etc. The study on this installation lasts from 8 to 36 hours with regular registration of these parameters. At the end of the study, a database is formed that reflects the change in all the values described above over time. Based on these data, it becomes possible to determine the thickness of organic deposits at each moment of the time, for this we write expression 1, which is the Poiseuille equation, which is a special case of the Darcy-Weisbach formula for the laminar flow regime when calculating pressure losses in the pipeline [24].

$$\Delta P = \frac{Q \cdot 128 \cdot \eta \cdot l}{\pi \cdot d_1^{\ 4}} \tag{1}$$

Transforming this expression, we get expression 2, which is an expression for determining the internal diameter of the test section.

$$d_1 = \left(\frac{Q \cdot 128 \cdot \eta \cdot l}{\pi \cdot \Delta P}\right)^{1/4} \tag{2}$$
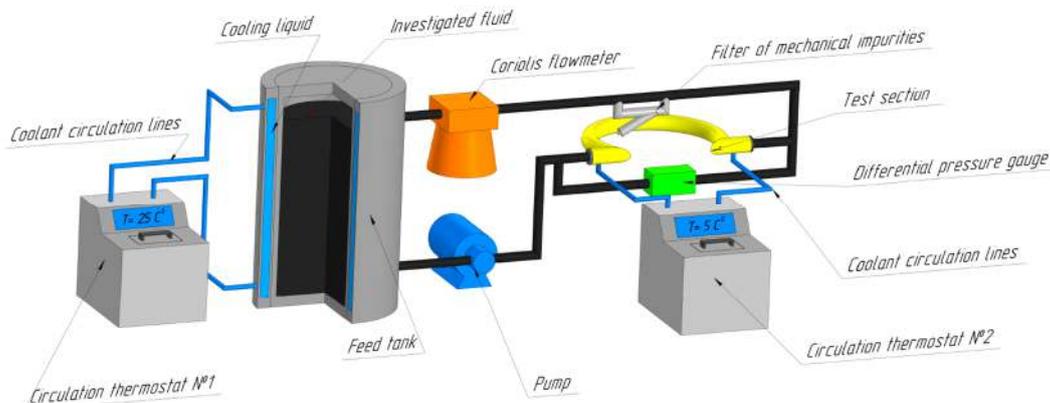

**Figure 1.** Laboratory installation "WaxFlowLoop"

For a reliable assessment of the thermal conductivity of organic deposits, it is necessary to know the dynamics of changes in the temperature of the inner surface of a particular point of the test section; however, this installation will only allow estimating the temperature at the outlet of the test section. To determine the correctness of taking this temperature as the temperature in the test section, modeling was carried out in the Ansys Fluent software package. The simulation results are shown in Figure 2.

From the modeling results, it becomes obvious that the flow temperature drops sharply at the entrance to the test section and its further decrease can be taken as insignificant. As a result, the temperature at the point of the test section in this method will be taken as the temperature at the outlet of the test section.

It is also important to note that in order to determine the thermal conductivity, it is necessary that all data recorded during the study change linearly, and the mass flow rate, the temperature at the inlet to the test section and in circulation thermostats change by no more than 5%. This value was obtained during laboratory tests and interpretation of their results.

To assess the thermal conductivity, the following initial data are required: the dynamic viscosity of oil at the temperature to which the test section is cooled and the test fluid is heated, the density of the mixture at the beginning of the study, the temperature at the inlet to the test section, the cooling temperature of the test section, at the outlet of the test section at the beginning of the study and finally, the thickness of organic deposits on the wall of the test section, the mass flow rate of the test fluid through the test section, the inner and outer diameters of the test section before paraffin formation, the thermal conductivity of the test section material, the thermal expansion coefficient of the oil.

The first step is to determine the thermal conductivity and heat capacity of the oil according to the empirical formulas of Craig, presented in expressions 3 and 4, respectively [25].
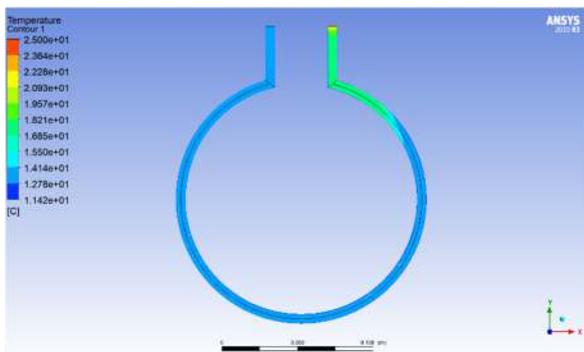
Figure 2. Modeling the temperature distribution in the test section during laboratory research

$$\lambda_T = \frac{0,00117}{\rho_{15}^{15}} \cdot (1,1474 - 0,00054 \cdot T) \tag{3}$$

$$C_T = \frac{1,687 + 0,00339 \cdot T}{\sqrt{\rho_{15}^{15}}} \tag{4}$$

After determining these parameters, it is necessary to determine a number of criteria for hydrodynamic and thermal similarity, namely: Reynolds, Prandtl and Grashof, the formulas for determining which are presented in expressions 5-7, respectively. Based on the obtained data values, the criterion is to select a formula to determine the Nu. Within the framework of this installation, it is proposed to use the formula given in expression 8.

$$Re = \frac{v \cdot d_1}{v} \tag{5}$$

$$Pr = \frac{C_T \cdot v \cdot \rho}{\lambda_T} \tag{6}$$

$$Gr = \frac{g \cdot \beta \cdot d_1^3}{v^2} \cdot \Delta T \tag{7}$$

$$Nu = 0,5 \cdot Re^{0.33} \cdot Gr^{0.1} \cdot Pr_{oil}^{0,43} \cdot \left(\frac{Pr_{oil}}{Pr_s}\right)^{0,25} \tag{8}$$

Taking into account the known value of the Nusselt coefficient, it becomes possible to determine the heat transfer coefficient from the fluid to the wall, presented in expression 9.

$$\alpha = \frac{Nu \cdot \lambda}{d_1} \tag{9}$$

Using this coefficient, we determine the value of the linear thermal resistance of heat transfer through the cylindrical wall (R_l) and the value of the linear heat flux density (q_l), according to expressions 10 and 11, respectively. It should be noted that the application of the classical Fourier heat transfer equation is due to the slow change in the temperature gradient and flow in the test section of the Wax Flow Loop installation [26]. In expression 11, the heat transfer coefficient from the test section to air is not taken into account due to its insignificant value and the high complexity of the calculation.

$$R_l = \frac{1}{\alpha \cdot d_1} + \left(\frac{1}{2\lambda_{steel}} \cdot ln\frac{d_1}{d_2}\right) \tag{10}$$

$$q_l = \frac{\pi \cdot \Delta T}{R_l} \tag{11}$$

Having determined the value of the linear density of the heat flux, it is necessary to take it as a constant for a given operating mode of the installation since the heat transfer mode remains stationary and the heat flux remains unchanged. Accordingly, in the process of formation of organic deposits, as the thermal resistance of the test section changes, due to the formation of

organic deposits, the temperature gradient will also change. Let us write expression 12, which reflects the change in the value of thermal resistance after the formation of organic deposits.

$$R_l^* = \frac{1}{\alpha \cdot d_1} + \left(\frac{1}{2\lambda_{steel}} \cdot ln\frac{d_1}{d_2}\right) + \left(\frac{1}{2\lambda_{wax}} * ln\frac{d_2}{d_3}\right) \quad (12)$$

Having transformed expression 11, taking into account expression 12, we write the formula for determining the thermal conductivity of organic deposits in the form of expression 13.

$$\lambda_{wax} = \frac{ln\frac{d_2}{d_3}}{2 \cdot (R_l^* - R_l)} \quad (13)$$

The method presented in this work allows us to evaluate the thermal conductivity of organic deposits without the use of additional research methods, but only based on the results of assessing the kinetics of wax deposits formation at the "WaxFlowLoop" installation.

The assumption of the application of this technique is the uniform distribution of the thickness of organic deposits along the length of the test section, since it is not possible to assess the actual profile of the adhered deposits. However, it should be noted that if there is an uneven distribution of organic deposits in the test section, this will not significantly affect its total thermal resistance.

3. RESULTS AND DISCUSSIONS

As an illustration of the work of this method, we present the processing of data from a real laboratory study. The initial data for processing are presented in Table 1.

Graphs reflecting the change in the main parameters of the study are shown in Figure 3.

**TABLE 1.** Parameters of laboratory research

Parameter	Dimesion	Value
Dynamic vicosity of oil 20 ℃	mPa·s	32.25
Dynamic vicosity of oil 5 ℃	mPa·s	96.7
Oil density	kg/m3	885.12
Thermal conductivity of the test section material	W/(m· °K)	90
Mass flow rate of liquid	kg/h	4.0
Temperature at the outlet of the test section — At the start of the study	℃	13.81
Temperature at the outlet of the test section — At the end of the study	℃	15.21
Cooling temperature of the test section	℃	5
Thickness of organic deposits at the end of the study	mm	0.495

As a result of processing this study, it was obtained that the average thermal conductivity of organic deposits is 0.247 W/(m·°K). Due to the fact that there were no available methods, techniques or empirical dependencies to determine this value, a comparison of this value with tabular values was carried out. The value obtained by the team of authors slightly differs from that given in the reference literature, which can be explained by differences in the fractional and component composition of the studied deposits.

This paper presents the results of processing a number of laboratory studies to determine the thermal conductivity of wax deposits (Figure 4). These studies were carried out on 20 formation fluid samples. These oils were selected from various production wells in the Perm Krai. The fractional composition was determined by gas chromatography for each of the studied fluids. In order to characterize the fractional composition of the fluid by one parameter, a value characterizing the ratio of low-molecular and high-molecular components in the studied fluid was developed. The formula for calculating this value is presented in expression 14. The results of determining this correlation dependence are shown in Figure 4.

(a)

(b)
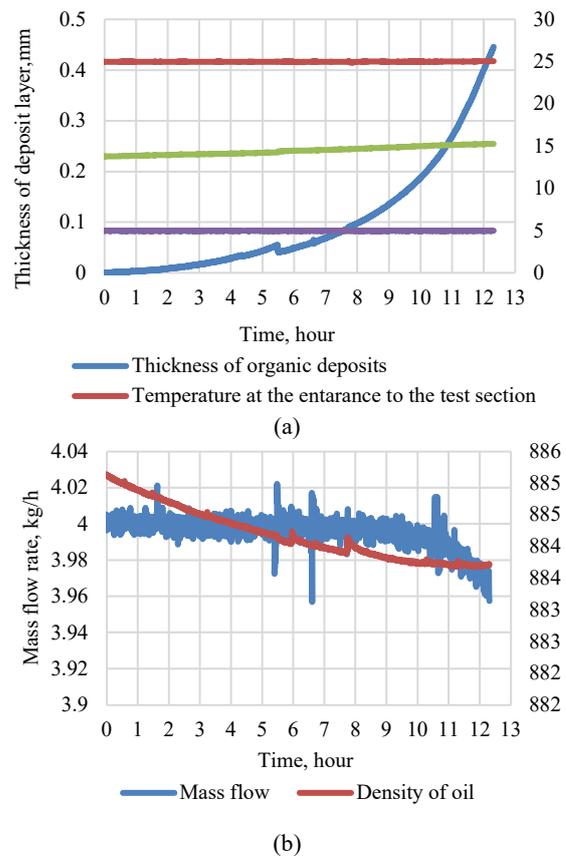
Figure 3. Changes in the operating temperature of the installation and the thickness of organic deposits (a), density and flow rate of the liquid (b)
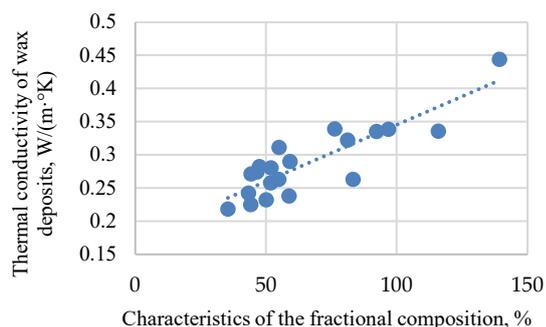
Figure 4. Dependence of wax deposits thermal conductivity on characteristics of fractional composition

$$X = \frac{\sum(C_5 - C_{16})}{\sum(C_{17} - C_{60})} * 100\% \qquad (14)$$

As can be seen from Figure 4, for the studied oils, the fractional composition characteristic is in the range of 35.4% to 139.1%. Analyzing the nature of the change in thermal conductivity, it is worth noting that there is a steady upward trend in this value with an increase in the characteristics of the fractional composition in the entire considered range. The presence of this dependence indicates a lower value of the thermal conductivity coefficient for heavy oils, which is explained by the content of high concentrations of resins and asphaltenes in them.

In addition to this parameter, the dependence between the thermal conductivity of wax deposits and the viscosity of the fluid under study is determined. This correlation is substantiated by a significant effect on the fluid viscosity of the content of high-molecular components. As is known, the thermal conductivity of hydrocarbons of the methane series decreases with increasing molecular weight, which is generally confirmed by this dependence shown in Figure 5.
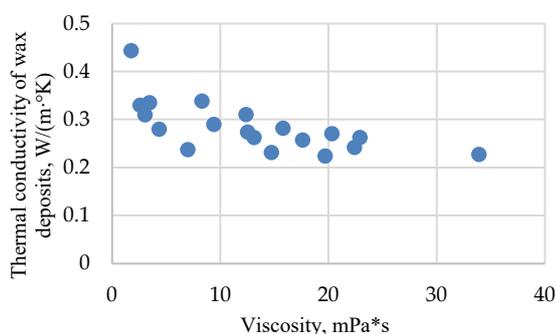
Figure 5. Dependence of wax deposits thermal conductivity on fluid viscosity

Analysis of Figure 5 confirms the theory of the influence of fluid composition on the thermal conductivity of wax deposits. The high content of heavy components causes an increase in fluid viscosity and a decrease in its thermal conductivity. The obtained correlation dependence confirms the previously put forward assumptions and shows that the estimation of the thermal conductivity of organic deposits is possible, including the results of fluid rheological studies, without carrying out an expensive study of the fractional composition.

The developed method makes it possible to determine the thermal conductivity of organic deposits in the process of paraffin formation, without changing their pore structure. The use of this method will make it possible to estimate this value with sufficient accuracy, which will allow the most accurate modeling of wax formation, the temperature of the inner surface of the production tubing and a linear oil pipeline. A feature of this method can be considered the conduct of research in a laminar mode and the study of exclusively degassed formation samples; however, this is a limitation of the laboratory installation. Determination of the correlation dependences between the thermal conductivity of wax deposits and the characteristic of the fractional composition will make it possible to estimate this value more correctly without carrying out long laboratory studies. Further research in this area can be aimed at influencing the thermal conductivity of organic deposits, the temperature of their formation, the presence of inclusions of oil and water phases.

4. CONCLUSIONS

As a result of the work performed, in the following should be noted:
1. The authors have developed a previously absent method for determining the thermal conductivity of organic deposits under conditions of paraffin formation without physical impact on the pore structure of deposits.
2. The value obtained as a result of the implementation of this method correlates with the data given in the referred literature.
3. Analysis of studies indicates the presence of a correlation between the thermal conductivity of deposits and the composition and properties of the initial fluid, as a result of which its assessment is possible without additional laboratory studies.
4. The application of the above methodology is possible to increase the accuracy of modeling the process of formation of organic deposits or the introduction of modern methods to combat these deposits.

5. ACKNOWLEDGEMENTS

6. REFERENCES

1. Ilushin, Pavel, Kirill Vyatkin, and Alexander Menshikov. "Development of a Methodology and Software Package for Predicting the Formation of Organic Deposits Based on the Results of Laboratory Studies", *Fluids* Vol. 6, No. 12, (2021), 446. https://doi.org/10.3390/fluids6120446

2. Vyatkin K., Mordvinov V., Ilushin P. and Kozlov A. "Influences of the Water Cut of Pumping Oil and the Mineralization of the Associated Water on the Rate of Sludging", *Applied Sciences,* Vol. 11, No. 15, (2021), 6678. DOI: 10.3390/app11156678

3. Safiulina A. G., Ibragimova D. A., Baibekova L. R., Soldatova R., Petrov S. M. and Bashkirtseva N. Y. "Modeling of Paraffin Wax Deposition Process in Poorly Extractable Hydrocarbon Stock", *Chemistry and Technology of Fuels and Oils,* Vol. 53, No. 6, (2018), 897-904.

4. Ljapin, A. Ju., Astahov, A. V. and Mihaljov, Ju. P. "Study of the crystallization temperature of paraffins in oil in order to reduce the formation of asphalt-resin-paraffin deposit", *Science and Technologies: Oil and Oil Products Pipeline Transportation*, Vol. 7, No. 6, (2017), 28-35. DOI: 10.28999/2541-9595-2017-7-6-28-35

5. Banki R., Hoteit H. and Firoozabadi A. "Mathematical formulation and numerical modeling of wax deposition in pipelines from enthalpy–porosity approach and irreversible thermodynamics", *International Journal of Heat and Mass Transfer,* Vol. 51, No. 13-14, (2008), 3387-3398. https://doi.org/10.1016/j.ijheatmasstransfer.2007.11.012

6. Goswant T. K. "How to Get Rid of Paraffin Deposition in Pipe Line. Chem", *Age India,* Vol. 20, No. 4, (2011), 15-16.

7. Ivanova, L. V., Burov, E. A. and Koshelev, V. N. "Asphalt-resin-paraffin deposits in production, transport and storage processes", *Oil and Gas Business*, Vol. 1, (2011), 268-284.

8. Abdullina A. and Fatykhov M. A. "Electromagnetic method of wax melting in a pipe", Automation, Telemechanization and Communication in the Oil Industry, No. 7, (2012), 25-28.

9. Ilushin, P., Vyatkin, K. and Kozlov, A. "Development of an Approach for Determining the Effectiveness of Inhibition of Paraffin Deposition on the Wax Flow Loop Laboratory Installation.", *Inventions*, Vol. 7, No. 1, (2022).

10. El-Dalatony M. M., Jeon B. H., Salama E. S., Eraky M., Kim W. B., Wang J. and Ahn T. "Occurrence and characterization of paraffin wax formed in developing wells and pipelines", *Energies,* Vol. 12, No. 6, (2020), 967-989. DOI: 10.3390/en12060967

11. Gilmutdinov N. R., Dmitriev M. E. and Mastobaev B. N., "New direstions of using asphalt-resinous paraffin deposits in the process of pipeline oil transportation", *Transport and Storage of Petroleum and Hydrocarbon Raw Material,* No. 2, (2015), 8-12.

12. Revel-Muroz P. A., Gilmutdinov N. R., Dmitriev M. E. and Mastobaev B. N. "Use of asphalt-resin-paraffin deposits as thermal and anticorrosive insulation of oil pipelines", *Transport*

and Storage of Petroleum and Hydrocarbon Raw Material, No. 3, (2016), 12-16.

13. Shchurova E. V., Krys A. O., Khuramshina R. A. and Valeev A. R. "Removal of asphalt-resin-paraffin deposits from oil storage tanks using ultrasonic action", *Transport and Storage of Petroleum and Hydrocarbon Raw Material,* No. 5-6, (2020), 29-33.

14. Ghasemi, M. Hadi, S. Hoseinzadeh, and Memon, S. "A dual-phase-lag (DPL) transient non-Fourier heat transfer analysis of functional graded cylindrical material under axial heat flux", *International Communications in Heat and Mass Transfer,* No. 131, (2022), 105858. https://doi.org/10.1016/j.icheatmasstransfer.2021.105858

15. Mugallimov F. M. and Abdullaev A. A. "Modeling the thermal regime when creating a controlled layer of ARPD on the inner surface of oil pipelines", *Transport and Storage of Petroleum and Hydrocarbon Raw Material,* No. 1, (2016), 9-12.

16. Sun D., Zhu Z., Hu Z. and Wu M. "Experimental and theoretical study on wax deposition and the application on a heat insulated crude oil pipeline in Northeast China", *Oil & Gas Science and Technology,* Vol. 73, No. 3, (2020), 1-11.

17. Hosseinipour A., Japper-Jaafar A., Yusup S. and Ismail L. "Application of the Avrami Theory for Wax Crystallisation of Synthetic Crude Oil", *International Journal of Engineering, Transactions A: Basics,* Vol. 32, No. 1, (2019), 18-27. DOI: 10.5829/IJE.2019.32.01A.03

18. Krivoshchekov, S. N., K. A. Vyatkin and A. V. Kozlov. "Modeling of Asphaltene-Resin-Wax Deposits Formation in a String of Hollow Rods During Simultaneous Separate Operation of Two Oil Reservoirs", *Chemical and Petroleum Engineering,* Vol. 57, No. 3, (2021), 213-219.

19. Hoseinzadeh, S., Sohani, A. and Ashrafi, T. G. "An artificial intelligence-based prediction way to describe flowing a Newtonian liquid/gas on a permeable flat surface", *Journal of Thermal Analysis and Calorimetry,* (2021), 1-7.

20. Al-Hasan, S. J. A., Balamuralikrishnan, R. and Altarawneh, M. "Eco-Friendly Asphalt Approach for the Development of Sustainable Roads", *Journal of Human, Earth, and Future,* Vol. 1, No. 3, (2020), 97-111. DOI: 10.28991/HEF-2020-01-03-01

21. Vyatkin K. A., Ilushin P. Y. and Kozlov A.V. "Forecasting the Value of the Linear Pipeline Cleaning Interval Based on the Laboratory Research", *International Review of Mechanical Engineering,* Vol. 15, No. 6, (2021), 294-300. DOI: 10.15866/ireme.v15i6.20811

22. Veiga H. M. B., Fleming F. P. and Azevedo L. F. A. "Wax deposit thermal conductivity measurements under flowing conditions", *Energy & Fuels,* Vol. 31, No. 11, (2017), 11532-11547.

23. Sousa, A. L., Matos, H. A. and Guerreiro, L. P. "Preventing and removing wax deposition inside vertical wells: a review", *Journal of Petroleum Exploration and Production Technology,* Vol. 9, No. 3, (2019), 2091-2107. DOI: 10.1007/s13202-019-0609-x

24. Adeyemi, T. S. "Analytical Solution of Unsteady-state Forchheimer Flow Problem in an Infinite Reservoir: The Boltzmann Transform Approach", *Journal of Human, Earth, and Future,* Vol. 2, No. 3, (2021), 225-233. DOI: 10.28991/HEF-2021-02-03-04

25. Bidmus H. O. and Mehrotra A.K. "Heat-transfer analogy for wax deposition from paraffinic mixtures", *Industrial & Engineering Chemistry Research,* Vol. 43, No. 3, (2004), 791-803. https://doi.org/10.1021/ie030573v

26. Ghasemi, M. H., Hoseinzadeh, S., Heyns, P. S. and Wilke, D. N. "Numerical Analysis of Non-Fourier Heat Transfer in a Solid Cylinder with Dual-Phase-Lag Phenomenon", *CMES-Computer Modeling in Engineering & Sciences,* Vol. 122, No. 1, (2020), 399-414.

Persian Abstract

چکیده

در طول تولید نفت، بروز چنین عارضه ای مانند تشکیل رسوبات موم غیر معمول نیست. مبارزه با این رسوبات و همچنین توسعه روش های نوین مقابله با آنها از مهمترین وظایف بهره برداران از زیر خاک است. بسیاری از روش‌های مدرن مدل‌سازی نیاز به تعیین دقیق عددی مانند هدایت حرارتی رسوبات آلی دارند. بر اساس تجزیه و تحلیل متون علمی، می توان نتیجه گرفت که هیچ روشی برای تخمین این مقدار در شرایط تشکیل موم بدون تأثیر بر ساختار منافذ آنها وجود ندارد. این مقاله روشی را برای تعیین این مقدار بر اساس نتایج مطالعه فرآیند تشکیل رسوبات آلی در تاسیسات آزمایشگاهی "حلقه جریان موم" بر اساس قوانین انتقال حرارت و جرم توصیف می کند. بر اساس نتایج به کارگیری این تکنیک، تعیین رسانایی حرارتی رسوبات آلی امکان پذیر می شود که مقدار آن با مقادیر ارائه شده در منابع مرجع و علمی مرتبط است. علاوه بر این، وجود یک همبستگی بین مقدار هدایت حرارتی رسوبات و ترکیب اجزای سیال مورد مطالعه تعیین شد. استفاده از روش توصیف شده این امکان را به شما می دهد که فرآیندهای تولید نفت را با دقت بیشتر شبیه سازی کنید و اثربخشی تکنولوژیکی استفاده از روش های مدرن مبارزه با سوب گذاری مواد آلی نظیر موم را تعیین کنید.

International Journal of Engineering

Nanostructured α-Fe₂O₃: Solvothermal Synthesis, Characterization, and Effect of Synthesis Parameters on Structural Properties

S. M. R. Shariatzadeh[a], M. Salimi*[a], H. Fathinejad[b], A. Hassani Joshaghani[a]

[a] Department of Chemical Engineering, Arak Branch, Islamic Azad University, Arak, Iran
[b] Department of Chemistry, Farahan Branch, Islamic Azad University, Farahan, Iran

A B S T R A C T

α-Fe₂O₃ is a stable, cheap, and non-toxic metal oxide with many advantages and different fields of application. Many attempts have been devoted to the synthesis of α-Fe₂O₃ with different crystal structures and morphologies to obtain the desired properties. In this research, nanostructured α-Fe₂O₃ were synthesized by a facile solvothermal route. The as-obtained samples are characterized by XRD, FESEM, EDS, FTIR, and BET surface area analysis. The results showed that the as-synthesized hematite consists of nanostructures with the morphology of distorted microspheres with an average diameter in the range of 1 to 1.5 μm each composed of self-assembled nanoparticles with an average size in the range of 10 to 30 nm. The results showed that the hematite nanostructures had a specific surface area of 41.86 m^2g^{-1}. The influence of temperature and duration of the solvothermal process as well as, calcination on the structural properties of the α-Fe₂O₃ samples was investigated. The results reveal that the crystallite size of the samples increases with increasing the temperature and duration of solvothermal treatment. Moreover, calcination leads to an increase in the crystallite size of the samples. The α-Fe₂O₃ nanostructures with a minimum crystallite size of 13.6 nm were synthesized at 150 °C for 4 h while the largest crystallite size of 75.4 nm was obtained at 180 °C and 8 h with subsequent calcination of the sample at 500 °C for 1 h. The results of the present study can be useful to enhance the properties of α-Fe₂O₃ nanostructures in various fields of application.

doi: 10.5829/ije.2022.35.06c.10

1. INTRODUCTION

Hematite (α-Fe₂O₃), the most stable form of iron oxides has drawn much attention due to its advantages and variety of applications [1, 2]. Various synthesis techniques including hydrolysis, chemical solution, electrospinning, molecular layer deposition, and solvothermal have been applied to prepare α-Fe₂O₃ nanostructures [3]. Among these, the hydro/solvothermal process has drawn much attention, as it is a one-step process with the possibility of controlling crystal structure and morphology [4-6]. The specific properties of nanostructures are widely affected by their structures and morphologies [7-9]. Therefore, various morphologies of α-Fe₂O₃ such as hexagonal plates [10],

rod and ellipsoidal particles [11], flower-like [12], and nanoparticles [13] have been synthesized.

In the solvothermal process, the properties of products are widely affected by the type of precursors, type of solvent, reaction temperature, and duration of the reaction. However, regarding the environmental aspects, it is often preferred to carry out the process using non-toxic and low-cost materials at a low level of energy consumption [14].

Ma et al. [15] synthesized α-Fe₂O₃ nanostructures with different sizes and shapes by changing reaction time and solvent via a simple hydrothermal process. α-Fe₂O₃ nanopolyhydra, nanoparticles and microcubes were obtained by different solvents and reaction times. Zhang et al. synthesized two different morphologies of α-Fe₂O₃ using two different solvents in a solvothermal process.

Corresponding Author Institutional Email: m-salimi@iau-arak.ac.ir
(M. Salimi)

3D flower-like α-Fe$_2$O$_3$ nanostructures and α-Fe$_2$O$_3$ nanoparticles were obtained with isopropanol and water as the solvent, respectively [16]. Trpkov et al. [17] synthesized α-Fe$_2$O$_3$ hierarchical superstructures by glycine-free and glycine-assisted hydrothermal method. The superstructures were composed of nanoparticles as building blocks with different morphology including mushroom-like, cube-like, and sphere-like, and dimensions of 1-5 µm. Cao et al. [18] synthesized flowerlike α-Fe$_2$O$_3$ nanostructures via a solvothermal route using FeCl$_3$.6H$_2$O, urea, ethanol, and microwave irradiation as the heating source.

The effect of crystallite size on various properties of hematite has been investigated [19, 20]. Nandiyanto et al. [21] studied the correlation between crystallite size and the photocatalytic activity of WO$_3$ particles. The photodegradation rate of curcumin was enhanced with increasing in crystallite size of the photocatalyst.

The present study consists of two phases. In phase 1, α-Fe$_2$O$_3$ is synthesized via a solvothermal process according to the previous study to investigate the effect of the heating source on the properties of the products. In the previous study solvothermal reaction was performed under microwave irradiation while in this study heating is performed by a standard laboratory oven. In phase 2, α-Fe$_2$O$_3$ is synthesized by solvothermal treatment under different conditions of temperature and duration of solvothermal treatment. The samples are characterized by several characterization techniques. The influence of the solvothermal parameters as well as calcination on the crystal structure of the products is investigated.

2. MATERIALS AND METHODS

2. 1. Materials   Ferric chloride hexahydrate (99.5% FeCl$_3$.6H$_2$O, Merck), urea (99.5%, ChemLab) and ethanol (99.9% C$_2$H$_5$OH, Merck) were used to synthesize α-Fe$_2$O$_3$ nanostructures. Deionized water was used in all cases. All the materials were of analytical grade and used without further purification.

2. 2. Synthesis of α-Fe$_2$O$_3$ Nanostructures   In phase 1, hematite nanostructures were synthesized via a solvothermal process according to the previous study [18]. A 1.89 g (7 mmol) of FeCl$_3$.6H$_2$O and 0.63 g (10.5 mmol) of urea were dissolved in 60 ml of absolute ethanol. The mixture was magnetically stirred at room temperature for 30 minutes to obtain a clear and homogeneous solution. The obtained solution was transferred into a 100 ml teflon-lined stainless steel autoclave. The autoclave was sealed and heated in a standard laboratory oven at 150 °C for 4 h. Then, the autoclave was naturally cooled down to room temperature. The obtained precipitates were collected by centrifugation at 4000 rpm, washed with absolute ethanol

5 times, and dried in an oven at 80 °C for 4 h. In phase 2, six samples of hematite were prepared under different conditions according to Table 1. The solvothermal process was performed at temperatures of 120 °C, 150 °C, and 180 °C, each for 4 h and 8 h. The other steps of synthesis including preparation of solution, separation, washing, and drying of the precipitates were the same as phase 1. Three of the as-synthesized samples were calcined at 500 °C in a muffle furnace for 1 h. The synthesis parameters and the sample names are listed in Table 1.

2. 3. Characterization   The crystal structure of the as-prepared samples was determined by XRD on XRD PANanalytical with Cu Kα radiation at λ=1.54060 Å. The crystallite size of the samples was calculated by Scherrer's equation as follows:

$$D \approx \frac{0.9\,L}{B\cos\theta} \qquad (1)$$

where D is the mean crystallite diameter, L is the wavelength of the X-ray applied, θ is the diffraction angle of the specified peak, and B is the full width at half maximum (FWHM) [22]. The morphology of the particles was investigated by FESEM with MIRA3TESCAN-XMU. The composition of the samples was determined by EDS along with FESEM. The type of bonding structure of the samples was examined by FTIR with Thermo AVATAR. The surface area of the products was studied on BELSORP MINI II by BET analysis.

3. RESULTS AND DISCUSSION

3. 1. Characterization   The phase and crystal structure of the products were analyzed by XRD analysis. The XRD pattern of the as-synthesized α-Fe$_2$O$_3$ is shown in Figure 1. The obtained XRD pattern illustrates diffraction peaks with 2θ at 24.2°, 33.1°, 35.7°, 40.9°,

TABLE 1. Different solvothermal conditions used for the synthesis of nanostructured α-Fe$_2$O$_3$

| Sample Name	Reaction Temperature (°C)	Reaction Time (h)	Calcination
F120-4	120	4	-
F120-8	120	8	-
F150-4	150	4	-
F150-4-C	150	4	Done
F150-8	150	8	-
F180-4	180	4	-
F180-4-C	180	4	Done
F180-8	180	8	-
F180-8-C	180	8	Done
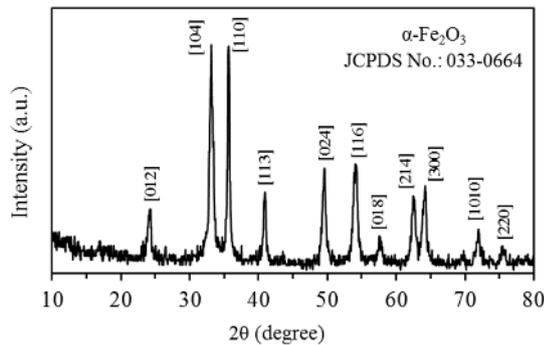
Figure 1. XRD pattern of the nanostructured α-Fe$_2$O$_3$ microparticles synthesized by solvothermal method at 150 °C for 4 h

49.5°, 54.1°, 57.6°, 62.5°, 64.1°, 71.9° and 75.5° which can be well ascribed to the standard peaks of the hematite structure (crystal system: hexagonal, space group: R-3c, cell parameters: a=b=5.034 Å, c=13.748Å, JCPDS No.: 033-0664) [23-25]. The obtained XRD pattern shows no peaks related to impurities and confirms that pure and single phase α-Fe$_2$O$_3$ has been successfully synthesized.

The morphology of the as-synthesized α-Fe$_2$O$_3$ was characterized using the FESEM. As can be seen in Figures 2(a), 2(b), and 2(c) the pure α-Fe$_2$O$_3$ consists of distorted microspheres with an average diameter in the range of 1 to 1.5 µm. The microspheres are composed of nanoparticles with an average size in the range of 10 to 30 nm. This morphology is different from the morphology of α-Fe$_2$O$_3$ synthesized via a solvothermal process by Cao et al. [18]. In their study, the same precursors and solvent with the microwave irradiation as the heating source were used and flowerlike nanostructures composed of nanopetals were obtained. In the present study, convection heating by a standard laboratory oven was used to carry out the reaction synthesis of α-Fe$_2$O$_3$. From the obtained results, it can be concluded that the source of energy used in the solvothermal process is a key factor, which can affect the morphology of the products.

The EDS pattern was taken to specify the composition of the sample. As shown in Figure 2(d) the EDS pattern confirms the presence of the elements Fe and O in the as-synthesized α-Fe$_2$O$_3$ nanostructures.

The chemical structure of the α-Fe$_2$O$_3$ samples was studied by FTIR analysis. The FTIR spectrum was obtained in the wavenumber range from 400 to 4000cm^{-1} at room temperature. As can be seen in Figure 3 two vibrational bands at 474 cm^{-1} and 562 cm^{-1} are related to the Fe-O stretching modes which confirm the formation of α-Fe$_2$O$_3$ crystals. The bands at 1633 cm^{-1} and 3417 cm^{-1} are related to the bending and stretching modes of the O-H groups respectively, that show the presence of the hydroxyl group and/or water molecules on the surface of α-Fe$_2$O$_3$ [26].
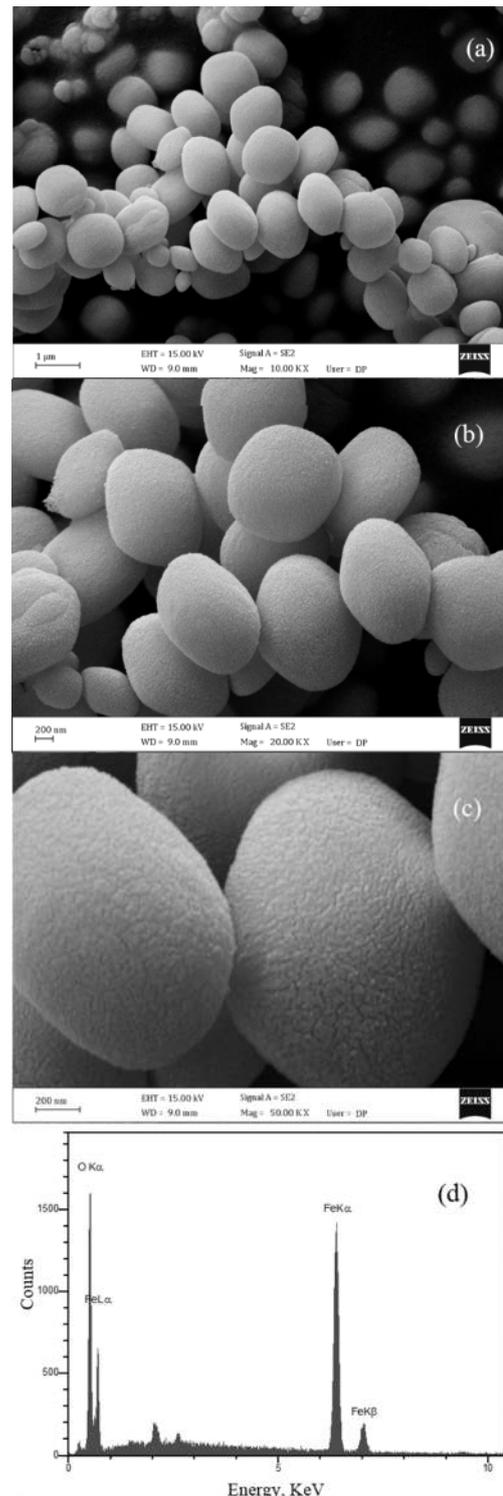

Figure 2. FESEM images (a), (b), (c), and EDS pattern (d) of the nanostructured α-Fe$_2$O$_3$ microparticles synthesized by solvothermal method at 150 °C for 4 h

Figure 4 displays the BET plot of the as-prepared α-Fe$_2$O$_3$ microparticles. The BET surface area and average pore size of the α-Fe$_2$O$_3$ microparticles are calculated to be
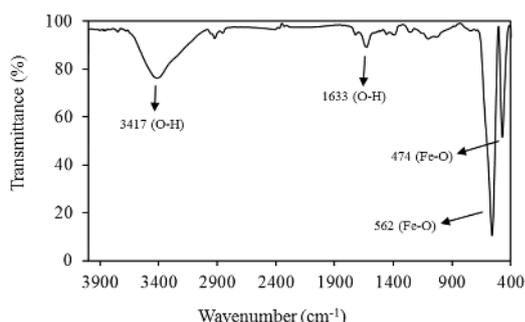
Figure 3. FTIR spectrum of the as-synthesized nanostructured α-Fe$_2$O$_3$ microparticles
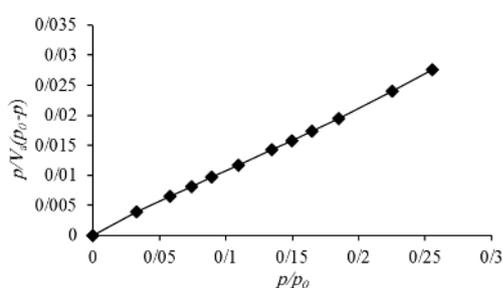
Figure 4. BET plot of the as-synthesized nanostructured α-Fe$_2$O$_3$ microparticles

41.86 m^2/g^{-1} and 3.45 nm respectively. This relatively high surface area of the samples is attributed to the nanostructured surface of the particles as confirmed by the FESEM. The large surface area is of great significance in some applications such as photocatalysis which adsorption has the main role in the process [27].

3. 2. Reaction Mechanism   In the solvothermal process, the OH$^-$ group is formed by adding urea to water molecules present in the solvent of ethanol (steps 1 and 2). The brown colloidal precipitates of Fe(OH)$_3$ are produced by the association of OH$^-$ and Fe^{+3} (step 3). High temperature and pressure of the solvothermal process leads to dehydration of Fe(OH)$_3$ and finally crystallization of the amorphous iron oxide to α-Fe$_2$O$_3$ crystals (step 4). Besides, urea has the role of a capping agent in the formation of the as-synthesized α-Fe$_2$O$_3$ nanostructures [18, 27].

1) $CO(NH_2)_2 + H_2O \rightarrow 2NH_3 + CO_2$
2) $NH_3 + H_2O \rightarrow NH_4^+ + OH^-$
3) $Fe^{3+} + 3OH^- \rightarrow Fe(OH)_3$
4) $2Fe(OH)_3 \rightarrow \alpha\text{-}Fe_2O_3 + 3H_2O$

3. 3. Effect of Synthesis Parameters on Purity and Phase Structure   In phase 2 of this study, the α-Fe$_2$O$_3$ samples were synthesized via the solvothermal

method, and the effect of synthesis parameters on the crystallite size of the products was investigated. The solvothermal reaction was performed at different reaction temperatures for different reaction times. Moreover, according to Table 1 three of the as-synthesized samples were calcined to determine the effect of calcination on the crystallite size of the samples.

The X-ray Diffraction (XRD) patterns of α-Fe$_2$O$_3$ samples were taken to determine the purity, phase, and crystal structure of the products. The XRD patterns of the samples are shown in Figure 5. For the sample F120-4, no distinctive peak of α-Fe$_2$O$_3$ can be identified in the obtained XRD pattern, which reveals that the sample prepared at the reaction temperature of 120 °C for a duration of 4 h has an amorphous phase. As can be seen in Figure 5, when reaction time increases from 4 h to 8 h and reaction temperature increases from 120 °C to 150 °C and 180 °C the diffraction peaks assigned to the α-Fe$_2$O$_3$, without any impurity peaks, appear in the obtained XRD patterns. Thus, except for the sample F120-4, the obtained XRD patterns for all other samples show diffraction peaks which can be well ascribed to the standard peaks of hematite structure with JCPDS No. 033-0664. This indicates when the reaction is performed at a low temperature of 120 °C and a low duration of 4 h, the activation energy is not enough for crystallization of the α-Fe$_2$O$_3$ nanostructures, and the sample phase remains amorphous. This is compatible with the findings in the previous studies [5].

The synthesis parameters used in this study and some previous studies are shown in Table 2. These data show that the nanostructured α-Fe$_2$O$_3$ can be synthesized at a relatively lower reaction temperature and shorter reaction time. These conditions are desirable due to the less energy and time consumption in the synthesis of nanostructured hematite.

TABLE 2. Solvothermal synthesis parameters of α-Fe$_2$O$_3$ in the present and previous studies

Reference	Reaction Time (h)	Reaction Temperature (°C)	α-Fe$_2$O$_3$ Morphology
Zhang et al. [16]	24	200	3D Flowerlike
Ayachi et al. [27]	10	200	Nanoplatelets
Liang et al. [28]	24	180	3D Multileaf
Majumder et al. [29]	8	180	3D Dendritic
Xiao et al. [30]	24	160	Burger-like
This study	4	150	Distorted microspheres
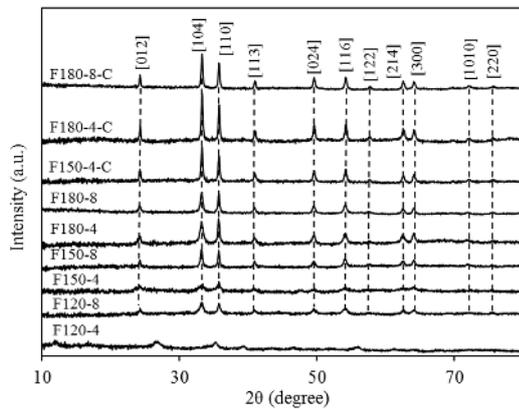
Figure 5. XRD patterns of hematite prepared by the solvothermal method at reaction temperatures of 120 °C, 150 °C, and 180 °C for reaction times of 4 h and 8 h. The samples assigned by C were calcined at 500 °C for 1 h

3. 4. Effect of Synthesis Parameters on Crystallite Size

**3. 4. 1. Reaction Temperature**   The mean crystallite size of the samples was calculated by equation (1) based on the obtained peak at θ=33.2 ° in the XRD patterns of hematite samples. The effect of the reaction temperature on the crystallite size of the samples was determined at 120 °C, 150 °C, and 180 °C. According to Figure 6, for the reaction time of 4 h the crystallite size of the α-Fe$_2$O$_3$ samples increases from19.7 nm to 24.4 nm when the reaction temperature increases from 150 °C to 180 °C. In addition, for the reaction time of 8 h, the crystallite size is 21.3, 25.4, and 31.9 nm at the temperature of 120 °C, 150 °C, and 180 °C, respectively. Thus, in the higher reaction temperature, hematite with a larger crystallite size is formed and this is in good compliance with the previous works [5, 31, 32].

3. 4. 2. Reaction Time   The effect of reaction time on the crystallite size of the samples was also investigated. The solvothermal reactions were carried out for reaction times of 4 h and 8h and the crystallite size was calculated by Equation (1). According to Figure 7 at reaction temperatures of 120 °C, 150 °C, and 180 °C the crystallite size of the samples increases when the reaction time increases from 4 h to 8 h. By increasing the solvothermal process time, the crystal growth occurs in a longer time, thus the samples with larger crystallite size can be prepared [31].

3. 4. 3. Calcination   The effect of calcination on the crystallite size of samples was evaluated for the three samples 150-4-C, F180-4-C, and F180-8-C. According to Figure 8, the crystallite size of the samples increases by calcination at 500 °C for 1 h. The growth in the crystallite size of the samples after calcination is due
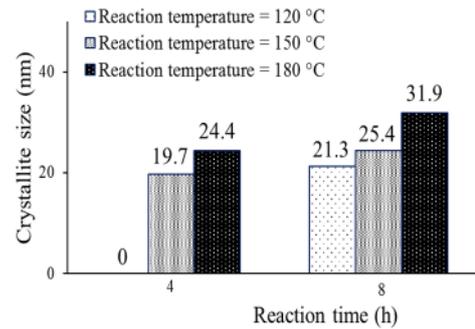
Figure 6. Effect of reaction temperature on the crystallite size of the as-synthesized α-Fe$_2$O$_3$
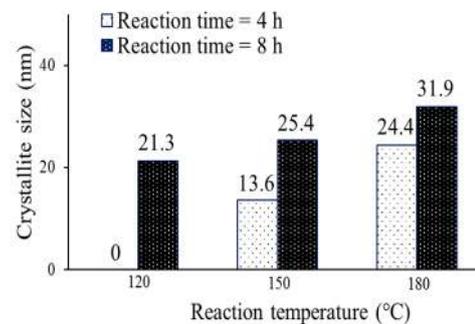
Figure 7. Effect of reaction time on the crystallite size of the as-synthesized α-Fe$_2$O$_3$
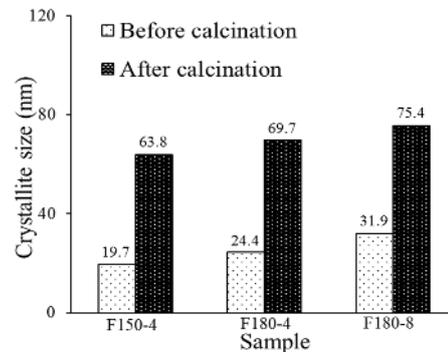
Figure 8. Effect of calcination on the crystallite size of the as-synthesized α-Fe$_2$O$_3$

to the reduction in activation energy of crystallization, which enhances the crystal growth rate in the as-prepared nanostructured hematite [32, 33]. The enhancement of crystallite size and subsequent low density of crystalline defects of the nanostructured α-Fe$_2$O$_3$ crystals is desirable in some applications [34, 35].

4. CONCLUSION

The nanostructured α-Fe$_2$O$_3$ was successfully synthesized via a facile one-step solvothermal process

using $FeCl_3.6H_2O$, urea, and ethanol treated at 150 °C for 4 h. The FESEM images showed that the samples are composed of distorted microspheres with an average diameter in the range of 1 to 1.5 µm and each microsphere is built from self-assembled nanoparticles with an average size in the range of 10 to 30 nm. The BET analysis showed a relatively high surface area of 41.86 m^2g^{-1} for the α-Fe_2O_3 nanostructures. The effect of solvothermal reaction parameters on the structural properties of the α-Fe_2O_3 nanostructures was investigated. It was found that an increase in reaction temperature and reaction time in the solvothermal process, leads to an increase in crystallite size of the products. In addition, the effect of calcination on the crystallite size was studied and the results showed that calcination enhanced the crystallite size of the nanostructured α-Fe_2O_3. The sample synthesized at 150 °C for 4 h had the smallest crystallite size of 13.6 nm. The sample that was treated at 180 °C for 8 h and then calcined at 500 °C for 1 h had the largest crystallite size of 75.4 nm. The obtained results can be suitable to synthesize α-Fe_2O_3 nanostructures with enhanced properties for different applications.

5. REFERENCES

1. Toghraei, M. and Siadati, H., "Electrodeposited co-pi catalyst on α-Fe_2O_3 photoanode for water-splitting applications", *International Journal of Engineering*, *Transactions C: Aspects,* Vol. 31, No. 12, (2018), 2085-2091. DOI: 10.5829/ije.2018.31.12c.13

2. Salman, K. D., "Synthesis and characterization unsaturated polyester resin nanocomposites reinforced by Fe_2O_3+Ni nanoparticles: Influence on mechanical and magnetic properties", *International Journal of Engineering*, *Transactions A: Basics,* Vol. 35, No. 1, (2022), 21-28. DOI: 10.5829/ije.2022.35.01A.03

3. Hitam, C. N. C. and Jalil, A. A., "A review on exploration of Fe_2O_3 photocatalyst towards degradation of dyes and organic contaminants", *Journal of Environmental Management*, Vol. 258, (2020), 110050. DOI: 10.1016/j.jenvman.2019.110050

4. Djurisic, A. B., Xi, Y. Y., Hsu, Y. F. and Chan, W. K., "Hydrothermal synthesis of nanostructures", *Recent Patents Nanotechnology*, Vol. 1, No. 2, (2007), 121-128. DOI: 10.2174/187221007780859591

5. Sha, G., Wang, T., Xiao, J. and Liang, C., "A mild solvothermal route to α-Fe_2O_3 nanoparticles", *Materials Research Bulletin*, Vol. 39, (2004), 1917-1921. DOI: 10.1016/j.materresbull.2004.06.002

6. Heidari, A., Younesi, H. and Zinatizadeh, A. A. L., "Controllable synthesis of flower-like Zno nanostructure with hydrothermal method (research note)", *International Journal of Engineering, Transactions B: Applications*, Vol. 22, No. 3, (2009), 283-290.

7. Gharibshahian, E., "The effect of polyvinyl alcohol concentration on the growth kinetics of ktiopo4 nanoparticles synthesized by the co-precipitation method", *HighTech and Innovation Journal*, Vol. 1, No. 4, (2020), 187-193. DOI: 10.28991/HEF-2021-02-02-05

8. Kien, P. H., Khamphone, Y. and Trang, G.T.T., "Study of effect of size on iron nanoparticle by molecular dynamics simulation", *HighTech and Innovation Journal*, Vol. 2, No. 3, (2021), 158-167. DOI: 10.28991/HIJ-2021-02-03-01

9. Hosseingholi, M., "Room temperature synthesis of n-doped urchin-like rutile TiO_2 nanostructure with enhanced photocatalytic activity under sunlight", *International Journal of Engineering*, *Transactions A: Basics,* Vol. 28, No. 10, (2015), 1401-1407. DOI: 10.5829/idosi.ije.2015.28.10a.01

10. Katsuki, H., Choi, E. K., Lee, W. J., Hwang, K. T., Cho, W.-S., Huang, W. and Komarneni, S., "Ultrafast microwave-hydrothermal synthesis of hexagonal plates of hematite", *Materials Chemistry and Physics*, Vol. 205, (2018), 210-216. DOI: 10.1016/j.matchemphys.2017.10.078

11. Wang, X., "Ammonium mediated hydrothermal synthesis of nanostructured hematite (α-Fe_2O_3) particles", *Materials Research Bulletin*, Vol. 47, (2012), 2513-2517. DOI: 10.1016/j.materresbull.2012.05.005

12. Zhang, Q., Lu, X., Chen, L., Shi, Y., Xu, T. and Liu, M., "Mesoporous flower-like α-Fe_2O_3 nanoarchitectures: Facile synthesis and their magnetic and photocatalytic properties", *Materials Letters*, Vol. 106, (2013), 447-451. DOI: 10.1016/j.matlet.2013.08.029

13. Khalil, M., Yu, J., Liu, N. and Lee, R.L., "Hydrothermal synthesis, characterization, and growth mechanism of hematite nanoparticles", *Journal of Nanoparticle Research*, Vol. 16, No. 2362, (2014), 1-10. DOI: 10.1007/s11051-014-2362-x

14. Byrappa, K. and Adschiri, T., "Hydrothermal technology for nanotechnology", *Progress in Crystal Growth and Characterization of Materials*, Vol. 53, No. 2, (2007), 117-166. DOI: 10.1016/j.pcrysgrow.2007.04.001

15. Ma, J., Lian, J., Duan, X., Liu, X. and Zheng, W., "A- Fe_2O_3: Hydrothermal synthesis, magnetic and electrochemical properties", *The Journal of Physical Chemistry C*, Vol. 114, No. 24, (2010), 10671-10676. DOI: 10.1021/jp102243g

16. Zhang, W., Chen, J., Wang, X., Qi, H. and Peng, K., "Self-assembled three-dimensional flower-like α-Fe_2O_3 nanostructures and their application in catalysis", *Applied Organometallic Chemistry*, Vol. 23, (2009), 200-203. DOI: 10.1002/aoc.1496

17. Trpkov, D., Panjan, M., Kopanja, L. and Tadić, M., "Hydrothermal synthesis, morphology, magnetic properties and self-assembly of hierarchical α-Fe_2O_3 (hematite) mushroom-, cube- and sphere-like superstructures", *Applied Surface Science*, Vol. 457, (2018), 427-438. DOI: 10.1016/j.apsusc.2018.06.224

18. Cao, C.Y., Qu, J., Yan, W.S., Zhu, J.F., Wu, Z.Y. and Song, W.G., "Low-cost synthesis of flowerlike alpha- Fe_2O_3 nanostructures for heavy metal ion removal: Adsorption property and mechanism", *Langmuir*, Vol. 28, No. 9, (2012), 4573-4579. DOI: 10.1021/la300097y

19. Fouad, D. E., Zhang, C., El-Didamony, H., Yingnan, L., Mekuria, T. D. and Shah, A. H., "Improved size, morphology and crystallinity of hematite (α-Fe_2O_3) nanoparticles synthesized via the precipitation route using ferric sulfate precursor", *Results in Physics*, Vol. 12, (2019), 1253-1261. DOI: 10.1016/j.rinp.2019.01.005

20. Valášková, M., Tokarský, J., Pavlovský, J., Prostějovský, T. and Kočí, K., "α-Fe_2O_3 nanoparticles/vermiculite clay material: Structural, optical and photocatalytic properties", *Materials*, Vol. 12, No. 11, (2019), 1880. DOI: 10.3390/ma12111880

21. Nandiyanto, A. B. D., Zaen, R. and Oktiani, R., "Correlation between crystallite size and photocatalytic performance of micrometer-sized monoclinic WO_3 particles", *Arabian Journal of Chemistry*, Vol. 13, No. 1, (2020), 1283-1296. DOI: 10.1016/j.arabjc.2017.10.010

22. Tadic, M., Panjan, M., Damnjanovic, V. and Milosevic, I., "Magnetic properties of hematite (α-Fe_2O_3) nanoparticles prepared by hydrothermal synthesis method", *Applied Surface*

Science, Vol. 320, (2014), 183-187. DOI: 10.1016/j.apsusc.2014.08.193

23. Zhu, Y., Peng, C., Gao, Z. F., Yang, H., Liu, W. M. and Wu, Z.-J., "Hydrothermal synthesis of CaFe₂O₄/α-Fe₂O₃ composite as photocatalyst and its photocatalytic activity", *Journal of Environmental Chemical Engineering*, Vol. 6, No. 2, (2018), 3358-3365. DOI: 10.1016/j.jece.2018.05.012

24. Tadic, M., Trpkov, D., Kopanja, L., Vojnovic, S. and Panjan, M., "Hydrothermal synthesis of hematite (α-Fe₂O₃) nanoparticle forms: Synthesis conditions, structure, particle shape analysis, cytotoxicity and magnetic properties", *Journal of Alloys and Compounds*, Vol. 792, (2019), 599-609. DOI: 10.1016/j.jallcom.2019.03.414

25. Bouziani, A., Park, J. and Ozturk, A., "Synthesis of α-Fe₂O₃/TiO₂ heterogeneous composites by the sol-gel process and their photocatalytic activity", *Journal of Photochemistry and Photobiology A: Chemistry*, Vol. 400, (2020), 112718. DOI: 10.1016/j.jphotochem.2020.112718

26. Lassoued, A., Lassoued, M. S., Dkhil, B., Ammar, S. and Gadri, A., "Synthesis, photoluminescence and magnetic properties of iron oxide (α-Fe₂O₃) nanoparticles through precipitation or hydrothermal methods", *Physica E: Low-dimensional Systems and Nanostructures*, Vol. 101, (2018), 212-219. DOI: 10.1016/j.physe.2018.04.009

27. Ayachi, A. A., Mechakra, H., Silvan, M. M., Boudjaadar, S. and Achour, S., "Monodisperse α-Fe₂O₃ nanoplatelets: Synthesis and characterization", *Ceramics International*, Vol. 41, (2015), 2228-2233. DOI: 10.1016/j.ceramint.2014.10.024

28. Liang, J., Li, L. and Kang, H., "Solvothermal synthesis, growth mechanism, and magnetic property of self-assembled 3d multileaf α-Fe₂O₃ superstructures", *Powder Technology*, Vol. 235, (2013), 475-478. DOI: 10.1016/j.powtec.2012.10.060

29. Majumder, S., Pal, S., Kumar, S. and Banerjee, S., "Photon upconversion in 3d dendritic α-Fe₂O₃", *Materialstoday: Proceedings*, Vol. 4, (2017), 5620-5624.

30. Xiao, C., Li, J. and Zhang, G., "Synthesis of stable burger-like α-Fe₂O₃ catalysts: Formation mechanism and excellent photo-fenton catalytic performance", *Journal of Cleaner Production*, Vol. 180, (2018), 550-559. DOI: 10.1016/j.jclepro.2018.01.127

31. Song, H., Sun, Y. and Jia, X., "Hydrothermal synthesis, growth mechanism and gas sensing properties of Zn-doped α-Fe₂O₃ microcubes", *Ceramics International*, Vol. 41, No. 10, (2015), 13224-13231. DOI: 10.1016/j.ceramint.2015.07.100

32. Pang, Y. X. and Bao, X., "Influence of temperature, ripening time and calcination on the morphology and crystallinity of hydroxyapatite nanoparticles", *Journal of the European Ceramic Society*, Vol. 23, No. 10, (2003), 1697-1704. DOI: 10.1016/S0955-2219(02)00413-2

33. Soo, J. Z., Ang, B. C. and Ong, B. H., "Influence of calcination on the morphology and crystallinity of titanium dioxide nanofibers towards enhancing photocatalytic dye degradation", *Materials Research Express*, Vol. 6, No. 2, (2018), 025039. DOI: 10.1088/2053-1591/aaf013

34. Wang, T., Yang, G., Liu, J., Yang, B., Ding, S., Yan, Z. and Xiao, T., "Orthogonal synthesis, structural characteristics, and enhanced visible-light photocatalysis of mesoporous fe2o3/tio2heterostructured microspheres", *Applied Surface Science*, Vol. 311, (2014), 314-323. DOI: 10.1039/C4CS00126E

35. Lukic, S., Menze, J., Weide, P., Busser, W., Winterer, M. and Muhler, M., "Decoupling the effects of high crystallinity and surface area on the photocatalytic overall water splitting over b-Ga₂O₃ nanoparticles by chemical vapor synthesis", *ChemSusChem*, Vol. 10, No. 21, (2017), 4190-4197. DOI: 10.1002/cssc.201701309

Persian Abstract

چکیده

α-Fe₂O₃ یک اکسید فلزی پایدار، ارزان و غیر سمی با مزایای زیاد و زمینه های کاربردی گوناگون می باشد. تلاش های زیادی برای سنتز α-Fe₂O₃ با ساختار های بلوری و مورفولوژی های متفاوت برای به دست آوردن خواص مطلوب صورت گرفته است. در این پژوهش، نانوساختار α-Fe₂O₃ با یک روش ساده حلالی حرارتی سنتز می شوند. نمونه های به دست آمده با استفاده از روش های پراش اشعه X (XRD)، میکروسکوپی الکترونی روبشی نشر میدانی (FESEM)، طیف سنجی پراش انرژی اشعه X (EDS)، طیف سنجی مادون قرمز تبدیل فوریه (FTIR)، و آنالیز مساحت سطح برونر-امت-تلر (BET) مشخصه یابی می شوند. نتایج نشان می دهد هماتیت سنتزی از نانوساختار هایی با مورفولوژی میکروکره های اعوجاج یافته با میانگین قطر در محدوده ۱ تا ۱.۵ میکرومتر تشکیل شده که هر میکروکره از نانوذرات خود تشکیل با اندازه میانگین ۱۰ تا ۳۰ نانومتر تشکیل یافته است. نتایج نشان می دهد نانوساختار های هماتیت مساحت سطح ویژه ای معادل ۴۱۸۶ متر مربع بر گرم دارند. تأثیر دما و زمان فرایند حلالی حراتی و نیز اثر کلسیناسیون بر روی ساختار بلوری نمونه های سنتز شده مورد بررسی قرار می گیرد. نتایج نشان می دهد با افزایش دما و زمان واکنش حلالی حرارتی، اندازه کریستالیت در نمونه ها افزایش می یابد. به علاوه، کلسیناسیون منجر به افزایش اندازه کریستالیت نمونه ها می گردد. نانوساختار های α-Fe₂O₃ با حداقل اندازه کریستالیت ۱۳.۶ نانومتر در دمای ۱۵۰ درجه سانتی گراد برای مدت ۴ ساعت سنتز شدند در حالی که بزرگ ترین اندازه کریستالیت برابر ۷۵.۴ نانومتر در دمای ۱۸۰ درجه سانتی گراد و ۸ ساعت و سپس کلسیناسیون نمونه در ۵۰۰ درجه سانتی گراد به مدت ۱ ساعت به دست آمد. نتایج این مطالعه می تواند در بهبود خواص نانوساختار های α-Fe₂O₃ در زمینه های مختلف کاربردی مفید واقع شود.

International Journal of Engineering

Journal Homepage: www.ije.ir

Numerical Investigation on Oscillation Behavior of a Non-isothermal Self-excited Jet in a Cavity: The Effects of Reynolds Number and Temperature Differences

M. Aminzadeh[a], J. Khadem*[a], S. A. Zolfaghari[a], A. Omidvar[b]

[a] Department of Mechanical Engineering, University of Birjand, Birjand, Iran
[b] Department of Mechanical and Aerospace Engineering, Shiraz University of Technology, Shiraz, Iran

P A P E R I N F O	*A B S T R A C T*
	A self-excited oscillating jet can be naturally produced by discharging a plane jet into a rectangular cavity due to pressure effects and without a need for external aid. In recent years, the self-oscillatory jet in non-isothermal conditions has attracted research interests because of its wide range of industrial applications. Therefore, the current study aimed to compare the oscillatory behavior of downward vertical self-excited jet with Reynolds number (Re) 1000 and 3000 under various temperature differences (0, 100, and 300 K) between inletflow and cavity's wall. Computational solutions were obtained using unsteady Reynolds averaged Navier-Stokes (URANS) and energy equations for an incompressible flow. The numerical simulation was carried out by the finite-volume based tool OpenFOAM code. The results showed that depending on the value of temperature difference, oscillatory and non-oscillatory flows were observed. Also, at Re=3000, the temperature differences can change oscillation frequency up to 10% compared to isothermal conditions. This value reaches 58% at Re=1000. The results indicated that where the Archimedes number is less than 0.1, the effects of temperature differences between jet and cavity walls on the oscillating behavior are negligible.

NOMENCLATURE

Ar	Archimedes number	v	Velocity component in y direction (m/s)
Co	Courant number	W	Width of cavity (m)
e	Thickness of nozzle (m)	x, y	Cartesian coordinate
FFT	Fast Fourier Transform	**Greek Symbols**	
f	Frequency (Hz)	α	Thermal diffusivity (m²/s)
g	Gravity (m/s²)	β	Thermal expansion coefficient (1/K)
k	Turbulence kinetic energy (m²/s²)	ν	Kinematic viscosity (m²/s)
L	Length of cavity (m)	ρ	Density (kg/m³)
P	Static pressure (Pa)	ω	Specific of dissipation rate (1/s)
Re	Reynolds number	**Subscripts**	
T	Temperature (K)	0	Jet inlet
t	Time (s)	c	Cavity
u	Velocity component in x direction (m/s)	eff	Effective

1. INTRODUCTION

Jet impingement is used in industrial applications such as cooling and heating processes because it provides a high heat transfer rate between walls and fluid [1]. It is desirable to develop the efficient cooling techniques to ensure performance and reliability of electronic devices [2]. Applying excited jets in the impinging flow can enhance thermal efficiency because their oscillating motion covers a much larger region of impingement

*Corresponding Author's Email: jkhadem@birjand.ac.ir (J. Khadem)

surface than steady jets [3]. The other significant feature of an excited jet is greater mixing rate with higher entrainment that can be used with advantage in combustion and cooling processes [4]. Several methods can excite the jet's flow. They can be classified into passive, active, and hybrid methods. In the passive technique, the jets become excited naturally and do not consume extra energy, so they are called self-excited jets. While, the active methods require an auxiliary device such as a fan, pump, or moving part for jet excitation. Therefore, the passive methods are more affordable and reliable than the active ones. Also, the hybrid methods combine two or more passive and/or active systems [5]. The passive methods attract the attention of engineers and researchers because of their simplicity, low maintenance, and cost. The passive self-exciting jets strongly depend on their geometric structures [6]. Many structures have been developed for self-excited jets, including annular, swirling, and sweeping jets [5].

The present study has considered one of the simplest geometry of a self-excited oscillating jet comprised of a planar jet discharged into a rectangular cavity (Figure 1). These oscillations are driven by the jet deflection mechanism produced by the pressure variations (Coanda effect) [6]. Shakouchi et al. [7] found that a pair of vortices formed on both sides of the jet has an essential role in oscillatory behavior. This self-excited oscillating jet can be operated as an impingement jet for intensifying heat transfer in various applications such as freezing of tissue, drying processes of textiles and paper, cooling of electronic components [3], heat treatment of different metals [5], film cooling, and food processing [8]. These various applications have led to numerous studies on the self-excited oscillating jets. Mataoui et al. [9] numerically and experimentally studied the interaction of a turbulent plane jet issuing into a rectangular cavity under isothermal conditions. They varied jet location inside the cavity and Reynolds number (Re) to observe jet oscillation frequency changes. They showed that oscillation frequency increases with Re and height of the jet exit and is decreased by increasing the distance between nozzle's exit and bottom plate in the isothermal self-excited oscillating jet.

Denisikhina et al. [10] indicated that oscillation's amplitude-frequency characteristics in a self-excited oscillatory jet could predict accurately by applying the large eddy simulation (LES) and three-dimensional unsteady Reynolds averaged Navier-Stokes (URANS) methods. Mataoui and Schiestel [6] investigated the effects of the cavity's aspect ratio on the jet flow regime. They showed that oscillation frequency is decreased moderately with cavity height. Also, frequency is independent of the length of the cavity when impingement distance exceeds a certain value. Righolt et al. [11] developed a zero-dimensional model of the delay differential equation type for quantitatively describing

the self-sustained oscillation of a confined jet. Iachachene et al. [12] numerically investigated the effects of convection heat transfer on a slot oscillating impinging jet. They presented a relation for calculating Nusselt number with Reynolds number and geometrical parameters. Mosavati et al. [13] numerically simulated vortex ring deformation of round and square self-excited jets in a confined cavity. Their results showed that nozzleṡ geometry shape does not affect on the side wall's impingement point and oscillation frequency. While square oscillating nozzle has a wider spread than round one, and both have a wider jet spread (40% higher) than the free jets. Carnero et al. [8] studied the self-sustained oscillations of two turbulent isothermal opposing impinging planar water jets discharging into an open cavity under crossflow. They indicated that Reynolds number of jets plays a vital role in flow motion and behavior of the switching jets.

Appling multiple nozzles is a way to improve jet performance that have many practical engineering applications [14,15]. Aminzadeh et al. [16] reported the characteristics of the oscillatory flow caused by a double-inlet jet in a rectangular cavity compared to those of a single-inlet jet. They did not considered the effects of non-isothermal conditions. Also, Aminzadeh et al. [17] numerically studied on effects of nozzle width of self-excited oscillating impinging jets in a heated cavity at a fixed flow rate. The results indicated that Nusselt number at the impingement wall linearly changed with oscillation frequency. In addition, the cooling performance of these jets was compared to that of conventional stationary impinging jets. Aminzadeh et al. [18] numerically investigated the buoyancy mediating effects on the performance and oscillating behavior of horizontal and vertical self-excited jets under different thermal boundary conditions of the end cavity's wall (heated, cooled, and adiabatic). The results showed that non-isothermal conditions did not significantly affect the oscillating behavior of horizontal jets contrary to vertical jets. Also, Aminzadeh et al. [19] investigated the effects of limited temperatue differences in a horizontal self-excited jet with a fixed inlet velocity.

Buoyancy and momentum are forces that impact the flow field of the jet under non-isothermal conditions. According to the previous studies of Aminzadeh et al. [18,19], the significant effect of non-isothermal conditions on a self-excited oscillating jet occurs when the jet is positioned vertically. In the vertical position relative to gravity, the buoyancy force is parallel to momentum force and can affect the oscillatory behavior of the self-excited jet. Also, the interaction between buoyancy and momentum basically depends on the amount of flow rate and temperature difference. In industrial applications, these jets experience different flow rates and thermal conditions. However, the effects of different inlet flow rates at various temperatures of the

cavity's wall were not investigated yet. So, the present study was designed to simulate the vertical self-excited oscillating jet with different inlet flow rates and cavity wall temperatures. A parametric study was done on the effects of inlet Reynolds number of a plane jet issuing into a hot cavity on the flow and thermal fields.

2. METHODS

2. 1. Description of Setup   This paper studied the self-excited jet in a vertical cavity, as depicted in Figure 1. This cavity has dimensions $L \times W$. A downward oriented plane jet of thickness e is inserted centrally to a depth l, which injects the airflow with Reynolds number Re_0 and temperature of T_0 into the cavity with uniform temperature T_c. The flow can exit from two openings located above the cavity. All geometric and flow parameters are presented in Table 1.

2. 2. Numerical Models   The unsteady Reynolds averaged Navier–Stokes equations (URANS) for turbulent incompressible flow in a two-dimensional domain must be solved to simulate the present work. This purpose was carried out by the finite-volume based tool OpenFOAM code, using the Buoyant Boussinesq Pimple Foam solver enclosed by the SST k-ω turbulence model. These governing equations can be presented as follows:

$$\frac{\partial \bar{u}}{\partial x} + \frac{\partial \bar{v}}{\partial y} = 0 \tag{1}$$

$$\frac{\partial \bar{u}}{\partial t} + \bar{u}\frac{\partial \bar{u}}{\partial x} + \bar{v}\frac{\partial \bar{u}}{\partial y} = -\frac{1}{\rho}\frac{\partial \bar{P}}{\partial x} + \nu_{\text{eff}}\left(\frac{\partial^2 \bar{u}}{\partial x^2} + \frac{\partial^2 \bar{u}}{\partial y^2}\right) \tag{2}$$

$$\frac{\partial \bar{v}}{\partial t} + \bar{u}\frac{\partial \bar{v}}{\partial x} + \bar{v}\frac{\partial \bar{v}}{\partial y} = -\frac{1}{\rho}\frac{\partial \bar{P}}{\partial y} + \nu_{\text{eff}}\left(\frac{\partial^2 \bar{v}}{\partial x^2} + \frac{\partial^2 \bar{v}}{\partial y^2}\right) + g\beta(\bar{T} - T_0) \tag{3}$$
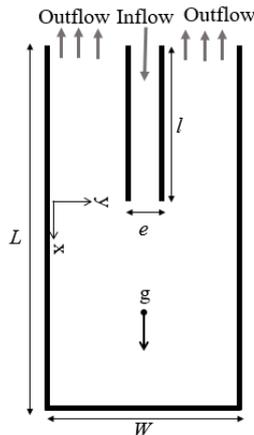
Figure 1. Studied configuration of a self-excited oscillating jet in a confined cavity

$$\frac{\partial \bar{T}}{\partial t} + \bar{u}\frac{\partial \bar{T}}{\partial x} + \bar{v}\frac{\partial \bar{T}}{\partial y} = \alpha_{\text{eff}}\left(\frac{\partial^2 \bar{T}}{\partial x^2} + \frac{\partial^2 \bar{T}}{\partial y^2}\right) \tag{4}$$

where $\bar{u}$ and $\bar{v}$ are mean velocity components, ρ denotes fluid density. ν_{eff} is effective viscosity and α_{eff} is effective thermal diffusivity. Mean temperature and static pressure are defined by $\bar{T}$ and $\bar{P}$, respectively. Also, β is the thermal expansion coefficient. Air was assumed as a Newtonian fluid with $\nu = 15.68\times10^{-6}$ m²/s and $\beta = 0.0033$ 1/K. At each time interval, the time step was checked out due to maintaining the Courant number ($Co = u\Delta t/\Delta x$) below 1. Constant values of temperature (T_0) and velocity (U_0) were imposed on the inlet boundary conditions. For all walls of jet and cavity, no-slip conditions and wall functions were applied. The jet walls temperature was considered to be equal to T_0. Three values of 0, 100, and 300 were considered for the temperature difference between cavity's walls and inlet flow ($\Delta T = T_c - T_0$). Therefore, T_c accepts values 300, 400, and 600 K. The outflow condition was considered at outlet boundaries for all variables except static pressure, which was set zero.

2. 3. Mesh Study of the Computational Domain
Structured and non-uniform grids were generated with a refinement around walls and near jet's exit to capture high gradients in the flow field. Several grids (20350, 23400, 26650, 30100, and 33000) were tested to ensure the grid independence of results and finally, a grid with 26650 cells was chosen as a sufficient grid resolution demonstrated in Figure 2.

2. 4. Validation of the Numerical Method   In order to validate the present numerical method, the experimental data of Mataoui et al. [9] and numerical results of Iachachene et al. [12] were used. Mataoui et al. [9] carried out an experiment on a self-excited jet discharged into a cavity at Reynolds numbers of 1300, 2600, and 4000 under isothermal conditions ($\Delta T = 0$). Measurements equipment and materials are represented in Table 2. They measured the frequency of jet oscillations. In the present work, the point with coordinates (25, 10cm) were utilized to calculate the oscillation frequency. The comparison between the

TABLE 1. Summary of simulation conditions

L (cm)	50
W (cm)	20
e (cm)	1
l (cm)	20
T_0 (K)	300
$\Delta T = T_c - T_0$	0, 100, 300
$Re_0 = U_0 e/\nu$	1000, 3000
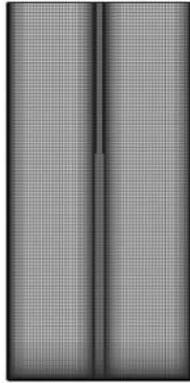
Figure 2. The grid arrangement of computational domain

current simulation and experimental results [9] is shown in Table 3. A good agreement between the present results and experimental data reported by Mataoui et al. [9] can be observed in Table 3. For the second validation step, a non-isothermal case with $\Delta T = 60$ K was investigated. The non-dimensional velocity components, temperature, and pressure for the specified points with coordinates of (x/e, y/e) ((16, 4), (16, 8), (16, 16) and (8, 4) cm, respectively) were extracted from the current numerical simulation and compared with the study by Iachachene et al. [12] in Figure 3. In this study , a jet with $Re_0 = 8500$ and a temperature of $T_0=300$K was discharged into a rectangular cavity with a constant temperature of $T_c=360$ K. These comparisons confirmed that the current numerical method is feasible and valid.

TABLE 2. Measurements equipment and materials [9]

Target	Equipment	Discription
air supply	Wind tunnel	-
Velocity measurement	Hot wire anemometry	5 μm diameter platinum-plated tungsten wire
Flow visualisation	White smoke generator	composed of droplets of vegetable oil mixed in carbon dioxide
	Camera	Shooting rate of two pictures per second

TABLE 3. The computed oscillation frequency of the present study and experiment done by Mataoui et al. [9]

	Re	4000	2600	1300
***f* (Hz)**	Present study	0.63	0.39	0.19
	Mataoui et al. [9]	0.62	0.40	0.20
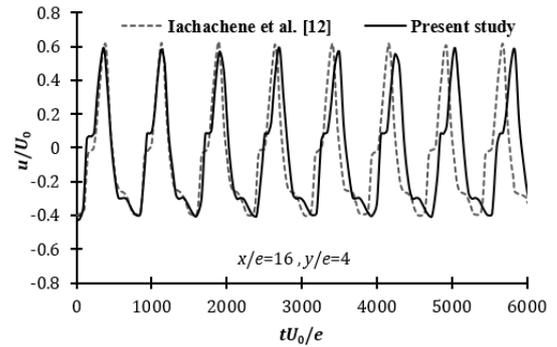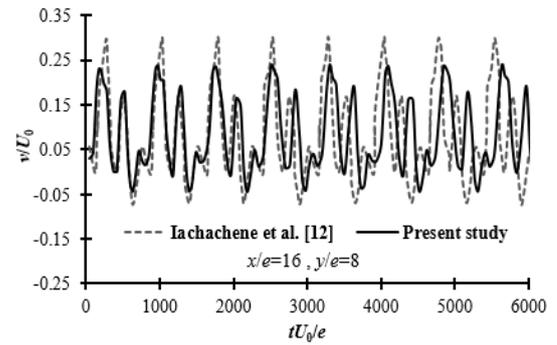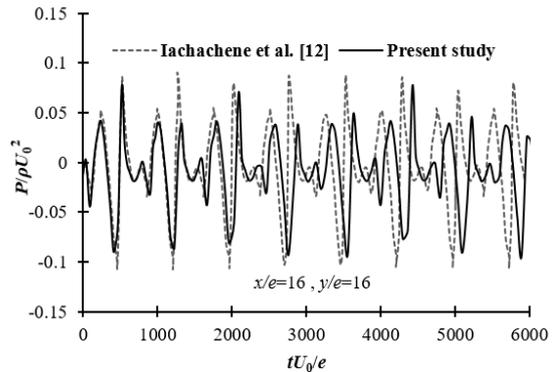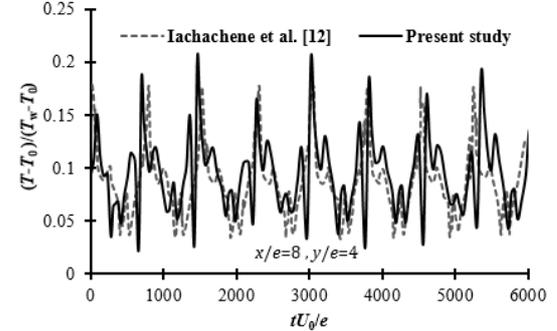
Figure 3. Comparison of dimensionless time evolution of (a) and (b) mean velocity components, (c) temperature and (d) pressure at $Re_0 = 8500$ and $\Delta T=60$ K between the present study and results reported by Iachachene et al. [12]
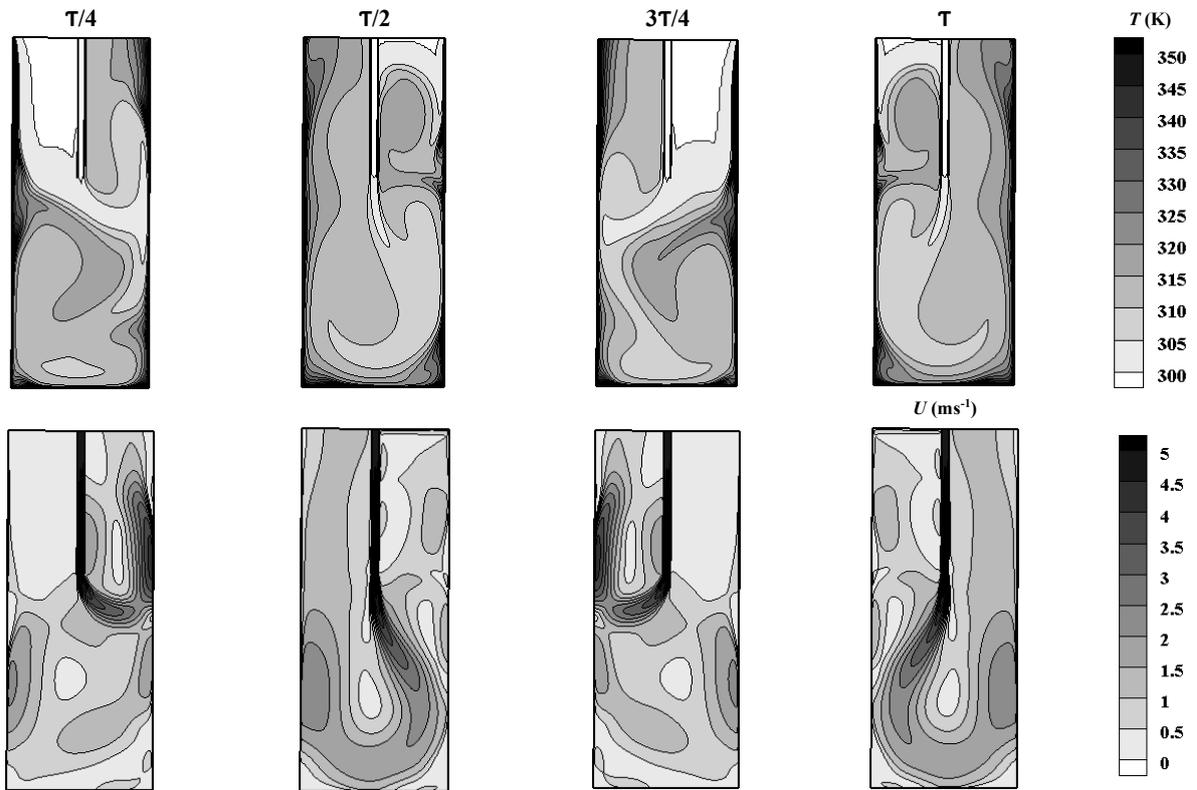
Figure 4. Temperature and velocity magnitude contours within one period of time (T=1.61 s) for *Re*=3000 and Δ*T*=100 K
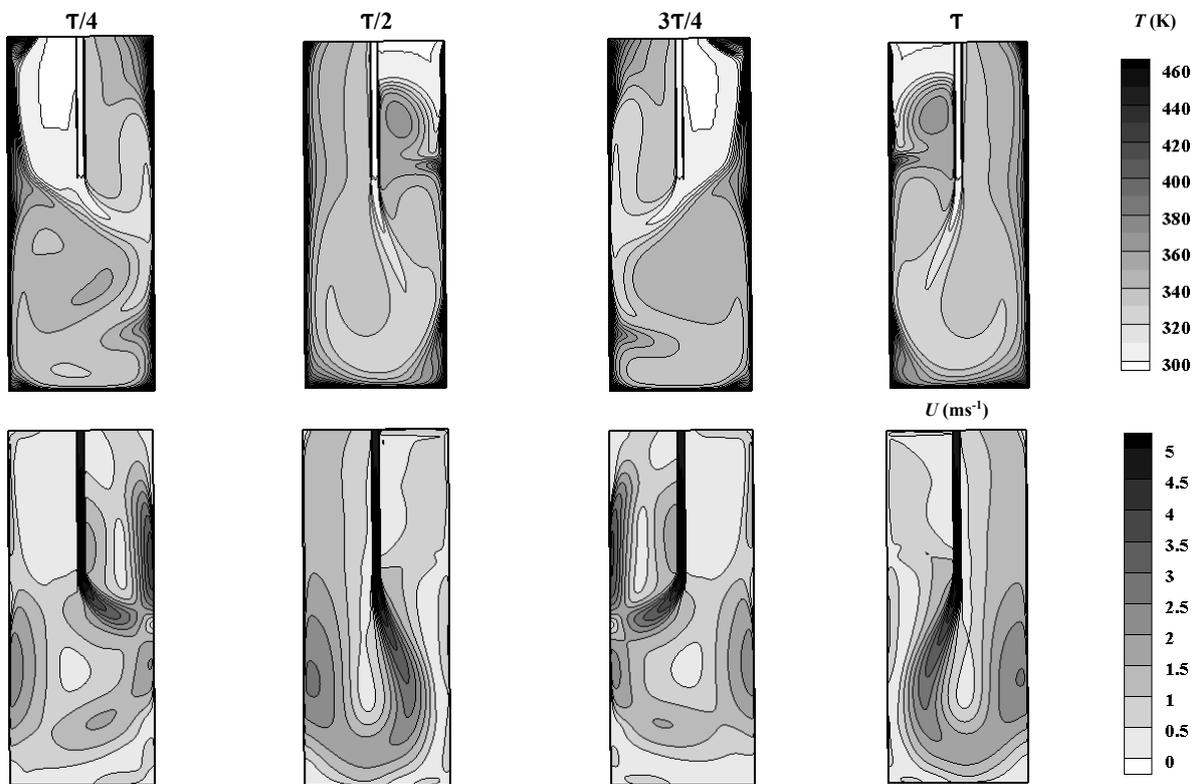
Figure 5. Temperature and velocity magnitude contours within one period of time (T=1.54 s) for *Re*=3000 and Δ*T*=300 K

3. RESULTS AND DISCUSSIONS

The self-excited jets produce an oscillatory flow that its oscillation frequency depends on the inlet velocity, geometric parameters, and thermal conditions [6, 17]. Several studies have been done on the influence of geometric parameters. In this study, the effect of inlet Reynolds number and cavity's wall temperature were studied on flow and thermal fields and oscillation characteristics of the self-excited jet. For this purpose, six cases were simulated, as depicted in Table 1.

Figures 4 and 5 show contours of temperature and velocity magnitude at four stages during one period of time for Re=3000 and temperature differences of 100 and 300, respectively. It should be noted that **τ** denotes oscillation period and each contour was provided after every quarter of the period. These figures illustrate the jet's flapping motions that oscillate right and left sides periodically. A comparison of Figures 4 and 5 reveals that increasing temperature differences from 100 to 300 K can almost increase the velocity magnitude in the cavity. In the vertically downward cavity, when the cold jet is discharged into the hot cavity, the momentum force and buoyancy force act in the same direction toward the bottom of the cavity. So, for Re=3000, increasing the temperature difference can raise velocity magnitude to some extent. This result is evidenced in Figure 6.

Figure 6 allows us to describe the time evolution of velocity magnitude at a specific point near the bottom wall of the cavity with coordinates (25, 10 cm) for all studied cases. As shown in Figure 6 (b), the temperature differences between the cavity's walls and inlet flow at Re=3000 can change the maximum velocity magnitude between 6 and 15% relative to the isothermal conditions. On average, for Re=1000, the temperature differences also increase the velocity magnitude. Interestingly, for Re=1000, the oscillation amplitude decreases with increasing the temperature difference until at ΔT=300 K, the jet stops flapping.

Figure 7 represents the temperature distribution over time for the specific point coordinates (25 10 cm) at each

(b) Re=3000
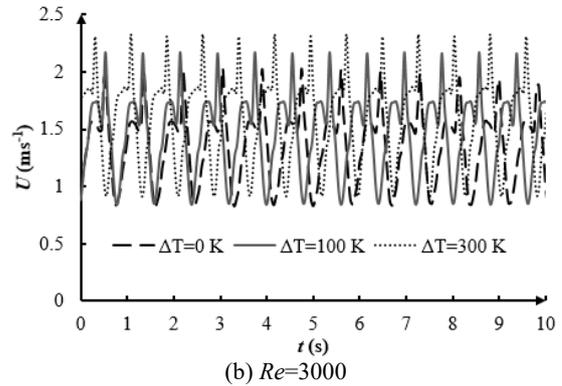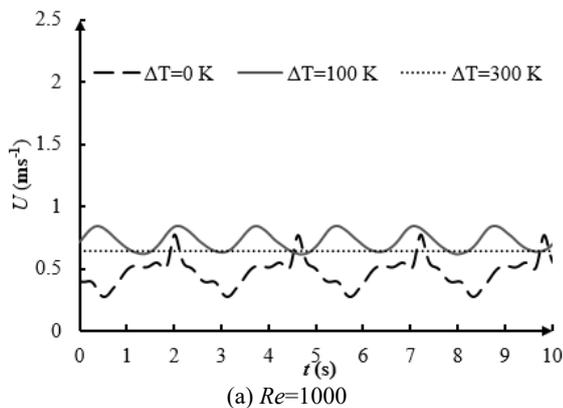
Figure 6. Time signal of the velocity magnitude in three temperature differences for Re: (a) 1000 and (b) 3000 at the location of x=25 and y=10 cm

(a) ΔT=100 K

(b) ΔT=300 K
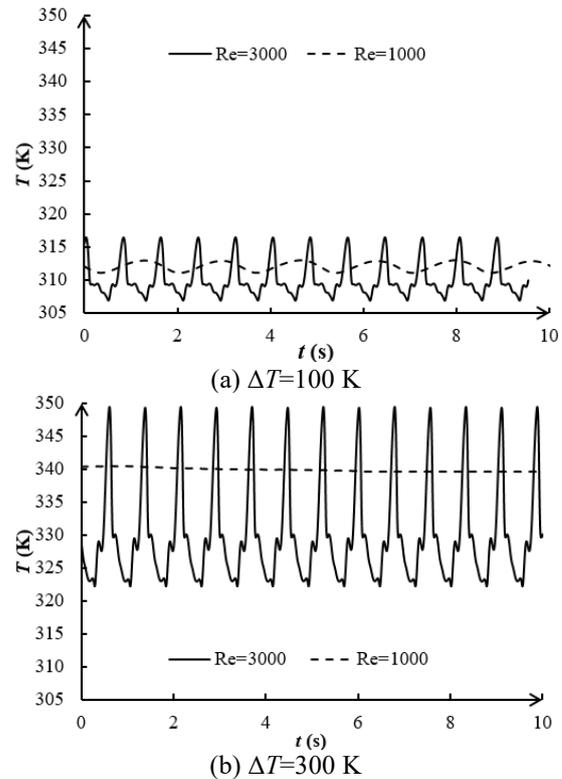
Figure 7. Time signal of the temperature in two Reynolds numbers for ΔT: (a) 100 K and (b) 300 K at the location of x=25 and y=10 cm

temperature difference. In ΔT=300 K, the amplitude of temperature oscillations for Re=3000 is enlarged nine times compared to Re=1000.

To investigate the oscillation frequency of self-excited jets, fast Fourier transform (FFT) was used. In this method, data of the specific point with coordinates (25, 10 cm) in the computational domain was extracted and applied as the input of FFT code, so the outputs are

(a) Re=1000

the frequencies. The maximum value of Fourier modes accurately determines the fundamental frequency [12]. As a sample, the output of FFT method is shown in Figure 8. The oscillation frequencies are extracted by the FFT method for all cases and reported in Table 4.

It can be deduced from Table 4 that for Re=3000, temperature differences can intensify the frequency by up to 10% in comparison with the isothermal self-excited jet. It is interesting to note that for Re=3000 the oscillation frequency slightly changes despite the temperature differences. This phenomenon is almost certainly due to the interaction between momentum and buoyancy forces. This interaction can be assessed by calculation of Archimedes number (Ar).

Ar is defined by the buoyancy to momentum ratio as $Ar = g\beta W \Delta T / U_0^2$ [20]. The results obtained from Ar calculations are presented in Table 4. At Re=3000, values of Ar are below 0.1 for both temperature differences of 100 and 300 K. It means that the role of buoyancy force, against momentum force is negligible in the flow field. Therefore, at Re=3000, changing cavity's thermal boundary conditions has little effect on the oscillation characteristics, i.e., the frequency and amplitude of oscillations.

As Table 4 shows, there is a significant difference in the frequency values between ΔT=100 K and isothermal conditions at Re=1000. As observed in Figures 6 and 7, in conditions of Re=1000 and ΔT=300 K, the flow has no oscillation motion. Indeed, for Re=1000 that has a weaker momentum force than Re=3000, values of Ar are larger than 0.1. Hence, buoyancy as well as temperature

difference, can play a key role in the behavior of self-excited jet. That's why changing ΔT from 0 to 100 can raise the oscillation frequency about 58%. But more increasing of ΔT to 300 K enlarges Archimedes number more than 0.7 and non-oscillatory flow was observed.

From a physical point of view, it can be said that the heated cavity's walls can strengthen the buoyancy mechanism and the tendency of the air inside the cavity to escape through the upper outlets increases. As a result, the pressure decreases locally due to the relative increase in air velocity adjacent to the lateral walls of the cavity. This can amplify the Coanda effect [6, 9] (oscillating behavior due to the drop in periodic pressures in the side walls) and increase the jet oscillation frequency. As can be seen in Table 4, at Re =3000, the frequency of jet oscillations increases as the cavity heats up. The same behavior is observed to some extent at Re =1000. Thus, at Re =1000, by providing the temperature difference of 100 K between the cavity walls and the jet, the frequency of jet oscillations increases from 0.19 (in the isothermal state) to 0.3. However, by raising the temperature difference to 300 K, an increase in the trend of frequency does not continue and the jet becomes non-oscillating. As can be seen in Table 4, as the temperature difference increases to 300 K, the Archimedes number (Ar) increases to about 0.78, which means that the ratio of buoyancy force versus momentum is significant. In such a situation, the opposition of these two mechanisms can cause instability in the oscillating jet behavior and makes it non-oscillating, or sometimes cause irregular random oscillations with limited amplitude, which are usually classified in the non-oscillating category [18].

In the case of Reynolds number 3000, because Ar is very small (much less than 0.1), an increase in the temperature difference between the jet and the wall, even up to 300 K, can not cause the buoyancy and momentum mechanisms to interfere and thus change the jet oscillation regime. The earlier work [18] showed that where Ar is less than 0.1, the effects of the cavity's thermal boundary conditions on the oscillating jet's behavior are not significant. However, in cases where Ar exceeds 0.1, the buoyancy effects due to the temperature difference influence the characteristics of oscillating flow.

Figure 8. Typical Fourier modes time signal of the mean velocity for Re = 3000 and ΔT=100 K

TABLE 4. Oscillation frequency of the studied cases

Re		1000			3000	
ΔT (K)	0	100	300	0	100	300
f (Hz)	0.19	0.30	Non-oscillatory flow	0.59	0.62	0.65
Ar	-	0.26	0.78	-	0.03	0.09

4. CONCLUSIONS

Numerical simulations were employed to investigate the effects of inlet flow rate in various temperature differences on the behavior of self-excited oscillating jet. In the recent years, studying the self-excited jet under non-isothermal conditions has received much attention due to its wide range of industrial applications. In the previous works, the effects of various Reynolds numbers and temperature differences on the oscillatory flow were

not investigated. For this purpose, a plane jet with a fixed temperature of 300 K and Reynolds numbers (Re=1000 and 3000) discharging vertically downward into a rectangular cavity was considered. In the studied problems, the cavity's walls experienced various temperatures to create temperature differences of 0, 100, and 300 K relative to inletflow. The key conclusions are as follows:

- With capturing the time variation of velocity magnitude in the specific point located at the computational domain, it was determined that at Re=3000, the temperature differences between cavity's walls and inlet jet could affect maximum velocity magnitude between 6 and 15% relative to the isothermal conditions.

- Also, time variation of the temperature at ΔT=300 K for the specific point showed that the amplitude of temperature oscillations for Re=3000 is enlarged by about nine times compared to Re=1000.

- It is deduced from the results that in Re=3000, the temperature differences can increase oscillation frequency up to 10% compared to isothermal conditions. This value equals to 58% at Re=1000.

- The jet at Re=1000 and ΔT=300 K acts as a non-oscillatory jet due to the interaction between momentum and buoyancy forces.

- For Archimedes number (Ar) below 0.1, the frequency and amplitude of oscillations are slightly dependent on the temperature differences.

- For Re=1000 and ΔT=300 K, the flow stopped oscillating. In this case, Archimedes number was enlarged more than 0.7, which is indicative of momentum weakness in driving the oscillating flow.

- Further experimental studies are require for prefect understand and more accurately identify complex phenomena that occur in the range of relatively low Reynolds numbers and high-temperature differences that the opposition of the buoyancy and momentum mechanisms may lead to instability of the oscillating jet.

5. REFERENCES

1. J. Vejrazka, J. Tihon, P. Mart, and V. Sobolík, "Effect of an external excitation on the flow structure in a circular impinging jet", *Physics of Fluids*, Vol. 17, No. 10, (2005), 1-14. DOI:10.1063/1.2084207

2. A. Husain and M. Ariz, "Thermal Performance of Jet Impingement with Spent Flow Management", *International Journal of Engineering, Transactions A: Basics*, Vol. 30, No. 10, (2017), 1599-1608. DOI: 10.5829/ije.2017.30.10a.22

3. X. Wen, J. Liu, Z. Li, D. Peng, W. Zhou, and K. Chun, "Jet impingement using an adjustable spreading-angle sweeping jet", *Aerospace Science and Technology*, Vol. 105, (2020), 105956. DOI: 10.1016/j.ast.2020.105956

4. [4]   M. Jahanmiri, "Static pressure distribution in an excited jet: some observations", *International Journal of Engineering*, Vol. 13, No. 3, (2000), 81-86.

5. H. M. Maghrabie, "Heat transfer intensification of jet impingement using exciting jets - A comprehensive review", *Renewable and Sustainable Energy Reviews*, Vol. 139, (2021), 110684. DOI: 10.1016/j.rser.2020.110684

6. A. Mataoui and R. Schiestel, "Unsteady phenomena of an oscillating turbulent jet flow inside a cavity : effect of aspect ratio", *Journal of Fluids and Structures*, Vol. 25, (2009), 60-79. DOI: 10.1016/j.jfluidstructs.2008.03.01

7. T. Shakouchi, Y. Yoshikazu, and T. Ito, "A study on oscillatory jet in a cavity : lst report, mechanism of oscillation", *Bulletin of JSME*, Vol. 25, No. 7, (1982), 767-769. DOI: 10.1299/jsme1958.25.1258

8. D. Carnero, C. Treviño, and L. Martínez-Suástegui, "Three-dimensional deflecting oscillation of turbulent planar opposed jets confined in an open cavity under crossflow", *Physics of Fluids*, Vol. 32, (2020), 105101. DOI: 10.1063/5.0021501

9. A. Mataoui, R. Schiestel, and A. Salem, "Flow regimes of interaction of a turbulent plane jet into a rectangular cavity: experimental approach and numerical modelling", *Flow, Turbulence and Combustion*, Vol. 67, (2001), 267-304. DOI: 10.1023/A:1015255211723

10. D. M. Denisikhina, I. . A. Bassina, D. A. Nikulin, and M. K. Strelets, "Numerical simulation of self-excited oscillation of a turbulent jet flowing into a rectangular cavity," *High Temperature*, Vol. 43, No. 4,(2005), 568-579. DOI: 10.1007/s10740-005-0098-0

11. B. W. Righolt, S. Kenjereš, R. Kalter, M. J. Tummers, and C. R. Kleijn, "Dynamics of an oscillating turbulent jet in a confined cavity", *Physics of Fluids*, Vol. 62, (2015), 395-406. DOI: 10.1063/1.4930926

12. F. Iachachene, A. Mataoui, and Y. Halouane, "Numerical investigations on heat transfer of self-sustained oscillation of a turbulent jet flow inside a cavity", *Journal of Heat Transfer*, Vol. 137, (2015), 1-10.

13. M. Mosavati, R. M. Barron, and R. Balachandar, "Characteristics of self-oscillating jets in a confined cavity", *Physics of Fluids*, Vol. 32, No. 11,(2020), 115103. DOI: 10.1063/5.0023833

14. N. Hnaien, S. Marzouk Khairallah, H. Ben Aissia, and J. Jay, "Numerical study of interaction of two plane parallel jets," *International Journal of Engineering, Transactions A: Basics*, Vol. 29, No. 10, (2016), 1421-1430. DOI: 10.5829/ije.2022.35.03c.06

15. K. Bouaraour and N. Hebbir, "Numerical study of twin jets interactions using Realizable model", *International Journal of Engineering, Transactions C: Aspects*, Vol. 35, No. 3, (2022), 544-551. DOI: 10.5829/ije.2022.35.03c.06

16. M. Aminzadeh, J. Khadem, S. A. Zolfaghari, and A. Omidvar, "Numerical comparative study between flow field characteristics of a double-inlet and single- inlet self-excited jet," in ISME 2020, (2020), 27-30.

17. M. Aminzadeh, J. Khadem, S. A. Zolfaghari, and A. Omidvar, "Numerical study of nozzle width effect on cooling performance of a turbulent impinging oscillating jet in a heated cavity", *International Communications in Heat and Mass Transfer*, Vol. 118, (2020), 104899. DOI: 10.1016/j.icheatmasstransfer.2020.104899

18. M. Aminzadeh, J. Khadem, S. Alireza, and A. Omidvar, "Computational study on self-oscillatory flow induced by vertical and horizontal jets in partially heated and cooled cavities," *International Communications in Heat and Mass Transfer*, Vol. 129, (2021), 105680. DOI: 10.1016/j.icheatmasstransfer.2021.105680

19. M. Aminzadeh, J. Khadem, A. Zolfaghari, and A. Omidvar,

"Influence of a non-isothermal conditions on oscillation characteristics of self-excited jet in a rectangular cavity," in 18th Fluid Dynamics Conference, (2019).

20. H. Yamasawa, T. Kobayashi, T. Yamanaka, N. Choi, and M. Matsuzaki, "Experimental investigation of difference in indoor environment using impinging jet ventilation and displacement ventilation systems", *International Journal of Ventilation*, (2020), 1-18. DOI: 10.1080/14733315.2020.1864572

Persian Abstract

چکیده

جت نوسانی خود-تحریک می‌تواند با تخلیه یک جت صفحه‌ای در یک حفره مستطیلی به دلیل اثرات فشار و بدون نیاز به کمک خارجی به طور طبیعی ایجاد شود. در سال‌های اخیر، جت خود-نوسانی غیر هم‌دما به دلیل کاربردهای صنعتی گسترده‌ای که دارد، مورد توجه محققین قرار گرفته است. بر این اساس، مطالعه حاضر به منظور مقایسه رفتار نوسانی جت خود-تحریک عمودی پایین‌زن با عدد رینولدز (Re) ۱۰۰۰ و ۳۰۰۰ تحت شرایط اختلاف دماهای مختلف بین جریان ورودی و دیواره‌های حفره (۰، ۱۰۰ و ۳۰۰) انجام شده است. محاسبات عددی با استفاده از معادلات گذرای ناویر-استوکس میانگین‌گیری شده به روش رینولدز (URANS) و معادله انرژی برای یک جریان تراکم‌ناپذیر به دست آمده است. شبیه‌سازی عددی توسط ابزار حجم محدود اپن‌فوم اجرا شده است. نتایج نشان داد که در حالات مورد بررسی، بسته به مقدار اختلاف دما، جریان های نوسانی و غیر نوسانی مشاهده می‌شود. همچنین در ۳۰۰۰=Re، اختلاف دما می‌تواند فرکانس نوسان را تا ۱۰ درصد نسبت به شرایط هم‌دما تغییر دهد. این مقدار در ۱۰۰۰=Re به ۵۸٪ می‌رسد. نتایج نشان داد در حالتی که عدد ارشمیدس کمتر از ۰.۱ است، تأثیر اختلاف دمای جت و دیواره حفره بر رفتار نوسانی ناچیز می‌باشد.

International Journal of Engineering

J o u r n a l   H o m e p a g e :   w w w . i j e . i r

Wheel Load Torque Emulation for Electric Propulsion Structure using Dual Induction Motors

S. Yahia Cherif[a], D. Benoudjit*[a,b], M. S. Nait-Said[a], N. Nait-Said[a]

[a] LSP-IE'2000 Laboratory, Electrical Engineering department, University of Batna 2, 05000, Batna, Algeria
[b] Health and Safety Institute, University of Batna 2, 53 route de Constantine, 05078, Batna, Algeria

ABSTRACT

Electric vehicle is an adaptation of conventional vehicle, with an integration of electrical motors. It seems to be one of the most promising technologies that can lead to significant improvements in vehicle performance and polluting emissions. However, for any vehicle in urban traffic requires regime changes, frequent acceleration, deceleration, and stopping phases, which lead to serious breakdowns. During the above phases, electric motors are continuously being exposed to thermal and mechanical effects.This paper highlights the possibility of representing the wheel load torque emulation of an electric propulsion structure using dual induction motors vector-controlled. The emulation of load torque acting on one of both electric motors placed at the rear wheels of electric vehicle (EV) structure is accomplished by a DC-generator coupled with an induction motor during vehicle drive cycle operation andunpredictable load profiles. Simulation results confirm widely the feasibility and the effectiveness of the proposed emulator scheme of induction motor-based vector-control in the electric vehicle application.

doi: 10.5829/ije.2022.35.06C.12

NOMENCLATURE

R_a, L_a	Armature resistance, armature inductance	ϕ_{rd}, ϕ_{rq}	Quadrate , direct rotor flux components
U_a, i_a	Armature voltage, armature current	L_r, T_r	Rotor induction, rotor time constant
K_ϕ	Constant based on flux and machine construction	ω_s, M	Synchronous angular speed, mutual inductance
i_{sd}, i_{sd}	Direct, quadrate stator current compnents	Ω	Speed of motor
Ω_o, Ω_{diff}	EV speed, speed-difference	$\Omega_{Left}, \Omega_{Right}$	Speeds of left motor 1, right motor 2
e_a	Generated voltage	R_s, L_s	Stator resistance and winding inductance
J_{IM}, J_{DCG}	IM inertia, DC-generator inertia	v_{sd}, v_{sq}	Stator voltage
f_{IM}, f_{DCG}	IM friction, DC-generator friction	σ	The redefined leakage inductance
T_L, T_e	Load torque, electromagnetic torque	$J_{tot}, *$	Total inertia, input command variable
e_d, e_q	Nonlinear coupling terms	θ_s	The rotor flux position angle
p	Number of pole pairs	f_{tot}	Total viscous friction of the coupled system

1. INTRODUCTION

Environment protection and energy conservation have urged the development of electric vehicle (EV). It seems to be one of the most promising technologies for the next century and will probably be one of the most interesting solutions to the rational and effective use of energy reducing environmental damage caused by conventional vehicles [1, 2].

Electric vehicles present a lot of similarities with conventional vehicles which are already optimized for minimum energy consumption in rolling. EV is an adaptation of conventional vehicle; with an integration of electrical motors.

Different research works of EV configurations and drive association possibilities can be found in literature, e.g., one to four electrical motors, direct current or alternative current motors, with or without a clutch and a

Corresponding Author Institutional Email:
d.benoudjitf@univ-batna2.dz (D. Benoudjit)

gearbox, etc. [3, 4]. Electric propulsion control system or power train is the main part of an EV. It consists of three main blocs: electric motors, power electronic converters and command or controller. The controller bloc is an essential part of an EV. Therefore, electric propulsion system cannot be designed without this bloc. In fact, it's undoubtedly essential to control or to get optimal operations during the different propulsion phases: starting, acceleration, deceleration, cruising and stopping phases. During the above operations, electric motors are continuously being exposed to load disturbances, road gradient, surface roughness and various traffic conditions effects. The occurred effects might influence electric motor control and from which the control of the vehicle might be lost. Therefore, in order to maintain desired performances even in the presence of any external disturbances, particularly, motor mechanical load changes. Motor control system with high robustness is an important challenge in research due to its different applications. Therefore, motor mechanical loads identification and analysis under parametric variations of the load are often problematic. Thus, several research studies in the literature have focused on EV emulation system, proposing different approaches [5-23]. In fact, motor mechanical load emulation allows to analyze a motor performance under real operation condition.

However, in most cases studied, the main elements for motor load emulation are an electric dynamometer and its control system. On this topic, main used strategies directly related to the control system include field-oriented control (F.O.C.), direct torque control (D.T.C.) and position control [6-11]. Other research works has been proposed in literature [12-21] using different test benches platforms with different emulation approaches.

The interest of the emulator is to be able to introduce different loads and disturbances which can be applied to the vehicle wheel and which in fact are reported on any profile. This explains why these applications are generated via a torque controller by a DC-generator. Therefore, the load emulation must follow any regime regarding load variation according to a desired load profile. In this context, after this brief outline (research background) of the most important studies related to the emulation system; this paper highlights the possibility of representing the wheel load torque emulation of an electric propulsion structure purposed for an EV using dual-induction motors vector-controlled, which separately drive the rear wheels of the vehicle. The aim of this paper is to check the wheel load torque emulator based propulsion structure performance in the face of the unpredictable load profiles acting on one of both electric motors encountered during vehicle drive cycle operation with specific maneuvers.

For this purpose, a control scheme was developed for a DC-generator coupled with an induction motor and takes into account the effect of rotational inertia. The

simulation results showed a good performance of the control system and also validated the feasibility of the proposed emulator scheme for three scenarios, of unpredictable load profiles as shown further from three loads profiles in section 4.

The paper is organized as follows. Section 2 presents the field-oriented control (FOC) of induction motor. In section 3, we will first present the proposed electric propulsion structure using dual induction motors, then the emulator block diagram. Simulation results are presented in section 4. Conclusion is done in section 5.

2. FIELD-ORIENTEDCONTROL

The complex mathematical model and non-linear characteristic make the control of an induction motor difficult and call for the use of a high performance control algorithms such as vector control, commonly called Field-Oriented Control (F.O.C.). This is a strategy that provides a decoupled control similar to a DC motor, between flux and torque of an induction motor [24-26]. With decoupling between magnetizing flux and torque, the torque producing component of the stator flux can be controlled independently.

Based on the orientation rotor flux process described by the imposed zero constraint of quadrate rotor flux component, such as [24, 25]:

$$\phi_{rq} = 0 \ \text{ and } \ \phi_{rd} = \phi_r \tag{1}$$

where ϕ_{rq}, ϕ_{rd} : quadrate, direct rotor flux components.

When the rotor flux orientation assumption is verified, the basic field-oriented control expressions of an induction motor (IM) are simplified as:
The stator voltage equations are given by [24, 25]:

$$v_{sd} = (R_s i_{sd} + \sigma L_s \frac{d i_{sd}}{dt}) + e_q \tag{2}$$

$$v_{sq} = (R_s i_{sq} + \sigma L_s \frac{d i_{sq}}{dt}) + e_d \tag{3}$$

The nonlinear coupling terms are [24]:

$$e_d = \omega_s (\sigma L_s i_{sd} + \frac{M}{L_r} \phi_r) \tag{4}$$

$$e_q = \frac{M}{L_r} \frac{d\phi_r}{dt} - \sigma L_s \omega_s \tag{5}$$

where R_s, L_s denote stator resistance, stator winding inductance. σ is the redefined leakage inductance. i_{sd}, i_{sq}, denote direct, quadrate stator current components. ω_s, M, L_r, ϕ_r are: synchronous angular speed, mutual inductance, rotor inductance and rotor flux, respectively.
The rotor flux formulation is [24]:

$$\phi_r = \frac{M}{1 + T_r S} i_{sd} \qquad (6)$$

T_r, S: rotor time constant, differential or laplaceoperator, respectively.

The rotor flux position angle can be derived by [24]:

$$\theta_S = \int (\omega_s + p\Omega) dt \qquad (7)$$

The electromagnetic torque is [24]:

$$T_e = p \frac{M}{L_r} \phi_{rd} i_{sq} \qquad (8)$$

p denotes the number of pole pairs. From Equation (8) it's very clear, that the electromagnetic torque can be controlled only from quadrate stator current component i_{sq} when the rotor flux is maintained constant. This is appropriate for EV applications, for which the loads can be largely varied. From this point of view, the induction motor does not operate normally in filed weakening region; thus, the flux must be maintained constant to its rated value.

3. ELECTRIC PROPULSION STRUCTURE

For conventional vehicle, when a turn is reached, the speed difference of the rear wheels is regulated via a mechanical differential in order to avoid vehicle slipping. This mechanical device is an arrangement of gears connecting two shafts on the same line and enabling one shaft to revolve faster than the other when required. So when the inner wheel speed is reduced, the outer one is increased. Besides the mechanical means, the differential action of an EV when cornering can be electrically provided by two electric motors operating at different speeds [3].

As can be seen from Figure 1, for the proposed electric structure, this difference is regulated by an electric differential based on two induction motors operating at difference speeds drives separately the rear wheels of the vehicle via fixed gearing [27].

The differential function has to verify the following expressions [28]:

$$\begin{cases} \Omega_{Left} = \Omega_o + \Omega_{diff} \\ \Omega_{Right} = \Omega_o - \Omega_{diff} \end{cases} \qquad (9)$$

where Ω_{Left}, Ω_{Right}: speeds of left motor 1, right motor 2.

Therefore, from the above system of equations (9), the vehicle speed Ω_o and the difference speed Ω_{diff} may be done simply by [28]:

$$\begin{cases} \Omega_o = \frac{1}{2}(\Omega_{Left} + \Omega_{Right}) \\ \Omega_{diff} = \frac{1}{2}(\Omega_{Left} - \Omega_{Right}) \end{cases} \qquad (10)$$
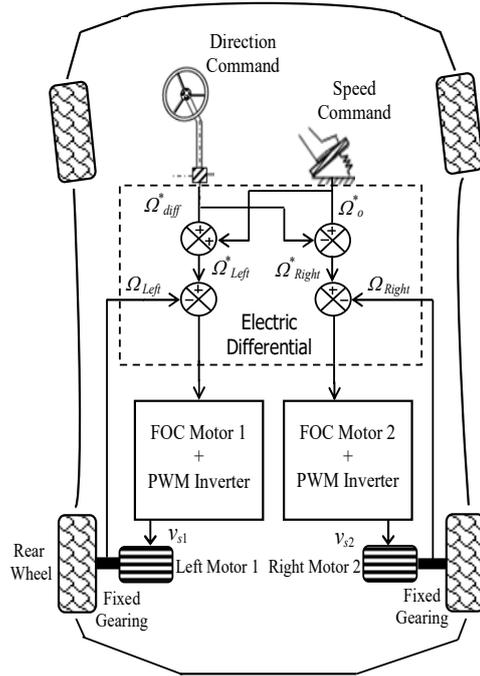
Figure 1. Electric propulsion structure

As mentioned before, for the purpose of emulating a wheel load torque acting on one of both electric motors for an EV structure, a control scheme consisting of an induction motor vector controlled connected to a DC-generator has been presented.

Let us first present the mathematical model of a DC-generator given by the following equations.

The armature voltage can be written as [21]:

$$U_a = -(R_a i_a + L_a \frac{di_a}{dt}) + e_a \qquad (11)$$

where R_a, L_a, i_a, denote armature resistance, armature inductance and armature current, respectively.

The generated voltage e_a is relative to rotational speed by [21]:

$$e_a = K_\phi \Omega \qquad (12)$$

where K_ϕ, Ω, denote a constant based on flux and machine construction, rotational speed.

The load torque is related to armature current bytorque constant [21].

$$T_L = -K_\phi i_a \qquad (13)$$

Knowing that the induction motor is coupled with a DC generator, the mechanical equation can be written as [21]:

$$T_e = J_{tot} \frac{d\Omega}{dt} + f_{tot} \Omega + T_L \qquad (14)$$

where T_e is the electromagnetic torque, Ω is the rotating speed, T_L is the load torque and J_{tot}, f_{tot} are total inertia, total viscous friction of the coupled system (Induction motor and DC-Generator) respectively, expressed by

$$J_{tot} = J_{IM} + J_{DCG} \tag{15}$$

$$f_{tot} = f_{IM} + f_{DCG} \tag{16}$$

Based on the system's block diagram shown in Figure 2, emulating wheel load torque is realized with a DC-generator torque control using a PI controller.

4. SIMULATION RESULTS AND DISCUSSION

The aim of this section is to check the wheel load emulator-based EV performance in the face of the load disturbances encountered during specific maneuvers.

Simulation results are carried out under a desired torque load for three different profiles (scenarios) using MATLAB/Simulink software package where rated data are given next in Tables 1 and 2.

The main idea is to test both a control scheme for torque load emulation acting on one of both electric motors encountered during vehicle drive cycle operation, taking into account the effect of rotational inertia, as well as to verify the validity of the electric differential principle resulting from the pruposed propulsion struture may be used in EV substituting the conventional mechanical differential system.

In order to verify the control scheme performances, particularly when the vehicle accomplishes the turning maneuvers, let us take a given speed profile for the EV defined as illustrated in Figures 3, 5, 7and the evolution of line stator current under the load perturbations based on three references profiles (references 1, 2 and 3) presented in Figures 4, 6 and 8, respectively.

From a starting point, the vehicle starts with a constant acceleration until attains the speed of 118 rad/s, then it will be maintained constant. After, the vehicle will turn left, the electric differentialaction allows the outer (right) wheel to rotate faster than the inner (left) wheel: $\Omega_{Right,} > \Omega_{Left}$. Then the vehicle should continue directly its trajectory by a constant cruising speed, it results inequality of the two motors speed: $\Omega_{Right} = \Omega_{Left}$.

As may be seen in Figures 3-8, for all scenarios the simulation results show that the load emulation method is effective, and has good adaptability to unpredictable load profiles associated with specifics vehicle maneuvers.

Figures 3, 5 and 7 show that the speed response follows its refernce precisely. The same figures also illustrate the time evolution of the first phase stator current. The current behave according to the dynamic behaviour of the motors,where its magnitude changes following the developed load torque.

Figures 4, 6 depict the load torque responses according to the load references 1 and 2, respectively. Desipate the load variation, the responses that were obtained arevery close for the desired and the emulated torque load with relatively very small emulation error.
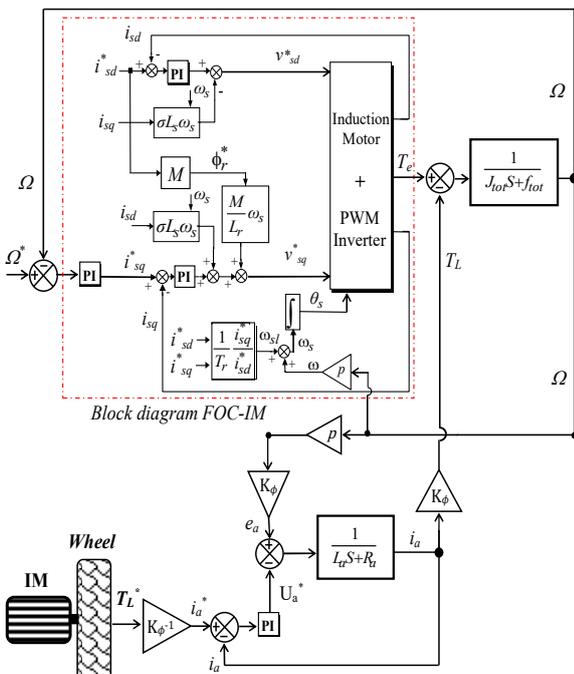

Figure 2. Emulator block diagram
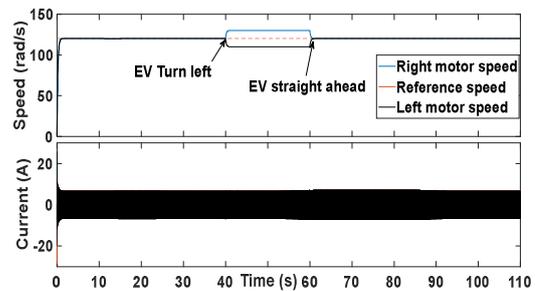
**Figure 3.** Speed and current evolution versus times
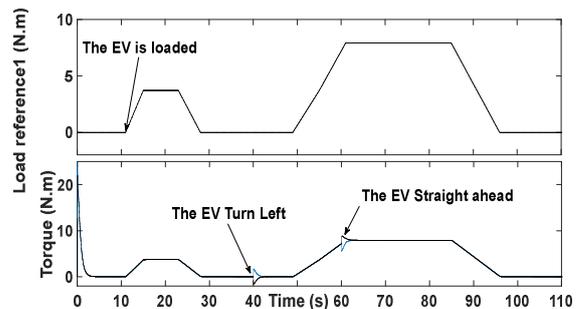
Figure 4. Torque response versus times for load reference 1

Further, to test severely the control scheme performances, another test is carried out, in Figures 7, 8 and its zoom in Figure 9 for the load perturbation profile (reference 3), taking into account the measurement noise effect.

In this case, reference load and the emulated load response show close correspondance, but associated with torque oscillations.


Figure 9. Zoom of torque response for load reference 3
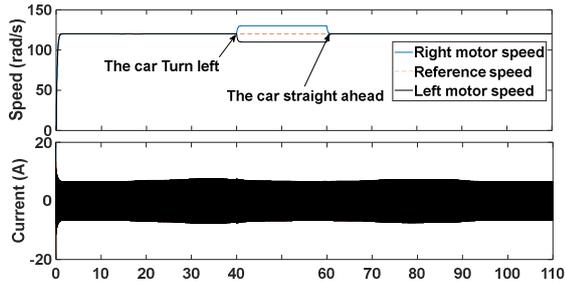
Figure 5. Speed and current evolution versus times
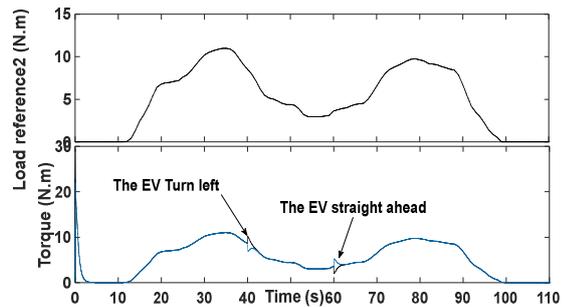
Figure 6. Torque response versus times for load reference 2

TABLE 1. Induction motor paprametrs

Parameters	Values	Unity
Power	1.1	kW
Speed	1400	rev. min^{-1}
Stator phase resistance R_s	7.5	Ω
Rotor phase resistance R_r	3.8	Ω
Stator inductance L_s	0.3594	H
Rotor inductance L_r	0.3032	H
Mutual inductance M	0.303	H
Rotor inertia J_{IM}	0.0052	Kg.m^2
Friction coefficient f_{IM}	0.0005	Nm.s.rd^{-1}
Number of pole pairs p	2	

TABLE 2. DC-Generator paprametrs

Parameters	Values	Unity
Power	1.5	kW
Speed	1400	rev. min^{-1}
Armature resistance R_a	1	Ω
Armature inductance L_a	0.005	H
Constant $K_\emptyset$	1	V.s
Inertia J_{DCG}	0.0015	Kg.m^2
Friction coefficient f_{DCG}	0.0001	Nm.s.rd^{-1}

Figure 7. Speed and current evolution versus times

5. CONCLUSIONS

In this paper, we focused on emulating a wheel load torque of an electric propulsion structure using dual induction motors vector-controlled. For that purpose, a control scheme using a DC-generator coupled with an induction motor has been adopted to carry-out control tests during specifics vehicle maneuvers for different unpredictable torque load profiles (scenarios).

Simulation results confirm widely the feasibility and the effectiveness of the emulation scheme applied for electric vehicle. In fact, the speed responses have a good

Figure 8. Torque response versus times for load reference 3

dynamic reference speed tracking, while the emulated torque load closely matches of the desired load torque with relatively very small emulation error for different scenarios, but only torque oscillations for the load profile with measurement noise effect exist.

The investigation of the impact of the emulation of more complex load behaviors, the variation in rotational inertia and a hot values of phase resistances on the emulation performance, this last case might be occurred. For example, when one wheel vehicle is stopped by a strong obstacle while the induction motor is called to develop an important torque under zero speed, as well as the implementation and experimental validation of the emulation scheme applied for EV propulsion structure via a test bench, which constitute others interesting topics, will be the subject of future works.

6. REFERENCES

1. Shao, L., Karci, A.E.H., Tavernini, D., Sorniotti, A. and Cheng, M., "Design approaches and control strategies for energy-efficient electric machines for electric vehicles—a review", *IEEE Access*, Vol. 8, (2020), 116900-116913, doi: 10.1109/ACCESS.2020.2993235.

2. Anto, A. and Sreethumol, M., "Review of electric vehicles", in 2018 International Conference on Control, Power, Communication and Computing Technologies (ICCPCCT), IEEE. (2018), 392-398.

3. Ehsani, M., Singh, K.V., Bansal, H.O. and Mehrjardi, R.T., "State of the art and trends in electric and hybrid electric vehicles", *Proceedings of the IEEE*, (2021), doi: 10.1109/JPROC.2021.3072788.

4. Chan, C.C., Bouscayrol, A. and Chen, K., "Electric, hybrid, and fuel-cell vehicles: Architectures and modeling", *IEEE Transactions on Vehicular Technology*, Vol. 59, No. 2, (2009), 589-598, doi: 10.1109/TVT.2009.2033605.

5. Zhang, Z., Wang, L., Zhang, J. and Ma, R., "Study on requirements for load emulation of the vehicle with an electric braking system", *IEEE Transactions on Vehicular Technology*, Vol. 66, No. 11, (2017), 9638-9653, doi: 10.1109/TVT.2017.2739425.

6. Fajri, P., Prabhala, V.A.K. and Ferdowsi, M., "Emulating on-road operating conditions for electric-drive propulsion systems", *IEEE Transactions on Energy Conversion*, Vol. 31, No. 1, (2015), 1-11, doi: 10.1109/TEC.2015.2481180.

7. Chandrasekaran, V., Sykora, B., Mishra, S. and Mohan, N., "A novel model based development of a motor emulator for rapid testing of electric drives", in 2020 IEEE Energy Conversion Congress and Exposition (ECCE), IEEE. (2020), 2395-2402.

8. Lei, B., Xiong, N., Li, S. and Ren, K., "An emulation system of dynamic mechanical loads based on dtc induction 110kw motor", in 2013 International Conference on Electrical Machines and Systems (ICEMS), IEEE. (2013), 519-522.

9. Zha, H., Zong, Z., Jiang, N. and Liu, Z., "Implementation of space vector modulated direct torque controll for electric vehicle dynamic emulation", in 2010 International Conference on Computer, Mechatronics, Control and Electronic Engineering, IEEE. Vol. 4, (2010), 503-507.

10. de Oliveira, C.M., de Aguiar, M.L., Guazzelli, P.R., de Castro, A.G., dos Santos, S.T. and Monteiro, J.R., "Analysis of the dynamic emulation problem for validation of position control algorithms in machine drives", in 2018 13th IEEE International Conference on Industry Applications (INDUSCON), IEEE. (2018), 1266-1273.

11. Rodič, M., Jezernik, K. and Trlep, M., "Dynamic emulation of mechanical loads—position control approach", in Proceedings of 14th International Power Electronics and Motion Control Conference EPE-PEMC 2010, IEEE. (2010), S10-23-S10-30.

12. Aiello, G., Scelba, G., Scarcella, G., Cacciato, M., Tornello, L., Palmieri, A., Vanelli, E., Pernaci, C. and Di Dio, R., "Real-time emulation of induction machines for hardware in the loop applications", in 2018 international symposium on power electronics, electrical drives, automation and motion (SPEEDAM), IEEE. (2018), 1340-1345.

13. Taleires Filho, J., Correia, W.B., Aguiar, V.d.P.B. and Pontes, R.S.T., "Motor test bench control for load profile emulation", in IECON 2019-45th Annual Conference of the IEEE Industrial Electronics Society, IEEE. Vol. 1, (2019), 6663-6668.

14. de Medeiros, L.O.C., Rodrigues, J.C.G., Rezek, A.J.J., de Oliveira Junior, N., Corrêa, R.D.L., Braga, A.V., Ogoulola, C.E.G., Silva, V.Z. and Ramos, M.L., "Implementation of a didactic platform for a generic load torque emulator using induction machines and pwm inverters", in 2019 IEEE 15th Brazilian Power Electronics Conference and 5th IEEE Southern Power Electronics Conference (COBEP/SPEC), IEEE. (2019), 1-6.

15. Ahmadi, R., Fajri, P. and Ferdowsi, M., "Dynamic modeling and stability analysis of an experimental test bench for electric-drive vehicle emulation", in 2013 IEEE Power and Energy Conference at Illinois (PECI), IEEE. (2013), 88-94.

16. Rodic, M., Jezernik, K. and Trlep, M., "Use of dynamic emulation of mechanical loads in the testing of electrical vehicle driveline control algorithms", in 2007 European Conference on Power Electronics and Applications, IEEE. (2007), 1-10.

17. Marignetti, F., D'Aguanno, D. and Volpe, G., "Design and experiments of a test equipment for hybrid and electric vehicle drivetrains", in 2017 twelfth international conference on ecological vehicles and renewable energies (EVER), IEEE. (2017), 1-6.

18. Xie, Q., Claudio Filho, H., Feng, G., Clandfield, W. and Kar, N.C., "Advanced vehicle dynamic model for ev emulation considering environment conditions", in 2017 IEEE 30th Canadian Conference on Electrical and Computer Engineering (CCECE), IEEE. (2017), 1-4.

19. Fajri, P., Lee, S., Prabhala, V.A.K. and Ferdowsi, M., "Modeling and integration of electric vehicle regenerative and friction braking for motor/dynamometer test bench emulation", *IEEE Transactions on Vehicular Technology*, Vol. 65, No. 6, (2015), 4264-4273, doi: 10.1109/TVT.2015.2504363.

20. Sehab, R. and Shanan, T., "Control laws for the emulation of an electric vehicle drivetrain by two electric machines", in 2013 IEEE Vehicle Power and Propulsion Conference (VPPC), IEEE. (2013), 1-7.

21. Antal, D., Kiss, T., Szemes, P.T. and Husi, G., "Labview based dc motor dynamic load emulation testbed for testing rapid prototyping servo drives", in 2016 International Symposium on Small-scale Intelligent Manufacturing Systems (SIMS), IEEE. (2016), 105-110.

22. Unni, A., Kumar, A.S., Manoj, R., Sunil, S. and VC, J.S., "Design and simulation of test-bed for of emulation electric vehicle dynamics", in 2021 Sixteenth International Conference on Ecological Vehicles and Renewable Energies (EVER), IEEE. (2021), 1-6.

23. Ma, R., Wang, L. and Zhang, J., "Novel pi control algorithm for dynamic emulation of mechanical loads during transmission shift of electric vehicles", in 2019 IEEE 2nd International Conference on Automation, Electronics and Electrical Engineering (AUTEEE), IEEE. (2019), 234-240.

24. Qinglong, W., Changzhou, Y. and Shuying, Y., "Indirect field oriented control technology for asynchronous motor of electric vehicle", in 2020 IEEE International Conference on Power, Intelligent Computing and Systems (ICPICS), IEEE. (2020), 673-677.

25. Xiao-Feng, X., Guo-Feng, L. and Rong-Tai, H., "A rotor field oriented vector control system for electric traction application", in ISIE'2000. Proceedings of the 2000 IEEE International Symposium on Industrial Electronics (Cat. No. 00TH8543), IEEE. Vol. 1, (2000), 294-299.

26. Ahallianath, K. and Beevi, W., "Indirect field oriented control of induction motor using predictive current controller", in 2015

International Conference on Control Communication & Computing India (ICCC), IEEE. (2015), 248-253.

27. Benoudjit, D., Nait-Said, N. and Nait-Said, M., "Differential speed control of a propulsion system using fractional-order controller", *Electromotion-Cluj Napoca-*, Vol. 14, No. 2, (2007), 91.

28. Yahia Cherif, S., Benoudjit, D., Nait-Said, M.S. and Nait-Said, N., "Comparative study between propulsion control system failures of an electrical vehicle piloted by foc and by dtc using dual-induction-motors structure", *Diagnostyka*, Vol. 21, (2020), https://doi.org/10.29354/diag/125307

Persian Abstract

چکیده

خودروی الکتریکی اقتباسی از وسیله نقلیه معمولی با ادغام موتورهای الکتریکی است. به نظر می رسد این یکی از امیدوارکننده ترین فناوری هایی است که می تواند به بهبود قابل توجهی در عملکرد خودرو و انتشار آلاینده ها منجر شود. با این حال، برای هر وسیله نقلیه ای در ترافیک شهری نیاز به تغییرات رژیم، شتاب گیری مکرر، کاهش سرعت و مراحل توقف است که منجر به خرابی های جدی می شود. در طول مراحل فوق، موتورهای الکتریکی به طور مداوم در معرض اثرات حرارتی و مکانیکی قرار می‌گیرند. این مقاله امکان نمایش گشتاور بار چرخ را در ساختار پیشرانه الکتریکی با استفاده از موتورهای القایی دوگانه با کنترل بردار نشان می‌دهد. تقلید گشتاور بار که بر روی یکی از هر دو موتور الکتریکی قرار گرفته در چرخ‌های عقب ساختار خودروی الکتریکی (EV)عمل می‌کند، توسط یک ژنراتور DC همراه با یک موتور القایی در طول عملیات چرخه رانندگی خودرو و پروفایل‌های بار غیرقابل پیش‌بینی انجام می‌شود. نتایج شبیه‌سازی بطور گسترده امکان‌سنجی و اثربخشی طرح شبیه‌ساز پیشنهادی کنترل بردار مبتنی بر موتور القایی در کاربرد خودروی الکتریکی را تأیید می‌کند.

International Journal of Engineering

Analyzing Factors Influencing Mobile Social Media Marketing Acceptance among Customers

H. Hamidi*[a], M. S. Rafebakhsh[b]

[a] Department of Information Technology, Faculty of Industrial Engineering, K. N. Toosi University of Technology, Tehran, Iran
[b] Science and Research Branch, Islamic Azad University, Tehran, Iran

P A P E R I N F O	A B S T R A C T
	The purpose of this paper is to investigate the effective factors in accepting marketing through mobile social media by end users. The research method, is descriptive-survey and the research type is practical based on the research purpose. The statistical population of this study is the online customers of mobile phones from the Mobile Online website in 2019. Infinite population (384) was selected as statistical sample according to Cochran formula. Data collection was accomplished through questionnaire which involves 25 questions. The reliability of the questionnaire using Cronbach's alpha coefficient was 87%, which indicates an appropriate reliability. The results showed the importance of the effective factor of profitability on the attitude towards mobile marketing and the orientation towards mobile marketing on mobile marketing activities is significant.

1. INTRODUCTION

In today's world, businesses are becoming more electronic, and e-trade is gaining new appearances every day. A new area in this area is electronic social media, which has gained tremendous popularity. Businesses such as companies are willing to use this form of communication as a means of communicating with their customers [1]. Competition in today's market is more diverse than ever before, which is why many companies are trying to figure out how to develop competitive strategies to help them grow and develop their business [2]. There is no doubt that today's world is intensely involved with the internet and the cyber world and companies have to admit it. Any business or commerce that realizes the necessity of this and enters it will be a step ahead of those that keep thinking traditionally, show resistance against the changes [3]. At the same time, the individuals in a community need to adapt to e-trade, online drug shopping, etc. for doing social, scientific, cultural, etc. affairs. The use capability of a website is a necessity for a company's survival. Mass markets have

been divided into sections due to the intensive competition. Moreover, public media have replaced many non-individual marketing communications with individual ones [4]. With the ever-increasing expansion of mobile devices, e-trade and e-marketing has gone beyond the internet, appearing in mobile phones. In recent years, mobile technologies have been rapidly developed. Thus, new and more sophisticated generations of mobile phones have emerged, allowing users to use all features of the media, providing customized ads in proportion to time and location, and providing services at the right time. This has enhanced the productivity of the ads. It should be noted that the popularity of social media, such as Facebook, Whatsapp, and Twitter, has affected e-business sections, such as mobile businesses [5]. Most organizations use social media as a form of Social Media Marketing to have interaction with their customers or potential customers. Although many mobile advertising centers have limited their marketing budgets and this reduced the effectiveness of their marketing plans, it is required that the researchers know the factors influencing the social

---

*Corresponding Author Institutional Email: h_hamidi@kntu.ac.ir (H. Hamidi)

media acceptance, attempting to measure the effects through the mutual effects and taking into account online traffic analysis. Despite all of these requirements, no study has been conducted on the factors affecting the mobile marketing acceptance among customers in a unit model in our country. The foreign studies, on the other hand, investigated this subject limitedly. Furthermore, the effects of the variables on each other in Iranian organizations remain unknown. Since the relationships between these variables have been separately investigated or measured with other variables in the previously conducted studies, they need to be explored. In the previous studies, the results indicated that more than two-thirds of the online shoppers who filled up their carts left the website without making any purchase and only 10% of shoppers make online purchases [6]. To study why most of the online shoppers search and do not purchase and how to motive them to make purchases, their motives to make the final purchase decisions, repurchase, and the influencing factors have to be discussed. In the physical purchase studies, the authors investigated the physical purchase behaviors of the customers from the two viewpoints of enjoyment and profit. But the quantitative studies on the effects of the online product recommendations are based on the customer's loyalty with the mediating role of customer decision-making effectiveness in the drug shopping communities. At the same time, the repurchase behavior of the customers is very considerable for all online shops and electronic retailers. In today's very competitive market, the managers of companies are searching for new ways to make the people know about their products and improve their brands. One of the ways is the social media that have brought a big change in e-marketing. There are windows to keep the customers loyal to survive in this competitive market [7, 8].

The main objective of this study is to investigate the effects of different factors on mobile marketing acceptance among customers. We also have other objectives that are:

1) To ascertain the effect of perceivable profitability on mobile social media marketing attitude;

2) To ascertain the effect of risk avoidance on mobile social media marketing attitude;

3) To ascertain the effect of inventions on mobile social media marketing attitude.

This paper is organized in the following manner: Section 1 provides an introduction to online businesses. Section 2 is a literature review along with factors influencing online marketing. In section 3, we make a conceptual model of the study and the hypotheses. Section 4 research methodology is discussed. In this section the identification method and information collection are discussed. Section 5 presents research findings and the target acceptance test results. Discussions of results are presented in section 6. Finally,

section 7 is the conclusion along with suggestions for future works and the limitations of the current study.

2. LITERATURE REVIEW

Marketing aims to make and keep communications with the customers and other companies. In this communication, a set of norms must be considered. Commitment, trust, and mutual benefit are the main communication elements. Moreover, cooperation, trust, and mutual relationships are of importance. Compared to the traditional marketing, the pattern of this type of marketing helps and is fair, thus providing both parties – i.e. marketers and customers – with a "win-win result" [9].

Other researchers had different views. Theodor Levitt mentions that selling something is not the end of a transaction, but the customers have to be made willing [9, 10]. This is why many companies add additional services to their products. This way, they are differentiated from their competitors. The additional services are seen as valuable by the customers. The quality enhancement of the services provided to the customers is also a necessary element in marketing. The set of the mentioned factors is an attempt that results in "the customer coming back to the company" [10].

Overby and Lee [11] identified the marketing elements as Commitment, the sustainable will to make the best attempt to keep the communication. Trust, trusting is the honesty of an exchange partner. Notification is a willingness to share the information that is useful for the broth parties. Communication value relationships are classified into different levels, from partners with close and mutual cooperation-based relationships to those with competitive and aggressive relationships [11].

Commitment and trust are two main components of marketing, being mentioned in most of the models. Commitment is generally the realization of the activities as they are promised. Companies are committed to each other when they value the relationships constructed between them. Trust is when Company A believes that: a) Company B keeps its promises that provide positive results for Company A, and b) Company B does not perform its unpredicted activities in a manner that imposes losses to Company A [12-14].

In the field of industrial marketing, Torabi et al. [15] and Sorce et al. [16] identified the steps that have to be made by organizations in a mutual relationship. The most important step is trust in which both organizations make efforts to enhance the mutual relationship and continue it as long as it is beneficial for both of them. Moreover, there has to be a high degree of trust between the two organizations. Mutual information circulation has also to exist continuously. It is concluded that it is very

necessary to have commitment, trust, long-term time horizon, and information circulation to construct a mutual relationship regardless of the nature of the industry [17, 18].

In general, to define cyber social media, it can be said that there is a website that provides its users the opportunity to search and share information by adding simple features. Social media is the gathering place of hundreds of millions of internet users who interact and exchange information regardless of the political borders, languages, gender, and cultures [19]. Table 1 summarizes the factors affecting mobile marketing and its supporting resources.

3. CONCEPTUAL MODEL

Marketing practices of this study provide insights into customers' and mobile marketing acceptance. Mobile

TABLE 1. Factors Affecting mobile marketing

Concept	Dimensions	Supporting Resources
Mobile marketing Communication Strategies	Customer acceptance	[20]
	Infrastructure	
	Social culture	
	Legal barriers	
Social Media Marketing	Customer services	[20, 21]
	Satisfaction enhancement	
	Customer loyalty	
Marketing Communications	Applicability	[22, 23]
	Credibility	
	Amusement	
Social Media and E-commerce	Customer friendly relationship	[24, 25]
	Stability	
	Compatibly	
	Operations	
Social Media Acceptance	Beneficiary interactions	[26]
	Customer interaction	
	Live, real, and friendly interaction	
Customer Online Purchase	Knowing Prices	[17]
	Repurchase	
	Visiting website	
	Internet skills	
	Easy purchasing	
Website Quality Effect on Repurchase Intention	Website design	[20]
	Transaction security information usefulness	
	Payment group and customer communication	

marketing attitudes indicate a common influence in the phone market. Mobile marketing attitudes significantly impact marketing practices. There have been many studies that have examined how mobile marketing impacts the relationship between technologies, attitudes toward mobile marketing, willingness or unwillingness to participate in mobile marketing, and technological factors [19].

Relying on this base, this study developed three customer features for mobile platforms and formulated a conceptual model for mobile marketing acceptance (see Figure 1).

The first part of the conceptual model links customers' understandings of mobile devices used and their features of the phone innovations, customers' understandings of phone attachment, and the willingness to risk avoidance in the marketing methods. The second part relates to the effects of mobile marketing attitude on the participation and real content marketing activities, including purchasing products or services and downloading music and mobile applications. This model also explores the direct effects of three personal features of innovation, attachment, and mean risk-taking on the perceived usefulness of the content, applications, and customers' attitude toward mobile marketing.

The following hypotheses are made in this study:
1) Perceived profitability affects mobile marketing attitude;
2) Risk avoidance affects mobile marketing attitude;
3) Innovations affect mobile marketing attitude;
4) Perceived profitability affects mobile marketing attitude with the mediating role of innovations;
5) Perceived profitability affects mobile marketing attitude with the mediating role of risk avoidance; and
6) Mobile marketing attitude affects mobile marketing activities.

4. METHODOLOGY

Accordingly, this study analyzed the factors that influence the acceptance of mobile marketing by consumers. In terms of the nature of the subject, this study is cross-sectional.
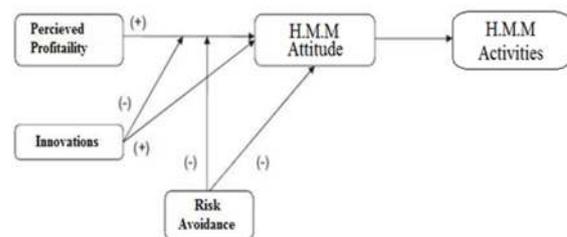
Figure 1. Conceptual model of present study

Statistical population refers to several desirable elements with at least one characteristic. A characteristic is an attribute that is shared among all the statistical populations and makes them different from the others [21]. The statistical population of this study consisted of the customers of Mobile Online drug shopping websites in 2021. According to Cochran's formula for an unlimited population, 384 individuals were selected. Sampling was performed using the Cochran formula for infinite populations. It samples as the ulated as:

$$n = \frac{Z_{\frac{\alpha}{2}}^2 \times \sigma^2}{\varepsilon^2} \tag{1}$$

In which n is the a ze, $Z_{\frac{\alpha}{2}}$ is the estimation, which is 1.6 considering the confidence level of 95%, ε is the permissible error, which is taken to be 0.05, and squared is the population variance. The population was 384 for 95% of confidence level and 0.5 standard deviations. This study used a simple random sampling method.

4. 1. Data Collection   This study used interviews with a set of managers and experts, particularly in the mobile bank. In general, the hypothesis and questions of the study is designed to investigate on mobile banking. Using the Likert scale, the views of the managers on the components were collected. To ensure the correctness and validity of the questionnaire, I was distributed Hamon 30employee in an experiment. Then, the defects were corrected, providing the final questionnaire. The test is shown in the following figure. Since the reliability is 0.863 (>05), the reliability was good. Cronbach's alpha is generally calculated as:

$$\alpha = \frac{kС̄}{V̄+(K-1)С̄} \quad OR \quad \alpha = \frac{k}{(K-1)}[1 - \frac{\sum_{i=1}^{k} S_i^2}{\sigma^2}] \tag{2}$$

where K is the number of the questions, S_i^2 is question variance, σ^2 is total variance of the questions, $\bar{C}$ is mean covariance of the questions, and $\bar{V}$ is mean variance [22].

4. 2. Respondents Frequency Distribution
Tables 2, 3, 4, and 5 represent gender, age, educational degree, and descriptive analysis results of the main variables, respectively.

5. FINDINGS

Structural Equation Model in PLS was employed to validate the theoretical model of the study and calculate

TABLE 2. Gender Distribution of Respondents

Gender	Frequency	Percentage
Male	149	38.7
Female	236	61.3
Total	385	100

TABLE 3. Age Distribution of Respondents

Age	Frequency	Percentage
<25	76	19 .7
25-30	130	3.8
31-35	127	33
36-40	36	9.4
>40	16	4.2
Total	385	100

TABLE 4. Educational Degree of Respondents

Educational Degree	Frequency	Percentage
Diploma or less	95	24.7
Bachelor	266	69.1
Maters or higher	24	6.2
Total	385	100

TABLE 5. Descriptive Analysis Results of the Main Variables

Variable	Mean	Standard Deviation	Lowest	Highest
Perceived profitability	3.866	0.409	2.56	4.72
mobile marketing attitude	4.140	0.621	2.00	5.00
mobile marketing activities	3.991	0.615	2.75	5.00
Innovations	3.834	0.578	2.33	5.00
Risk avoidance	3.446	0.795	1.25	5.00

the effect coefficients. The multivariable structural equation model is a general and strong model of multivariable regression, and more specifically a linear regression model extension that allows the author to test multiple regression equations simultaneously. Structural equations are used in general to determine the relationships between variables through a set of equations. The main question of the study was answered by employing a structural equation model. SmartPLS software was used to answer the main question of the study. The model was first fitted, followed by testing the hypotheses.

A. Factor Loading Test   Before testing the main model and hypotheses, the variable measurability of the questionnaire was tested using second-order factor loading analysis. The main components are comprised of sub-components which are themselves tested by a set of questions. As their form the study variables, the loading factor analysis is second-ordered here. Figure 2 represents the model with the loading factors.
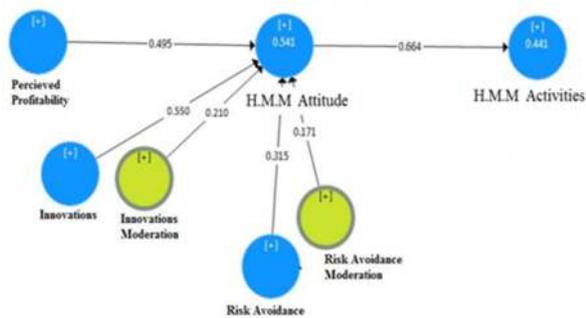
Figure 2. Loading Factors of the Structures and Variable Indicators

B. Cronbach's Alpha and Composite Reliability
Composite reliability (CR) indicators and Cronbach's alpha were used to examine the questionnaire reliability. The indicators have to be greater than 0.7 to confirm the reliability. Table 6 gives Cronbach's alphas.

As is shown in Table 6, all the coefficients are greater than 0.7, confirming the reliability of the variables. Table 7 shows the AVE for the variables.

As it is shown in Table 7, all the AVEs are greater than 0.5, representing a high validity for the latent variables. Table 8 indicates the main first-order square root AVE diagonal values of the latent variables and sub-diagonal correlation values between them.

At is shown in Table 8, the main diagonal values are greater than the sub-diagonal ones, representing a good validity and fitting for the variables.

5. 1. T-values   In the structural model fitting using t-values, the values have to be greater than 1.96 to

TABLE 6. Cronbach's Alpha of Variables

Variable	Cronbach's Alpha	CR
Perceived profitability	0.800	0.861
Mobile marketing attitude	0.829	0.921
Mobile marketing activities	0.668	0.937
Innovations	0.816	0.867
Risk avoidance	0.741	0.835

TABLE 7. Convergent Validity Results for Latent Variables

Variable	AVE
Perceived profitability	0.594
Mobile marketing attitude	0.854
Mobile marketing activities	0.881
Innovations	0.522
Risk avoidance	0.561

**TABLE 8.** Divergent Validity Matrix under Fornell-Larker method

Variables	Perceived profitability	Mobile marketing attitude	Mobile marketing activities	Innovations	Risk avoidance
Perceived profitability	961.1				
Mobile marketing attitude	650.0	942.0			
Mobile marketing activities	479.0	513.0	804.0		
Innovations	778.0	638.0	4032.0	964.0	
Risk avoidance	270.0	623.0	457.0	242.2	748.0

confirm their significance at the confidence level of 95%. Figure 3 shows the significant coefficients of the structural fitting.

According to Figure 3, the t-values are shown for the relationships between the variables at the confidence level of 95%.

5. 2. General Model Fitting   Goodness of Fitting (GOF) is used in the general part of the structural equation model. The author can investigate the fitting of the testing and structural part of the study to control the general fitting using this criterion. GOF was introduced by Naghsh Nilchi et al. [14]. It is calculated as:

$$GOF = \sqrt{communality * R\ square} \qquad (3)$$
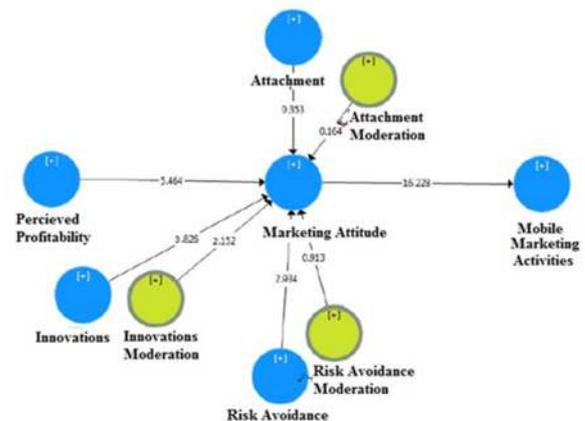
Figure 3. T-values for Structural Fitting

It is obtained from from the mean shared values of the first-order latent variables. To calculat$\overline{R^2}$,squared is needed to be calculated for all the latent variables of the model, including first- and second-order. Table 9 demonstrates the values obtained for R^2 and COMMUNALITIES.

TABLE 9. Squared and COMMUNALITIES Results

Variables	R^2	COMMUNALITIES
Perceived profitability	0.678	0.770
Mobile marketing attitude	0.634	0.854
Mobile marketing activities	0.760	0.882
Innovations	0.642	0.522
Risk avoidance	0.200	0.561

TABLE 10. GOF results

GOF	R^2	COMMUNALITIES
0.678	0.609	0.756

Given the three GOF values, 0.01, 0.25, and 0.36, as weak, medium, and strong, 0.675 is a strong value of GOF for the model (Table 10).

5. 3. Testing the Hypotheses   For the hypotheses that were tested, smart PLS was employed. This section consists of two parts: 1. (investigating the t-values for the hypotheses, and 2. (investigating the standardized loading factors. Table 11 shows the regression coefficient estimated for the hypotheses.

TABLE 11. Regression Coefficients

Hypothesis	Coefficient	T-value	Result
1: Perceived profitability → marketing attitude	0.495	5.464	Supported
2: Risk avoidance → marketing attitude	0.315	2.934	Supported
3: Innovations → marketing attitude	0.550	3.826	Supported
6: Perceived Profitability ↓→ marketing attitude, mediating innovations	0.210	2.152	Rejected
7: Perceived Profitability ↓→ marketing attitude, mediating risk avoidance	0.171	0.913	Rejected
8: mobile marketing attitude → marketing activities	0.664	16.228	Supported

6. DISCUSSION

Social media marketing is a new and powerful marketing tool in cyberspace. It's technology marketing on an intermediate-less, rapid, and less limited space. The use of this type of marketing can help a company attract a large number of customers. This could transform the market in a short period. In addition to making companies different from their competitors, by gaining customers and fans and receiving their immediate feedback directly on their websites, this considerably helps the companies. Social media marketing is using social media to gain traffic to a given website, or to attract attention to a given topic.

In today's intensively competitive market, Managers of companies are searching for new ways to inform people about their products and brands. One of the ways is social media, which has brought a dramatic transformation in online businesses and marketing. To survive in this competitive market, there are windows to keep the customers loyal [12]. One of the windows is to use optimal and continuous use of the online media communities. It provides companies with much popularity and many potential advantages, such as easy and wide access, various perception costs, and efficiency in communications [23]. Thus, for the success of companies in the market, it is important to study the factors driving social media acceptance through new marketing and advertisement practices in online media communities.

7. CONCLUSION

According to the tables and t-values, all the hypotheses were supported. The t-value between perceived profitability and mobile marketing attitude was 5.464, which is greater than 1.96. This indicates the significant effect of the perceived profitability on mobile marketing attitude at the confidence level of 95%. Customers may choose the facts created by the company that is consistent with their beliefs and attitudes. As a fact, they keep the facts to rebuild an image of it whenever they remember the company. This is associated with brand recognition. Participation in an e-commerce relationship somewhat creates customers' attachments to the online vendor to receive their products and services. It is only through participation in an exchange relationship a customer acquires experience, value, and satisfaction. This is why profitability satisfaction is an important customer condition. T-value between risk avoidance and mobile marketing attitude was 2.934 (>1.96). This demonstrates the significant effect of risk avoidance on mobile marketing attitude at the confidence level of 95% (Hypothesis 2). To explain this hypothesis, it can be said that risk avoidance can be seen as an individual's

confident expectation from an online and risky situation in which the customer's weaknesses will not be used. Vendors need to make trust aiming to change a customer from a curious visitor into an individual willing to exchange through the website not giving up until their online purchases are completed. T-value for innovations and mobile marketing attitude was 3.826 (>1.96). This confirmed the significant effect of innovations on mobile marketing attitude at the confidence level of 95% (Hypothesis 3). Innovations are a transaction means and increased online drug shopping increases the consideration of the customer's expectations. Non-consideration of innovations for ease of purchasing is among the most important reasons for the customers not to make purchases. Perceived innovations are an important variable in customers' purchase decisions. Thus, Hypothesis 5 is rejected. T-value for perceived profitability and mobile marketing attitude with the mediating role of innovations was 2.152 (>1.96) at the confidence level of 95%. This supports Hypothesis 6. T-value for perceived profitability and mobile marketing attitude with the mediating role of risk avoidance was 0.913 (<1.96)and the confidence level of 95%, indicating the insignificant effect of perceived profitability on mobile marketing attitude. Thus, Hypothesis 7 is rejected. T-value for mobile marketing attitude and mobile marketing activities was 16.228 (>1.96). This shows the significant effect of mobile marketing attitude on mobile marketing activities at the confidence level of 95%. Hence, Hypothesis 8 is supported.

8. SUGGESTION FOR THE FUTURE WORKS

By conducting similar studies in other regions and provinces and comparing the results with those of your current study, your findings can contribute to your scientific achievements. Different sample sizes and types can support or refute previous studies. Therefore, since this study was conducted in a specific organization and the sample size was limited, additional studies need to be conducted in other organizations. It is suggested to use other questionnaires for testing the variables of the current study and comparing the results.

9. LIMITATIONS

The limitations of any study are not always apparent, but that does not mean that the results of the study cannot be used. However, since it is necessary to mention some limitations faced by this study, the limitations are as follows:

Findings were obtained from the data collection period. Hence, the findings are valid for a short period. Time can change the variables. This study was conducted in 2019. Care must be taken when extending the results to future years. A major limitation of any study is the inability to extend its results to other statistical populations. This is true for the current study in that its results cannot be extended to other regions or populations. Non-response from a segment of the population, uncaring responses to the questions, and a bias that some of the respondents may have toward specific questions are some of the important limitations of scientific studies. This also applies to the current study.

10. REFERENCES

1. Ahn, T., Ryu, S. and Han, I., "The impact of web quality and playfulness on user acceptance of online retailing", *Information & Management*, Vol. 44, No. 3, (2007), 263-275, doi: 10.1016/j.im.2006.12.008.

2. Hamidi, H., A combined fuzzy method for evaluating criteria in enterprise resource planning implementation, in Intelligent systems: Concepts, methodologies, tools, and applications. 2018, IGI Global.639-670.

3. Boyd, D.M. and Ellison, N.B., "Social network sites: Definition, history, and scholarship", *Journal of Computer-mediated Communication*, Vol. 13, No. 1, (2007), 210-230, doi: 10.1111/j.1083-6101.2007.00393.x.

4. Daraei, A. and Hamidi, H., "An efficient predictive model for myocardial infarction using cost-sensitive j48 model", *Iranian Journal of Public Health*, Vol. 46, No. 5, (2017), 682, doi. http://ijph.tums.ac.ir/index.php/ijph/article/view/9918

5. Verdery, A.M., Entwisle, B., Faust, K. and Rindfuss, R.R., "Social and spatial networks: Kinship distance and dwelling unit proximity in rural thailand", *Social Networks*, Vol. 34, No. 1, (2012), 112-127, doi: 10.1016/j.socnet.2011.04.003.

6. Kim, J.K., Cho, Y.H., Kim, W.J., Kim, J.R. and Suh, J.H., "A personalized recommendation procedure for internet shopping support", *Electronic Commerce Research and Applications*, Vol. 1, No. 3-4, (2002), 301-313, doi: 10.1016/j.elerap.2012.04.002.

7. Hamidi, H., Vafaei, A. and Monadjemi, S.A., "Analysis and design of an abft and parity-checking technique in high performance computing systems", *Journal of Circuits, Systems, and Computers*, Vol. 21, No. 03, (2012), 1250017, doi. https://doi.org/10.1142/S021812661250017X

8. Kuan, H.-H., Bock, G.-W. and Vathanophas, V., "Comparing the effects of website quality on customer initial purchase and continued purchase at e-commerce websites", *Behaviour & Information Technology*, Vol. 27, No. 1, (2008), 3-16, doi: 10.1080/01449290600801959.

9. Minarti, S.N. and Segoro, W., "The influence of customer satisfaction, switching cost and trusts in a brand on customer loyalty–the survey on student as im3 users in depok, indonesia", *Procedia-Social and Behavioral Sciences*, Vol. 143, (2014), 1015-1019, doi: 10.1016/j.sbspro.2014.07.546.

10. Panasenko, N., "Czech and slovak family patterns and family values in historical, social and cultural context", *Journal of Comparative Family Studies*, Vol. 44, No. 1, (2013), 79-98, doi: 10.3138/jcfs.44.1.79.

11. Overby, J.W. and Lee, E.-J., "The effects of utilitarian and hedonic online shopping value on consumer preference and intentions", *Journal of Business Research*, Vol. 59, No. 10-11, (2006), 1160-1166, doi: 10.1016/j.jbusres.2006.03.008.

12. Sagone, E. and De Caroli, M.E., "The "portrait" of values in family: A cross-age study in sicilian context", *Procedia-Social and Behavioral Sciences*, Vol. 127, (2014), 194-198, doi: 10.1016/j.sbspro.2014.03.239.

13. Sen, R., King, R.C. and Shaw, M.J., "Buyers' choice of online search strategy and its managerial implications", *Journal of Management Information Systems*, Vol. 23, No. 1, (2006), 211-238, doi: 10.2753/MIS0742-1222230107.

14. Nilchi, A.N., Vafaei, A. and Hamidi, H., "Evaluation of security and fault tolerance in mobile agents", in 2008 5th IFIP International Conference on Wireless and Optical Communications Networks (WOCN'08), IEEE. (2008), 1-5.

15. Torabi, A., Hamidi, H. and Safaie, N., "Effect of sensory experience on customer word-of-mouth intention, considering the roles of customer emotions, satisfaction, and loyalty", *International Journal of Engineering*, *Transactions C: Aspects,* Vol. 34, No. 3, (2021), 682-699, doi: 10.5829/ije.2021.34.03c.13.

16. Sorce, P., Perotti, V. and Widrick, S., "Attitude and age differences in online buying", *International Journal of Retail & Distribution Management*, Vol. 33, No. 2, (2005), doi: 10.1108/09590550510581458.

17. Shin, J.I., Chung, K.H., Oh, J.S. and Lee, C.W., "The effect of site quality on repurchase intention in internet shopping through mediating variables: The case of university students in south korea", *International Journal of Information Management*, Vol. 33, No. 3, (2013), 453-463, doi: 10.1016/j.ijinfomgt.2013.02.003.

18. Scarpi, D., "Work and fun on the internet: The effects of utilitarianism and hedonism online", *Journal of Interactive Marketing*, Vol. 26, No. 1, (2012), 53-67, doi: 10.1016/j.intmar.2011.08.001.

19. Sahin, A., Zehir, C. and Kitapçı, H., "The effects of brand experiences, trust and satisfaction on building brand loyalty; an empirical research on global brands", *Procedia-Social and Behavioral Sciences*, Vol. 24, (2011), 1288-1301, doi: 10.1016/j.sbspro.2011.09.143.

20. Hamidi, H., Vafaei, A. and Monadjemi, S.A.H., "Analysis and evaluation of a new algorithm based fault tolerance for computing systems", *International Journal of Grid and High Performance Computing*, Vol. 4, No. 1, (2012), 37-51, doi: 10.4018/jghpc.2012010103.

21. Yang, B., Kim, Y. and Yoo, C., "The integrated mobile advertising model: The effects of technology-and emotion-based evaluations", *Journal of Business Research*, Vol. 66, No. 9, (2013), 1345-1352, doi: 10.1016/j.jbusres.2012.02.035.

22. Hamidi, H. and Safaie, N., "Effect of motivation, opportunity and ability on human resources information security management considering the roles of attitudinal, behavioral and organizational factors", *International Journal of Engineering, Transactions C: Aspects*, Vol. 34, No. 12, doi: 10.5829/ije.2021.34.12c.07.

23. Tsai, H.-T. and Huang, H.-C., "Determinants of e-repurchase intentions: An integrative model of quadruple retention drivers", *Information & Management*, Vol. 44, No. 3, (2007), 231-239, doi: 10.1016/j.im.2006.11.006.

24. Yang, K. and Lee, H.J., "Gender differences in using mobile data services: Utilitarian and hedonic value approaches", *Journal of Research in Interactive Marketing*, (2010), doi: 10.1108/17505931011051678.

25. Alvanchi, A., Didehvar, N., Jalilehvand, M., Adami, P. and Shahmir, S., "Semi-augmented reality, a novel approach to improve customer safety in the pre-sale process of under construction buildings", *International Journal of Engineering, Transactions A: Basics*, Vol. 34, No. 10, (2021), doi: 10.5829/ije.2021.34.10a.01.

26. Mohammadi, S., Nikkhahan, B. and Sohrabi, S., "An analytical survey of" on-site customer" practice in extreme programming", in International Symposium on Computer Science and its Applications, IEEE. (2008), 1-6.

Persian Abstract

چکیده

هدف مقاله حاضر بررسی عوامل مؤثر در پذیرش بازاریابی موبایل رسانه اجتماعی، توسط مصرف‌کنندگان می‌باشد. روش تحقیق، روش توصیفی-پیمایشی و نوع پژوهش با توجه به هدف تحقیق کاربردی بوده و جامعه آماری این پژوهش شامل مشتریان خرید آنلاین از وب‌سایت آنلاین می باشد. بر اساس فرمول کوکران برای جامعه نامحدود (۳۸٤) نفر به‌عنوان نمونه آماری انتخاب شد. ابزار جمع‌آوری اطلاعات پرسشنامه استاندارد مشتمل بر ۲٥ سؤال مورد سنجش قرارگرفته شده است. پایایی پرسشنامه با استفاده از ضریب آلفای کرونباخ ۸۷٪ تعیین گردید که نشان‌دهنده‌ی پایایی مناسب ابزار اندازه‌گیری بود. نتایج نشان‌دهنده اهمیت تأثیر گذار عامل سوداوری، بر نگرش به بازاریابی همراه بوده و جهت گیری نسبت به بازاریابی همراه بر فعالیت های بازاریابی همراه قابل توجه می باشد.

AIMS AND SCOPE

The objective of the International Journal of Engineering is to provide a forum for communication of information among the world's scientific and technological community and Iranian scientists and engineers. This journal intends to be of interest and utility to researchers and practitioners in the academic, industrial and governmental sectors. All original research contributions of significant value focused on basics, applications and aspects areas of engineering discipline are welcome.

This journal is published in three quarterly transactions: Transactions A (Basics) deal with the engineering fundamentals, Transactions B (Applications) are concerned with the application of the engineering knowledge in the daily life of the human being and Transactions C (Aspects) - starting from January 2012 - emphasize on the main engineering aspects whose elaboration can yield knowledge and expertise that can equally serve all branches of engineering discipline.

This journal will publish authoritative papers on theoretical and experimental researches and advanced applications embodying the results of extensive field, plant, laboratory or theoretical investigation or new interpretations of existing problems. It may also feature - when appropriate - research notes, technical notes, state-of-the-art survey type papers, short communications, letters to the editor, meeting schedules and conference announcements. The language of publication is English. Each paper should contain an abstract both in English and in Persian. However, for the authors who are not familiar with Persian, the publisher will prepare the latter. The abstracts should not exceed 250 words.

All manuscripts will be peer-reviewed by qualified reviewers. The material should be presented clearly and concisely:
- *Full papers* must be based on completed original works of significant novelty. The papers are not strictly limited in length. However, lengthy contributions may be delayed due to limited space. It is advised to keep papers limited to 7500 words.
- *Research* notes are considered as short items that include theoretical or experimental results of immediate current interest.
- *Technical notes* are also considered as short items of enough technical acceptability with more rapid publication appeal. The length of a research or technical note is recommended not to exceed 2500 words or 4 journal pages (including figures and tables).

Review papers are only considered from highly qualified well-known authors generally assigned by the editorial board or editor in chief. Short communications and letters to the editor should contain a text of about 1000 words and whatever figures and tables that may be required to support the text. They include discussion of full papers and short items and should contribute to the original article by providing confirmation or additional interpretation. Discussion of papers will be referred to author(s) for reply and will concurrently be published with reply of author(s).

INSTRUCTIONS FOR AUTHORS

Submission of a manuscript represents that it has neither been published nor submitted for publication elsewhere and is result of research carried out by author(s). Presentation in a conference and appearance in a symposium proceeding is not considered prior publication.

Authors are required to include a list describing all the symbols and abbreviations in the paper. Use of the international system of measurement units is mandatory.

- On-line submission of manuscripts results in faster publication process and is recommended. Instructions are given in the IJE web sites: www.ije.ir-www.ijeir.info
- Hardcopy submissions must include MS Word and jpg files.
- Manuscripts should be typewritten on one side of A4 paper, double-spaced, with adequate margins.
- References should be numbered in brackets and appear in sequence through the text. List of references should be given at the end of the paper.
- Figure captions are to be indicated under the illustrations. They should sufficiently explain the figures.
- Illustrations should appear in their appropriate places in the text.
- Tables and diagrams should be submitted in a form suitable for reproduction.
- Photographs should be of high quality saved as jpg files.
- Tables, Illustrations, Figures and Diagrams will be normally printed in single column width (8cm). Exceptionally large ones may be printed across two columns (17cm).

PAGE CHARGES AND REPRINTS

The papers are strictly limited in length, maximum 6 journal pages (including figures and tables). For the additional to 6 journal pages, there will be page charges. It is advised to keep papers limited to 3500 words.

Page Charges for Papers More Than 6 Pages (Including Abstract)	
For International Author ***	$55 / per page
For Local Author	100,000 Toman / per page

AUTHOR CHECKLIST

- Author(s), bio-data including affiliation(s) and mail and e-mail addresses).
- Manuscript including abstracts, key words, illustrations, tables, figures with figure captions and list of references.
- MS Word files of the paper.